SAIL AEROFOIL
APPLIED TO A
VERTICAL-AXIS WIND TURBINE

BY

J. ROBERT

A Thesis submitted to the Faculty of Graduate Studies and Research in partial fulfillment of the requirements for the degree of Master of Engineering.

Department of Mechanical Engineering
McGill University

Montréal, Québec, Canada

March 1977

SAIL AEROFOIL APPLIED TO A VERTICAL-AXIS WIND TURBINE

SUMMARY

With the growing interest in wind energy, the vertical-axis wind turbine which is relatively cheap and is insensitive to wind direction is becoming increasingly popular. The feasibility of using sailwings instead of rigid blades has already been established experimentally. In this study, two-dimensional tests of the sail aerofoil are presented. The results are related to the characteristics of sailwings and two-dimensional sails. A theory for the wind turbine is outlined and extensions are developed for turbines of high solidity. A computer program for this theory is used to determine the relative merit of various shapes of sail aerofoils when applied to a vertical-axis wind turbine. The present knowledge indicates that a three-bladed vertical-axis wind turbine using dacron sailwings with a leading edge to chord ratio of 10% would be close to an optimum design if operated with a solidity of about 1.0.

RESUME

Etant donné l'intérêt croissant que suscite l'énergie éolienne, la turbine à vent à axe vertical, de par son faible coût initial et son insensibilité à la direction du vent, monte en popularité. Il a déjà été démontré expérimentalement par le passé qu'il est possible d'utiliser des "aile-voiles" plutôt que des pales rigides. Cette étude comprend des tests du "profil-voile" en deux dimensions. Les résultats sont comparés avec les charactéristiques des "aile-voile" et des voiles à deux dimensions. Une théorie des turbines à vent est décrite et est modifée quelque peu pour tenir compte des turbines ayant une grande surface de pales par rapport à la surface balayée. Un programme d'ordinateur pour cette théorie permet de comparer le rendement de différentes sections de "profil-voile" dans une turbine à axe vertical. Jusqu 'à présent il semble que la meilleure configuration pour une telle turbine comprend trois "aile-voiles" faites de dacron avec un bord d'attaque ayant un diamètre de 10% de la corde et une somme des cordes des pales environ égale au rayon lorsque mesurés au plan de symétrie de la turbine.

ACKNOWLEDGEMENTS

The author would particularly like to thank Dr. B.G. Newman for his guidance and help throughout this investigation. He also wishes to thank Mr. Joe Dubik, who gave useful technical assistance, Rosemary Swain, who handled the laborious task of typing, and the National Research Council, whose scholarship gave financial support. The author would also like to thank his wife Lise who encouraged him throughout and helped with the finishing touches. The work was supported by the National Research Council on Grant Number A7096 (Grantee: Dr. B.G. Newman).

TABLE OF CONTENTS

NOTATION

(The Symbols not Included in this List are Defined in the Text)

A		Frontal area of the wind turbine.
c		Chord
$\bar{c}$		Mean chord: area/span of a wing.
c_o		Maximum chord of the sail aerofoil (fabric just taut).
C_d	$\frac{\text{drag}}{\frac{1}{2}\rho V_\alpha{}^2\bar{c}l}$	Drag coefficient of a wing or aerofoil.
C_D	$\frac{D}{\frac{1}{2}\rho V^2 A}$	Wind turbine drag coefficient based on ambient windspeed.
C_{DD}	$\frac{D}{\frac{1}{2}\rho V_D^2 A}$	Wind turbine drag coefficient based on disc velocity.
$C_{D_{PL}}$	$\frac{\text{drag}}{\frac{1}{2}\rho V^2 A}$	Theoretical drag coefficient of a "fully solid" wind turbine.
C_L	$\frac{\text{lift}}{\frac{1}{2}\rho V_\alpha^2 cl}$	Lift coefficient.
$C_{m_{\frac{1}{4}}}$	$\frac{\text{moment}}{\frac{1}{2}\rho V^2 l}$	Coefficient of moment about the quarter-chord point.
C_N	$\frac{\text{normal force}}{\frac{1}{2}\rho V_\alpha^2 cl}$	Normal force coefficient.
C_P	$\frac{P}{\frac{1}{2}\rho V^3 A}$	Power coefficient of the wind turbine.
$C_{P_{id}}$		Ideal power coefficient.
$C_{P_{max}}$		Maximum power coefficient.

C_Q	$\frac{\text{torque}}{\frac{1}{2}\rho V^2 A 2R}$	Torque coefficient of the wind turbine.
C_T	$\frac{\text{thrust}}{\frac{1}{2}\rho V_\alpha^2 c l}$	Thrust coefficient.
d		Leading edge diameter.
D		Drag of the wind turbine.
h		Tunnel width.
H		Height of the wind turbine.
l		Length of a blade.
L/D		Lift to drag ratio.
N		Number of blades of a wind turbine.
$\frac{Nc}{R}$,		Solidity of the wind turbine at the plane of symmetry y = 0.
p_{in}		Static pressure measured inside the sail aerofoil.
p_r		Static pressure at a reference hole in the wind tunnel wall.
p_∞		Pressure far away.
P		Power of a wind turbine.
P_{id}		Power of an ideal wind turbine.
r		Local radius at a given height in the wind turbine.
R		Maximum radius of the wind turbine.
Re	$\frac{\rho V(\text{dim})}{\mu}$	Reynolds number based on a characteristic dimension (dim).
Re_{wd}	$\frac{\rho V(2R)}{\mu}$	Wind turbine Reynolds number based on the diameter.
Re_{bl}	$\frac{\rho V_\alpha C}{\mu}$	Local Reynolds number of a wind turbine blade.
t		Thickness of a wing or aerofoil.

V	Ambient windspeed.
V_{α}	Local windspeed relative to a blade.
V_D or V_d	Disc velocity (velocity at the actuator disc location).
V_{TS}	Velocity in the test section.
w	Angular velocity of the turbine.
$\frac{wR}{V}$	Tip speed ratio.
x	Exponent in the theory allowing for high solidity.
X-tension	Force on the trailing edge of the sail-aerofoil in a direction parallel to the chord line.
Y-tension	Force on the trailing edge of the sail aerofoil in a direction perpendicular to the surface of the aerofoil.
y	Vertical position within the wind turbine measured from the plane of symmetry.
α	Local angle of attack of the wind relative to a blade.
δ	Blade tilt angle with respect to the axis of the wind turbine.
ε_s	Solid blockage correction for wind tunnel measurements.
ε_w	Wake blockage correction for wind tunnel measurements.
$\eta \; \frac{27}{16} \frac{P}{\frac{1}{2}\rho AV^3}$	Betz efficiency.
ρ	Air density.
θ	Angular position of a blade within the wind turbine.
μ	Air viscosity.

1. INTRODUCTION

For a long time, man has been trying to harness wind energy. The first windmills apparently appeared about 2000 years ago, equipped with primitive sails. The 18th century saw the largest number of these, mostly for milling flour or pumping water, a familiar example being the Dutch windmill. With the advent of the steam engine in the 19th century, they were slowly abandoned. Then, electricity came into the picture in the 20th century and wind machines, like the American multibladed type, regained popularity by generating electricity in remote places.

Most windmills had a horizontal axis; those with a vertical-axis, of the drag type, being considered inefficient and slow. More recently, the National Research Council of Canada developed a vertical-axis wind turbine which was very efficient when operating at a high tip speed ratio (Figure 1). Tests were made by South and Rangi (1971, 1972). The design was simple and suitable mostly for large production. An attempt was made at McGill (Robert 1975) to design a cheap wind turbine with sails which would be suitable for the third world, and that would still retain one of the major advantages of vertical-axis turbines, namely that they are insensitive to the wind direction.

Since the drag of the blades is of prime importance, it was decided that sailwings, developed by Sweeney (1961) at Princeton University, would probably be more suitable than conventional sails for that application. A sailwing consists of fabric wrapped around a leading edge, usually circular in cross-section, and pulled taut to form a sort of flexible hollow wing (Figure 2). Models of vertical-axis wind turbines using sailwings were built and tested (Robert 1975). It was seen that the leading edge should not be too flexible. The model shown in Figure 3 was fully self-starting and featured a low tip speed ratio of around unity. Its low power coefficient of 0.02 was attributed to the use of a porous fabric (parachute silk). A subsequent model reached a power coefficient of 0.16 and had non-porous sailwings made of calendered dacron, mounted parallel to the rotating axis (Figure 4). The efficiency of various types of turbines is shown in Figure 5.

The behaviour of sailwings is difficult to predict owing to the difficulty of controlling all the parameters characterizing it (Figure 2). For instance, the chord must narrow down near the middle of the span in order that tension be maintained everywhere along the trailing edge. That tension has components in three perpendicular directions and is difficult to analyze. The sailwing, when loaded, becomes twisted towards mid-span. The camber may or may not be constant along the span. Also, the thickness (that is leading edge diameter) to chord ratio varies since the chord length changes along the span. A better understanding of sailwings was therefore desirable before proceeding further with the testing of particular sailwing wind turbines.

This thesis is devoted to the study of the sail aerofoil, which is the two-dimensional version of the sailwing with a rigid trailing edge, and should help to understand better the behaviour of sailwings by testing the effect of changing only one parameter at a time. It was found necessary to use a rigid trailing edge (Figure 6) for testing the sail aerofoil, in order to obtain constant chord, camber and tension along the span, and to avoid twisting. This rigid trailing edge was hinged about a longitudinal axis passing through the trailing edge thereby simulating the tensioning wire or seam normally found in a sailwing. Endplates were added to preserve two-dimensionality.

Wind tunnel testing of the sail aerofoil was performed for a full range of angles of attack 0° to 180° and the Reynolds numbers varied from 9×10^4 to 18×10^4 (up to 30×10^4 at small angles of attack). Different geometries were tested by varying the distance between the leading edge and the trailing edge, thus changing the camber and the tension in the fabric. Three leading edge diameters were tested, giving a thickness to chord ratio of 6.4%, 9.7% and 13%. Measurements were taken of the lift, the drag, the two components of the force exerted by the trailing edge to balance the tension in the fabric, and the static pressure inside the sail aerofoil. Comparisons are made with sail-wings, sails and rigid aerofoils.

The data on lift and drag were inserted in a computer program to evaluate the performance of a two-dimensional vertical-axis wind turbine, in an attempt to give a preliminary assessment of the optimum design. The Betz-Glauert theory is used to determine the air speed at the plane of the turbine and is extended to allow for wind turbines of a high solidity. An attempt is also made to modify the theory to account also for the interference between the upstream and downstream blades.

2. WIND TURBINE THEORY

2.1 Introduction

The performance of a wind turbine can be predicted from a knowledge of the aerodynamic characteristics of its blades. By vectorial addition of the velocity of the blade and of the wind passing through the turbine, it is possible to determine the local windspeed and angle of attack on an element of a blade in a given position. By summing up the torque contributions of the lift and drag as the blade revolves, the complete torque of the turbine can be determined.

In the above theory, allowance must be made for the reduction of speed as the flow approaches the turbine (outflow factor). Following Templin, this disc velocity V_D is estimated using theories which relate it to the drag D of the turbine itself.

2.2 Betz-Glauert Theory

In this theory reported by Glauert (Durand 1963) and Fales (Marks 1967), the wind turbine is represented by an actuator disc through which the velocity is uniform. The streamline pattern shown in illustration 1 is assumed.

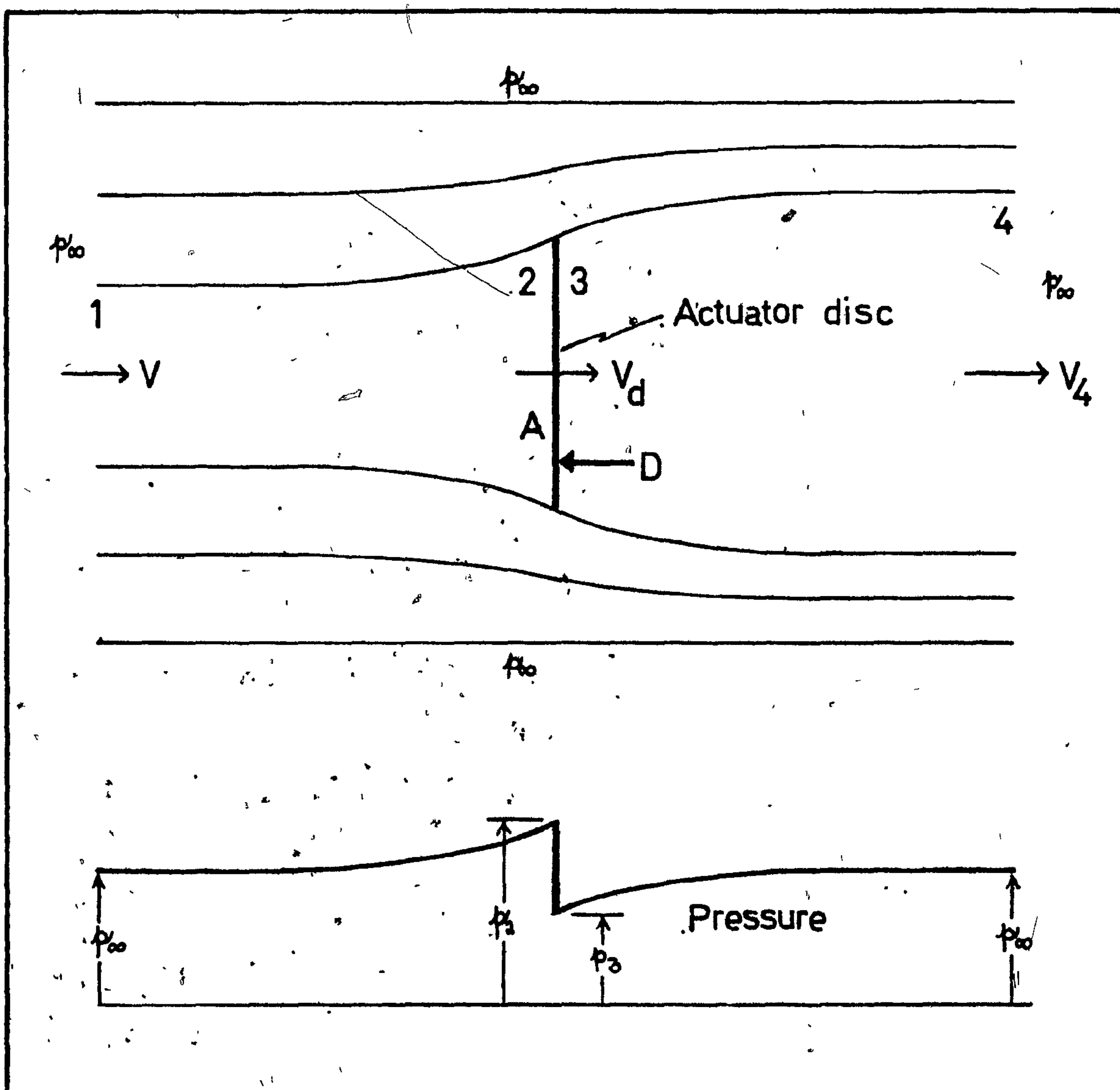

ILLUSTRATION 1 - Streamline Pattern and Pressure Profile.

Bernoulli's equation is applied in the steady flow from 1 to 2 and from 3 to 4:

$$P_\infty + \tfrac{1}{2}\rho V^2 = p^2 + \tfrac{1}{2}\rho V_D{}^2$$

$$p_3 + \tfrac{1}{2}\rho V_D{}^2 = p_\infty + \tfrac{1}{2}\rho V_4{}^2$$

The momentum equation is used from 1 to 4 for a large control volume with sides composed of streamlines far away.

$$D = \rho A\ V_D\ (V - V_4)$$

Noticing that:

$$D = (p_2 - p_3)A$$

the disc velocity becomes:

$$V_D = \tfrac{1}{2}\ (V + V_4)$$

That is, the disc velocity is the arithmetic mean between V and V_4. The wake velocity V_4 has values between 0 and V. This imposes the limitation that V_D lies between the ambient windspeed and half of it.

$$\frac{V}{2} < V_D \leq V$$

The coefficient of drag can be written:

$$C_D = \frac{D}{\frac{1}{2}\rho A V^2} = 4\,\frac{V_D}{V}\left(1 - \frac{V_D}{V}\right) \qquad 2.2\text{-}1$$

Notice it has values between 0 and 1. This equation is plotted in Figure 7.

The required relationship between the disc velocity and the drag coefficient correctly giving $\frac{V_D}{V} = 1$ when $C_D = 0$ is then:

$$\frac{V_D}{V} = \frac{1}{2} + \frac{1}{2}\sqrt{1 - C_D} \qquad 2.2\text{-}2$$

The theory can also be used to predict the power output of an ideal wind turbine by assuming that all of the turbine drag is converted to shaft power:

$$P_{id} = D\,V_D$$

And the power coefficient is:

$$C_{P_{id}} = \frac{D V_D}{\frac{1}{2}\rho A V^3} = C_D\,\frac{V_D}{V} \qquad 2.2\text{-}3$$

Using the drag expression 2.2-1

$$C_{P_{id}} = 4 \left(\frac{V_D}{V}\right)^2 \left(1 - \frac{V_D}{V}\right) \qquad 2.2\text{-}4$$

This ideal power will reach a maximum of:

$$C_{P_{max}} = \frac{16}{27} \text{ (or 59.3\%) at } \frac{V_D}{V} = \frac{2}{3}$$

in which case, the drag coefficient is:

$$C_D = \frac{8}{9}$$

This theory has an important limitation. It is possible to conceive a wind turbine that would have such a high solidity that the disc velocity would become less than half the ambient windspeed and the wake would become theoretically infinite in extent, or there would be backflow in the wake. The actuator disc theory cannot handle that case.

2.3 Extension of Betz-Glauert Theory to Allow for High Solidity

The Betz-Glauert theory is extended to cases with high solidity and low disc velocity. Let us assume that the disc velocity ratio depends on the ratio of the actual drag of the wind turbine to the drag of a "fully solid" wind turbine:

$$\frac{V_D}{V} = f\left(\frac{C_D}{C_{D_{PL}}}\right)$$

Where: $C_{D_{PL}}$ = drag coefficient of a "fully solid" wind turbine (i.e. drag of a circular plate in the case of a horizontal axis turbine).

There are two limiting conditions: when the wind turbine has zero solidity (i.e. there are no blades, $C_D = 0$), the disc velocity ratio should be unity, and when it is fully solid ($C_D = C_{D_{PL}}$), the disc velocity ratio should be zero:

$$C_D = 0 \Rightarrow \frac{V_D}{V} = 1.0$$

$$C_D = C_{D_{PL}} \Rightarrow \frac{V_D}{V} = 0$$

A simple function that satisfies (*) the above conditions is:

$$\frac{V_D}{V} = \left(1 - \frac{C_D}{C_{D_{PL}}}\right)^x$$

Where: x is a constant exponent which will be determined.

(*) $1 - \left(\frac{C_D}{C_{D_{PL}}}\right)^x$ was also tried but did not match Glauert's theory nearly so well.

This relation may be inverted to isolate C_D:

$$C_D = C_{D_{PL}} \left(1 - \left(\frac{V_D}{V}\right)^{\frac{1}{x}}\right)$$

Using equation (2.2-3), the ideal power coefficient becomes:

$$C_{P_{id}} = C_{D_{PL}} \frac{V_D}{V} \left(1 - \left(\frac{V_D}{V}\right)^{\frac{1}{x}}\right)$$

And the maximum ideal power coefficient is now:

$$C_{P_{max}} = \frac{C_{D_{PL}}}{x + 1} \left(\frac{x}{x + 1}\right)^x$$

And occurs at:

$$\frac{V_D}{V} = \left(\frac{x}{x + 1}\right)^x$$

Now, the two constants $C_{D_{PL}}$ and x can be adjusted so as to obtain the same maximum ideal power coefficient as in the Glauert theory, and at the same disc velocity ratio:

$$C_{P_{max}} = \frac{16}{27} \qquad \text{at } \frac{V_D}{V} = \frac{2}{3}$$

In this case, the values of the two constants are:

$$C_{D_{PL}} = 1.11467 \text{ and } x = 0.254$$

yielding the final form of the relation allowing for high solidities:

$$\frac{V_D}{V} = \left(1 - \frac{C_D}{1.11467}\right)^{0.254}$$

A graph of this equation is shown in Figure 7 and of the ideal power coefficient in Figure 8. It is encouraging that the computed value of $C_{D_{PL}}$ is of the right order for a bluff body.

2.4 Extension of Betz-Glauert Theory to Allow for Wake Interference

Another problem specific to vertical-axis wind turbines, is that the wind passes twice through the area swept by the blades. The interference of the upwind blades on the down-wind blades can be treated by crudely representing the turbine by two actuator discs in tandem. The second disc velocity is then lower than the first. The streamline pattern is shown in Illustration 2.

HARK'S ON COPY

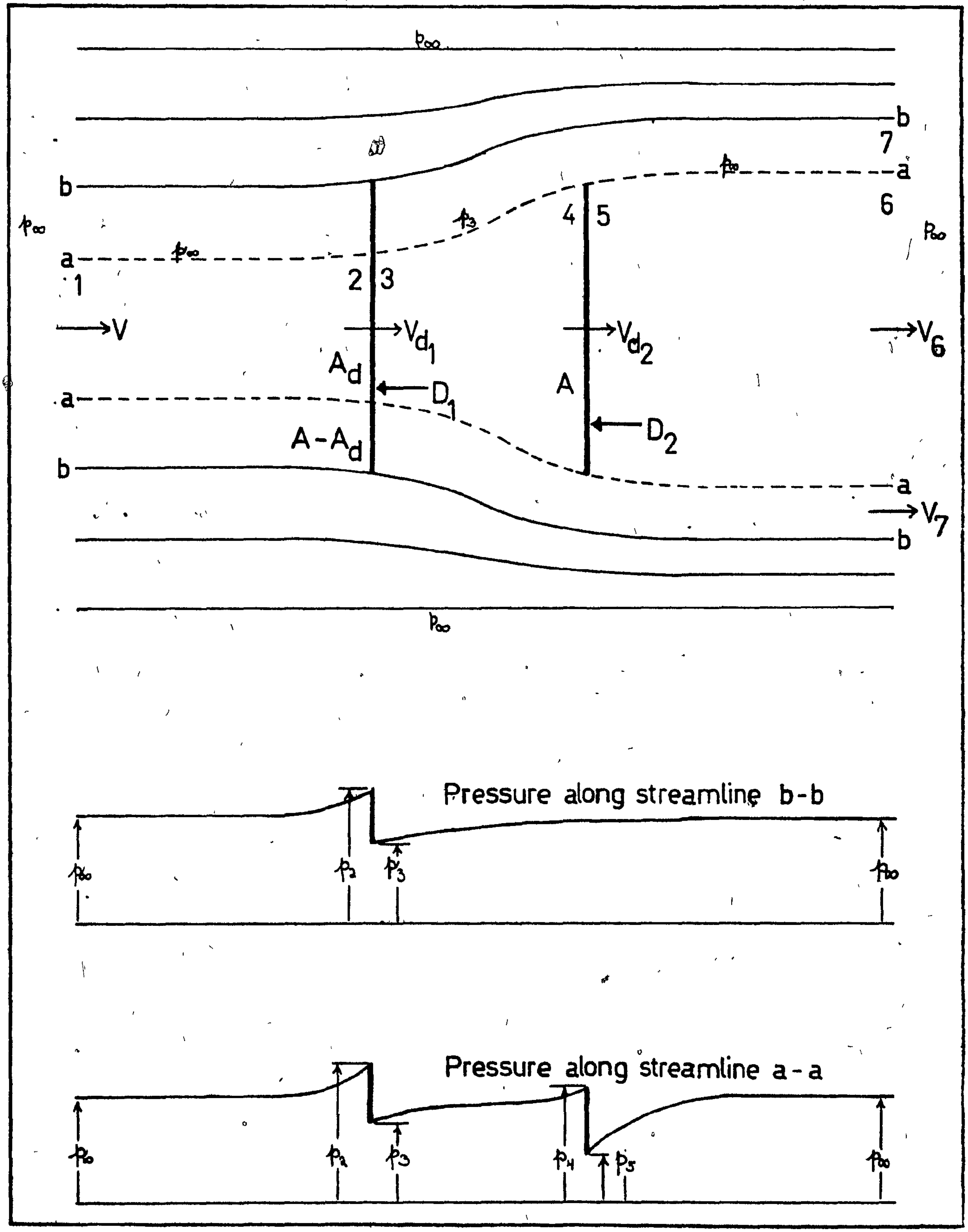

ILLUSTRATION 2 - Streamline Pattern and Pressure Profile (Wake Interference)

The Bernoulli's equation is applied:

$$1 \rightarrow 2 : \quad p_\infty + \tfrac{1}{2}\rho V^2 = p_2 + \tfrac{1}{2}\rho V_{D_1}^2 \qquad 2.4\text{-}1$$

$$3 \rightarrow 7 : \quad p_3 + \tfrac{1}{2}\rho V_{D_1}^2 = p_\infty + \tfrac{1}{2}\rho V_7^2 \qquad 2.4\text{-}2$$

$$3 \rightarrow 4 : \quad p_3 + \tfrac{1}{2}\rho V_{D_1}^2 = p_4 + \tfrac{1}{2}\rho V_{D_2}^2 \qquad 2.4\text{-}3$$

$$5 \rightarrow 6 : \quad p_5 + \tfrac{1}{2}\rho V_{D_2}^2 = p_\infty + \tfrac{1}{2}\rho V_6^2 \qquad 2.4\text{-}4$$

The momentum equation is used for a large control volume with the sides composed of streamlines far away:

$$\rho A V_{D_2} (V - V_6) + \rho(A - A_D) V_{D_1} (V - V_7) - (D_1 + D_2) = 0 \qquad 2.4\text{-}5$$

The momentum equation is also used for a smaller control volume with sides composed of the streamlines a - a. It is assumed that the drag of the area A_D of the first disc is simply: $\frac{A_D}{A} D_1$. A justification of the use of p_3 and p_∞ in the following momentum equation is given in the next paragraph.

$$1 \rightarrow 3 : \rho A V_{D_2} (V - V_{D_1}) + (p_\infty - p_3) A_D - \frac{A_D}{A} D_1 = 0 \qquad 2.4\text{-}6$$

$$3 \rightarrow 6 : \rho A V_{D_2} (V_{D_1} - V_6) + (p_\infty - p_3) A - D_2 = 0 \qquad 2.4\text{-}7$$

Finally, the drag of the two discs is:

$$D_1 = (p_2 - p_3)A \qquad 2.4\text{-}8$$

$$D_2 = (p_4 - p_5)A \qquad 2.4\text{-}9$$

When applying the momentum equation to the innermost control volume, the pressures must be carefully estimated. By assuming p_∞ from 1 to 2, a positive thrust is neglected, the pressure being actually larger than p_∞. By assuming p_3 from 3 to 4, a positive thrust is neglected, the pressure being actually larger than p_3. By assuming p_∞ from 5 to 6, a negative thrust is neglected, the pressure being actually less than p_∞. As can be seen from the sketch of the pressure profile, $(p_2 - p_\infty)$ is likely to be less than $(p_\infty - p_5)$. Thus, the positive thrust 1 to 2 is smaller than the negative thrust 5 to 6. Also, in the mid-section, the positive thrust 3 to 4 is small because it is applicable to a small area $(A-A_D)$. Hopefully, the negative thrust 3 to 4 compensates the two smaller positive thrusts and the momentum equations are justified.

In the previous 9 equations, there are 11 unknowns: A_D, V_{D_1}, V_{D_2}, V_6, V_7, p_2, p_3, p_4, p_5, D_1, D_2. Thus, it is possible to solve in terms of 2 of the unknowns: D_1 and D_2.

Combining 2.4-1, 2.4-2 and 2.4-8, we obtain:

$$\frac{V_7}{V} = \sqrt{1 - C_{D_1}} \qquad 2.4\text{-}10$$

HARK'S ON COPY

Using this result with 2.4-2, 2.4-3, 2.4-4 and 2.4-9, we have:

$$\frac{V_6}{V} = \sqrt{1 - C_{D_1} - C_{D_2}} \qquad 2.4\text{-}11$$

Those two results together with 2.4-2 and 2.4-7 yield:

$$V_{D_2} = \frac{V_{D_1} + V_6}{2} \qquad 2.4\text{-}12$$

This means that the second disc velocity is the average between the first disc velocity and the inner wake velocity. Making use of equation 2.4-6, the area ratio is found to be:

$$\frac{A_D}{A} = \frac{V_{D_1} + V_6}{V_{D_1} + V} \qquad 2.4\text{-}13$$

Combining all the equations into 2.4-5, we finally obtain the first disc velocity ratio (plotted in Figure 7):

$$\frac{V_{D_1}}{V} = \sqrt{3 - 2\sqrt{1 - C_{D_1}} - C_{D_1}} + \sqrt{1 - C_{D_1}} - 1 \qquad 2.4\text{-}14$$

Notice that the first disc velocity ratio is a function of the drag of the first disc only, and does not depend on the drag of the second disc. The maximum C_{D_1} is 1.0 at $V_{D_1}/V = \sqrt{2} - 1$, that is .4142.

Using 2.4-11 and 2.4-12, we get the second disc velocity (plotted in Figure 7 for three different values of $\frac{V_{D_1}}{V}$):

$$\frac{V_{D_2}}{V} = \frac{1}{2}\frac{V_{D_1}}{V} + \frac{1}{2}\sqrt{1 - C_{D_1} - C_{D_2}} \qquad 2.4\text{-}15$$

The maximum theoretical value of C_D (i.e. $C_{D_1} + C_{D_2}$) is 1.0. These relations can be inverted to give the drag coefficients as functions of the disc velocity ratios:

$$C_{D_1} = \frac{(1 - \beta_1^2)(\beta_1^2 + 4\beta_1 - 1)}{4\beta_1^2}$$

$$C_{D_2} = 1 - C_{D_1} - (2\beta_2 - \beta_1)^2$$

Where: $\beta_1 = \frac{V_{D_1}}{V}$ and $\beta_2 = \frac{V_{D_2}}{V}$

The ideal power coefficient is obtained by letting all the drag do useful work:

$$C_{P_{id}} = \frac{D_1 V_{D_1}}{\frac{1}{2}\rho A V^3} + \frac{D_2 V_{D_2}}{\frac{1}{2}\rho A V^3}$$

$$C_{P_{id}} = C_{D_1} \frac{V_{D_1}}{V} + C_{D_2} \frac{V_{D_2}}{V}$$

The maximum ideal power coefficient is calculated by trial and error:

$$C_{P_{max}} = .60662 \qquad \text{at} \quad \frac{V_{D_1}}{V} = .873$$

$$\text{and} \quad \frac{V_{D_2}}{V} = .580$$

For computer applications, it is sometimes desirable to use the drag coefficient C_{DD_1} based on the disc velocity rather than the ambient windspeed:

$$C_{DD_1} = \frac{D_1}{\frac{1}{2}\rho A V_{D_1}^2} = \frac{C_{D_1}}{(\frac{V_D}{V})^2}$$

That coefficient has the advantage that, whenever the blade characteristics are available at only a single value of the Reynolds number, it is not necessary to iterate to find the proper drag and disc velocity of the wind turbine. It is given by:

$$C_{DD_1} = \frac{(1 - \beta_1^2)(\beta_1^2 + 4\beta_1 - 1)}{4\beta_1^4}$$

Where: $\beta_1 = \frac{V_{D_1}}{V}$

It is usually necessary to invert this relation to obtain the disc velocity ratio as an explicit function of C_{DD_1}. Owing to the difficulty of inverting the relation, a least-squares curve-fitting of several functions was made and the best one chosen. The accuracy of the fit was better than $\pm$ .4% at any point.

$$\frac{V_{D_1}}{V} = \frac{1}{4.6926} \ln \left(\frac{43.142}{C_{DD_1} + 0.39019}\right)$$

Table 1 summarizes the three theories previously described.

Theory:	<u>Betz-Glauert Actuator Disc</u>	<u>Theory for High Solidity</u>	<u>Double Disc Theory for Wake Interference</u>
Sketch:			
Disc Velocity Ratio:	$\frac{V_D}{V} = \frac{1}{2} + \frac{1}{2}\sqrt{1-C_D}$	$\frac{V_D}{V} = (1 - \frac{C_D}{1.115})^{0.254}$	$\frac{V_{D_1}}{V} = \sqrt{3-2\sqrt{1-C_{D_1}} - C_{D_1}} + \sqrt{1-C_{D_1}} - 1$ $\frac{V_{D_2}}{V} = \frac{1}{2}\frac{V_{D_1}}{V} + \sqrt{1-C_{D_1} - C_{D_2}}$
Lowest Disc Velocity Ratio $\frac{V_D}{V}$	0.5	0.0	$\sqrt{2} - 1 = .4142$
Maximum C_D	1	1.115	1
Maximum C_{DD}	4	∞	5.828
Maximum $C_{P_{id}}$	16/27 = .593	16/27 = .593	.607
Iterative Technique Required for Single Re blade characteristics	No	No	Yes

TABLE 1 : Summary of the Wind Turbine Theory and its Extensions

2.5 Blade Element Analysis

The purpose of the blade element analysis is to calculate the torque and power output of a wind turbine at a given rotational speed in a given ambient windspeed. Note that there are two unknown quantities which are dependent on each other: the disc velocity and the drag of the turbine. The method for solving this problem usually consists of the following three steps. First, a disc velocity is assumed and the drag of the turbine is found by integrating the contribution of each blade element as the blade revolves using the known blade characteristics. Secondly, by using a theory similar to the theories previously explained, the disc velocity ratio associated with that drag is calculated, and is compared with the disc velocity assumed in the first step. The correct disc velocity can then either be directly found, if the blade characteristics are available at only a single Reynolds number, or by iteration between the first and the second step. Thirdly, once the disc velocity is established, the torque output of the turbine can be found by integrating the contribution of each blade element as the blade revolves, using again the blade characteristics. The power output is finally found by multiplying the torque output by the rotational speed.

The integration of the torque or drag contributions of a blade element requires the determination of the local velocity V_α and local angle of attack α of the relative wind on a blade element, at any given angular position θ and angular speed wr. The velocity diagram is shown in Illustration 3 for the case of a blade tilted at an angle δ with respect to the vertical axis of a wind turbine. Notice that V_α is in the plane of the aerofoil cross-section.

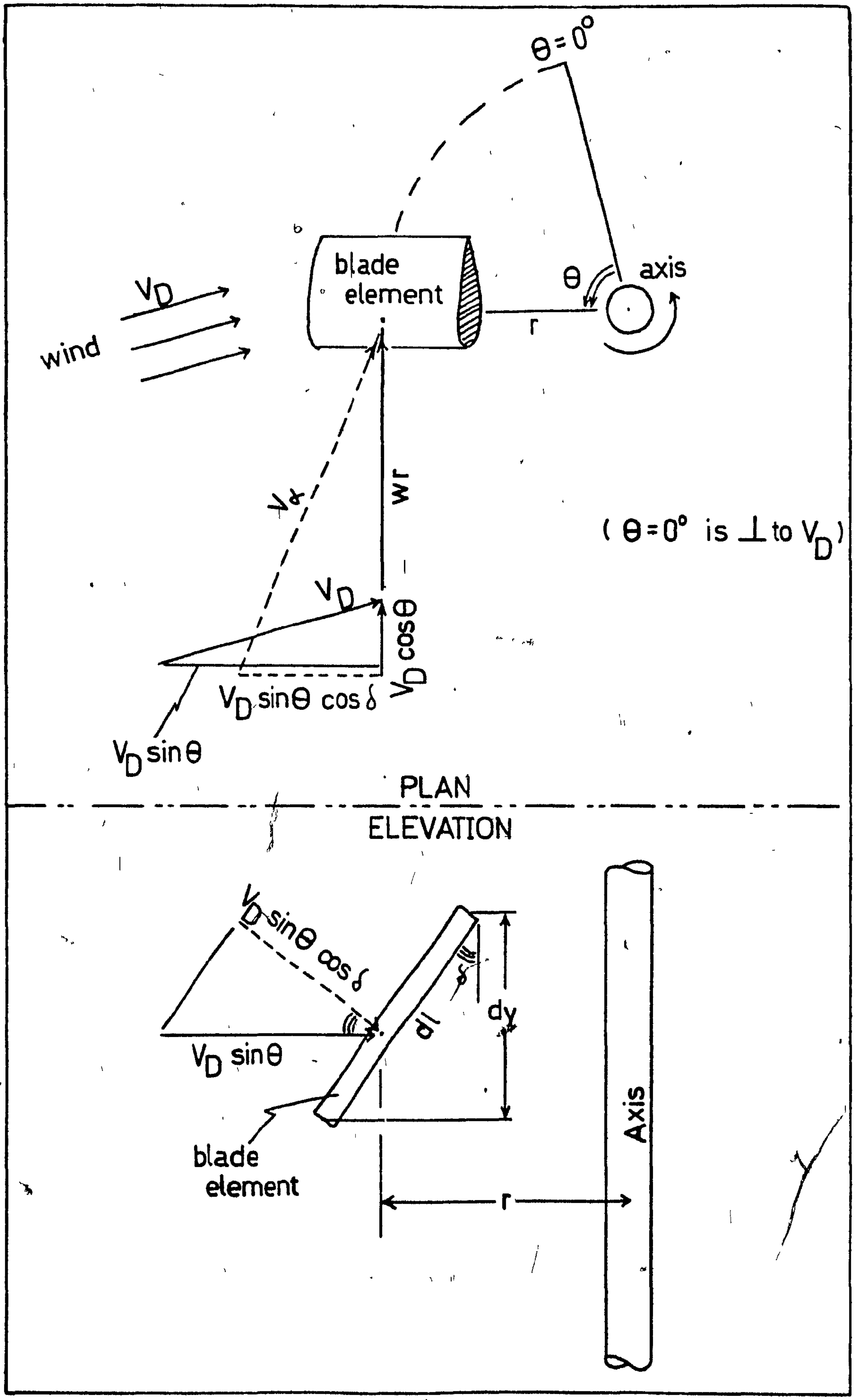

ILLUSTRATION 3: Velocity Diagram of a Blade Element

From this velocity diagram, it is seen that:

$$V_\alpha^2 = (V_D \sin\theta \cos\delta)^2 + (V_D \cos\theta + wr)^2 \qquad 2.5\text{-}1$$

$$\alpha = \tan^{-1} \frac{V_D \sin\theta \cos\delta}{wr + V_D \cos\theta} \qquad 2.5\text{-}2$$

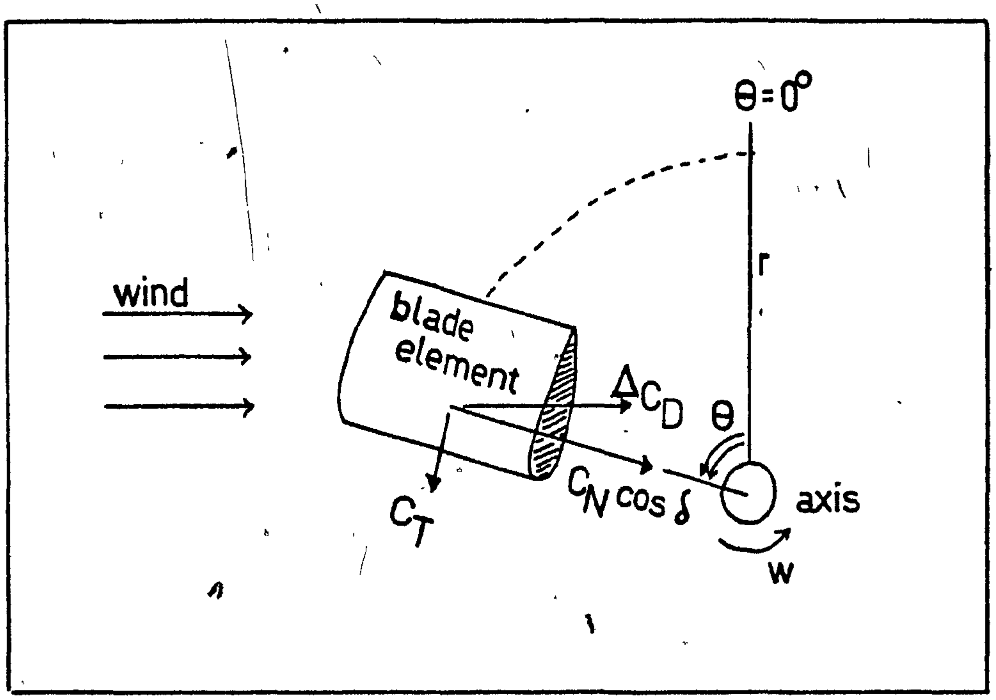

ILLUSTRATION 4: Force Diagram of a Blade Element

The contribution ΔC_D of a blade element to the total drag coefficient C_D of the turbine is found from the thrust and normal force characteristics of the aerofoil. According to the force diagram of Illustration 4, it is:

$$\Delta C_D = C_N \cos\delta \sin\theta - C_T \cos\theta$$

The drag coefficient C_D of the turbine must not be confused with the drag coefficient C_d of the aerofoil. If the characteristics of the aerofoil are expressed as lift and drag, they can be converted to thrust and normal force according to equations 3.2-1 and 3.2-2. The contributions to the turbine drag are averaged through a revolution and are integrated along the length of the blades. Since the wind turbine is symmetrical about the equatorial plane and its drag is the same from the upstream and downstream surfaces swept by the blades (except if wake interference is allowed), the integration of the elements of drag can usually be limited to a quarter of the surface generated by the rotating blades:

$$C_D = \frac{2}{\pi} N \int_0^{L/2} \int_0^{\pi} (C_N \sin\theta \cos\delta - C_T \cos\theta) d\theta \, \frac{\frac{1}{2}\rho V_\alpha^2 c \, dl}{\frac{1}{2}\rho V^2 A}$$

Since $dl = dy/\cos\delta$, we can rewrite this in a more appropriate dimensionless form:

$$C_D = \frac{2}{\pi} N \frac{HR}{2A} \int_{0}^{1}\int_{0}^{\pi} \left(\frac{V_\alpha}{V}\right)^2 \frac{c}{R} \left(C_N \sin\theta - C_T \frac{\cos\theta}{\cos\delta}\right) d\theta \, d\left(\frac{y}{H/2}\right)$$

Where local incidence and velocity are rewritten non-dimensionally from 2.5-1 and 2.5-2:

$$\left(\frac{V_\alpha}{V}\right)^2 = \left(\frac{V_D}{V} \sin\theta \cos\delta\right)^2 + \left(\frac{V_D}{V} \cos\theta + \frac{wR}{V} \frac{r}{R}\right)^2$$

$$\alpha = \tan^{-1} \frac{\frac{V_D}{V} \sin\theta \cos\delta}{\frac{wR}{V} \frac{r}{R} + \frac{V_D}{V} \cos\theta}$$

The thrust and normal coefficients are those at the local incidence α and at the following Reynolds number:

$$Re_{bl} = Re_{wd} \frac{V_\alpha}{V} \frac{c}{2R}$$

where: Re_{wd} = wind turbine Reynolds number based on the diameter

Re_{bl} = local Reynolds number of a blade element based on its chord.

The torque output of the turbine is obtained by averaging the contributions to torque of a blade element as it revolves and integrating them over the length of the blade. The torque contribution of a blade element is simply the thrust multiplied by the local radius arm and the torque coefficient is then:

$$C_Q = \frac{2}{\pi} N \int_0^{L/2} \int_0^{\pi} r \, C_T \, d\theta \, \frac{\frac{1}{2}\rho V_\alpha^2 c\, dl}{\frac{1}{2}\rho V^2 A (2R)}$$

Rewriting in a dimensionless form:

$$C_Q = \frac{1}{\pi} N \frac{HR}{2A} \int_0^1 \int_0^{\pi} \left(\frac{V_\alpha}{V}\right)^2 \frac{c}{R} \frac{r}{R} \frac{C_T}{\cos\delta} \, d\theta \, d\left(\frac{y}{H/2}\right)$$

And the power coefficient is:

$$C_P = 2 \, C_Q \frac{wR}{V}$$

The efficiency of the turbine is defined as the ratio of the actual power to the maximum theoretical power from an ideal actuator-disc turbine of area A. According to the Betz-Glauert theory, this is:

$$\eta = \frac{P}{16/27 \; 1/2 \rho A V^3} = \frac{C_P}{16/27}$$

2.6 Computer Program

The computer program listed in Appendix A is a modification to the more general program and was used to predict the performances of a "two-dimensional" vertical-axis wind turbine (that is, infinite in height and having sail aerofoils parallel to the axis) using the theory allowing for high solidity. A description of the program and the notation are also included in Appendix A.

The main objective of the program is to calculate the torque and power output of a vertical-axis wind turbine at chosen values of the rotational speed and ambient windspeed. The data used to run the program are the thrust and normal coefficients of the sail aerofoil at various angles of attack and Reynolds numbers. However, it is still possible to run the program using blade characteristics at a single Reynolds number.

The main program can be divided in three steps, applicable to each tip speed ratio at which performances are calculated.

1. Assume a disc velocity and numerically integrate the drag of the turbine (that is, the force that tends to capsize the turbine).

2. By using the theory allowing for high solidity, calculate the disc velocity corresponding to the drag of the turbine.

   Compare the calculated disc velocity with the assumed value. If they do not match closely enough, a new suitable assumption for the disc velocity is made. Steps 1 to 3 are repeated until there is agreement between the assumed and the calculated disc velocity.

3. Once the disc velocity is established, the torque output can be numerically integrated, and the power output calculated from the torque.

A sample of data cards required to run the program is shown in Appendix B, together with a printout and some explanatory notes. The experimental data shown are those of a slightly loose nylon sail aerofoil having a leading edge of 0.25 inch. The output results were used to draw the third curve shown in Figure 72, (solidity of 0.15). Notice the program did not terminate on its own but was manually interrupted after the calculations for a tip speed ratio of 4.6 were printed: further printing was found to be useless since a negative torque was already attained at that tip speed ratio.

3. EXPERIMENTS

3.1 Apparatus

The McGill 3 ft. X 2 ft. closed-working-section, open-return, low-speed wind tunnel (Wygnanski and Newman 1961) was used for testing the sail aerofoil. The maximum speed is about 170 ft./sec. and the turbulence level is about .4%. A two-component balance was available for measuring lift and drag. It featured a double flexure table whose displacement was detected with two variable reluctance transducers.

The breadth of the tunnel being 3 ft., a maximum sail aerofoil chord of 4 in. could be used in order to maintain wake blockage corrections on the aerodynamic forces below 5% for the most useful range of angles of attack (<30°). With such a chord, the Reynolds number can attain about 35 X 10^4. A little analysis on the trailing edge of the sail aerofoil showed that the bending would be excessive if the span would equal the tunnel height. Therefore, it was decided to divide the tunnel into two one-foot halves by using a plate. A sail aerofoil was mounted on the balance in the bottom half. To ensure uniformity in speed, another sail aerofoil was mounted at the same angle of attack in the top half, and it was used at the same time for measurement of the tension forces acting on the trailing edge. Such information is needed to design a wind turbine using sails with a tensioning wire at the trailing edge.

Drawings of the apparatus are shown in Figures 9, 10 and 11. Besides the dividing plate, other plates were added on the floor and on the roof of the tunnel. These would permit flush mounting of the sail aerofoil endplates, thereby reducing the tare drag. The two struts required to rigidly connect the endplates of the bottom sail aerofoil were shielded to further reduce the tare drag. Dummy shields were also mounted behind the top sail aerofoil to ensure similarity of the two halves of the tunnel, and hence preserve the flow calibration. Each end of the trailing edges terminated in a pin which was freely pivoted in a slide that allowed adjustment of the chord length. An exception was the top pin of the upper sail aerofoil which was somewhat longer, protruded through the tunnel roof, and was centered in a larger hole by adjusting extension springs hooked to the pin (Figure 10). This provided a null method of measurement of the forces on the trailing edge in two horizontal directions: perpendicular and parallel to the chord of the sail aerofoil. The static pressure was measured inside the sail aerofoil, just behind the leading edge.

HARK'S ON COPY

3.2 Data Reduction

Wind Tunnel Interference

Since the experiments were performed in a closed working section, corrections must be applied so that the results are similar to those found in free air. There are four main corrections: solid blockage, wake blockage, lift effect and pressure gradient.

The proportional increase in velocity at the aerofoil, due to solid blockage, is given by Batchelor (1944) using ideal flow theory:

$$\varepsilon_s = \frac{\pi^2}{12}\,\frac{1}{h^2}\,(1 + 3\sec^2\frac{\pi a}{h})\,(r^2 - \frac{\chi^2 - 1}{3}\,b^2\cos 2\alpha)$$

Where a is the offset of the aerofoil from the tunnel centre-line (in these tests, a = 0), χ and b are parameters used in the Joukowski transformation of the theoretical derivation. This can be rewritten (without restriction on the value of α):

$$\varepsilon_s = \frac{\pi^2}{12}\,\lambda\,(\frac{t}{h})^2$$

Where: $\lambda = \lambda_0 + k_1 \sin^2\alpha$

$$\lambda_0 = 4\left(\frac{r^2}{t^2} - \frac{\chi^2 - 1}{3} - \frac{b^2}{t^2}\right)$$

$$k_1 = \frac{8}{3}\,(\chi^2 - 1)\,\frac{b^2}{t^2}$$

A practical value of λ can be extracted from Pankhurst and Holder (1952) with the restriction that α is small:

$$\lambda = 0.5 + 0.42\,\frac{c}{t} + 0.47\,\left(\frac{c}{t}\right)^2\,\alpha^2$$

Then, with no restriction on α, the solid blockage is assumed to be:

$$\varepsilon_s = \frac{\pi^2}{12}\left(\frac{t}{h}\right)^2\left(0.5 + 0.42\,\frac{c}{t} + 0.47\,\left(\frac{c}{t}\right)^2\sin^2\alpha\right)$$

Notice the solid blockage is estimated by using ideal flow theory, and is certainly not accurate for large angles of attack, where the flow is separated. But the corrections are quite small, less than 1%.

The wake blockage also causes an increase in velocity, as given by Pankhurst and Holder (1952):

$$\varepsilon_w = \frac{1}{4}\,\frac{c}{h}\,C_{d_T}$$

where the subscript T refers to the coefficient as measured in the tunnel.

The lift and drag were corrected for the so-called lift effect. The very small corrections on the angle of attack were neglected, since they did not justify the additional complexity. Pankhurst and Holder (1952) give the following lift effect corrections:

$$C_{L_F} - C_{L_T} = \frac{-\pi^2}{48} \left(\frac{c}{h}\right) C_{L_T}$$

$$C_{d_F} - C_{d_T} = \frac{\pi}{96} \left(\frac{c}{h}\right)^2 C_{L_T} \left(C_{L_T} + 4C_{m_{\frac{1}{4}T}}\right)$$

Where the subscript F refers to the value of the coefficients in free air. Since the moment coefficient was unknown, it was left out of the corrections.

The pressure gradient due to the wake of the aerofoil, added to the pressure gradient of -.0007 per inch due to boundary layer growth in the tunnel, incur a correction on the drag (buoyancy) as given by Pankhurst and Holder (1952).

$$C_{d_F} - C_{d_T} = \frac{\pi}{2} \lambda \frac{t^2}{c} \frac{dC_p}{dx}$$

Where $\frac{dC_p}{dx} = \frac{-\pi}{6} \frac{c}{h^2} C_{d_T} - .0007$ (per inch)

The corrections are summarized in Table 2, where C_{force} is any force coefficient other than lift and drag coefficient, and were applied to all the data presented in this thesis.

	Solid Blockage	Wake Blockage	Lift Effect	Pressure Gradient	Total Correction for $0^\circ < \alpha < 20^\circ$	Total Correction for $0^\circ < \alpha < 180^\circ$
$\frac{C_{d_F}}{C_{d_T}} = 1.0$	$-2\varepsilon_s$ $< 1\%$	$-2\varepsilon_w$ $< 12\%$	$+\frac{\pi}{96}\left(\frac{c}{h}\right)^2 \frac{C_{L_T}^{\,2}}{C_{D_T}}$ $< .1\%$	$-\frac{\pi}{2}\lambda\frac{t^2}{c}\left(\frac{-dC_p}{dx}\right)\frac{1}{C_{d_T}}$ $< .5\%$	$< 3\%$	$< 14\%$
$\frac{C_{L_F}}{C_{L_T}} = 1.0$	$-2\varepsilon_s$ $< 1\%$	$-2\varepsilon_w$ $< 12\%$	$-\frac{\pi^2}{48}\left(\frac{c}{h}\right)^2$ $< .3\%$		$< 3\%$	$< 13\%$
$\frac{Re_F}{Re_T} = 1.0$	$+\varepsilon_s$ $< .5\%$	$+\varepsilon_w$ $< 6\%$			$< 1.5\%$	$< 7\%$
$\frac{C_{Force_F}}{C_{Force_T}} = 1.0$	$-2\varepsilon_s$	$-2\varepsilon_w$			$< 3\%$	$< 13\%$

TABLE 2: Corrections for Wind Tunnel Interference

Calibration Curves

A pitot-static traverse was made at the sail-aerofoil location at different tunnel speeds. The velocity in the apparatus (without the sail aerofoil) was calibrated versus a reference gauge pressure ($p_\infty - p_r$) at the upstream static holes in the tunnel wall. The contraction produced by the three plates of the apparatus caused an increase of 9 to 11% in velocity as compared with the empty tunnel. This is consistent with the 11% geometric area reduction.

The coefficient of drag of the end plates was found to be from .005 to .006, decreasing slightly with the Reynolds number. These figures are consistent for turbulent flow past a smooth flat plate. A smooth cylinder 2 inches in diameter was tested to check the accuracy of the apparatus Its drag coefficient was found to be about 1.2 at a Reynolds number between 3×10^4 and 10×10^4 and corresponds to accepted values (Schlichting 1968) for infinitely long cylinders.

Since the calculations were performed on a computer, equations were fitted to the calibration curves of the drag of the endplates and the velocity in the upper and lower test sections. Notice that the calibration actually varies with the Reynolds number although, for convenience, the variation is expressed as a function of the reference pressure, assuming a standard room temperature of $68^{\circ}F$ and standard pressure.

$$\frac{\frac{1}{2}\rho V_{TS}^2}{p_\infty - p_r} = 1.076\ (p_\infty - p_r)^{.02189} \quad \text{upper section}$$

$$\frac{\frac{1}{2}\rho V_{TS}^2}{p_\infty - p_r} = 1.151 - \frac{.1836}{(p_\infty - p_r) + 2.067} \quad \text{lower section}$$

$$C_{d_{endplates}} = \left(5.102 + \frac{.358}{(p_\infty - p_r) \times 1.08}\right) \times 10^{-3}$$

Where: $1\text{ mb} < (p_\infty - p_r) < 11\text{ mb}$

The upper and lower velocities would normally be equal but differed slightly. The helical tension springs required for measuring the force on the trailing edge of the sail-aerofoil, showed a definite threshold load to initiate extension, followed by a constant spring rate. Different springs were used, the stiffer being used for measuring large forces. Each spring was characterized by two constants K and K_o, the equation being:

$$F = K_o + K\ (X - X_o)$$

Where: F = Load

K_o = Threshold load to initiate extension.

K = Spring rate.

X_o = Initial length.

X = Measured length.

Since the trailing edge may sometimes produce a force F_y, perpendicular to the sail-aerofoil, which is less than the threshold load of the softest spring, it was necessary to have another spring pulling sufficiently in the opposite direction to take up the threshold load.

However, the trailing edge force F_x, parallel to the sail-aerofoil, was always larger than the spring threshold load, thus requiring only one spring.

The calibration of the balance was linear.

Evaluation of the Coefficients

The coefficients of lift and drag were evaluated in the usual manner, after subtraction of the tare drag of the endplates in the latter case. The thrust and normal coefficients could then be calculated according to:

$$C_T = C_L \sin\alpha - C_d \cos\alpha \qquad 3.2\text{-}1$$

$$C_N = C_L \cos\alpha + C_d \sin\alpha \qquad 3.2\text{-}2$$

Since the springs for measuring the force on the trailing edge were connected to the hinge pin some distance above the end of the trailing edge, the coefficient of the force on the trailing edge was obtained by multiplying the measured coefficient by the leverage ratio, assuming that the force on the whole trailing edge acts at the mid-point.

In order to compare one set of results with another, it is usually desirable to perform the experiments at some chosen values of the Reynolds number. In practice, this cannot be done easily, mainly because the tunnel interference corrections vary with the angle of attack. However, by suitable interpolation, all the coefficients could be brought back to some fixed values of the Reynolds number.

The pressure coefficient inside the sail aerofoil is defined as:

$$C_{p_{in}} = \frac{p_{in} - p_{TS}}{\frac{1}{2}\rho V_{TS}^2}$$

and was rewritten more conveniently:

HARK'S ON COPY

$$C_{p_{in}} = \frac{(p_r - p_{TS}) - (p_r - p_{in})}{\frac{1}{2}\rho\, V_{TS}^2}$$

Where: p_{in} is the static pressure inside the sailwing.

p_{TS} is the static pressure in the free stream of the test section.

p_r is the reference pressure at the static hole of the tunnel.

V_{TS} is the velocity in the test section.

The value $(p_r - p_{in})$ was measured during the tests, whilst the static pressure drop $(p_r - p_{TS})$ was determined from the previous calibration of the test section.

3.3 Experimental Procedure

At each angle of attack, three to five wind tunnel speeds were used, in a decreasing order. Once the speed had settled down, the springs for measuring the trailing edge force were adjusted until the top pin of the trailing edge was centred in its hole. The voltages from the lift and drag balance were then recorded, as well as the manometer readings for the tunnel speed and for the pressure inside the sail aerofoil. The spring displacements were measured with a vernier-caliper. The shape taken by the sail was observed through the plexiglass window at the top.

HARK'S ON COPY

The electrical balance consists of a plate, held by flat springs, to which is attached variable reluctance displacement transducers in two perpendicular directions. Thus, with no force exerted on the balance, the voltage readings are not necessarily zero. After completing a test at three to five different windspeeds at a given angle of attack, the tunnel was stopped and the zero-lift and zero-drag voltages were recorded. Since the balance had a tendency to stick slightly in the absence of vibrations, as when the tunnel was off, a small electric motor was run continuously on top of the tunnel in order to cause small vibrations. The wind-off readings could then be taken with a sufficient degree of confidence.

The camber was varied by changing the chord length, thereby changing also the slackness of the fabric. For each leading edge diameter, the largest chord length tested was c_o, attained when the fabric was just taut, with the wind off. Different leading edge diameters were tested. Since the fabric width was constant a smaller value of c_o was chosen for a larger leading edge in order to produce a comparable tautness of the sail.

3.4 Tests Performed

The Reynolds number chosen for the tests on sail aerofoils ranged from 9×10^4 to 30×10^4. The highest values were chosen to match approximately the highest local velocity expected to be found in a 12 ft. diameter vertical-axis wind turbine with 3 sail aerofoils having a chord of 25% the radius of the turbine, in a 12 mph wind. Here, the optimum tip speed ratio was assumed to be 1.0, as obtained in previous tests on a model (Robert, 1975).

$$\text{maximum } Re_{blade} = \left(\frac{wR}{V} + 1\right) \frac{Re_{wd}}{2} \frac{c}{R} = 34 \times 10^4$$

Where: $$Re_{wd} = \frac{VD}{\nu} = 135 \times 10^4$$

Most of the tests were performed using a sail made of un-calendered nylon of 1.2 oz./sq. yd., but in one test, cal-endered dacron of 1.6 oz./sq. yd. was used. The dacron was stiffer and non-porous. The nylon was very slightly porous. Measurements of the porosity were made on circular pieces of nylon 1.5 inch in diameter, using a displacement flow-meter. The mean velocity through the fabric was proportional to the pressure drop across it, the constant varying from

.032 to .048 ft/s/mb, depending on the specimen. The pressure drop was varied from 0 to 11 mb, corresponding somewhat to the range expected in the present tests on sail aerofoils, assuming a maximum pressure drop coefficient across the fabric of 1.0:

$$C_{\Delta p} = \frac{\Delta p}{\frac{1}{2}\rho V_{TS}^2} = \leq 1.0$$

Since the dacron cloth was much stiffer, and had less tendency to camber, the value of c_o was deliberately chosen smaller than for the nylon in order to attain a comparable camber, the two fabrics being cut to identical sizes.

The tests are summarized in Table 3.

HARK'S ON COPY

Fabric	Leading Edge Diameter: Inch	Leading Edge Diameter: % c	Chord: Inch	Chord: % c	Lift	Drag	Thrust	Normal	X-tension	Y-tension	L/D	Pressure	Range of Angle
					FIGURE NUMBER								
Taut Nylon	0.250	6.4%	3.910	100%	12	19	28	35	42	47	52	-	180^{o}
Slightly Loose Nylon	0.250	6.4%	3.850	98.5%	13	20	29	36	-	-	53	-	180^{o}
Loose Nylon	0.250	6.4%	3.790	96.9%	14	21	30	37	43	48	54	-	180^{o}
Taut Dacron	0.375	9.7%	3.845	99.2%	15	22	31	38	44	49	55	59	20^{o}
Taut Nylon	0.375	9.7%	3.875	100%	16	23	32	39	45	50	56	60	180^{o}
Loose Nylon	0.375	9.7%	3.755	96.9%	17	24	33	40	-	-	57	61	180^{o}
Taut Nylon	0.500	13%	3.840	100%	18	25	34	41	46	51	58	62	180^{o}

TABLE 3: Summary of Tests on Sail Aerofoils

4. DISCUSSION

4.1 Experimental Observations

Surprisingly no flapping of the sail aerofoil was observed during the tests even when the fabric was loose. This is an indication that the flapping observed on three-dimensional sailwings (Robert 1975) is due only to the freedom of the trailing edge to move sideways, and not to the flexibility of the sail. There was no zero-lift condition when the sail aerofoil was facing the wind: at 0° angle of attack, depending on the initial state, the sail aerofoil would either assume a positive or a negative camber, thus producing a positive or a negative lift. By external action, the sail could be made to flip from one side to the other and be stable in each position.

The lower sail aerofoil, mounted on the balance plate, strongly vibrated at angles of attack between 40° and 140°, thereby limiting the maximum safe tunnel speed at these angles. This must be attributed to the largely separated flow. The unsteady forces were not damped by the balance or by the cantilevered arrangement on top of it. Some vibrations of the top trailing edge, especially the uppermost spring-held portion, were also observed, but were much less than the lower sail aerofoil. The tunnel speed itself was unstable at those angles of attack, oscillating about ±5% with a period of roughly 10 seconds.

The shape taken by the sail could be observed through the transparent indexing plate at the top. The camber increased with the windspeed at small angles of attack, in the case of a tight sail aerofoil. At larger angles or for a loose sail, the camber increased only slightly with the windspeed. In general, the camber increased from 0° to 90° and then decreased from 90° to 180°. This can be attributed to the normal force. The following model shown in Illustration 5 approximates very roughly a section of the sail aerofoil.

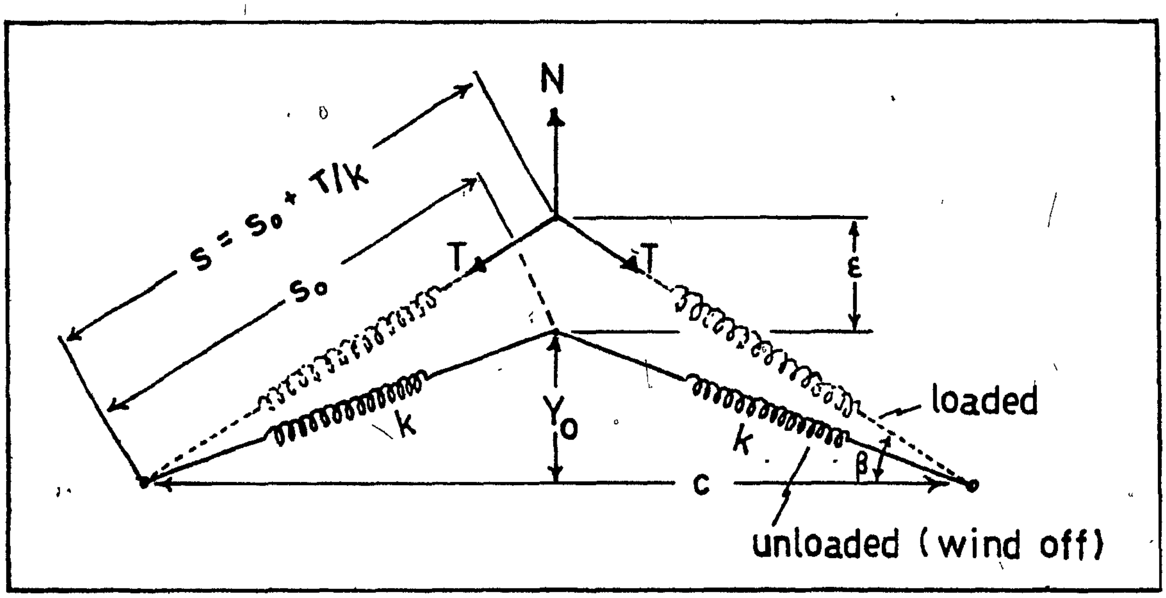

Illustration 5: Crude Model of a Sail Aerofoil Section

Where: N = normal force (concentrated at the middle of the sail)

T = tension in the fabric

β = angle of the two springs modelling the fabric

K = spring rate

Y = amount of camber

Y_o = initial camber (wind off)

ε = increase in camber $\varepsilon = (Y - Y_o)$

s = length of fabric

s_o = initial length of fabric (fabric just taut)

If the following assumptions are made:

$\varepsilon << Y$ (change in camber small compared to the camber)

$\frac{T}{K} << \varepsilon$ (extension of the fabric small compared to increase in camber)

$Y << C$ (camber ratio is small)

then one obtains the following result:

$$\varepsilon \approx \frac{\ell 1}{8K} C_N \frac{(\frac{1}{2}\rho V^2)}{(\frac{Y_o}{C})^2}$$

This very crude analysis shows that the change in camber is proportional to the square of the windspeed, and the effect is more pronounced in the case of a small initial camber ratio, that is a taut sail aerofoil. The change in camber is also proportional to the normal coefficient, which increases from 0° to 90° and decreases from 90° to 180°. This agrees somewhat with the observations.

The thickness measured at the point of maximum camber reduced as the windspeed increased. At a given windspeed, the thickness of taut sail aerofoils was nearly constant through the range of angles of attack. In the case of loose sail aerofoils, some ballooning was observed at small surface angles, that is 0° to 20° and 160° to 180°. This phenomenon clearly depends partly on the internal pressure within the aerofoil.

The distance from the point of maximum camber to the leading edge, given as a percentage of the chord, moved gradually from 40% to 50% as the angle of attack increased from 0° to 180°.

The stretchability of the uncalendered nylon was found to be about $160 \ \dfrac{\text{lb./in.}}{\text{in./in.}}$.

4.2 Experimental Results

Lift (Figures 12 to 18)

The lift curve slope is in general very high at small angles of attack. In Figure 12, it reaches 1.6 (2π) between 2.5° and 5°. This high value can be attributed to the change in camber: as the angle of attack increases from 0° to the stall, the sail aerofoil becomes more cambered, causing a large increase in lift.

Between 0° and 20°, the lift coefficient increases markedly with the Reynolds number in the case of a taut sail aerofoil, but is rather unaffected in the case of a loose sail aerofoil. This can be explained also by the camber. As shown in the previous Section 4.1, the camber of a taut sail aerofoil shows more increase with the windspeed than the camber of a loose sail aerofoil. To be precise, this increase in lift is not actually a Reynolds number effect, but strictly a wind pressure ($\frac{1}{2}\rho V^2$) effect. Notice that a Reynolds number of 18 X 10^4 corresponds to a dynamic pressure of about 4.5 mb. Since the dacron fabric did not stretch appreciably under tension, its camber was probably not affected much by the wind pressure and explains why its lift coefficient does not vary with the Reynolds number (Figure 15).

The lift coefficient increases with the slackness of the sail. With a 1/4" leading edge, the maximum lift coefficient before the stall is 1.35 for a taut sail, 1.70 and 1.80 for slightly loose and loose sail, respectively (Figures 12, 13 and 14). The stalling angle also increases with the slackness of the sail aerofoil.

The lift coefficient is not much affected by the leading edge diameter.

The stalling angle of the dacron sail aerofoil is larger than that of the nylon sail aerofoil and reaches a higher value of lift coefficient before the stall occurs (Figures 15 and 16).

As mentioned earlier, there is no zero-lift condition even at an angle of attack of 0°. Notice that if the curve of the lift coefficient would be drawn for negative angles of attack, it would start with a negative lift coefficient at 0°. Actually, it is possible to obtain either negative or positive lift for a certain range of small angles of attack, perhaps -1° to $+1^{\circ}$. It is also interesting to note that the maximum negative lift near 170° is usually as high as the positive value near 10° but does not appear so much affected by the Reynolds number.

<u>Drag</u> (Figures 19 to 25; a printout for small angles of attack 0° to 20° is given in Figures 26 and 27).

The drag at an angle of attack of 0° increases with the leading edge diameter: the drag coefficient of taut nylon sail aerofoils is 0.03, 0.05 and 0.06 for leading edge diameters of 0.25, 0.375 and 0.5 inch respectively (Figures 26 and 27). This can be attributed to a more adverse pressure gradient over the rear portion of the aerofoil as the diameter of the leading edge increases.

In general, the drag coefficient at angles of attack below the stall decreases slightly with the Reynolds number. For example, the drag coefficient of a taut nylon sail aerofoil with a leading edge of 0.25 in. is 0.09 for Re = 9×10^4 and is 0.05 for Re = 30×10^4, at an angle of attack of 5° (Figure 26).

The stalling angle is somewhat affected by the Reynolds number, as can be seen in Figure 13: it is 13° at low Reynolds number and 15° at high Reynolds number. The stall is characterized by an increase in drag and is caused by separation of the flow from the back of the aerofoil. At large Reynolds numbers, there is less tendency for the flow to separate since a greater proportion of the boundary layer is turbulent, and thus the stall occurs at a larger angle of attack.

The drag coefficient is greatly affected by the tautness of the sail aerofoil and by the leading edge diameter, especially at small angles of attack from 0^{o} until the stall. At larger angles of attack, say past 20^{o}, the drag coefficient is more or less similar for all cases of tautness and leading edge size. The drag at 0^{o} increases with the leading edge diameter and with the looseness of the sail aerofoil. From 0^{o} until the stall, no such general comment can be made and each case deserves special attention. For the sakeness of clarity, four cases are drawn: two leading edge diameters, each with a taut or a loose fabric, as shown in Illustration 6.

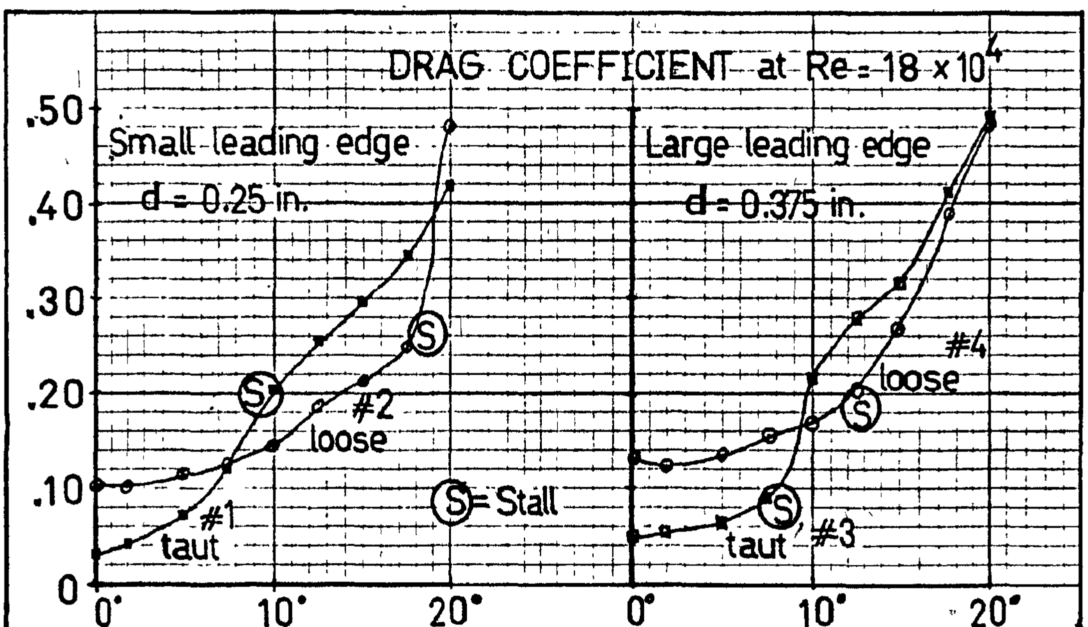

Illustration 6: Drag Coefficient of Four Shapes of Sail Aerofoil

In the first case, a taut sail aerofoil with a small leading edge, the stall is early and smooth, suggesting a premature turbulent separation around the small radius of the leading edge, followed by a re-attachment and a progressive turbulent separation on the back of the aerofoil.

The second case, a loose sail aerofoil with a small leading edge, shows a high initial drag followed by a low drag curve slope and finally a late and abrupt stall. It is very possible that, because of the large camber, some separation occurs on the concave surface of the aerofoil at low α, just behind the leading edge, explaining the high initial drag. At larger angles of attack, there is less and less tendency for this separation to occur as the stagnation point moves downward around the leading edge, and the drag remains nearly constant. The abrupt stall suggests that a laminar separation occurs later on top of the aerofoil.

The third case, a taut sail aerofoil with a large leading edge, shows an early and abrupt stall, characteristic of a laminar separation. This is reasonable in view of the leading edge diameter which is larger than in the first case.

The fourth case, a loose sail aerofoil with a large leading edge, is characterized by a large initial drag followed by a low drag curve slope and a smooth stall. The large initial drag and the small drag curve slope may be due to separation underneath the aerofoil, as explained in the second case. The smooth stall may indicate that the leading edge radius was large enough to cause a transition from a laminar to a turbulent boundary layer before separation occurred. It is not known why this did not seem to occur in the third case.

The drag coefficient of the dacron sail aerofoil (Figure 22) is much less than that of a comparable sail aerofoil made of nylon (Figure 23). At an angle of attack of 0°, it is about 40% less. Also, the stalling angle is larger, 18° compared with 10°.

<u>Thrust</u> (Figures 28 to 34)

The thrust coefficient is calculated from the lift and drag coefficients according to $C_T = C_L \sin\alpha - C_d \cos\alpha$. The value of the thrust coefficient is rather small in general and does not exceed 0.3. Since it is calculated by taking the difference between two relatively large coefficients, the percentage of error can become quite large and may explain why the graphs show some fluctuations.

At small angles of attack, the thrust coefficient of taut nylon sail aerofoils drastically decreases at low Reynolds numbers. This is consistent with the decrease in lift of the taut nylon sail aerofoil at low Reynolds numbers. In the case of the loose nylon or taut dacron aerofoils, there is not such a decrease.

The slackness of the sail increases the maximum thrust available and also increases the angle of attack at which this maximum occurs, 8° to 18°, when the leading edge is 0.25 in. The 0.375 in (9.7% of the chord) leading edge diameter seems to give better thrust for taut sail aerofoils than the two other diameters tested. (Figures 28, 32 and 34.)

The sail aerofoil made of dacron has a substantially better thrust than a comparable nylon sail aerofoil (Figures 31, and 32).

Normal Force (Figures 35 to 41)

The normal coefficient is calculated from the lift and drag coefficient according to $C_N = C_L \cos\alpha + C_d \sin\alpha$. At small angles of attack, say between 0° and 20°, the curves of the normal coefficient are very similar to the curves of lift coefficient, and the same comments apply.

At larger angles of attack, especially around 90°, the normal coefficient decreases with increasing leading edge diameter. This is most probably due to the reduced size of the wake for the larger leading edge radius to which the flow remained attached longer. With a small diameter leading edge, the normal coefficient reaches a value of 1.90-2.00 (Figures 35, 36, and 37), which is consistent with the accepted value of 2.0 for an infinitely long flat plate held perpendicular to the stream.

<u>X-tension</u> (Figures 42 to 46)

The coefficient of X-tension, defined as the force on the trailing edge in the plane of the sail aerofoil in a direction parallel to the chord line, shows very large random variations in the first set of experiments using taut nylon and a 0.25 in. leading edge (Figure 42), especially at angles of attack less than 40°. These fluctuations should be considered as results of experimental inexperience and have no meaning. With increasing familiarity, it was possible to get more consistent results, as shown in the next four figures.

In general, the X-tension coefficient has a very high value, from 1 up to 6, as compared with the other force coefficients that do not exceed 2 in most cases.

When the sail aerofoil is held taut, the X-tension coefficient clearly decreases as the Reynolds number goes up. Assuming that the tension in the fabric depends directly on the normal force, one would not expect any decrease in the X-tension coefficient, since the normal coefficient is either constant or increases with the Reynolds number. It is thought that the camber, which increases with the dynamic pressure, is responsible for lowering the fabric tension required to balance the normal force. Using again the crude model outlined at the beginning of the discussion, we have:

$$T_X = \frac{N \cos\beta}{2 \sin\beta}$$

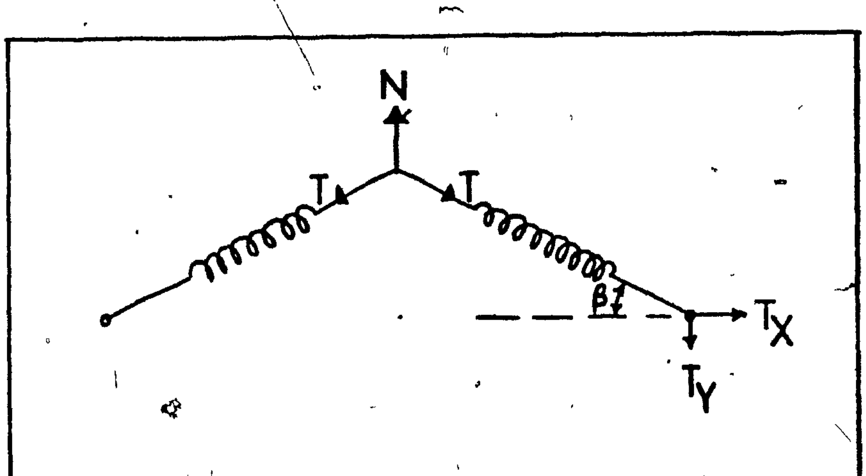

and approximately:

$$C_{T_X} \doteq \frac{C_N}{2\sin\beta}$$

When the windspeed increases, the camber increases and so does the angle β, thereby reducing C_{T_X}. As explained earlier in the discussion, the increase in camber with the windspeed is larger when the sail is taut, thus explaining that the X-tension coefficient does not vary so much in the case of a loose sail aerofoil, (Figure 43). Also, since the camber is larger in the case of a loose sail aerofoil, the X-tension coefficient is then smaller, in the range 1 to 2.5.

In general, the leading edge diameter does not seem to affect the X-tension very much.

<u>Y-tension</u> (Figures 47 to 51)

The coefficient of Y-tension, defined as the tension in the trailing edge in a direction perpendicular to the chord plane of the sail aerofoil, is generally low, from 0 to 1.3, as compared with the X-tension coefficient. Its value would be expected to lie between $\frac{C_N}{4}$ and $\frac{C_N}{2}$, depending on the position of the center of pressure which normally lies between $\frac{C}{4}$ and $\frac{C}{2}$. The test results seem to confirm this.

Lift to Drag Ratio (Figures 52 to 58)

The lift to drag ratio increases greatly with the Reynolds number when the sail aerofoil is taut and has a small leading edge, but not so much when it is loose or has a larger leading edge. This is to be mostly attributed to the increase in lift as the Reynolds number increases, and partly to the decrease in drag.

Although the lift increases significantly with the slackness of the fabric, the maximum lift to drag ratio diminishes because of the additional drag. This is just opposite to the behaviour of the maximum thrust coefficient. One would normally tend to associate a high thrust to a high lift to drag ratio. The reason for this apparent contradiction is that the two maximums do not occur at the same angle of attack. For instance, the maximum thrust coefficient occurs in the range 8° to 18°, close to the stalling angle, and in that range, the lift coefficient increases with the slackness of the fabric but the drag remains rather unaffected. On the other hand, the maximum lift to drag ratio occurs in the range 4° to 8°, where the drag increases faster than the lift as the sail aerofoil tension is diminished.

In the case of taut sail aerofoils, the leading edge 0.375 in. in diameter (9.7% of the cord) gives a higher maximum lift to drag ratio to the sail aerofoil than the other two diameters tested (0.25 and 0.5 inch).

The maximum lift to drag ratio of the dacron sail aerofoil is roughly equal to that of the nylon sail aerofoil at high Reynolds number, but does not diminish so much as the Reynolds number decreases.

Pressure Inside the Sail Aerofoil (Figures 59 to 62)

The static pressure was measured inside some of the sail aerofoils, just behind the leading edge, in order to get a rough idea of its value. It is found to be usually less than the ambient static pressure. This is understandable if one assumes that the pressure inside the sail aerofoil settles down at a value midway between the external mean pressure on the concave surface and the mean external pressure on the convex surface. It is thought that the rate of flow in and out of the inside cavity in the sail aerofoil depends on the porosity of the fabric and the size of the endgap between the edge of the fabric and the endplate, with the latter probably more important for the fabric tested here. If the geometry is such that the gap is the same for the concave and the convex surface, then the flow in should equal the flow out, the same porosity applying to both surfaces. In general, the static pressure coefficient inside the sail aerofoil diminishes with increasing Reynolds number. There is no apparent reason for this, although it may be due to unequal distortion of the end gaps.

The pressure inside the dacron sail aerofoil is higher than inside the nylon sail aerofoil, and can even become larger than the ambient static pressure. Since the dacron is non-porous, this suggested a defect in the geometry of the edge of the fabric such that the endgap is larger at the edge of the concave surface than at the edge of the convex surface.

4.3 Comparison Between Various Aerofoils and Wings

The large number of data on sail aerofoils becomes more meaningful when they are related to some other types of aerofoils and wings. Usually, a direct comparison is very difficult to make and one cannot conclude that one type is better than another. In the following discussion, some data on sailwings from various sources are presented together with data on two-dimensional sails.

McGill Sailwing

A three-dimensional sailwing was tested in previous work (Robert 1975). The data were obtained in the same wind tunnel, but the set-up was different. The sailwing was mounted with its span parallel to a pivoting shaft and the torque on the shaft was measured. A first set of experiments was made with the chord of the sailwing in a tangential position with respect to the pivoting shaft and yielded the thrust coefficient shown in Figure 63. A second set of experiments with the chord of the sailwing in a radial position yielded the normal coefficient shown in Figure 64. The lift and drag coefficients obtained by calculations are shown in Figures 65 and 66.

The sailwing was 9 in. long with a mean chord of 3 in. The chord actually varied from 3.5 in. at the edges to 2.5 in. at mid-span. The leading edge diameter was 0.25 in., that is 8.3% of the mean chord. The calendered dacron of 1.6 oz./sq. yd. was held taut. A sketch of that sailwing is shown in Figure 2.

The data on this sailwing are not too reliable, especially the drag coefficient which dropped to zero at an angle of attack of 0^{o}. This is understandable since small errors in the measurement of the thrust and normal coefficients can cause large variations in the calculated drag coefficient at small angles of attack. Notice that the procedure was opposite to that used with the sail aerofoil, in that the thrust and normal force were measured, and the lift and drag derived from these.

Although it is rather unusual to establish a comparison between a finite aspect ratio wing and a two-dimensional aerofoil without applying some corrections for tip vortices, it will be done here since it is thought that these corrections would be small compared to discrepancies arising from other three-dimensional characteristics of the sailwing, such as twist and trailing edge flexibility.

The sail aerofoil which resembles the sailwing the most closely is the taut dacron sail aerofoil but since its characteristics are available only from 0° to 20°, it is necessary to use the taut nylon sail data from 20° to 180°. Both of these have a leading edge diameter of 0.375 inch, that is 9.7% of the chord.

The lift of the sailwing was zero at 0° (Figure 65) since the sailwing fluttered when facing the wind. The sail aerofoil does not flutter and produces either a positive or a negative lift (Figure 15). The lift of the sailwing increased markedly with the Reynolds number and this was attributed to an increase in wind pressure that produced more camber. Notice the increase in camber was probably not due to the stretching of the fabric, since dacron was used, but was achieved through a reduction in chord length allowed by the flexible trailing edge. The lift of the dacron sail aerofoil does not depend on the free stream dynamic pressure because the trailing edge is restrained and the dacron does not stretch appreciably, so that the camber change is minimal.

The sailwing stalled later than the sail aerofoil, mostly because of the twist which reduced the local angle of attack near mid-span. To be exact, the sailwing probably stalled early near the edges, while the mid-span had not yet reached maximum lift. This probably explains why the maximum lift coefficient was low and the stall was smooth, when compared to the sail aerofoil. Another possible effect of the twist is the positive lift of the sailwing at an angle of attack of 90°, in contrast with the sail aerofoil which exhibits nearly zero lift at this angle of attack.

At 0°, the drag coefficient of the sailwing was .06 to .08 (Figure 66) as compared to .03 for the sail aerofoil (Figure 22). The larger value was probably attributable to the fluttering. With increasing angle of attack, the drag coefficient of the sailwing did not rise so sharply as that of the sail aerofoil (Figure 23), probably because of the twist. Near 90^{O}, the maximum drag coefficient of the sailwing does not exceed 1.3, compared to 1.9 for the sail aerofoil. This is certainly another effect of the twist which allows air to "escape" sideways thereby reducing the average pressure in front of the sailwing. The drag coefficient of the sailwing generally decreased with the Reynolds number although this is not apparent from the limited set of data given in Figure 66.

The thrust coefficients of sail aerofoils and sailwings are much different. In the range of angles of attack from 0^{O} to 20^{O}, the thrust coefficient of the sailwing was very dependent on the Reynolds number (Figure 63). The thrust coefficient of the sail aerofoil does not vary much when dacron fabric is used, but varies widely when nylon is used (Figures 31 and 32).

Another characteristic of the sailwing is that the thrust coefficient remained positive and relatively high at all angles of attack except below 5^{O} or 7^{O}. The thrust coefficient of the sail aerofoil is also negative below 4^{O} and the rises rapidly until it reaches the stall angle, at which incidence it drops sharply to negative values, and then fluctuates at low positive values for larger angles. From the stall angle until about 80°, the sailwing has a larger thrust than the sail aerofoil probably because the twist tends to increase the lift and decrease the drag in that range.

The lift to drag ratio of the sailwing, although important, is not discussed here in view of the unreliability of the drag data.

Princeton Sailwing

Some research on sailwings was undertaken at Princeton University by Sweeney (1961), for application to low-speed flight. Wind tunnel tests were made on a sailwing having an aspect ratio of 6, a taper ratio of 0.33 and a leading edge of 12% of the mean chord (Figure 67). The data were available for a limited range of angles of attack at two Reynolds numbers. Cotton duck sails were used, untreated at first, and then impregnated with light wax in order to reduce porosity. No mention was made of the amount of tension, although it appears from some of the pictures that the fabric was very taut. The drag was not corrected for tares.

The maximum lift coefficient was 0.86 at Re = 15×10^4 and compares to 1.25 for the McGill sailwing (Figure 65) at Re = 17.7×10^4. The lift curve slope was somewhat less too. Both sailwings show an increase in lift with the Reynolds number. Treating the Princeton sailwing with wax surprisingly reduced the lift and Sweeney attributed this to an increase in stiffness which limited the camber change.

The drag coefficient of the Princeton sailwing was 0.05 at 0° (Figure 67) and was reported to be actually less, perhaps half (see next paragraph), because the data were not corrected for tares. The drag coefficient of the McGill sailwing was higher, 0.06 at 0° (Figure 66), although the thickness to chord ratio was smaller. Since the drag at 0° was sensitive to the tension in the fabric, this would suggest that the Princeton sailwing was more taut. Surprisingly, the drag of the Princeton sailwing increased with the Reynolds number and the author attributed this to a greater leakage through the porous fabric. This explanation is acceptable in view of the following argument: flow through the tiny holes of a porous fabric is probably laminar and proportional to the pressure drop across the fabric, that is, proportional to the windspeed squared.

Then the ratio of the flow through the fabric to the flow near the surface of the sailwing would increase with the Reynolds number, thicken the boundary layer and usually increase the drag.

The lift to drag ratio of the untreated Princeton sailwing shown in Figure 67 does not correspond to the curves of lift and drag simply because the drag was corrected for tares in this case. These values of lift to drag ratio suggest that the corrected drag coefficient was about half of the measured value. The maximum lift to drag ratio was about 11 at an angle of attack of 4°. A sail aerofoil with a similar leading edge and at a Reynolds number of 13×10^{4} has a maximum lift to drag ratio of 12 at an angle of 5° (Figure 58). The lift to drag ratio of the Princeton sailwing would be expected to rise to about 16 for the treated sailwing assuming that the same corrections would apply to the drag coefficient.

The NASA Sailwing

A complete full-scale model of an airplane using the sailwing concept was tested by the NASA in the Langley full-scale tunnel and is reported by Fink (1967). The wind had an aspect ratio of 11.5 and a taper ratio of 0.4. The leading edge was a D-spar drooped 8° (Figure 68), its thickness being about 13% of the chord. The Reynolds number was 85×10^4, which is high compared to the other tests previously mentioned. The lift and drag of the sailwing alone were determined by subtracting the measured characteristics of the fuselage alone and are shown in Figure 68.

The maximum lift coefficient of 1.5 of the NASA sailwing is quite high when compared to the other sailwings and can perhaps be attributed to the higher Reynolds number. At an angle of attack of 0°, the drag coefficient is very low, only 0.025, as compared to about .06 for the McGill sailwing. This low value can be attributed partly to the high Reynolds number, partly to the efficient D-spar leading edge which may well reduce flow separation and partly to the higher aspect ratio. The lift to drag ratio is very high, around 28.

The 2-D Sail

It is possible that the sailwing may be used on sailboats with some advantage. Since comparisons between the sailwing and the ordinary sail is rather difficult, owing to the number of parameters to be controlled, the comparison is made between two-dimensional sails and sail aerofoils. Some tests on sails were reported by Chapleo (1968) and the characteristics are reproduced in Figure 69. The tests were made to study the effect of a gap between the mast and the sail and were comparative; thus, insufficient attention was paid to controlling or measuring the spanwise variation in camber and twist and the sails were probably not truly two-dimensional in the sense defined in this study (that is, no variation along the span). The mast was of commercial "pear shaped" section with a ratio of mast thickness/mast chord of 0.77. The comparison will be established between that sail and the slightly loose nylon sail aerofoil with a leading edge of 0.25 in.

The maximum lift of the sail was 1.7 and is equal to that of the sail aerofoil at a similar Reynolds number (Figure 13). The minimum drag coefficient of the sail was 0.065 and compares with 0.068 for the sail aerofoil (Figures 20 and 26). In general, the lift and drag curves of the sail were similar in shape to those of the sail aerofoil. The maximum lift to drag ratio of the sail aerofoil is 16 (Figure 53), compared to 14 for the sail. It is possible that a comparison with the dacron sail aerofoil may be more appropriate, although the leading edge was larger. The dacron aerofoil had a maximum lift to drag ratio of 18, a minimum drag coefficient of .025 and a maximum lift coefficient of 1.4 at an appropriate value of the Reynolds number.

Hang-Glider Sailwing

Some data on sailwings are given by Stong (1974). The sailwing was used in a hang-glider, an ultralight glider from which the pilot is suspended by a harness. Apparently the sailwing had a span of 34 feet, an area of 158 square feet and an aspect ratio of 7.25:1. It had a wing taper of 0.33. The coefficient of lift is reproduced in Figure 70. The windspeed, although not stated, was probably in the range 20 to 40 mph. This would mean a Reynolds number, based on a mean chord of 4.7 ft., of about 90 X 10^4 to 180 X 10^4. The maximum lift coefficient was 2.0 and is higher than that of the NASA sailwing which was 1.5 at a Reynolds number of 85 X 10^4. Some comparative tests could establish whether the D-spar leading edge of the NASA sailwing is actually more efficient at certain angles. The maximum lift to drag ratio was reported to be about 14.

Summary

A summary of the main characteristics of the various aerofoils and wings presented in this section is given in Table 4. Some data on the NACA 0012, a rigid symmetrical aerofoil currently in use in vertical-axis wind turbines (Templin 1974), are included.

		Taut Nylon Sail Aerofoil d = 0.375 in.	Taut Dacron Sail Aerofoil d = 0.375 in.	McGill Dacron Sailwing	Princeton Treated Cotton Sailwing	NASA Sailwing	2-D Sail	Hang-Glider Sailwing	NACA 0012 Aerofoil
*Thickness/Chord		9.7%	9.7%	8.3%	12%	13%	4.7%	12%	12%
C_L	At the Stall	1.2	1.4	1.25	0.9	1.5	1.7	2.0	1.25
	Higher Re	More Lift	Same Lift	More Lift	More Lift	-	-	-	Same Lift
C_d	At 0^o	.047	.028	.06	-	0.025	0.07	-	0.015
	At 5^o	.063	.054	.09	-	0.060	0.065	-	0.015
	At the Stall	≈.10	.15	.10	-	0.20	0.30	-	0.075
	Higher Re	Less Drag	Less Drag	Less Drag	More Drag	-	-	-	Less Drag
Maximum Lift/Drag		15	16	-	≈16	28	14	14	60
Maximum Thrust		0.06	0.22	0.33	-	-	-	-	0.30
Reynolds Number X 10^4		18	18	18	15	85	23	90-180	180

TABLE 4 Summary of Aerofoils and Wings Characteristics

4.4 Computer Simulation of Wind Turbines

In assessing the relative merit of various shapes of sail aerofoils for application to a vertical-axis turbine, it is readily seen that a single characteristic curve may not be a fair basis for comparison. For instance, one might assume that the sail aerofoil with the highest thrust coefficient may yield the best wind turbine performances, but the normal coefficient should also be taken into account. A high value of the latter may cause the disc velocity through the turbine to become low enough to impair the performance. The approach taken here is to insert the curves of the thrust and normal coefficient in the computer program simulating a vertical-axis wind turbine.

A wind turbine will operate best at a certain solidity, which will vary depending on the shape of the aerofoil. So, it was found necessary to determine the optimum solidity for each shape of sail aerofoil in order to compare the performances. In a realistic wind turbine with the blades tilted with respect to the axis, the solidity and the local blade Reynolds number will vary along the span of the blades, thus leading to many possible combinations of the parameters. To avoid this difficulty, it was decided to simulate a two-dimensional turbine having constant-chord blades mounted parallel to the axis. The number of blades is held constant while the chord is varied.

The computer program was run in the past (Robert 1975) and duplicated very accurately the predictions of the performances of the NRC wind turbine (Templin 1974). However, when it was used to predict the performances of a wind turbine model with sailwings, such as the model shown in Figure 4, it yielded a power coefficient curve that coincided with the experimental curve only in the low tip speed region. The maximum predicted power coefficient was about twice the measured value and occurred at a tip speed about 50% higher than in the experiments. There are various reasons for this discrepancy among which are the higher solidity encountered in sailwing wind turbines, the flapping of the sailwing as the camber changes in each rotation and the possible inaccuracy of the data on the thrust and normal coefficient of the sailwing. However, the program seemed to be useful for comparative purposes since it qualitatively reproduced the measured effect of a change in solidity or Reynolds number (Robert 1975).

The computer simulations of a two-dimensional wind turbine using the sail aerofoil data available are shown in Figures 71 to 77. In each case, the optimum solidity may be identified. In some instances, such as in Figure 71, the performance curve of the higher solidity cases could not be completed since the disc velocity was readily falling to zero. The best performances were achieved by the dacron sail aerofoil (Figure 74). Among the remaining sail aerofoils, all made of nylon, the slightly loose case with a leading edge of 0.25 in. gave the best results (Figure 72).

The effect of varying the turbine Reynolds number was simulated (Figure 78) and the power coefficient was not much affected. Notice the program made the necessary interpolation in the input data for thrust and normal coefficients over the available range of Reynolds number. The value at the limit of the range was assumed to extend outside that range.

Great care must be used when interpreting the foregoing computer simulations. The curves should be used for comparative purposes only. The maximum power coefficient has no meaning in itself for two reasons: first, the program has not yet proven reliable when predicting performances of sailwing or sail aerofoil wind turbines and second, the simulation is very unrealistic since an actual wind turbine would be fitted with sailwings and not sail aerofoils. Also, the optimum solidity and tip speed ratio shown in the curves may have no direct application to a realistic sailwing turbine. It is thought that such a turbine would operate at a lower tip speed ratio, and would consequently perform best with a higher solidity, because the sailwing has more drag than the sail aerofoil and, moreover, the blade drag of an actual fully rigged turbine is usually higher than in theory, as reported by Templin (1974).

The theory allowing for high solidity was used throughout the foregoing computer simulation. It was shown in previous work (Robert 1975) that, for low solidities, it duplicated faithfully the predictions made with the Betz-Glauert theory, but it could deal with higher solidities, where a lower disc velocity ratio is likely to occur. The double disc turbine theory was also tried and gave a maximum power coefficient about 5% less than with the Betz-Glauert theory in the case of the NRC wind turbines. It cannot handle high solidities and is therefore not usually applicable to sail turbines. The modified computer program for this theory is therefore not presented.

5. CONCLUSIONS

The main aerodynamic characteristics of the sail aerofoil have been obtained experimentally and helped to provide some insight into the behaviour of sailwings. The tension in the trailing edge is seen to be a very important parameter and deserves much attention if further experimentation is to be undertaken. Generally, an increase in looseness of the sail increased the camber and with it the lift and the drag, but decreased the lift-to-drag ratio. The properties of the fabric are also critical. The porosity should be minimal for low drag but it is difficult to study its effect alone since a reduced porosity is usually accompanied by a larger stiffness. The leading edge diameter should be about 10% of the chord for good thrust and lift-to-drag ratio.

The tests revealed that the most distinctive feature of the sailwing was the twist, which is due to the spanwise flexibility of the trailing edge. This is seen to cause fluttering and largely increases the drag at an angle of attack of 0°. At large angles of incidence, the twist reduces the local angle of attack near mid-span, thereby decreasing the drag and resulting in a lift with a lower maximum value spread over a much smoother stall. Despite the low aspect ratio

(3.0) of the sailwing, it generally had better thrust chracteristics than the sail aerofoil, especially at large angles of attack, but these are seen to deteriorate at low Reynolds numbers.

The characteristics of the sail aerofoil are seen to be slightly better but similar to those of a two-dimensional sail. Generally, the lift to drag ratio of sailwings and sails is below 30 while it may exceed 60 for rigid wings, owing to their lower drag.

The computer program was found to predict well the performance of low solidity, high speed, vertical-axis wind turbines using the Betz-Glauert theory. An extension to that theory was used in the program to treat the case of the sailwing wind turbine, operating at a higher solidity, and the predicted power output was about twice as high as that found in model tests. Another modification to the theory was made to account for wake interference, but introduced additional complexity and could not handle cases of high solidity. The program, including the extension for high solidity, can hopefully reproduce the relative effect of changing some of the parameters for sailwing turbines, such as the solidity, the Reynolds number and the characteristics of the sails.

The data collected on the sail aerofoil were inserted for comparative purposes into the computer program for simulating a two-dimensional vertical-axis wind turbine and the taut dacron sail aerofoil with a leading edge to chord ratio of 9.7% was seen to perform best.

Tests so far on the vertical-axis sailwing wind turbine indicate that the optimum tip speed ratio is low and the turbine is not highly efficient, but it is self-starting, cheap and probably suitable for third-world technology. It is suggested that the following parameters would be close to the optimum design:

1. Solidity close to 1.0

2. Sailwing: chord to radius ratio 10%
   taper ratio 2:1
   calendered dacron (or other impervious fabric)

3. Three sailwings for positive starting torque in any position.

4. Tilt angle of the sailwings from the axis: 30°.

5. Provision for high tensioning of the sailwing.

6. REFERENCES

CHAPLEO, A.Q. 1968 'A Review of Two-Dimensional Sails', Southampton University Yacht Research, SUYR Report No. 23.

DURAND, W.F. 1963 'Aerodynamic Theory', Vol. IV, Dover.

FALES, E.N. 'Windmills' in Marks (1967).

FINK, MARVIN P. 1967 'Full-Scale Investigation of the Aerodynamic Characteristics of a Model Employing a Sailwing Concept', Langley Research Center, NASA TN D-4062.

GLAUERT 'Windmill and Fans' in Durand (1963).

MARKS, L.S. 1967 'Standard Handbook for Mechanical Engineers', McGraw-Hill.

ROBERT, J. 1975 'Vertical-Axis Sailwing Windmill; Preliminary Work', Department of Mechanical Engineering, McGill University, Montreal, Unpublished Report.

SCHLICHTING, H. 1968 'Boundary Layer Theory', McGraw-Hill, New York.

SOUTH, P. and RANGI, R.S. 1971 'Preliminary Tests of a High Speed Vertical-Axis Windmill Model', National Research Council of Canada, NRC NAE LTR-LA-74.

SOUTH, P. and RANGI, R.S. 1972 'A Wind Tunnel Investigation of a 14 ft. Diameter Vertical-Axis Windmill', National Research Council of Canada, NRC NAE LTR-LA-105.

STONG, C.L. 1974 'Hang Gliding, or Sky Surfing, With a High Performance Low-Speed Wing', Scientific American, December 1974, Vol. 23, no. 6, p. 138.

SWEENEY, T.E. 1961 'Exploratory Sailwing Research at Princeton', Department of Aeronautical Engineering, Princeton University, Report No. 578.

TEMPLIN, R.J. 1974 'Aerodynamic Performance Theory for the NRC Vertical-Axis Wind Turbine', National Research Council of Canada, NRC NAE LTR-LA-160.

7. LIST OF FIGURES

	SAIL AEROFOIL DATA	FABRIC	LEADING EDGE
22	Drag Coefficient	Taut Dacron	0.375 in.
23	Drag Coefficient	Taut Nylon	0.375 in.
24	Drag Coefficient	Loose Nylon	0.375 in.
25	Drag Coefficient	Taut Nylon	0.5 in.

26 Sail Aerofoil Drag Coefficient from 0^{o} to 20^{o}: printout.

27 Sail Aerofoil Drag Coefficient from 0^{o} to 20^{o}: printout continued.

	SAIL AEROFOIL DATA	FABRIC	LEADING EDGE
28	Thrust Coefficient	Taut Nylon	0.25 in.
29	Thrust Coefficient	Slightly Loose Nylon	0.25 in.
30	Thrust Coefficient	Loose Nylon	0.25 in.
31	Thrust Coefficient	Taut Dacron	0.375 in.
32	Thrust Coefficient	Taut Nylon	0.375 in.
33	Thrust Coefficient	Loose Nylon	0.375 in.
34	Thrust Coefficient	Taut Nylon	0.5 in.
35	Normal Coefficient	Taut Nylon	0.25 in.
36	Normal Coefficient	Slightly Loose Nylon	0.25 in.
37	Normal Coefficient	Loose Nylon	0.25 in.
38	Normal Coefficient	Taut Dacron	0.375 in.
39	Normal Coefficient	Taut Nylon	0.375 in.
40	Normal Coefficient	Loose Nylon	0.375 in.
41	Normal Coefficient	Taut Nylon	0.5 in.

	SAIL AEROFOIL DATA	FABRIC	LEADING EDGE
42	X-Tension Coefficient	Taut Nylon	0.25 in.
43	X-Tension Coefficient	Loose Nylon	0.25 in.
44	X-Tension Coefficient	Taut Dacron	0.375 in.
45	X-Tension Coefficient	Taut Nylon	0.375 in.
46	X-Tension Coefficient	Taut Nylon	0.5 in.
47	Y-Tension Coefficient	Taut Nylon	0.25 in.
48	Y-Tension Coefficient	Loose Nylon	0.25 in.
49	Y-Tension Coefficient	Taut Dacron	0.375 in.
50	Y-Tension Coefficient	Taut Nylon	0.375 in.
51	Y-Tension Coefficient	Taut Nylon	0.5 in.
52	Lift to Drag Ratio	Taut Nylon	0.25 in.
53	Lift to Drag Ratio	Slightly Loose Nylon	0.25 in.
54	Lift to Drag Ratio	Loose Nylon	0.25 in.
55	Lift to Drag Ratio	Taut Dacron	0.375 in.
56	Lift to Drag Ratio	Taut Nylon	0.375 in.
57	Lift to Drag Ratio	Loose Nylon	0.375 in.
58	Lift to Drag Ratio	Taut Nylon	0.5 in.
59	Pressure Coefficient	Taut Dacron	0.375 in.
60	Pressure Coefficient	Taut Nylon	0.375 in.
61	Pressure Coefficient	Loose Nylon	0.375 in.
62	Pressure Coefficient	Taut Nylon	0.5 in.
63	Sailwing Thrust Coefficient		
64	Sailwing Normal Coefficient		

8. FIGURES

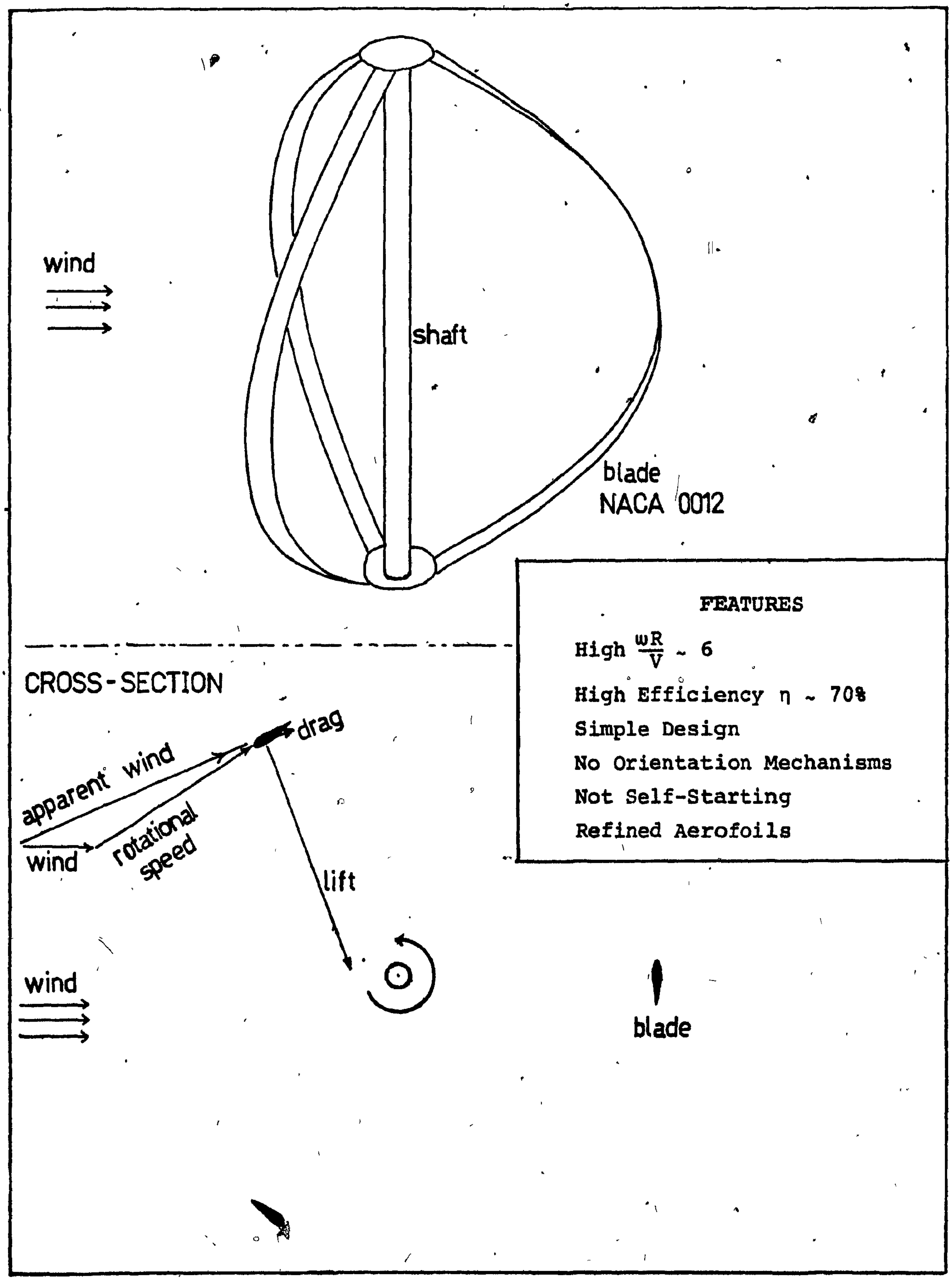

FIGURE 1 : NRC vertical-axis wind turbine.

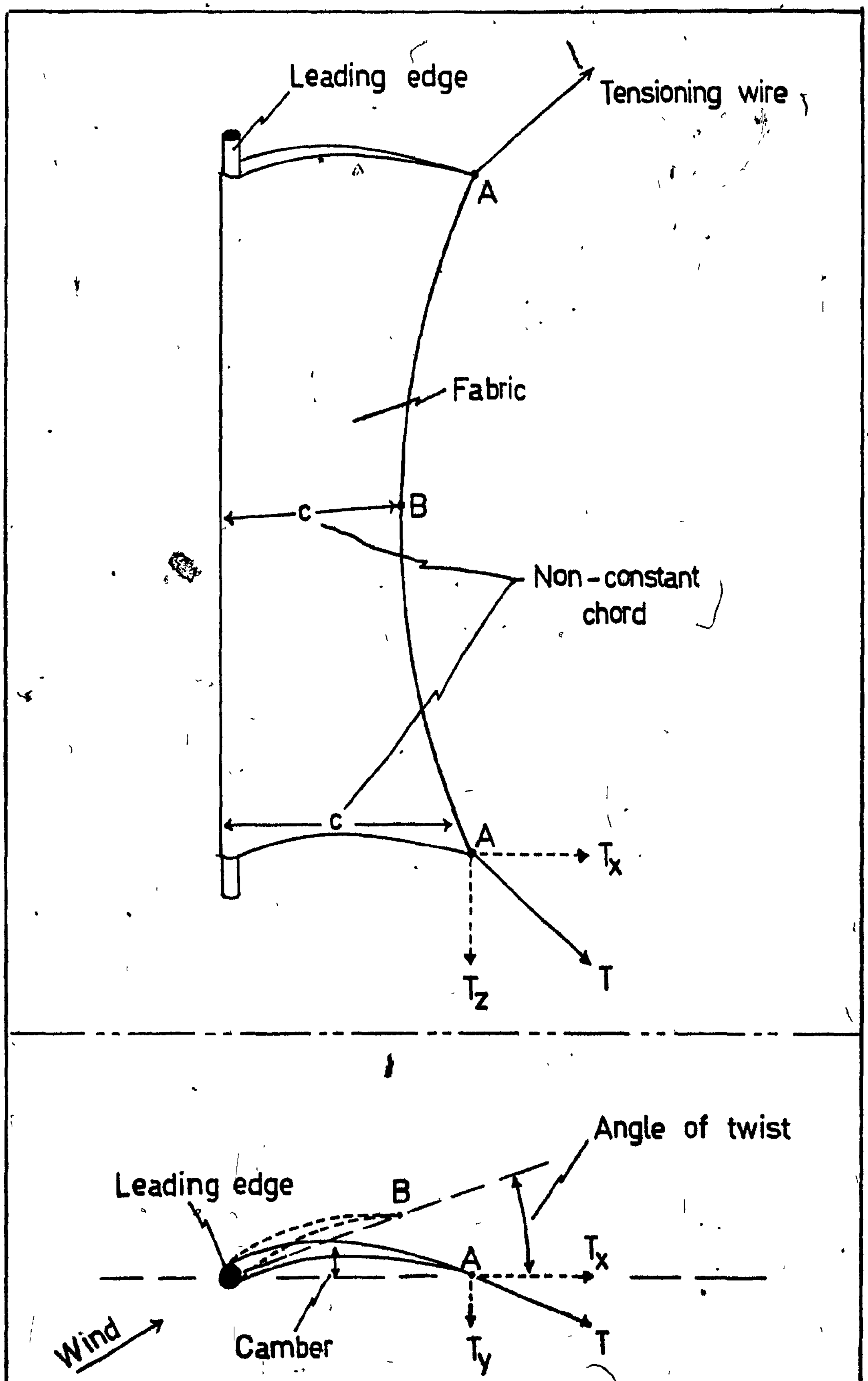

FIGURE 2 : The sailwing.

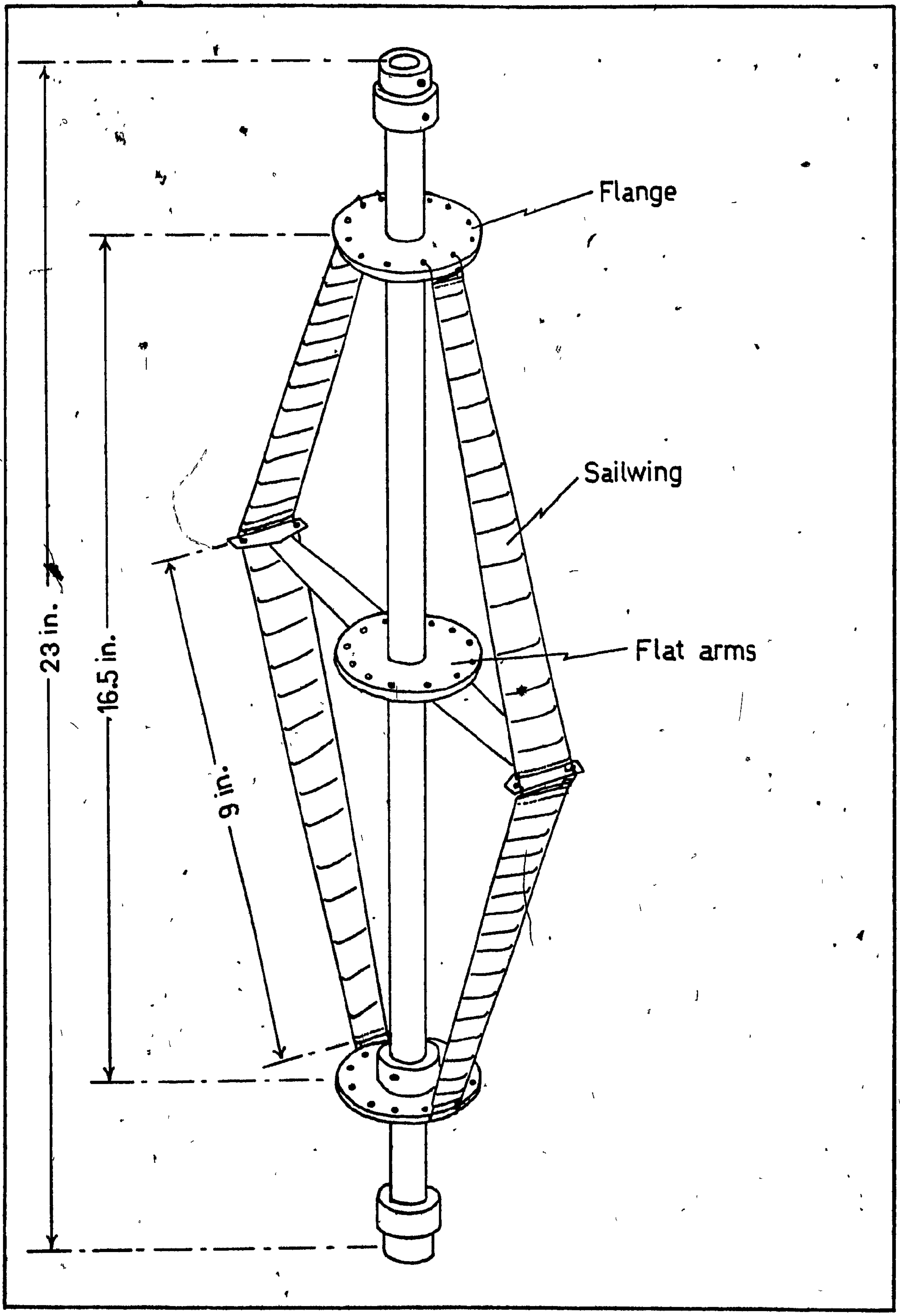

FIGURE 3 : Vertical-axis sailwing wind turbine model.

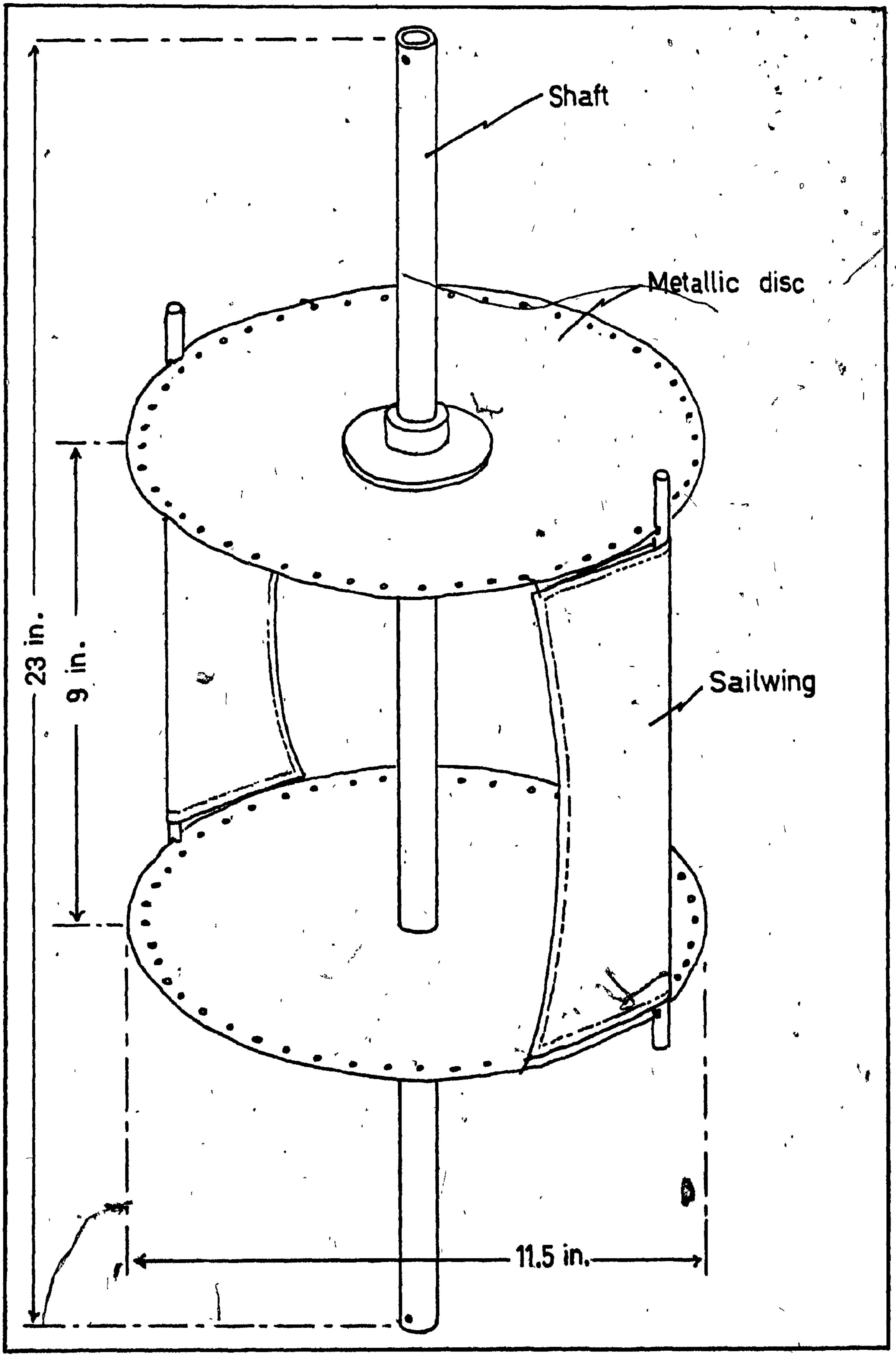

FIGURE 4 : Vertical-axis sailwing wind turbine model.

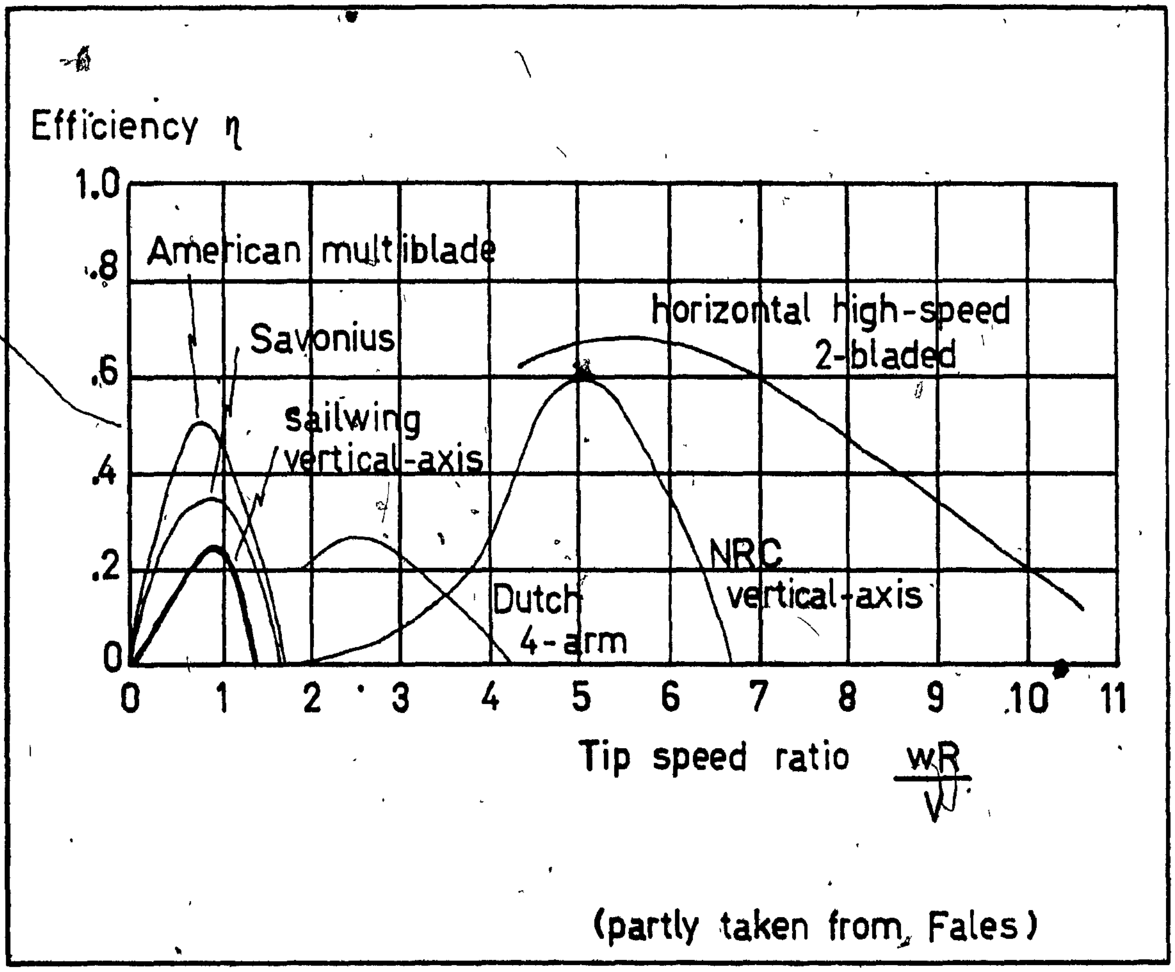

FIGURE 5 : Efficiency of various wind turbines.

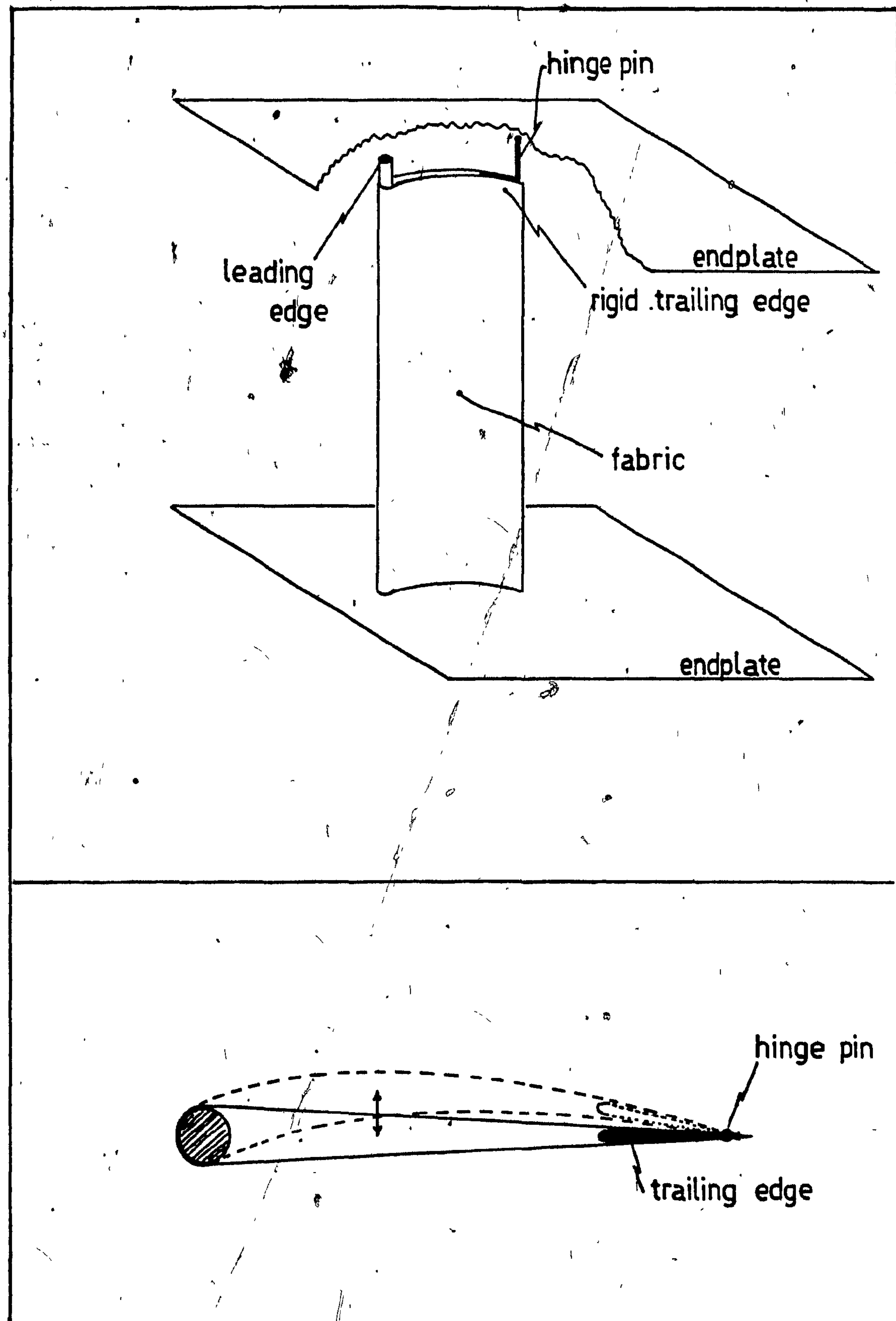

FIGURE 6 : The sail-aerofoil.

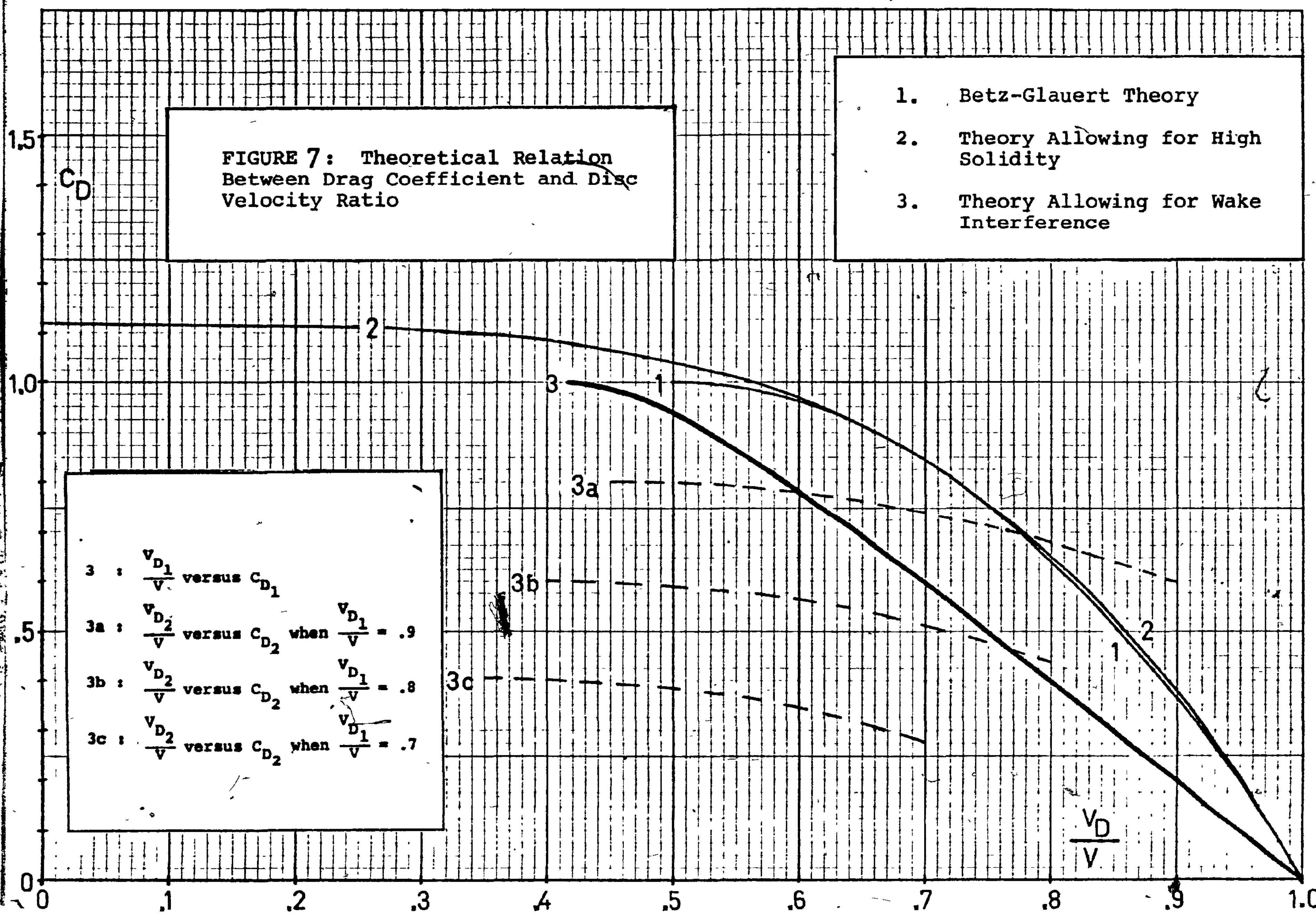

FIGURE 7: Theoretical Relation Between Drag Coefficient and Disc Velocity Ratio

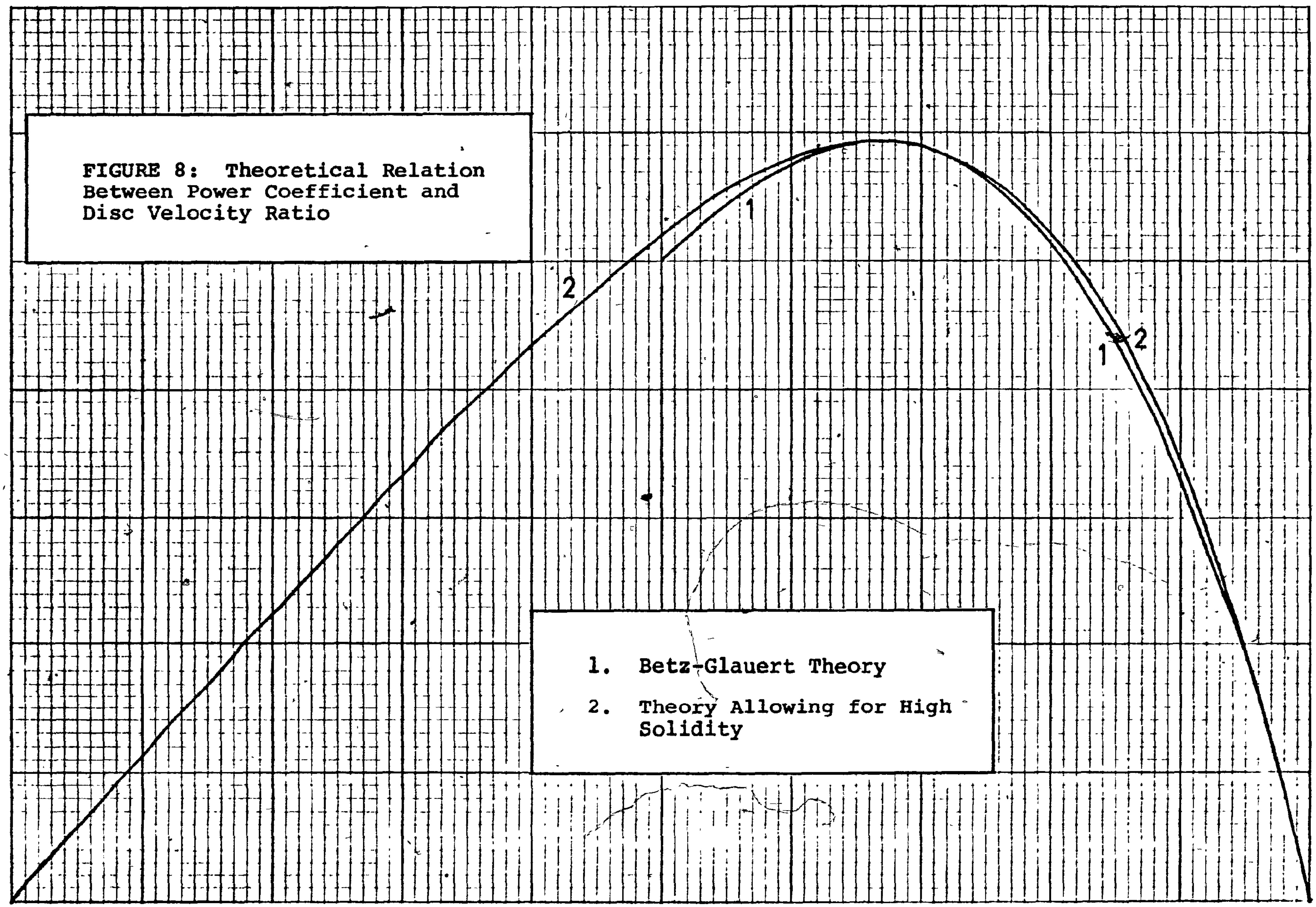
FIGURE 8: Theoretical Relation Between Power Coefficient and Disc Velocity Ratio
1
2
1
2
1. Betz-Glauert Theory
2. Theory Allowing for High Solidity

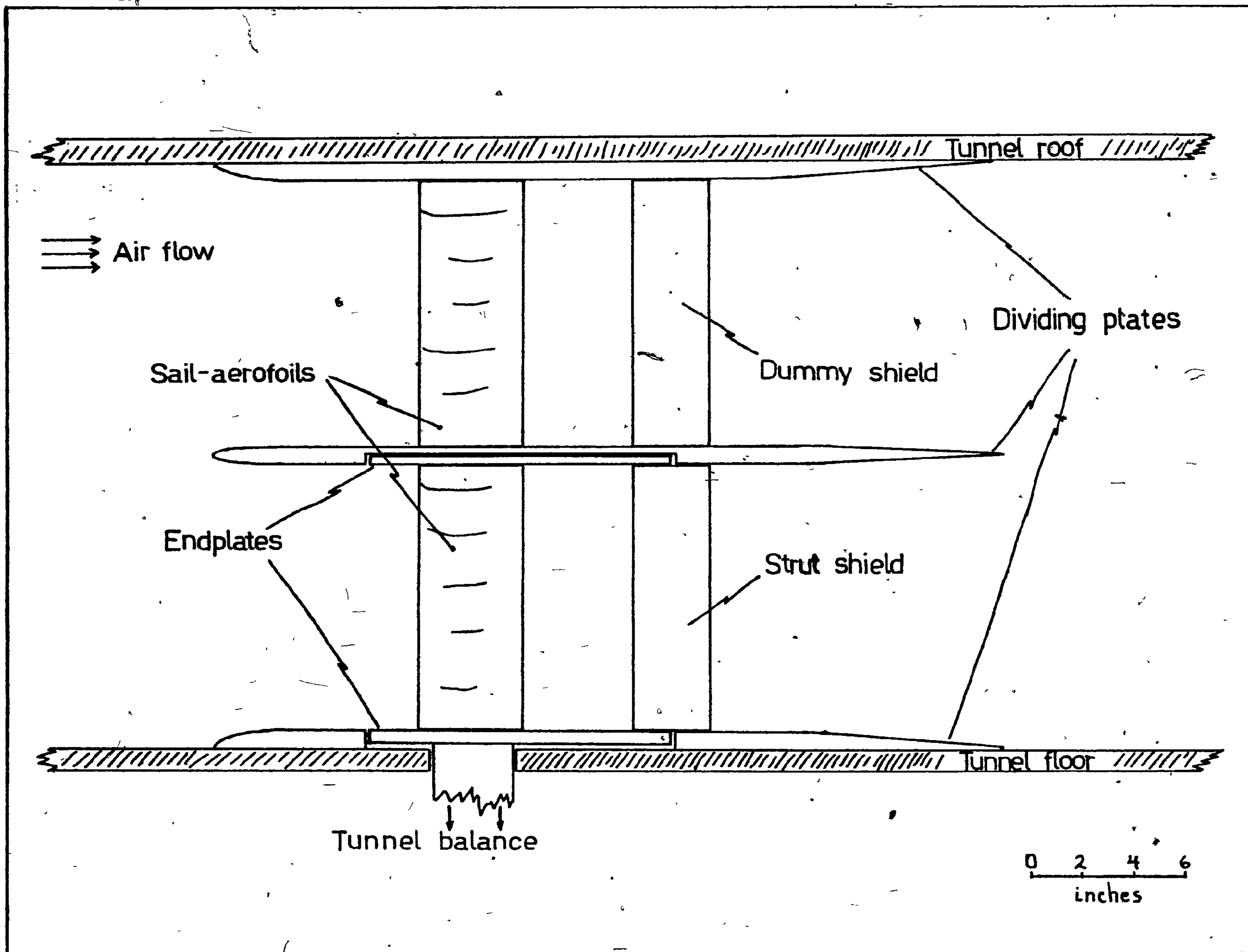

FIGURE 9 : Side view of the set-up for testing the sail aerofoil.

FIGURE 10 :

UPPER SAIL-AEROFOIL ASSEMBLY

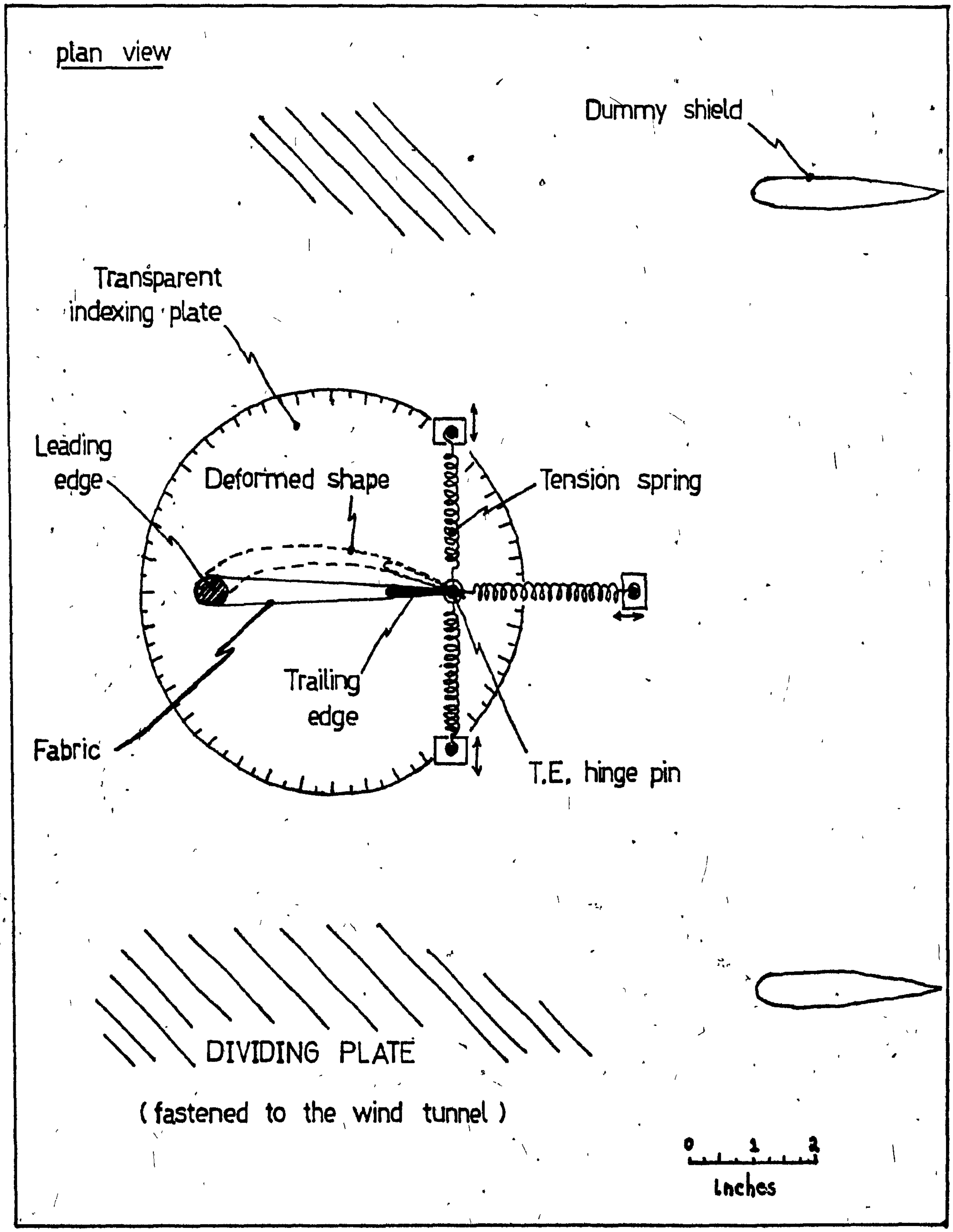

FIGURE 11 :

BOTTOM SAIL-AEROFOIL ASSEMBLY

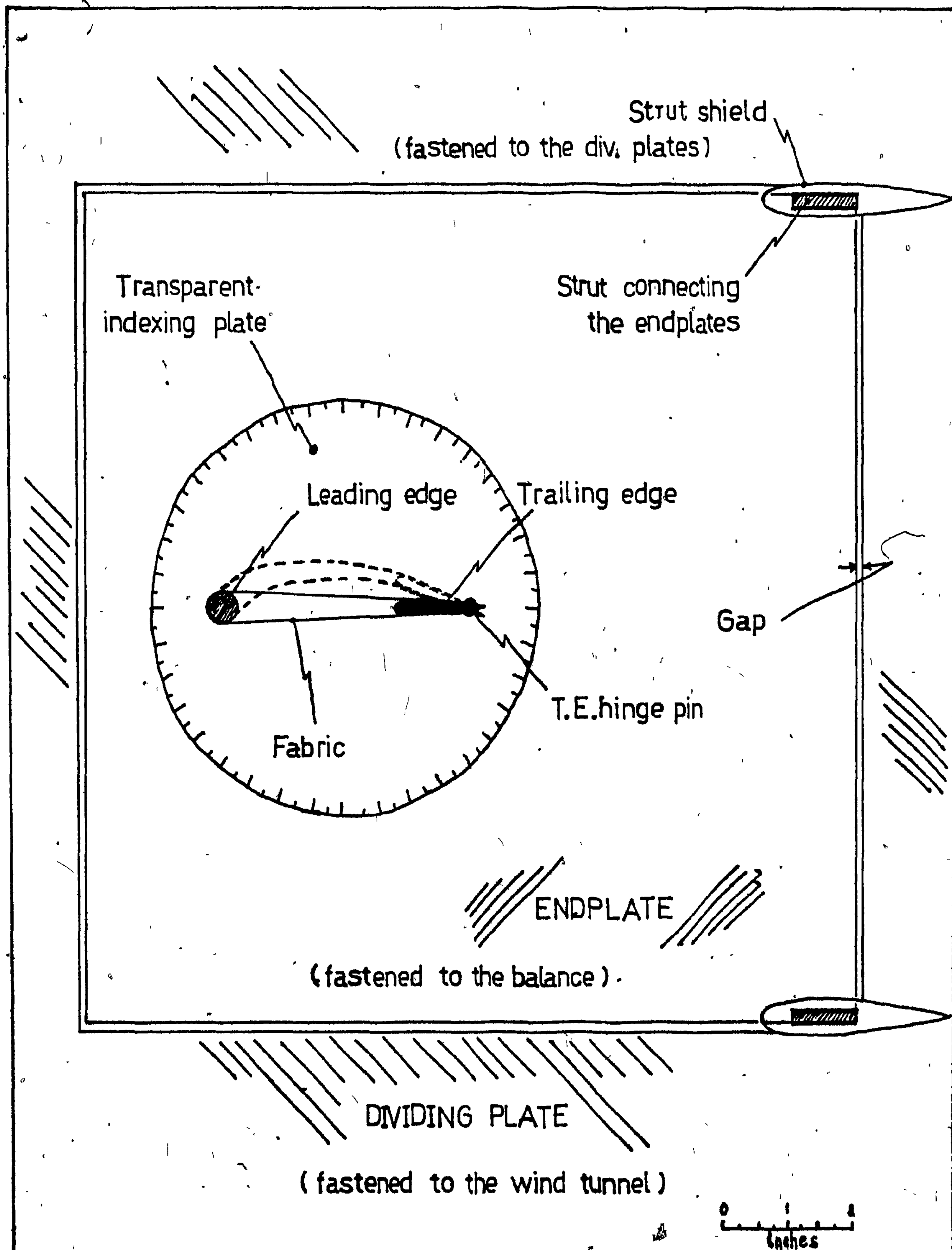

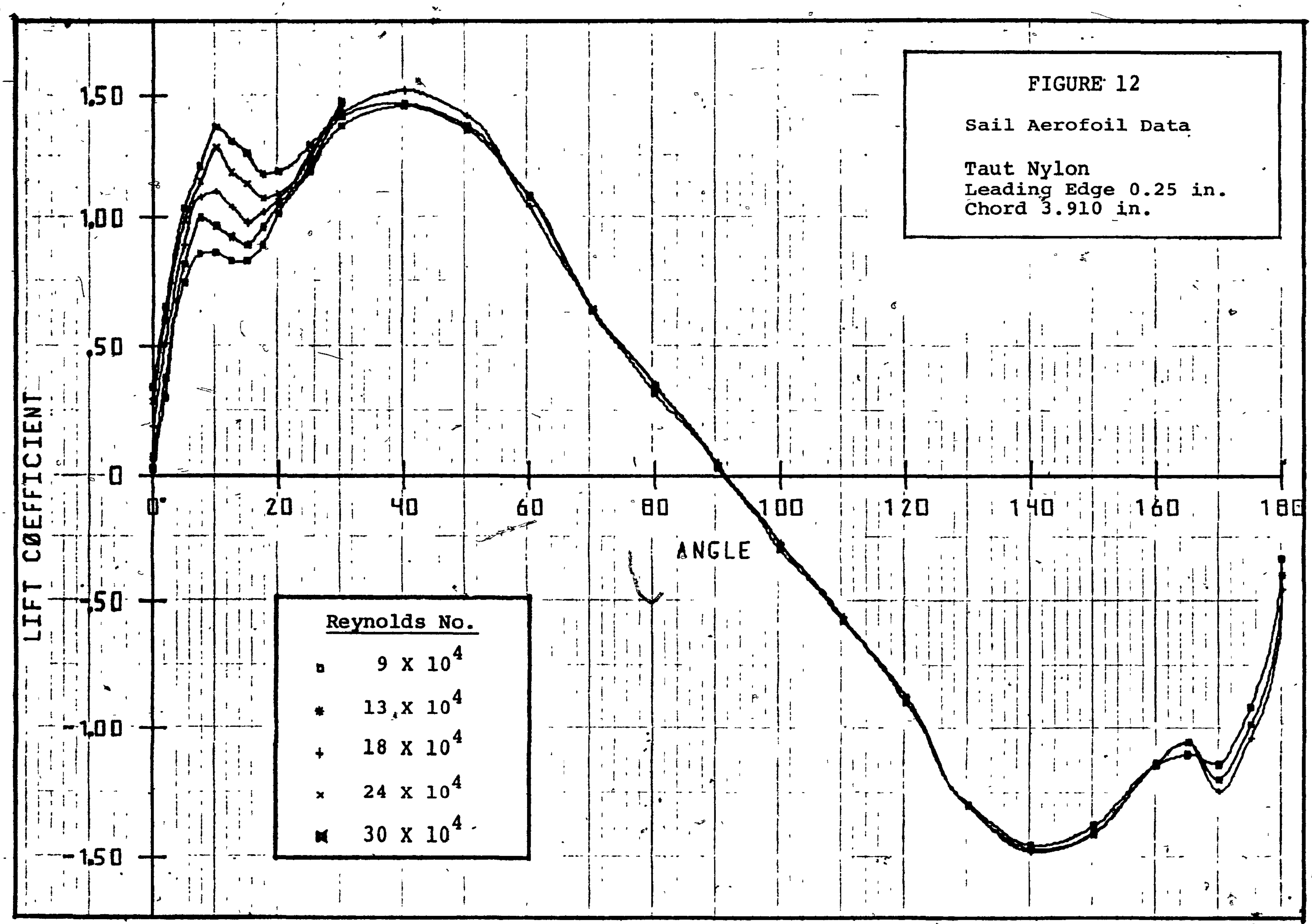
FIGURE 12
Sail Aerofoil Data
Taut Nylon
Leading Edge 0.25 in.
Chord 3.910 in.
LIFT CØEFFICIENT
ANGLE
1.50
1.00
.50
0
-.50
-1.00
-1.50
0°
20
40
60
80
100
120
140
160
180
Reynolds No.
9 X 10^4
13 X 10^4
18 X 10^4
24 X 10^4
30 X 10^4

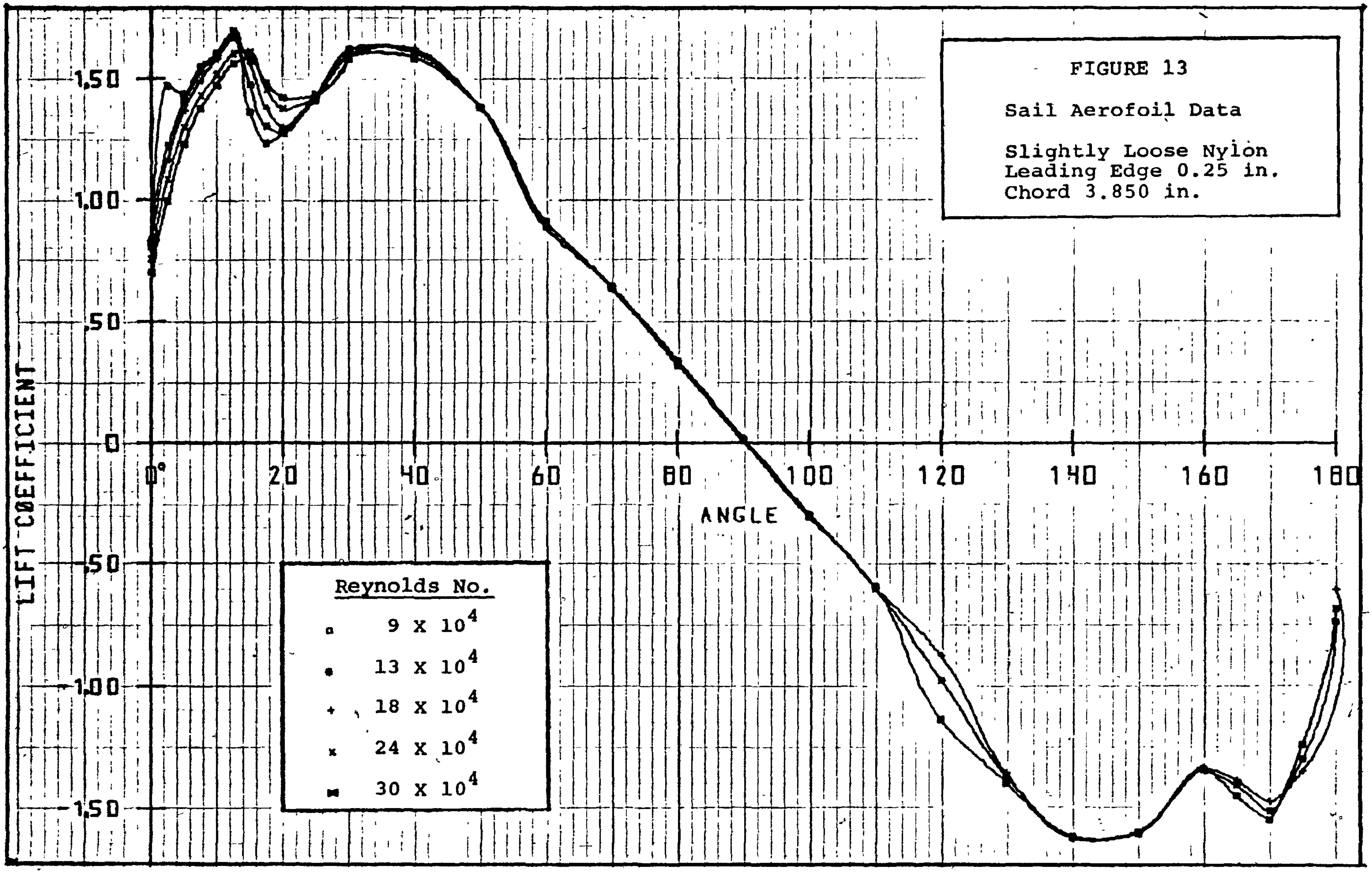
FIGURE 13
Sail Aerofoil Data
Slightly Loose Nylon
Leading Edge 0.25 in.
Chord 3.850 in.
Reynolds No.
9 X 10^4
13 X 10^4
18 X 10^4
24 X 10^4
30 X 10^4
LIFT COEFFICIENT
ANGLE
1.50
1.00
.50
0
-.50
-1.00
-1.50
0°
20
40
60
80
100
120
140
160
180

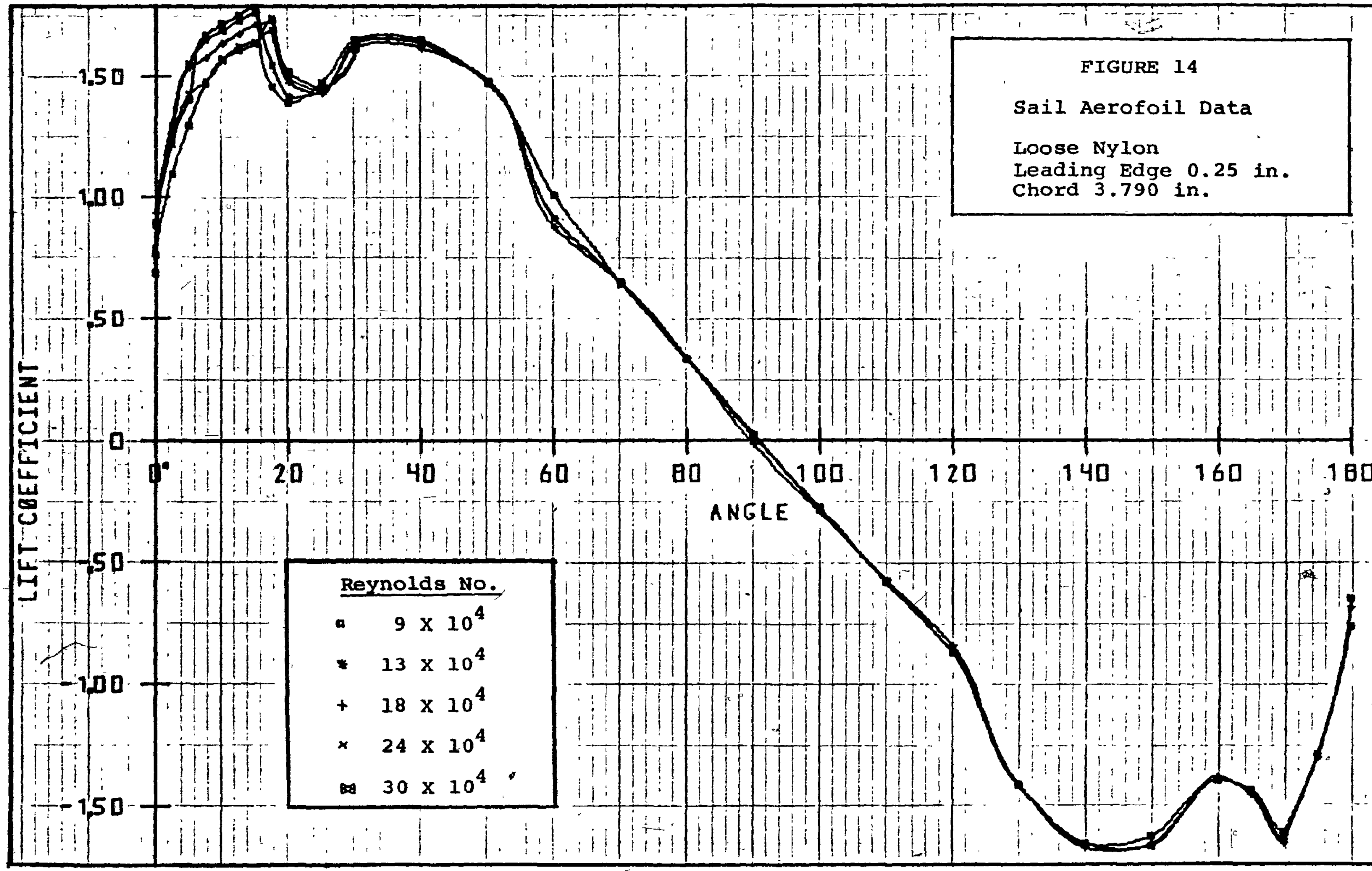
FIGURE 14
Sail Aerofoil Data
Loose Nylon
Leading Edge 0.25 in.
Chord 3.790 in.
LIFT COEFFICIENT
ANGLE
1.50
1.00
.50
0
-.50
-1.00
-1.50
0°
20
40
60
80
100
120
140
160
180
Reynolds No.
9 X 10^4
13 X 10^4
18 X 10^4
24 X 10^4
30 X 10^4

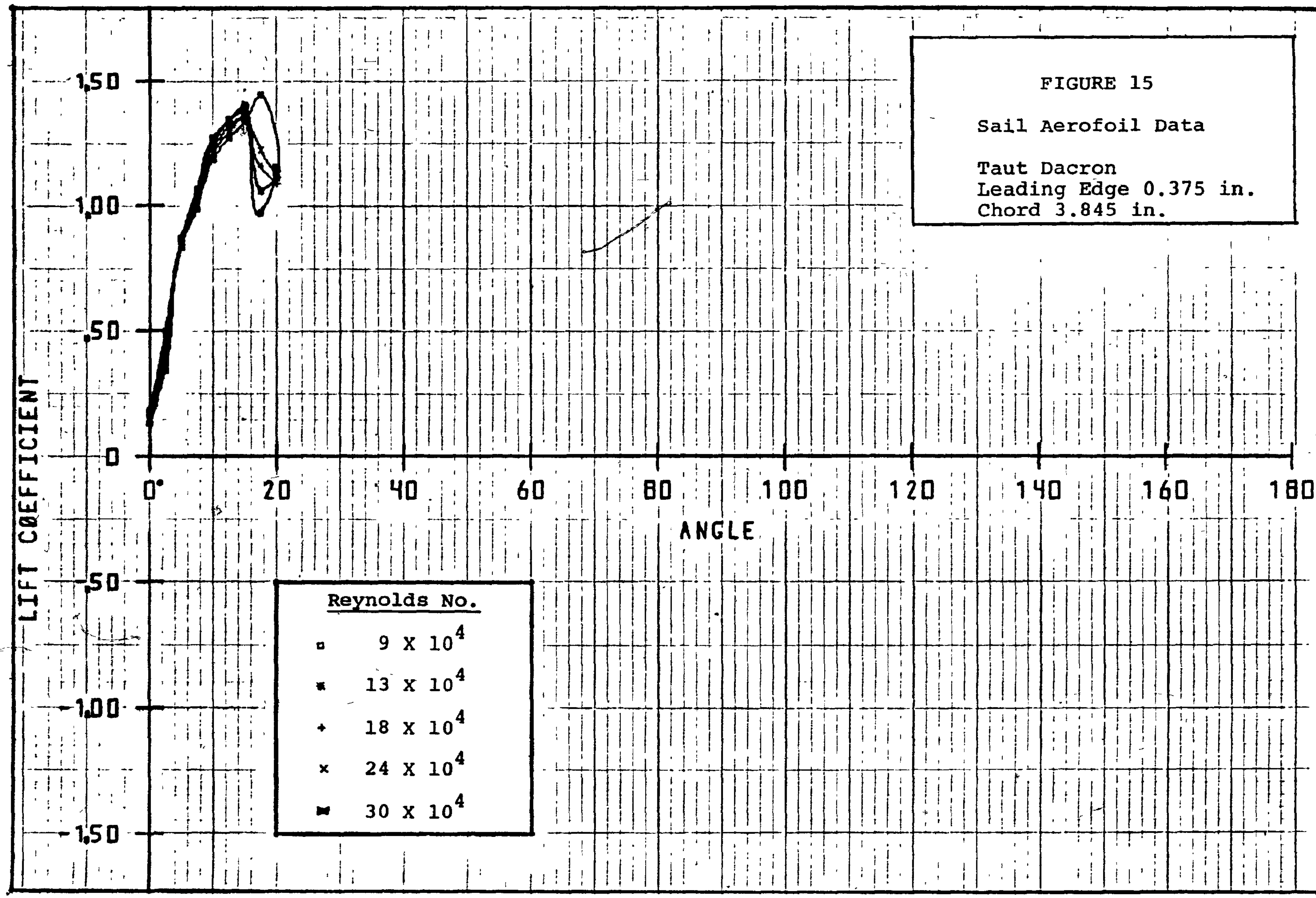
FIGURE 15
Sail Aerofoil Data
Taut Dacron
Leading Edge 0.375 in.
Chord 3.845 in.
LIFT COEFFICIENT
1.50
1.00
.50
0
-.50
-1.00
-1.50
0°
20
40
60
80
100
120
140
160
180
ANGLE
Reynolds No.
9 X 10^4
13 X 10^4
18 X 10^4
24 X 10^4
30 X 10^4

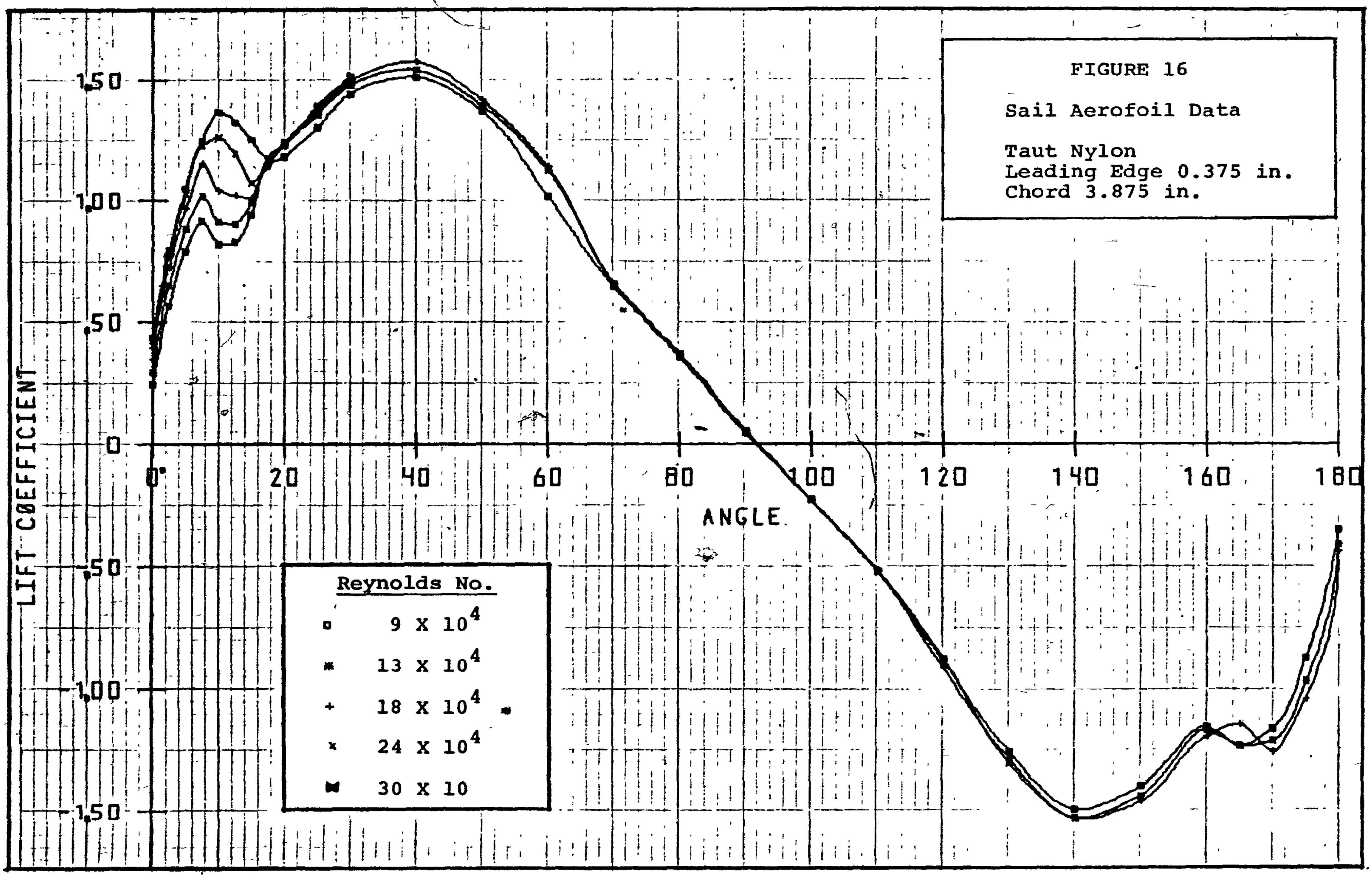

FIGURE 16
Sail Aerofoil Data
Taut Nylon
Leading Edge 0.375 in.
Chord 3.875 in.
LIFT COEFFICIENT
1.50
1.00
.50
0
-.50
-1.00
-1.50
0°
20
40
60
80
100
120
140
160
180
ANGLE
Reynolds No.
9 X 10^4
13 X 10^4
18 X 10^4
24 X 10^4
30 X 10

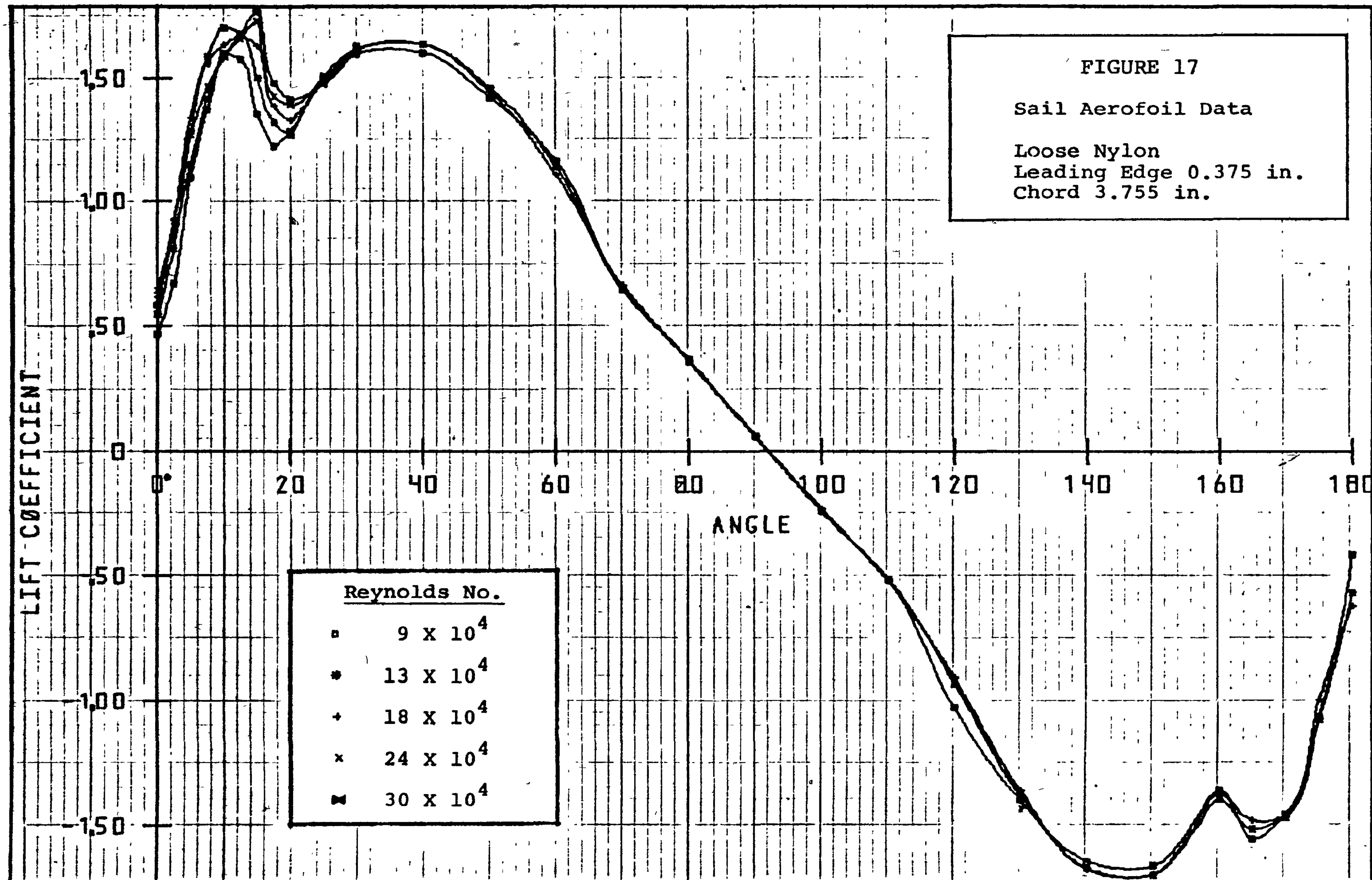

FIGURE 17
Sail Aerofoil Data
Loose Nylon
Leading Edge 0.375 in.
Chord 3.755 in.
LIFT COEFFICIENT
ANGLE
1.50
1.00
.50
0
-.50
-1.00
-1.50
0°
20
40
60
80
100
120
140
160
180
Reynolds No.
9 X 10^4
13 X 10^4
18 X 10^4
24 X 10^4
30 X 10^4

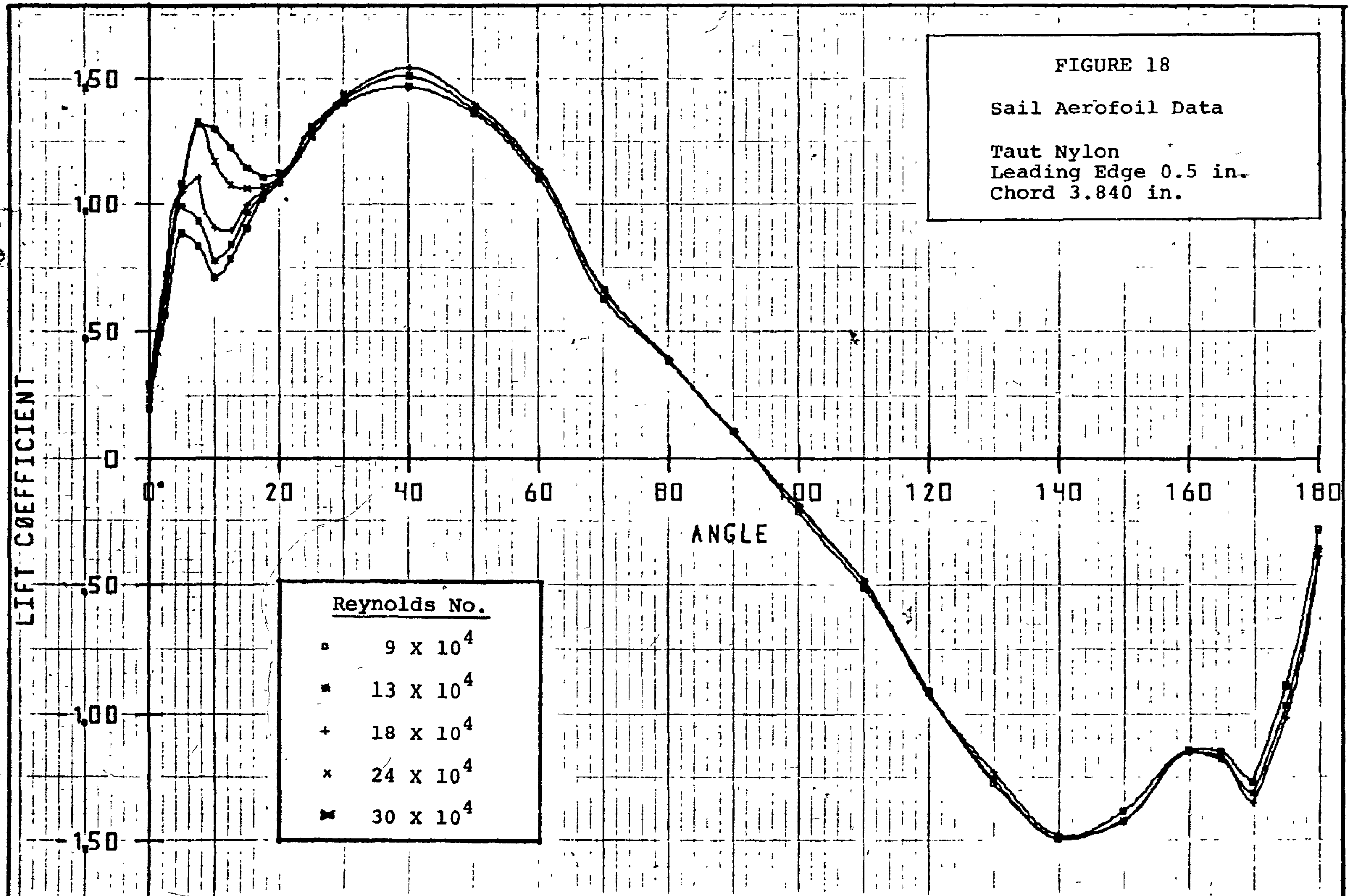

FIGURE 18
Sail Aerofoil Data
Taut Nylon
Leading Edge 0.5 in.
Chord 3.840 in.
LIFT COEFFICIENT
1.50
1.00
.50
0
-.50
-1.00
-1.50
0°
20
40
60
80
100
120
140
160
180
ANGLE
Reynolds No.
9 X 10^4
13 X 10^4
18 X 10^4
24 X 10^4
30 X 10^4

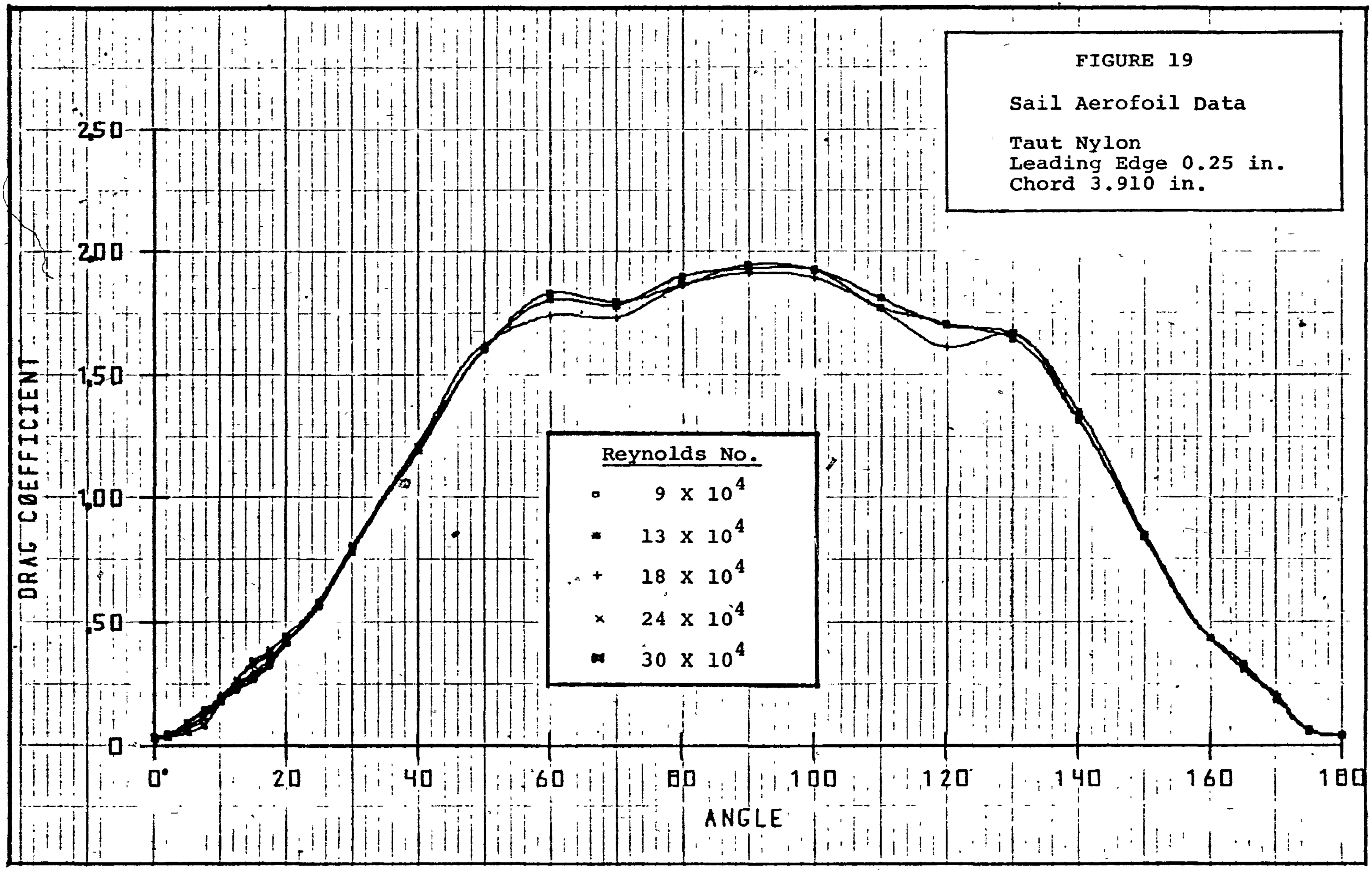
FIGURE 19
Sail Aerofoil Data
Taut Nylon
Leading Edge 0.25 in.
Chord 3.910 in.
Reynolds No.
9 X 10^4
13 X 10^4
18 X 10^4
24 X 10^4
30 X 10^4
DRAG COEFFICIENT
2.50
2.00
1.50
1.00
.50
0
0°
20
40
60
80
100
120
140
160
180
ANGLE

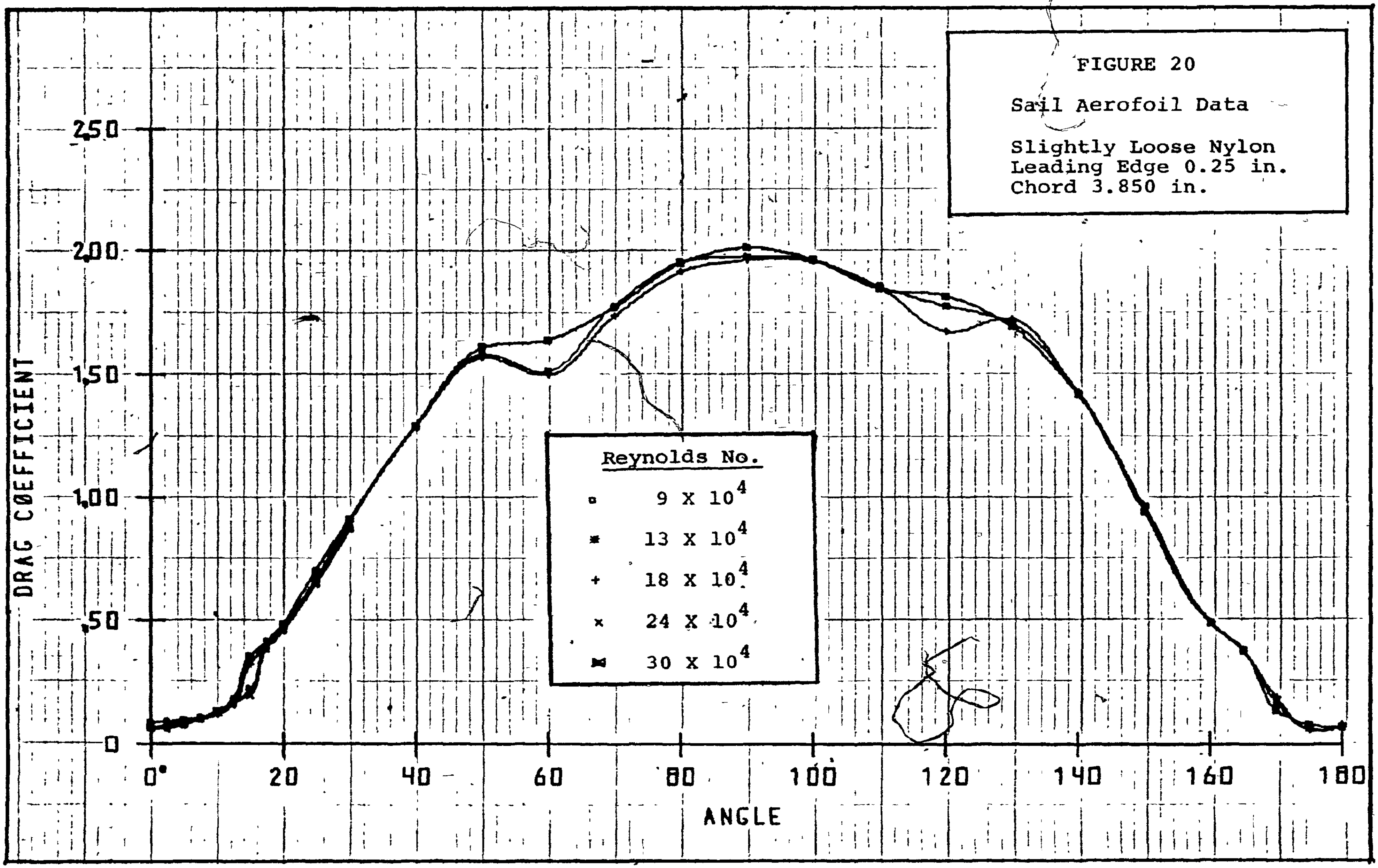
FIGURE 20
Sail Aerofoil Data
Slightly Loose Nylon
Leading Edge 0.25 in.
Chord 3.850 in.
Reynolds No.
9 X 10^4
13 X 10^4
18 X 10^4
24 X 10^4
30 X 10^4
DRAG COEFFICIENT
2.50
2.00
1.50
1.00
.50
0
0°
20
40
60
80
100
120
140
160
180
ANGLE

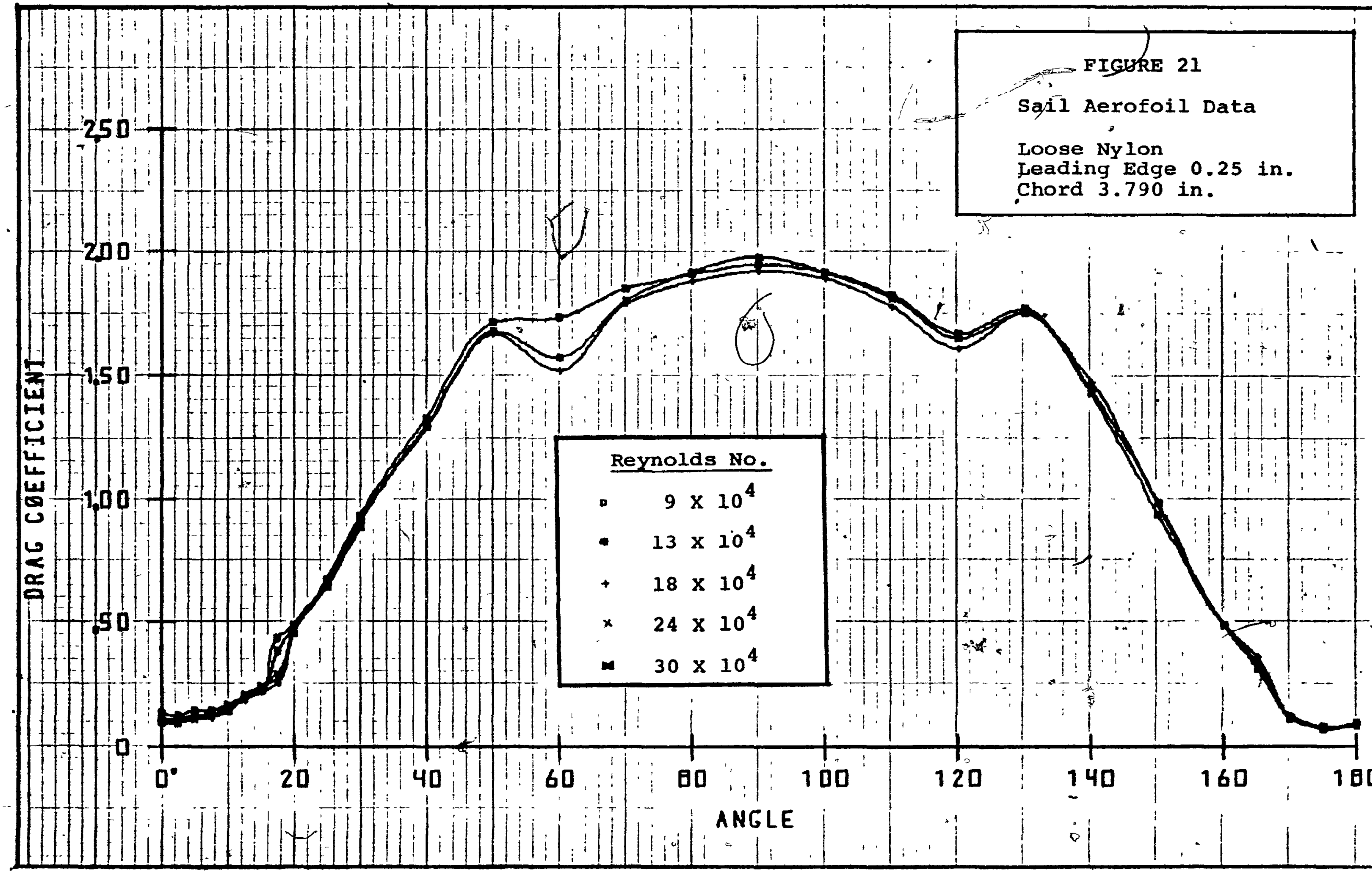

FIGURE 21
Sail Aerofoil Data
Loose Nylon
Leading Edge 0.25 in.
Chord 3.790 in.
Reynolds No.
9 X 10^4
13 X 10^4
18 X 10^4
24 X 10^4
30 X 10^4
DRAG COEFFICIENT
2.50
2.00
1.50
1.00
.50
0
0°
20
40
60
80
100
120
140
160
180
ANGLE

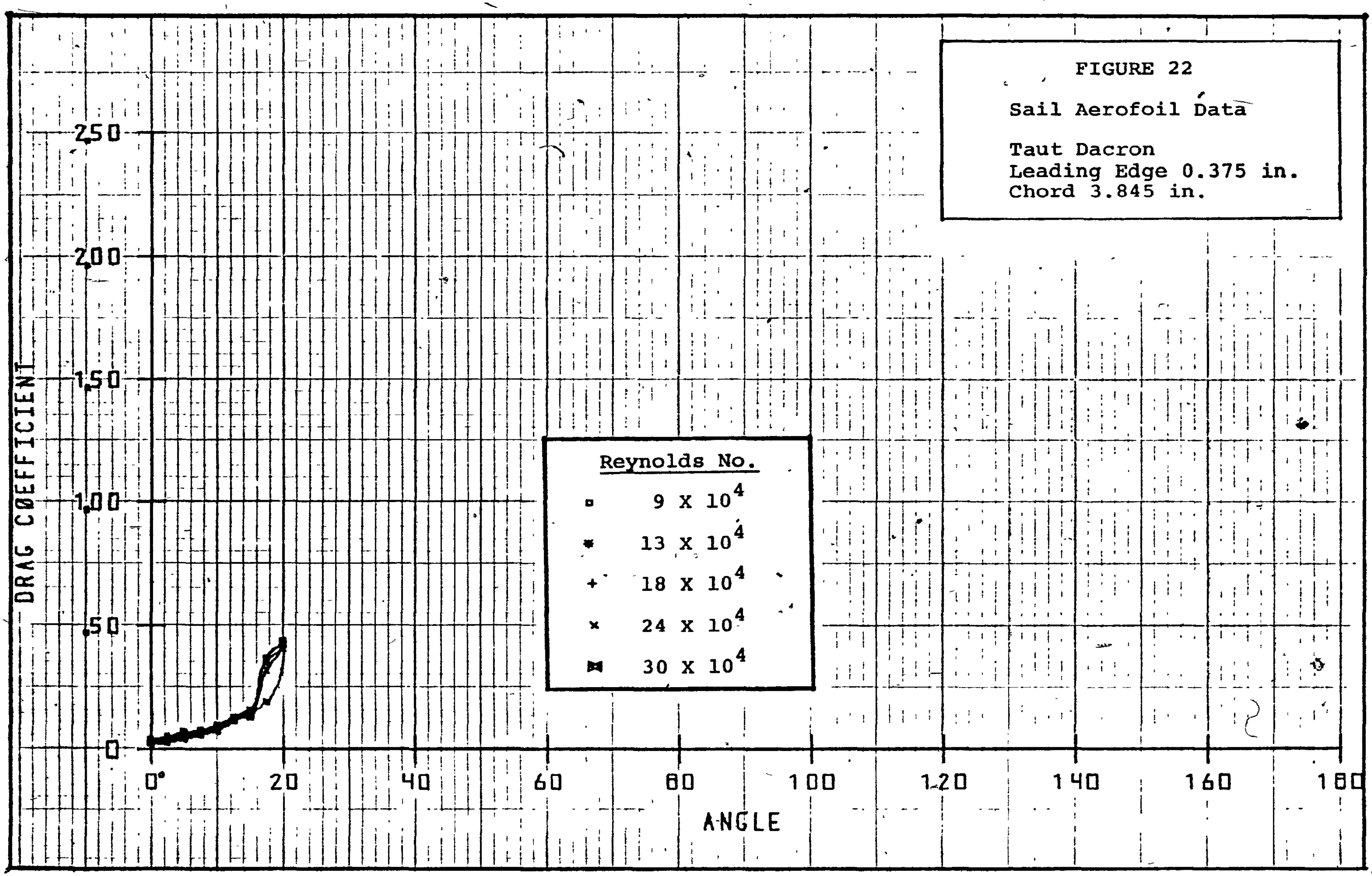

FIGURE 22
Sail Aerofoil Data
Taut Dacron
Leading Edge 0.375 in.
Chord 3.845 in.
Reynolds No.
9 X 10^4
13 X 10^4
18 X 10^4
24 X 10^4
30 X 10^4
DRAG CØEFFICIENT
2.50
2.00
1.50
1.00
.50
0
0°
20
40
60
80
100
120
140
160
180
ANGLE

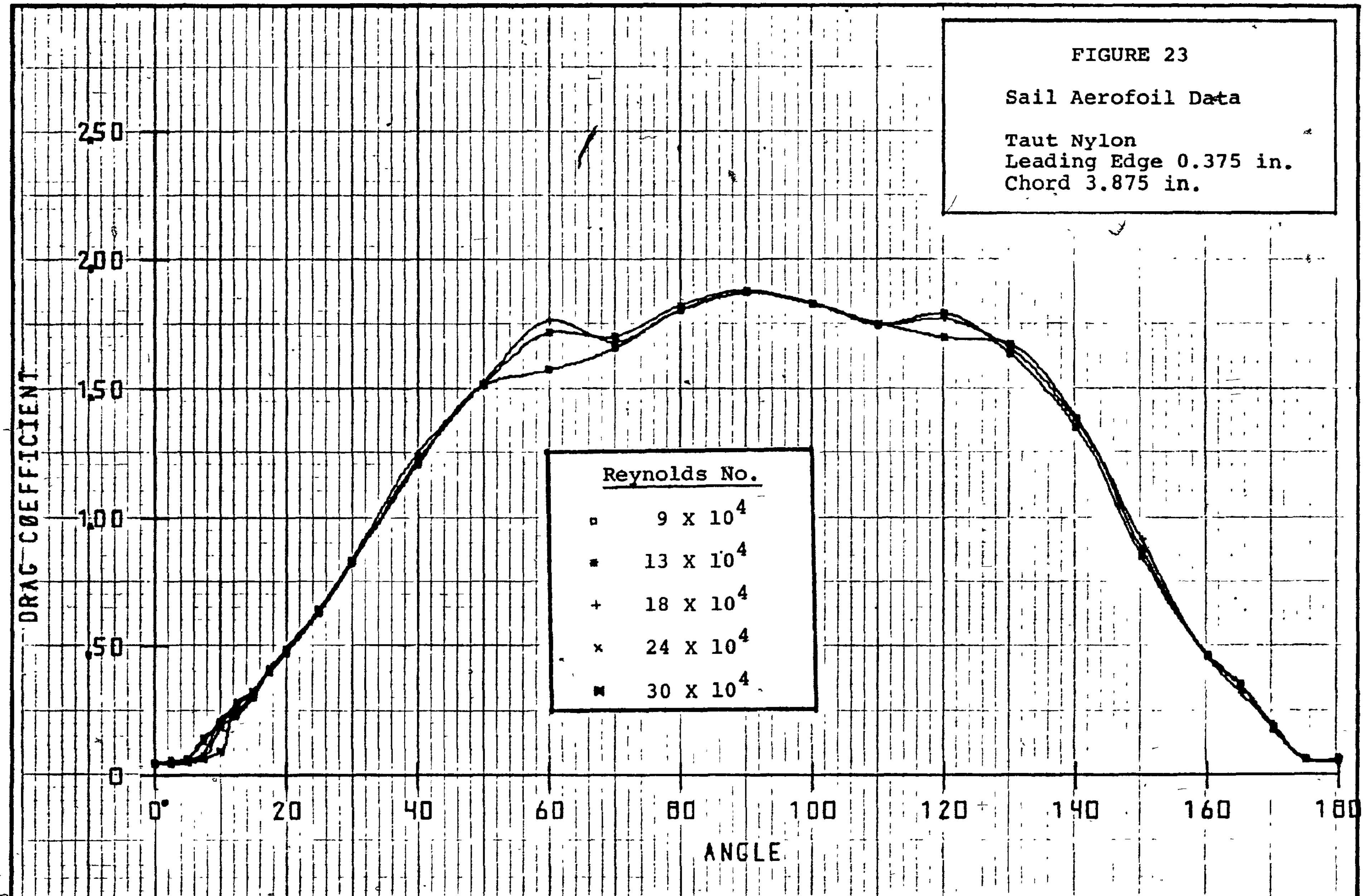
FIGURE 23
Sail Aerofoil Data
Taut Nylon
Leading Edge 0.375 in.
Chord 3.875 in.
Reynolds No.
9 X 10⁴
13 X 10⁴
18 X 10⁴
24 X 10⁴
30 X 10⁴
DRAG COEFFICIENT
2.50
2.00
1.50
1.00
.50
0
0°
20
40
60
80
100
120
140
160
180
ANGLE

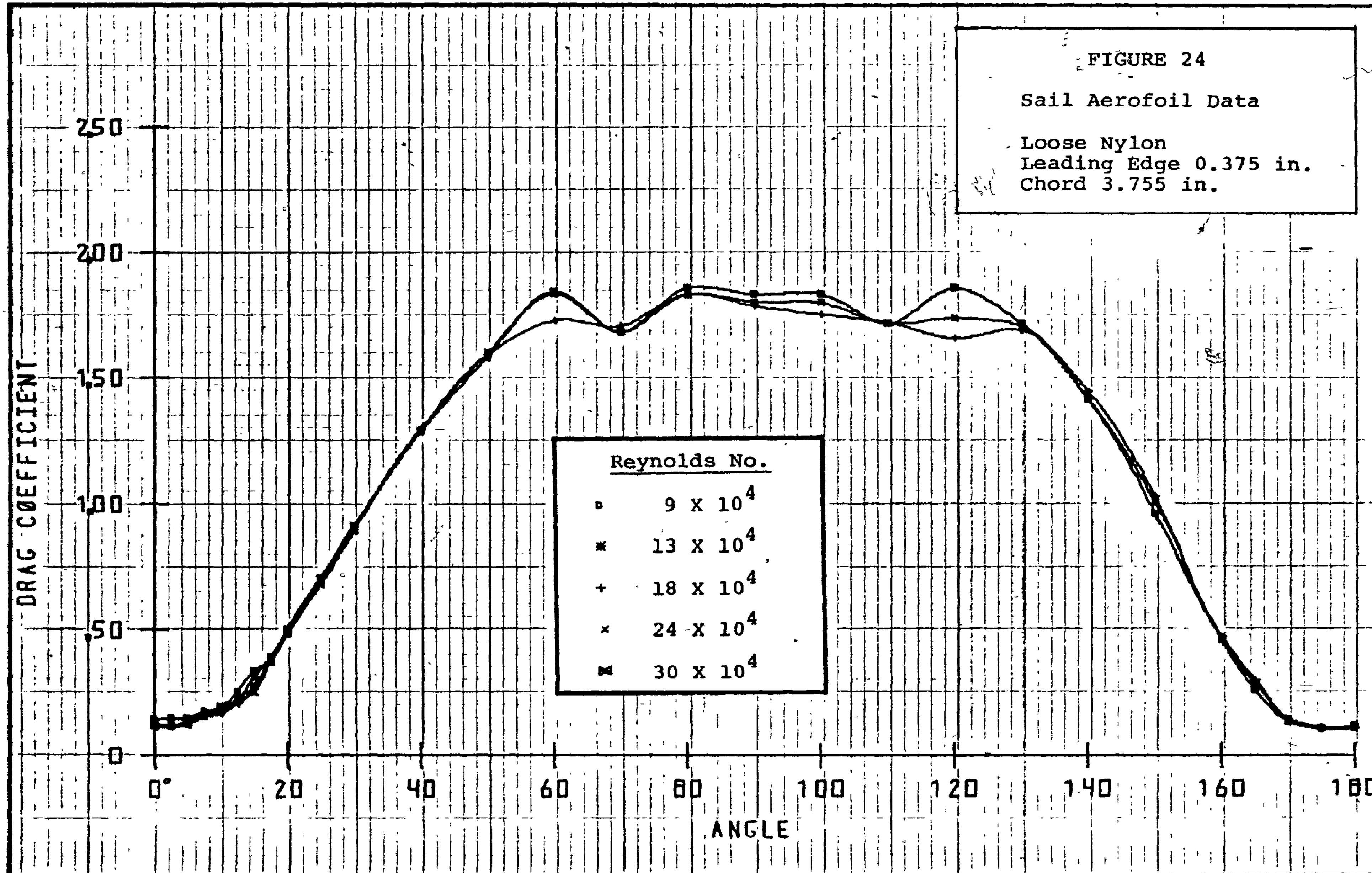
FIGURE 24
Sail Aerofoil Data
Loose Nylon
Leading Edge 0.375 in.
Chord 3.755 in.
Reynolds No.
9 X 10^4
13 X 10^4
18 X 10^4
24 X 10^4
30 X 10^4
DRAG COEFFICIENT
2.50
2.00
1.50
1.00
.50
0
0°
20
40
60
80
100
120
140
160
180
ANGLE

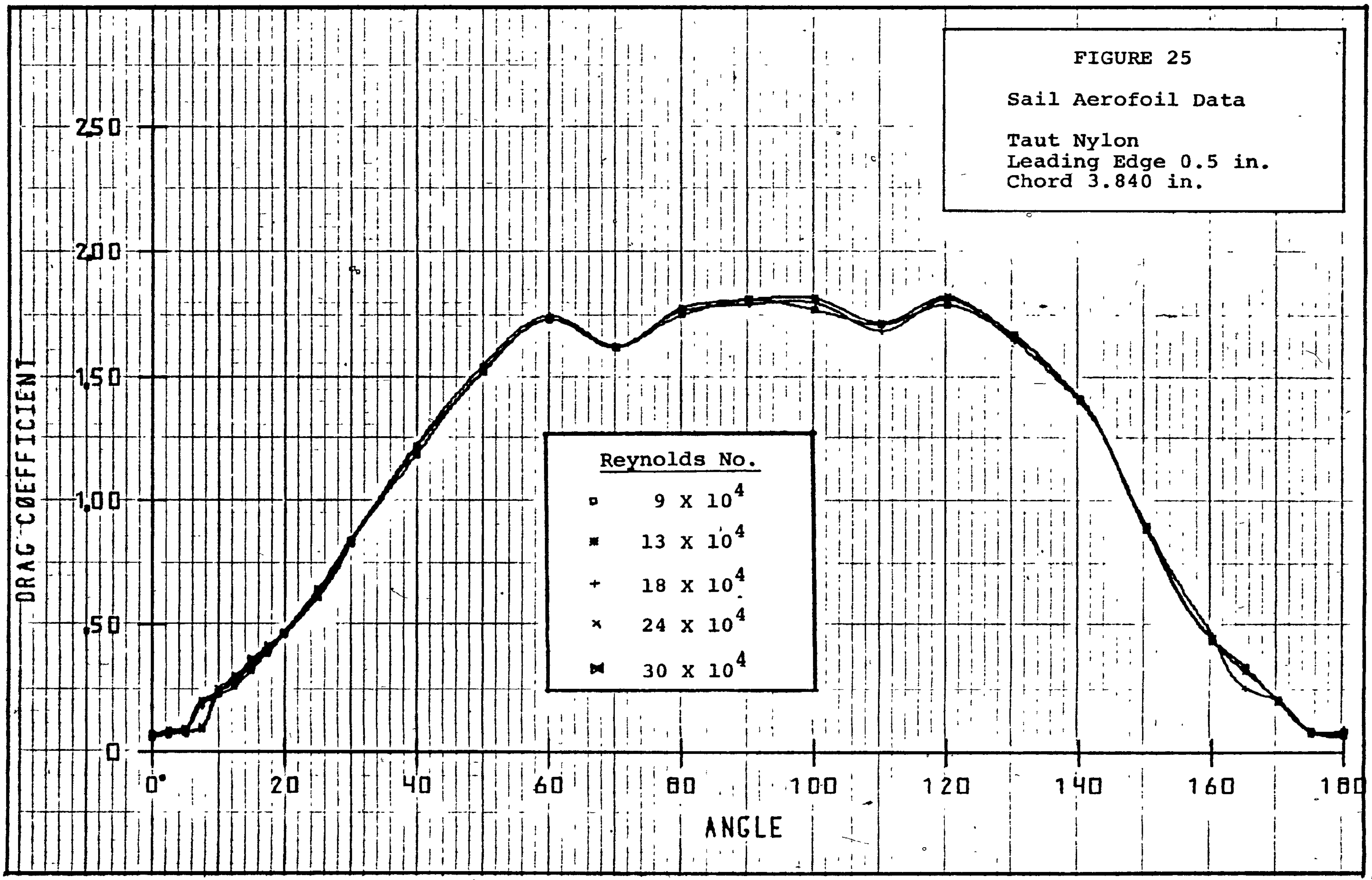
FIGURE 25
Sail Aerofoil Data
Taut Nylon
Leading Edge 0.5 in.
Chord 3.840 in.
Reynolds No.
9 X 10^4
13 X 10^4
18 X 10^4
24 X 10^4
30 X 10^4
DRAG COEFFICIENT
2.50
2.00
1.50
1.00
.50
0
0°
20
40
60
80
100
120
140
160
180
ANGLE

FIGURE 26: Sail Aerofoil Drag Coefficient from 0° to 20°

Taut Nylon Leading Edge 0.25 in. Chord 3.910 in.

α	Re = 9	13	18	24	30 $\times 10^4$
0.0	0.036	0.030	0.033	0.031	0.027
2.0	0.047	0.035	0.042	0.040	0.[illegible]34
5.0	0.091	0.086	0.073	0.065	0.054
7.5	0.145	0.136	0.125	0.108	0 080
10.0	0.184	0.198	0.205	0 195	0.178
12.5	0.229	0.241	0.254	0.267	0.265
15.0	0.270	0.279	0.295	0 327	0.339
17.5	0.327	0.337	0.346	0.359	0.379
20.0	0.409	0 412	0.417	0 421	0 442

Slightly Loose Nylon Leading Edge 0.25 in. Chord 3.850 in.

α	Re = 9	13	18	24	30 $\times 10^4$
0.0	0 088	0.076	0.069	0.070	0.066
2.5	0.097	0.079	0.073	0.068	0.067
5.0	0.101	0.089	0.082	0.082	0.082
7.5	0.109	0.103	0.105	0.104	0.107
10.0	0.133	0.130	0.124	0.132	0.137
12.5	0.180	0.171	0.158	0.166	0.174
15.0	0.356	0.356	0.319	0.195	0.218
17.5	0.415	0.406	0.404	0.399	0.384
20.0	0.486	0.474	0.467	0.463	0.459

Loose Nylon Leading Edge 0.25 in. Chord 3.790 in.

α	Re = 9	13	18	24	30 $\times 10^4$
0.0	0.133	0.114	0.102	0.098	0.099
2.5	0.124	0.110	0.101	0.094	0.094
5.0	0.144	0.125	0.114	0.109	0.114
7.5	0.147	0.125	0.121	0.125	0.144
10.0	0.156	0.147	0.144	0.152	0.167
12.5	0.192	0.189	0.187	0.169	0.203
15.0	0.222	0.218	0.213	0.229	0.242
17.5	0.436	0.383	0.250	0.268	0.288
20.0	0.487	0.485	0.481	0.468	0.456

Taut Dacron Leading Edge 0.375 in. Chord 3.845 in.

α	Re = 9	13	18	24	30 $\times 10^4$
0.0	0.036	0.030	0.028	0.024	0.020
2.5	0.047	0.041	0.034	0.031	0.023
5.0	0.063	0.058	0.054	0.047	0.040
7.5	0.072	0.068	0.064	0.058	0.053
10.0	0.090	0.087	0.081	0.077	0.071
12.5	0.121	0.125	0.118	0.112	0.109
15.0	0.127	0.156	0.153	0.146	0.141
17.5	0.364	0.365	0.350	0.318	0.188
20.0	0.433	0.430	0.408	0.405	0.422

Figure 27 - Sail Aeroroil Drag Coefficient from 0° to 20°
(continued)

Taut Nylon   Leading Edge 0.375 in.   Chord 3.875 in.

α	Re = 9	13	18	24	30 X 10^4
0.0	0.048	0.046	0.047	0.051	0.049
2.5	0.060	0.055	0.053	0.050	0.046
5.0	0.064	0.066	0.063	0.058	0.050
7.5	0.147	0.137	0.088	0.074	0.067
10.0	0.198	0.211	0.217	0.190	0.094
12.5	0.233	0.251	0.279	0.286	0.277
15.0	0.306	0.317	0.316	0.323	0.327
17.5	0.408	0.415	0.413	0.406	0.402
20.0	0.476	0.484	0.491	0.487	0.475

Loose Nylon   Leading Edge 0.375 in.   Chord 3.755 in.

α	Re = 9	13	18	24	30 X 10^4
0.0	0.145	0.141	0.129	0.120	0.117
2.5	0.150	0.147	0.121	0.120	0.115
5.0	0.152	0.141	0.134	0.129	0.127
7.5	0.176	0.164	0.157	0.156	0.168
10.0	0.193	0.180	0.169	0.177	0.191
12.5	0.249	0.221	0.204	0.213	0.224
15.0	0.336	0.311	0.266	0.252	0.277
17.5	0.381	0.393	0.392	0.388	0.371
20.0	0.501	0.488	0.485	0.485	0.484

Taut Nylon   Leading Edge 0.5 in.   Chord 3.840 in.

α	Re = 9	13	18	24	30 X 10^4
0.0	0.056	0.060	0.062	0.063	0.061
2.5	0.066	0.077	0.072	0.073	0.069
5.0	0.080	0.083	0.080	0.075	0.071
7.5	0.190	0.200	0.176	0.085	0.090
10.0	0.228	0.239	0.245	0.254	0.230
12.5	0.265	0.283	0.292	0.308	0.305
15.0	0.335	0.354	0.355	0.368	0.373
17.5	0.401	0.410	0.407	0.413	0.418
20.0	0.463	0.472	0.465	0.464	0.464

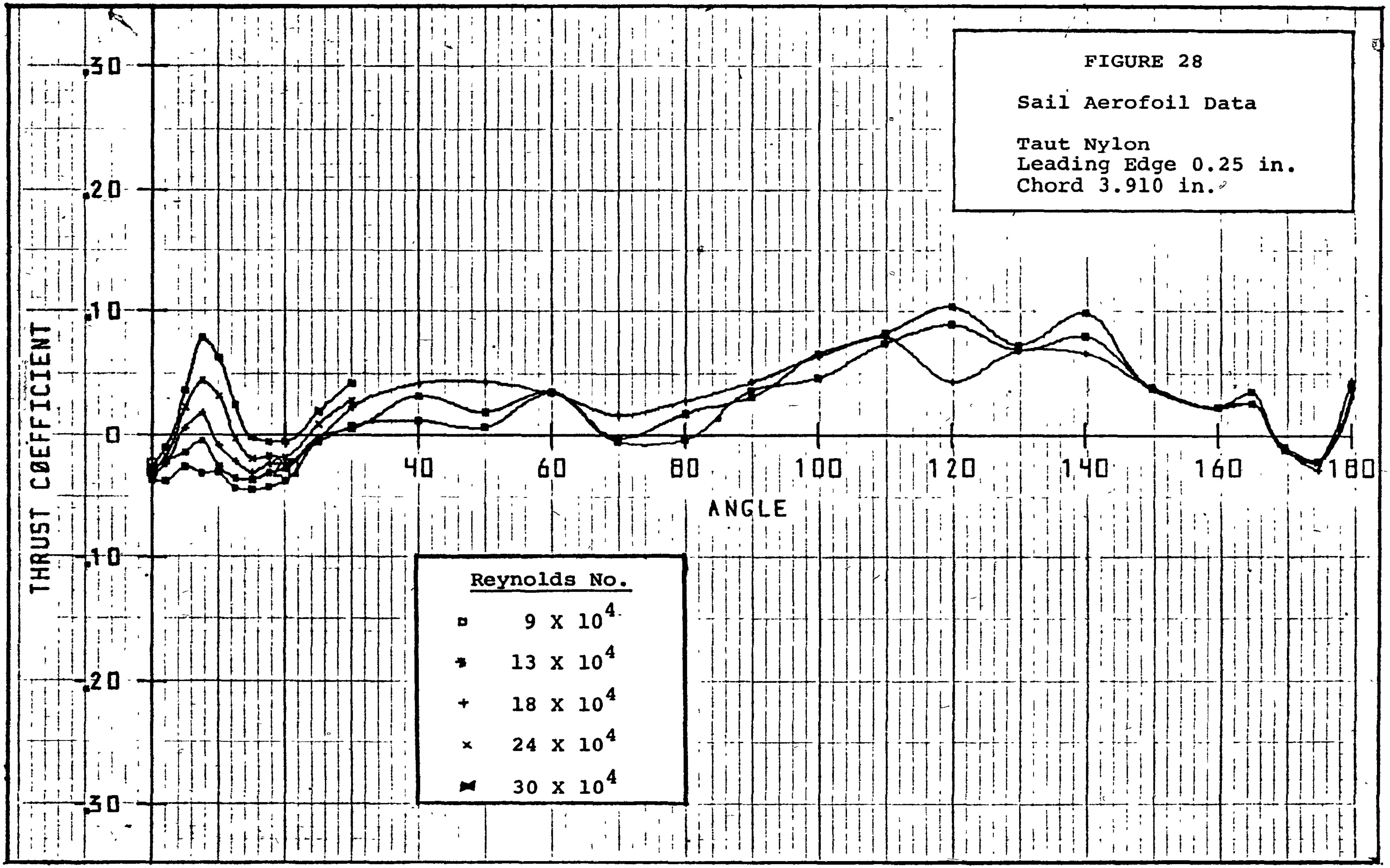

FIGURE 28
Sail Aerofoil Data
Taut Nylon
Leading Edge 0.25 in.
Chord 3.910 in.
.30
.20
.10
0
.10
.20
.30
THRUST COEFFICIENT
40
60
80
100
120
140
160
180
ANGLE
Reynolds No.
9 X 10^4
13 X 10^4
18 X 10^4
24 X 10^4
30 X 10^4

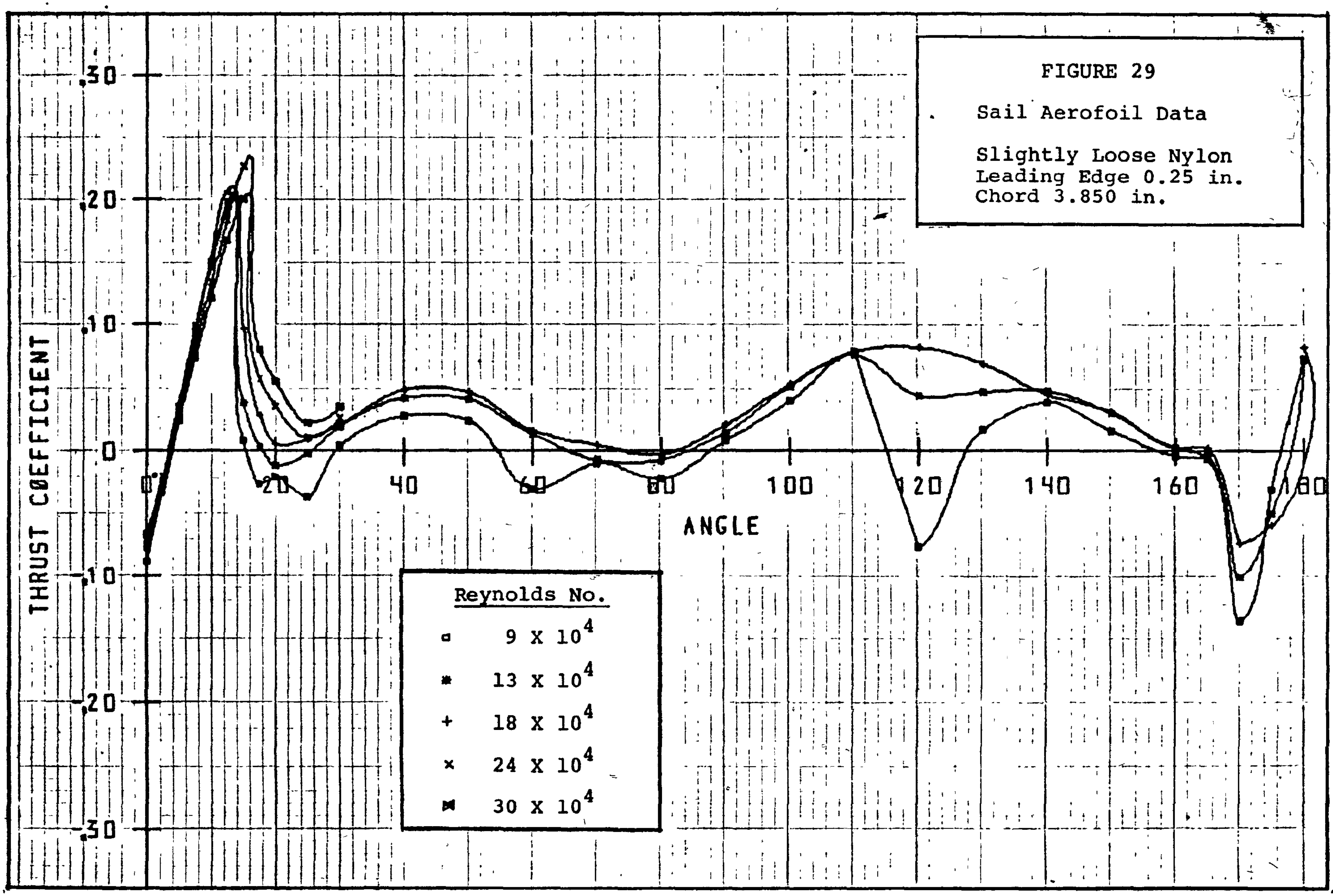
FIGURE 29
Sail Aerofoil Data
Slightly Loose Nylon
Leading Edge 0.25 in.
Chord 3.850 in.
THRUST COEFFICIENT
.30
.20
.10
0
.10
.20
.30
0
20
40
60
80
100
120
140
160
180
ANGLE
Reynolds No.
9 X 10^4
13 X 10^4
18 X 10^4
24 X 10^4
30 X 10^4

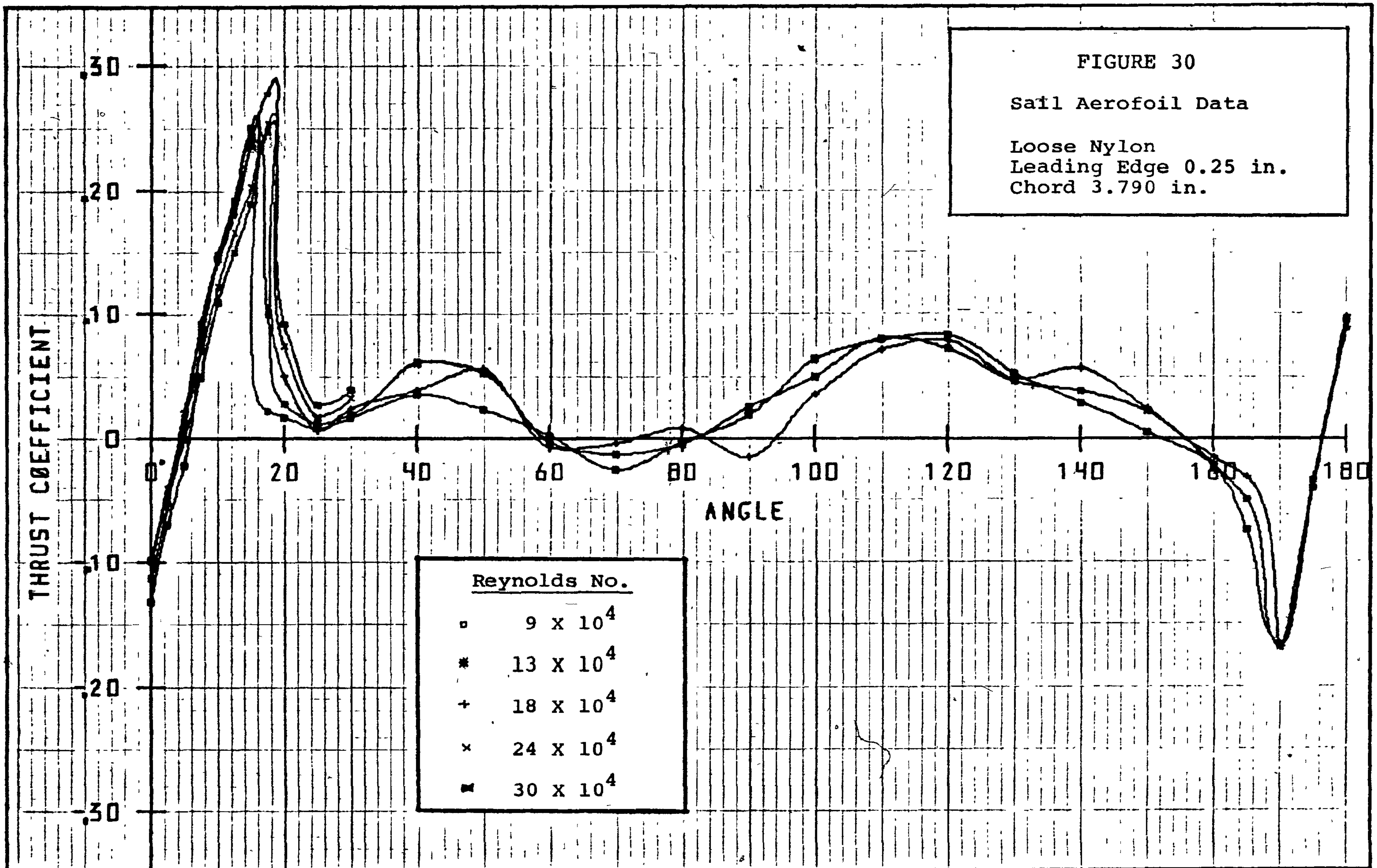

FIGURE 30
Sail Aerofoil Data
Loose Nylon
Leading Edge 0.25 in.
Chord 3.790 in.
THRUST COEFFICIENT
.30
.20
.10
0
-.10
-.20
-.30
0°
20
40
60
80
100
120
140
160
180
ANGLE
Reynolds No.
9 X 10⁴
13 X 10⁴
18 X 10⁴
24 X 10⁴
30 X 10⁴

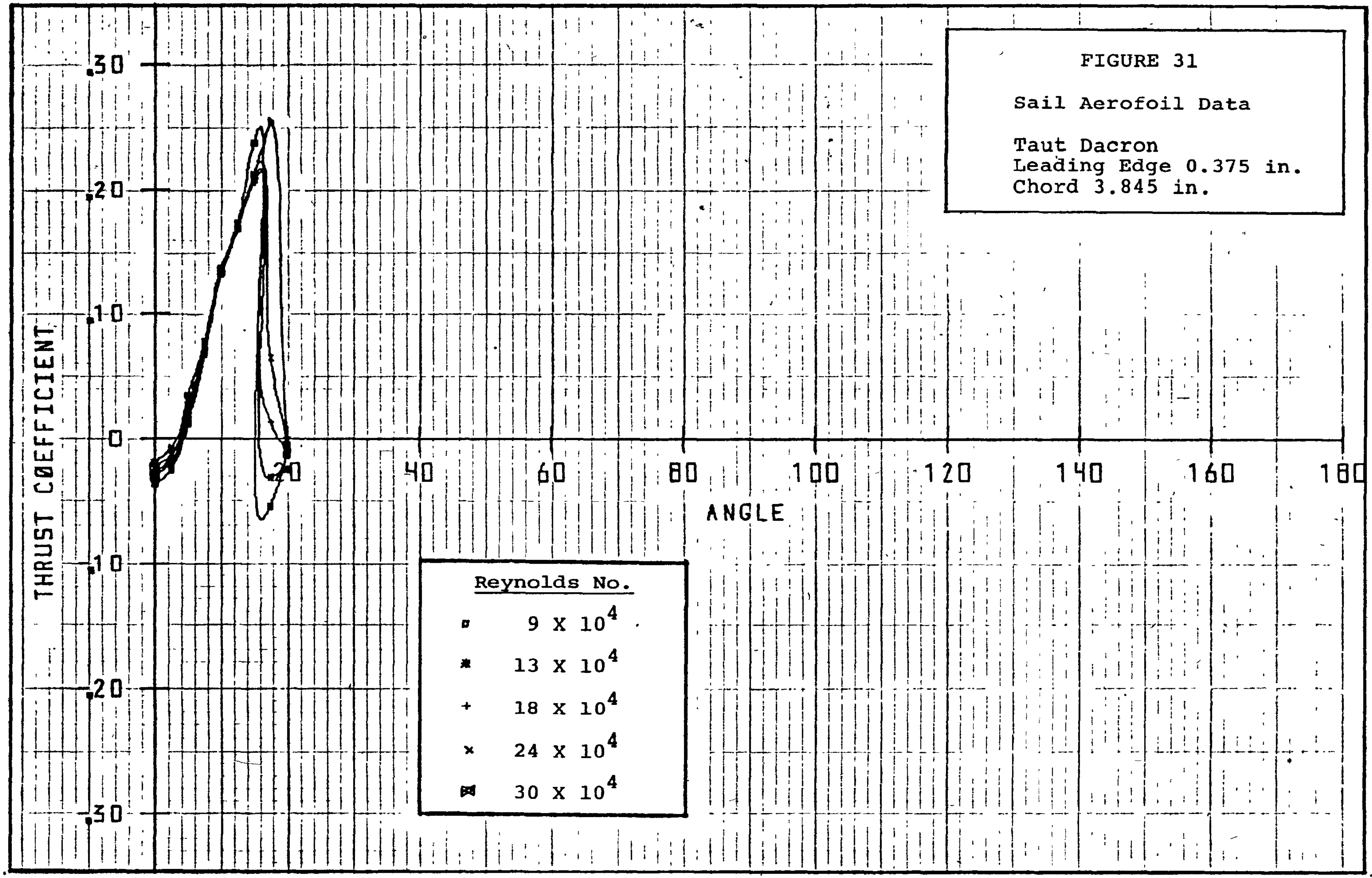
FIGURE 31
Sail Aerofoil Data
Taut Dacron
Leading Edge 0.375 in.
Chord 3.845 in.
THRUST COEFFICIENT
.30
.20
.10
0
.10
.20
.30
20
40
60
80
100
120
140
160
180
ANGLE
Reynolds No.
9 X 10^4
13 X 10^4
18 X 10^4
24 X 10^4
30 X 10^4

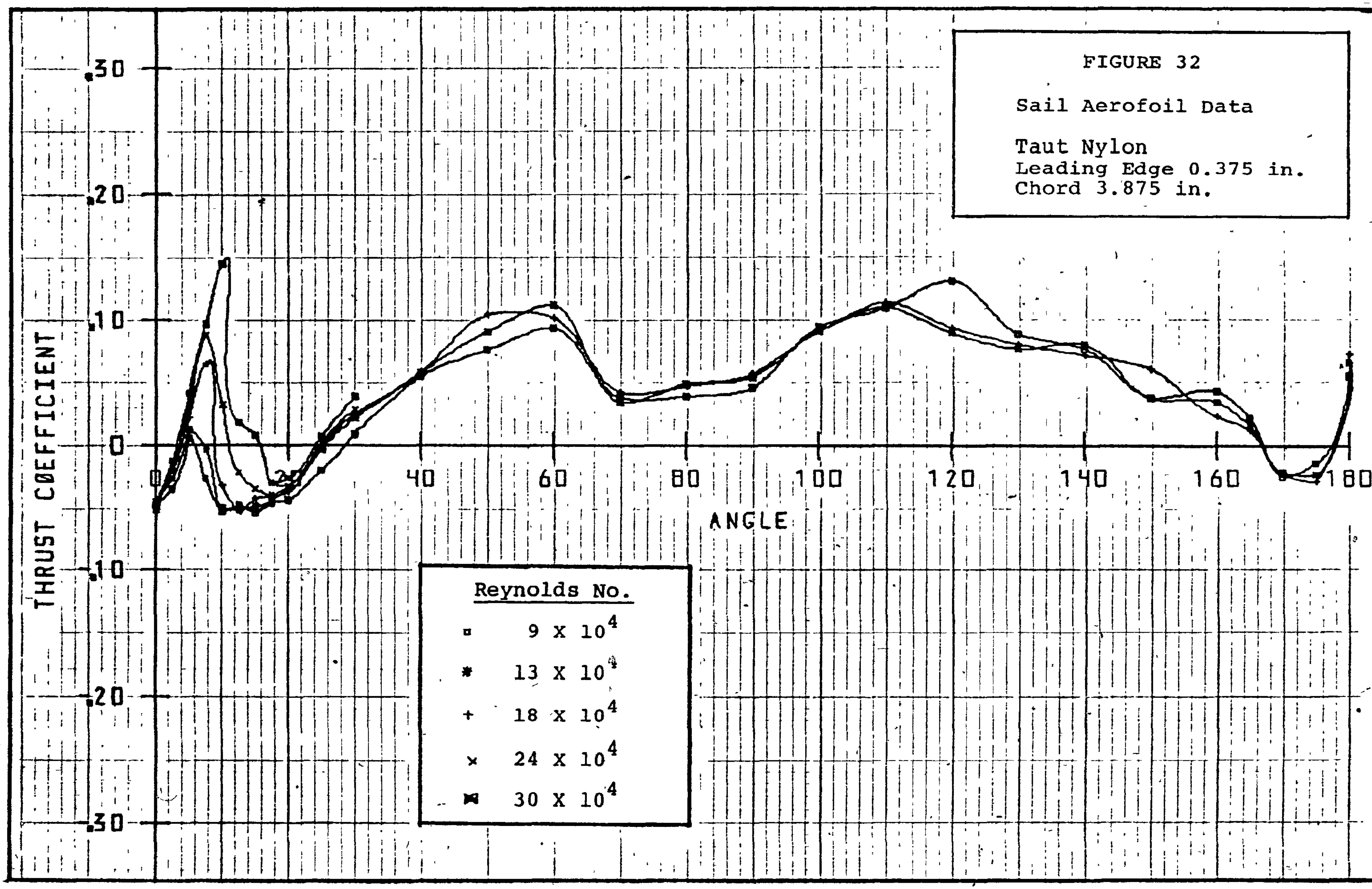
FIGURE 32
Sail Aerofoil Data
Taut Nylon
Leading Edge 0.375 in.
Chord 3.875 in.
THRUST CØEFFICIENT
.30
.20
.10
0
-.10
-.20
-.30
0
20
40
60
80
100
120
140
160
180
ANGLE
Reynolds No.
9 X 10^4
13 X 10^4
18 X 10^4
24 X 10^4
30 X 10^4

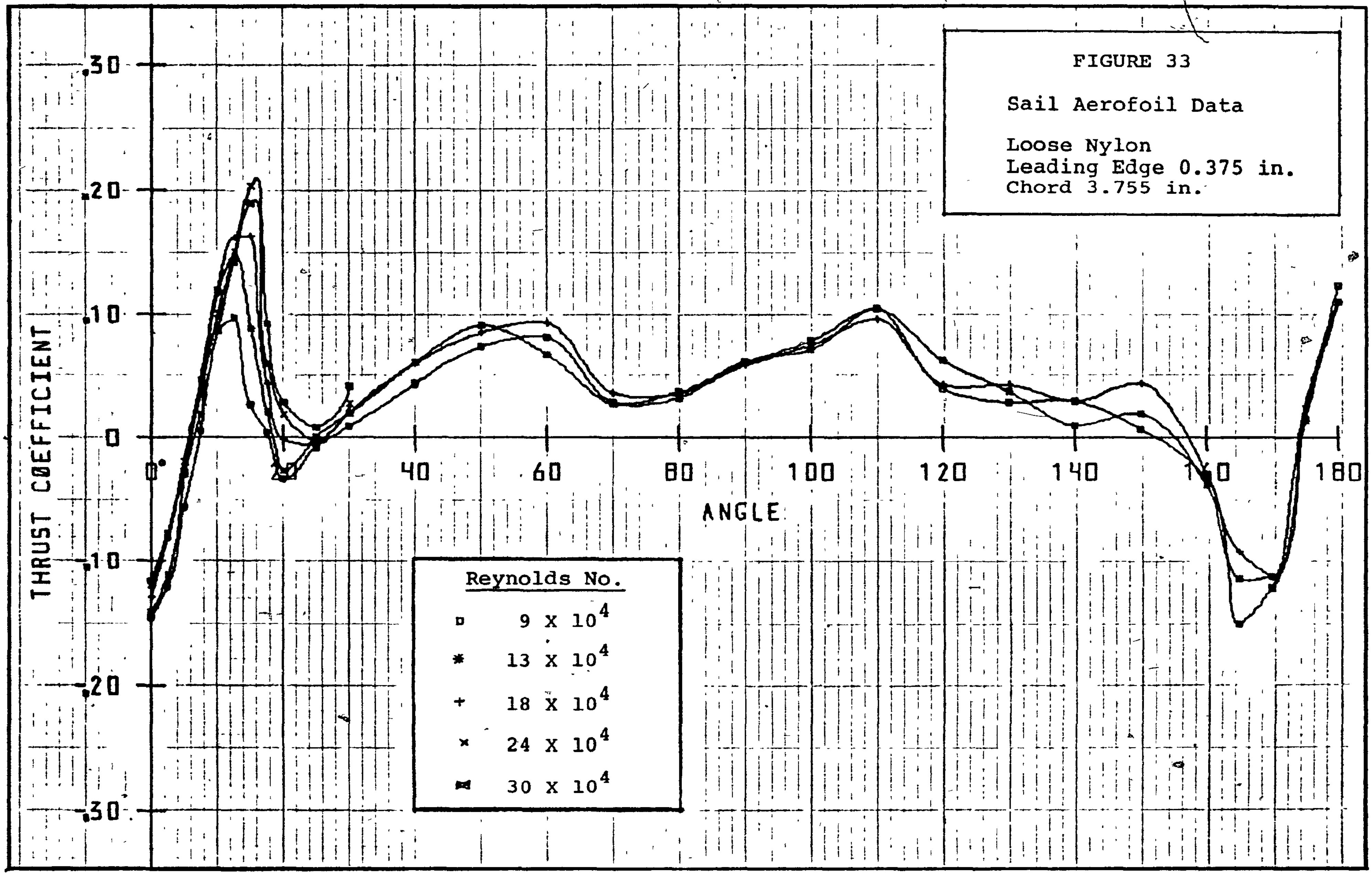
FIGURE 33
Sail Aerofoil Data
Loose Nylon
Leading Edge 0.375 in.
Chord 3.755 in.
THRUST CØEFFICIENT
.30
.20
.10
0
.10
.20
.30
0°
20
40
60
80
100
120
140
160
180
ANGLE
Reynolds No.
9 X 10^4
13 X 10^4
18 X 10^4
24 X 10^4
30 X 10^4

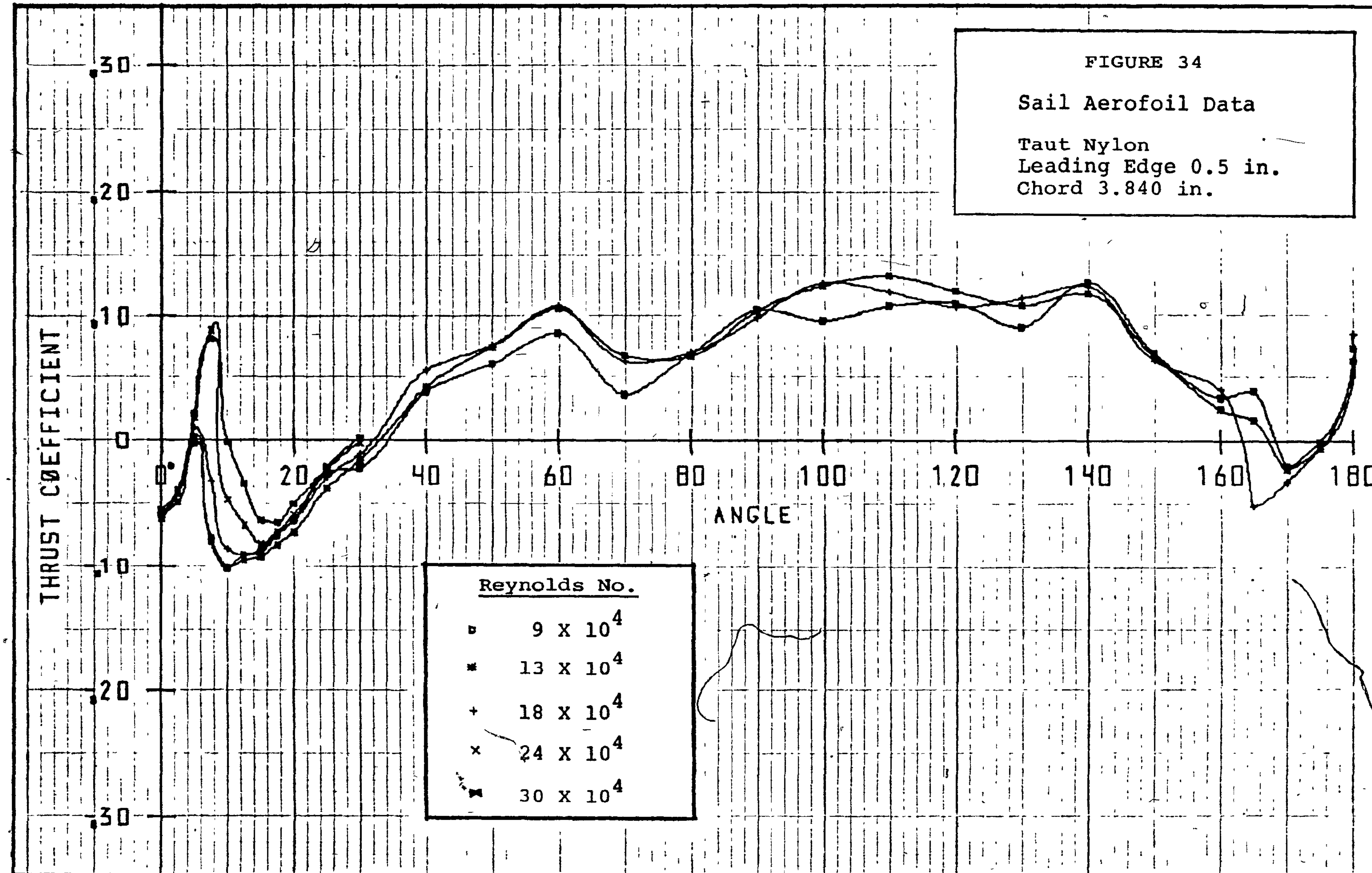
FIGURE 34
Sail Aerofoil Data
Taut Nylon
Leading Edge 0.5 in.
Chord 3.840 in.
THRUST COEFFICIENT
.30
.20
.10
0
-.10
-.20
-.30
0°
20
40
60
80
100
120
140
160
180
ANGLE
Reynolds No.
9 X 10^4
13 X 10^4
18 X 10^4
24 X 10^4
30 X 10^4

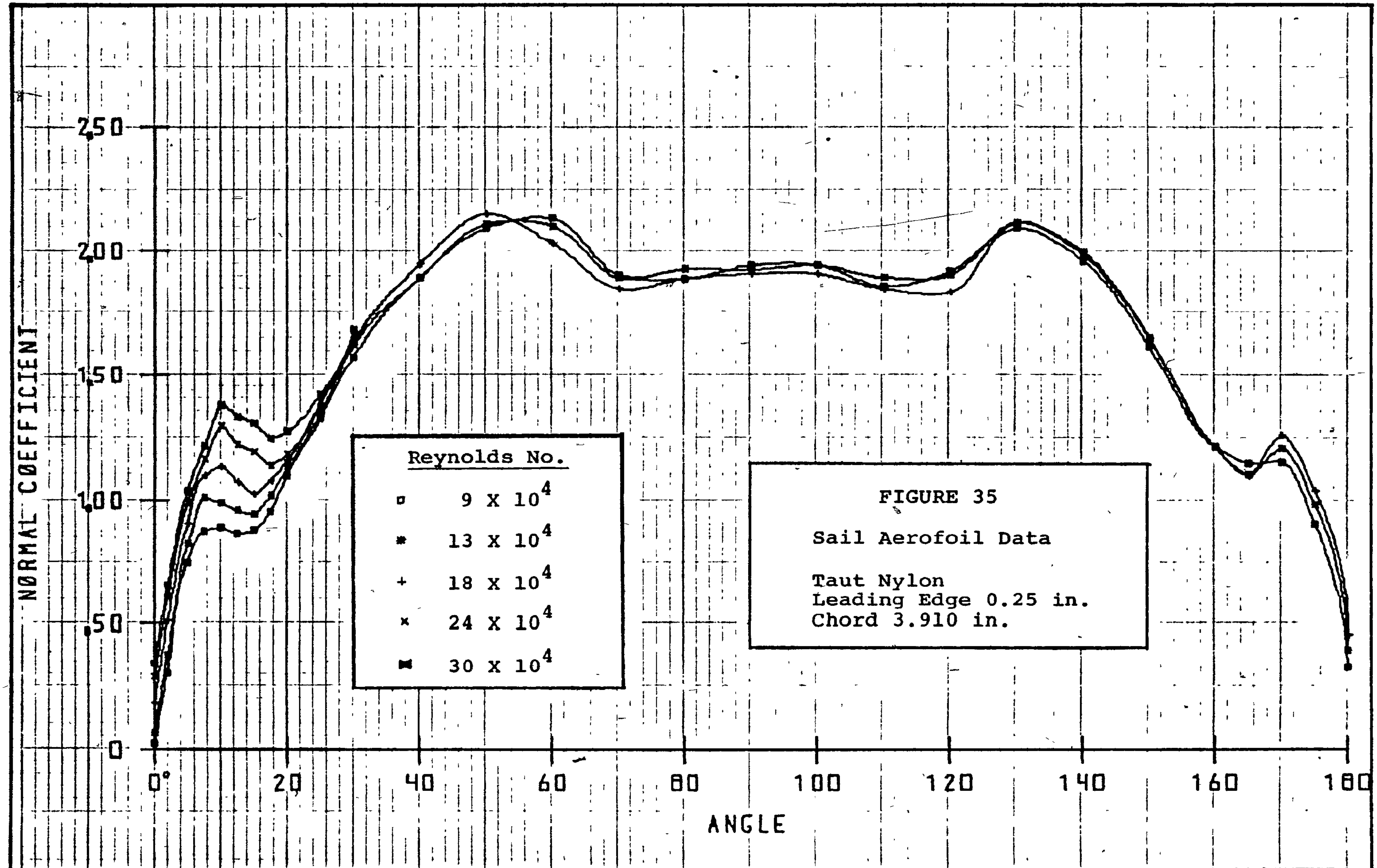

NØRMAL CØEFFICIENT
250
200
150
100
50
0
0°
20
40
60
80
100
120
140
160
180
ANGLE
Reynolds No.
9 X 10^4
13 X 10^4
18 X 10^4
24 X 10^4
30 X 10^4
FIGURE 35
Sail Aerofoil Data
Taut Nylon
Leading Edge 0.25 in.
Chord 3.910 in.

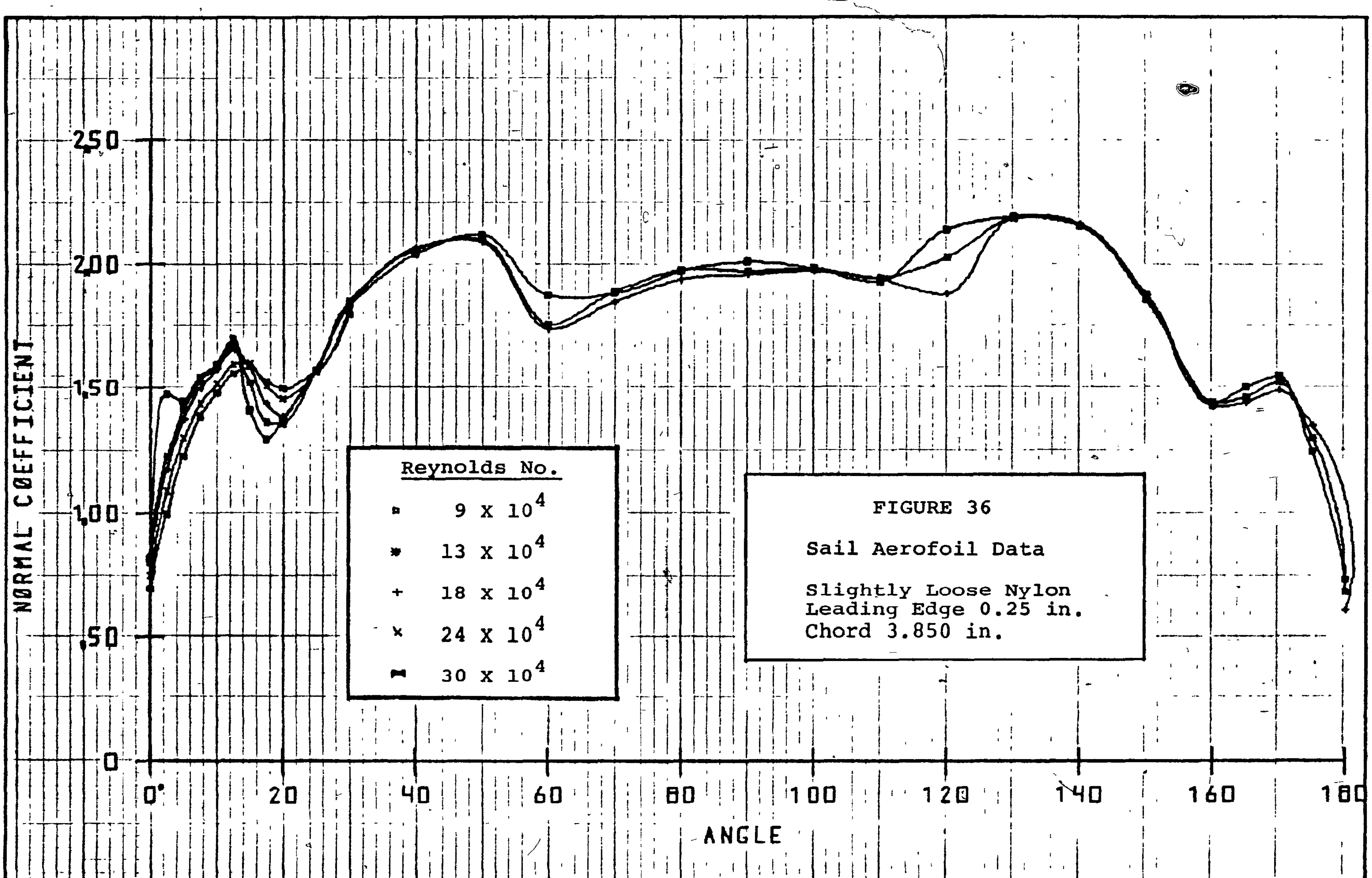

NORMAL COEFFICIENT
2.50
2.00
1.50
1.00
.50
0
0°
20
40
60
80
100
120
140
160
180
ANGLE
Reynolds No.
9 X 10^4
13 X 10^4
18 X 10^4
24 X 10^4
30 X 10^4
FIGURE 36
Sail Aerofoil Data
Slightly Loose Nylon
Leading Edge 0.25 in.
Chord 3.850 in.

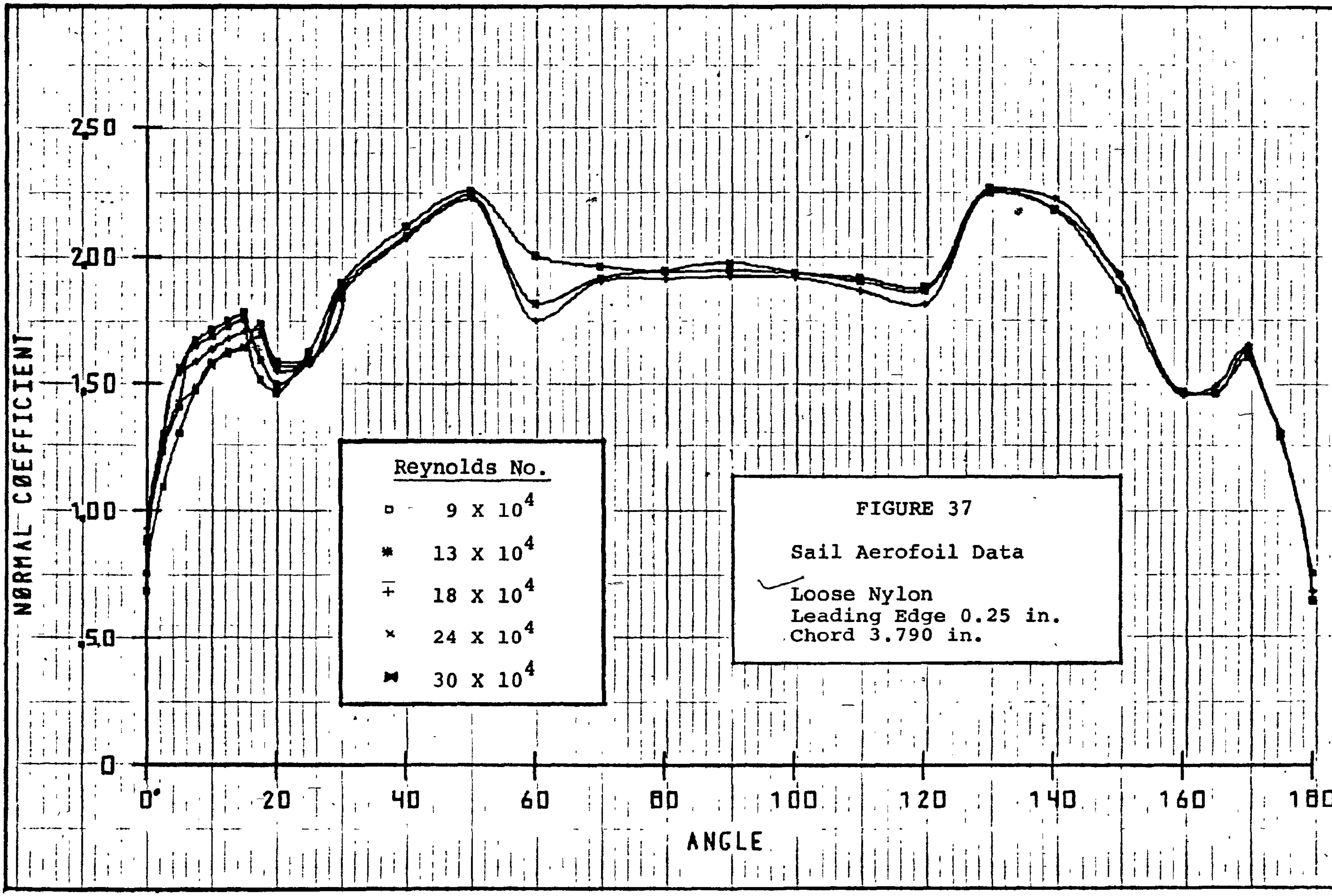

FIGURE 37

Sail Aerofoil Data

Loose Nylon
Leading Edge 0.25 in.
Chord 3.790 in.

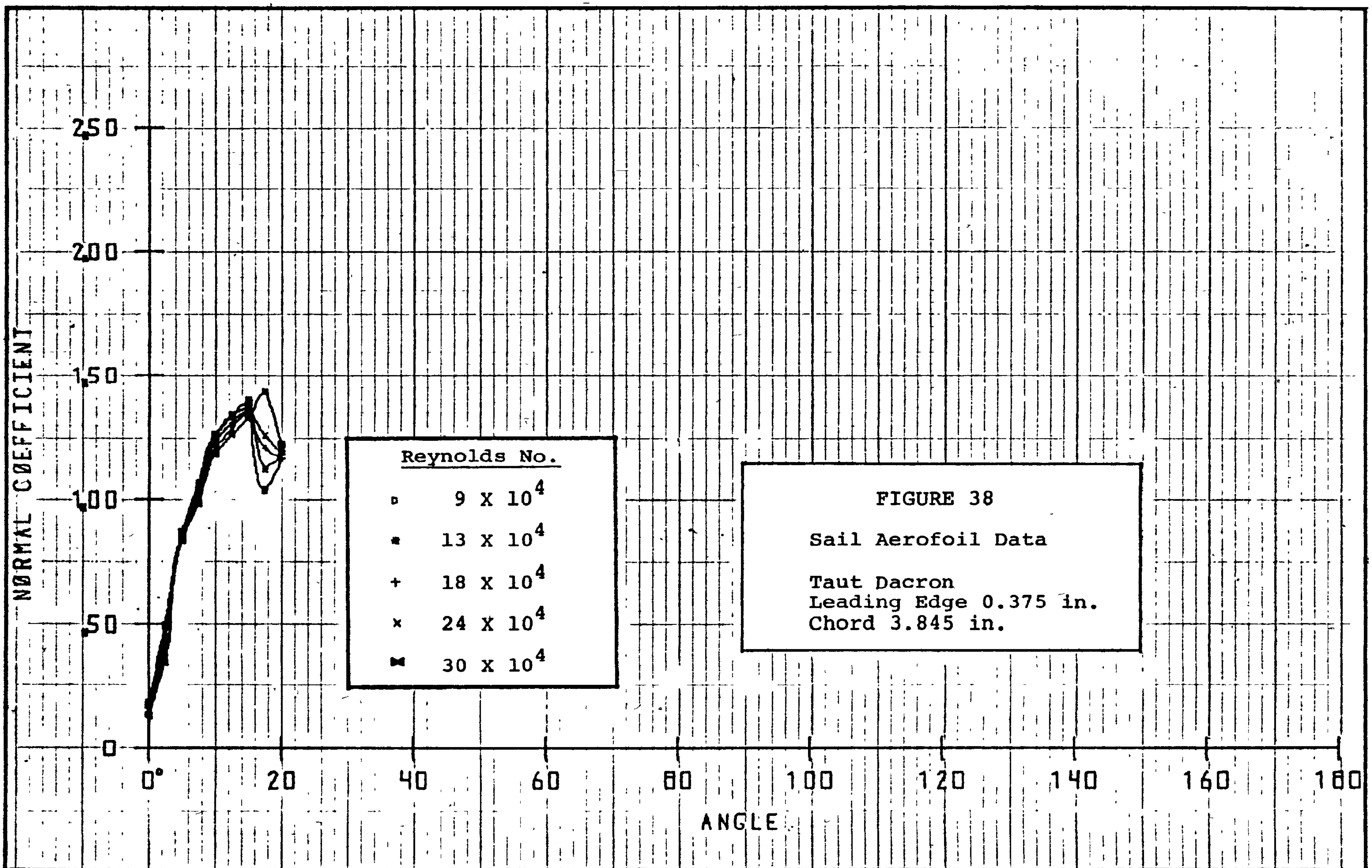
NØRMAL CØEFFICIENT
250
200
150
100
50
0
0°
20
40
60
80
100
120
140
160
180
ANGLE
Reynolds No.
9 X 10^4
13 X 10^4
18 X 10^4
24 X 10^4
30 X 10^4
FIGURE 38
Sail Aerofoil Data
Taut Dacron
Leading Edge 0.375 in.
Chord 3.845 in.

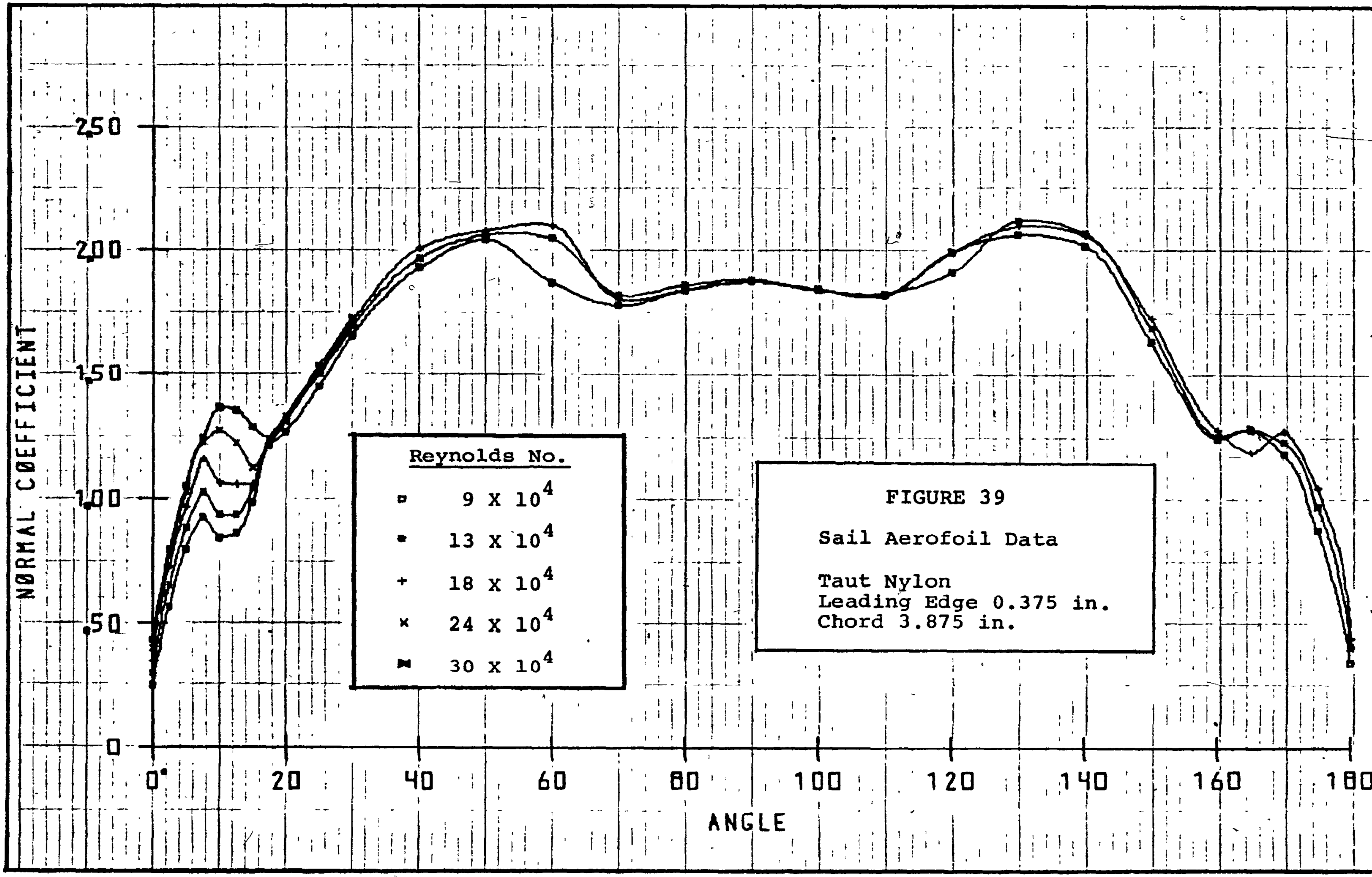

FIGURE 39

Sail Aerofoil Data

Taut Nylon
Leading Edge 0.375 in.
Chord 3.875 in.

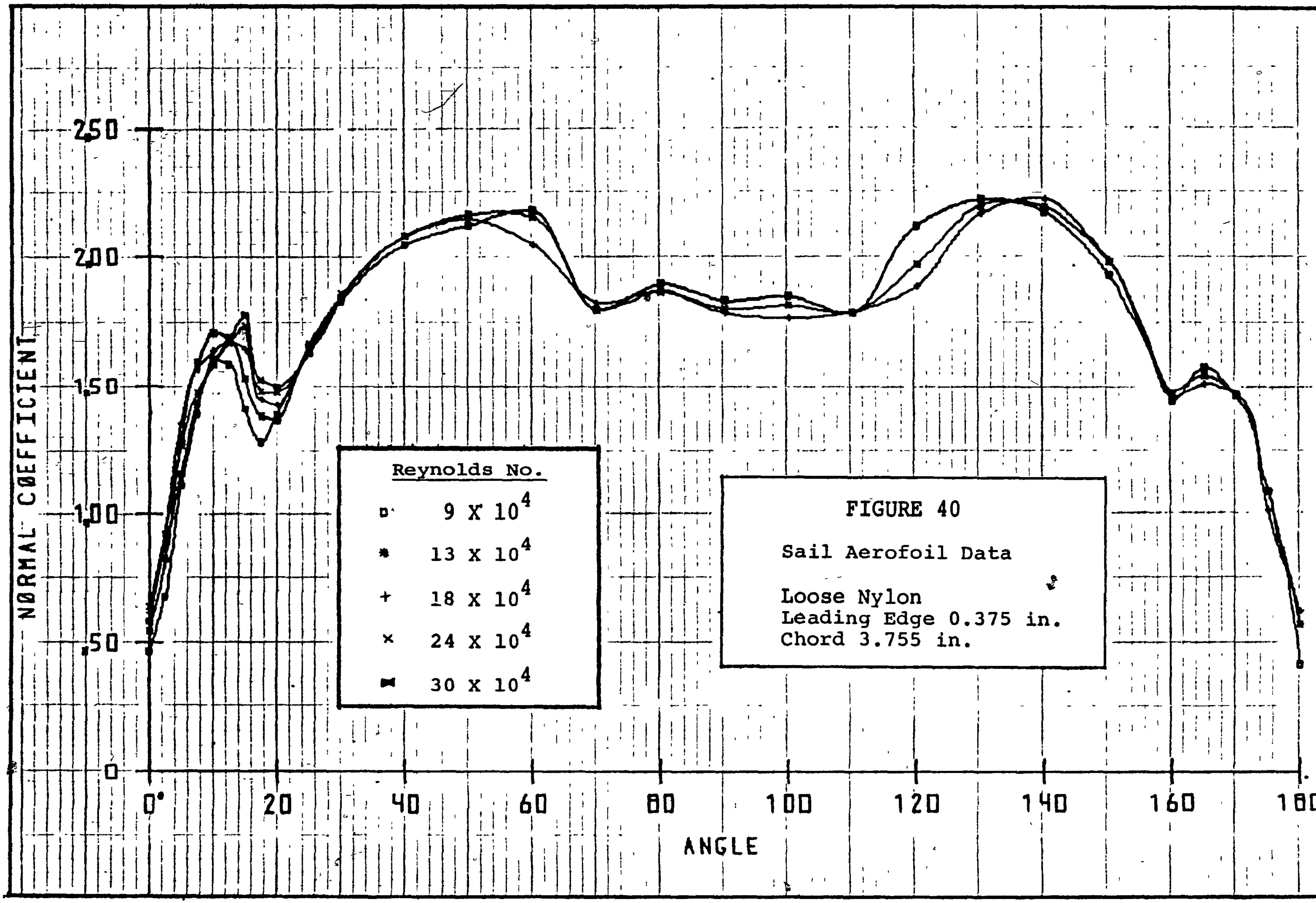

FIGURE 40

Sail Aerofoil Data

Loose Nylon
Leading Edge 0.375 in.
Chord 3.755 in.

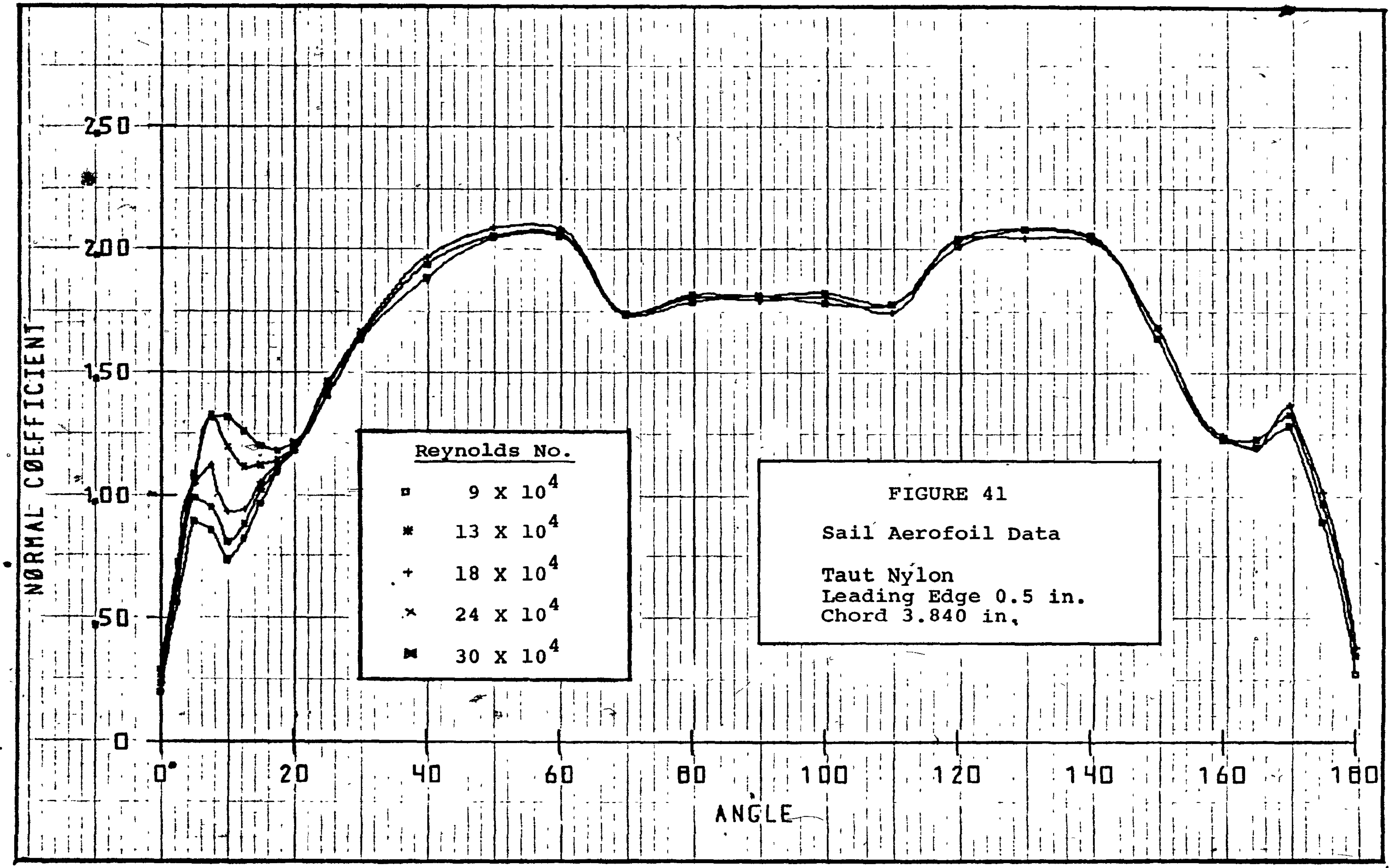

NORMAL COEFFICIENT
2.50
2.00
1.50
1.00
.50
0
0°
20
40
60
80
100
120
140
160
180
ANGLE
Reynolds No.
9 X 10^4
13 X 10^4
18 X 10^4
24 X 10^4
30 X 10^4
FIGURE 41
Sail Aerofoil Data
Taut Nylon
Leading Edge 0.5 in.
Chord 3.840 in.

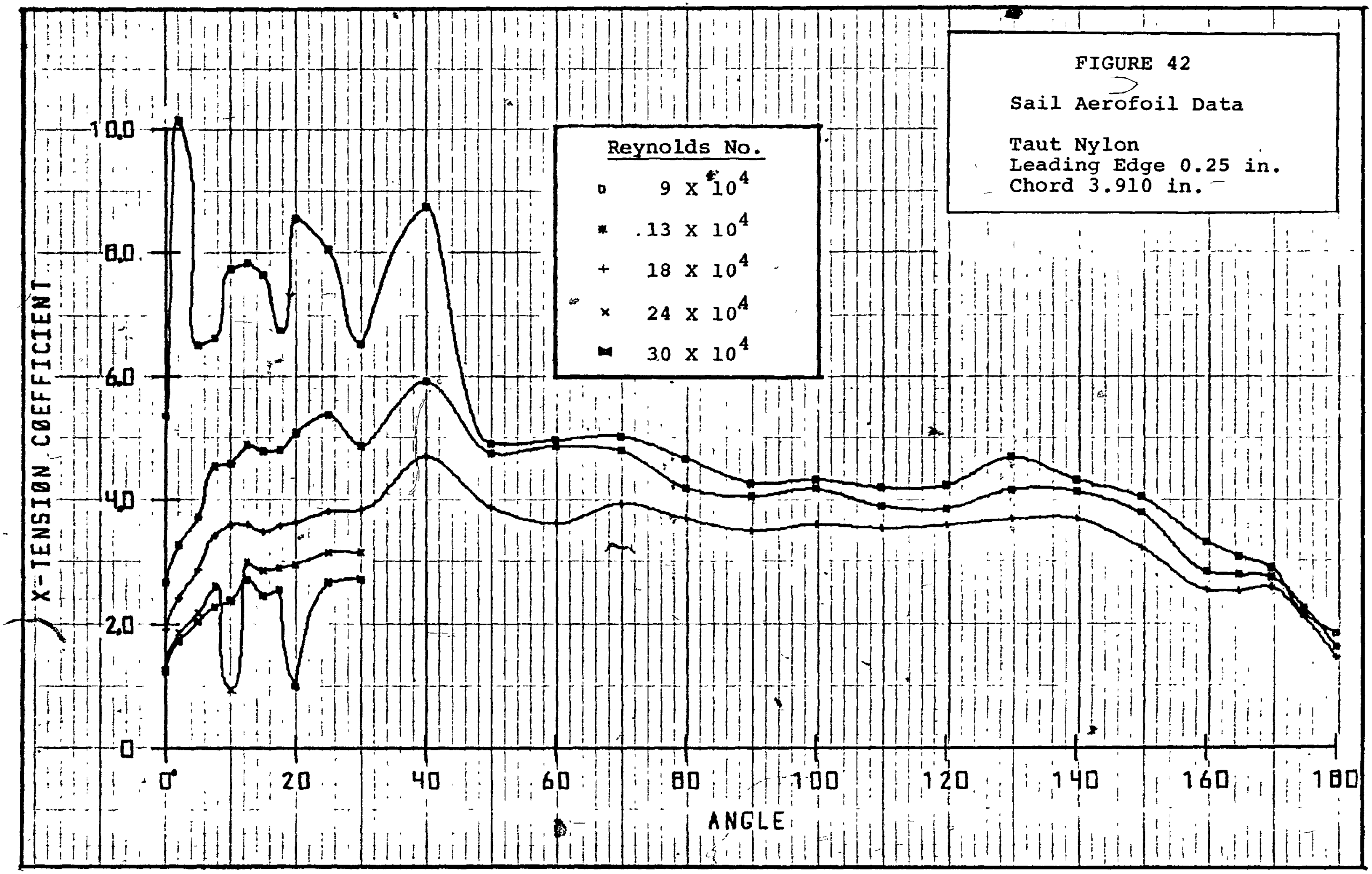

FIGURE 42
Sail Aerofoil Data
Taut Nylon
Leading Edge 0.25 in.
Chord 3.910 in.
Reynolds No.
9 X 10^4
.13 X 10^4
18 X 10^4
24 X 10^4
30 X 10^4
X-TENSIØN CØEFFICIENT
10.0
8.0
6.0
4.0
2.0
0
0°
20
40
60
80
100
120
140
160
180
ANGLE

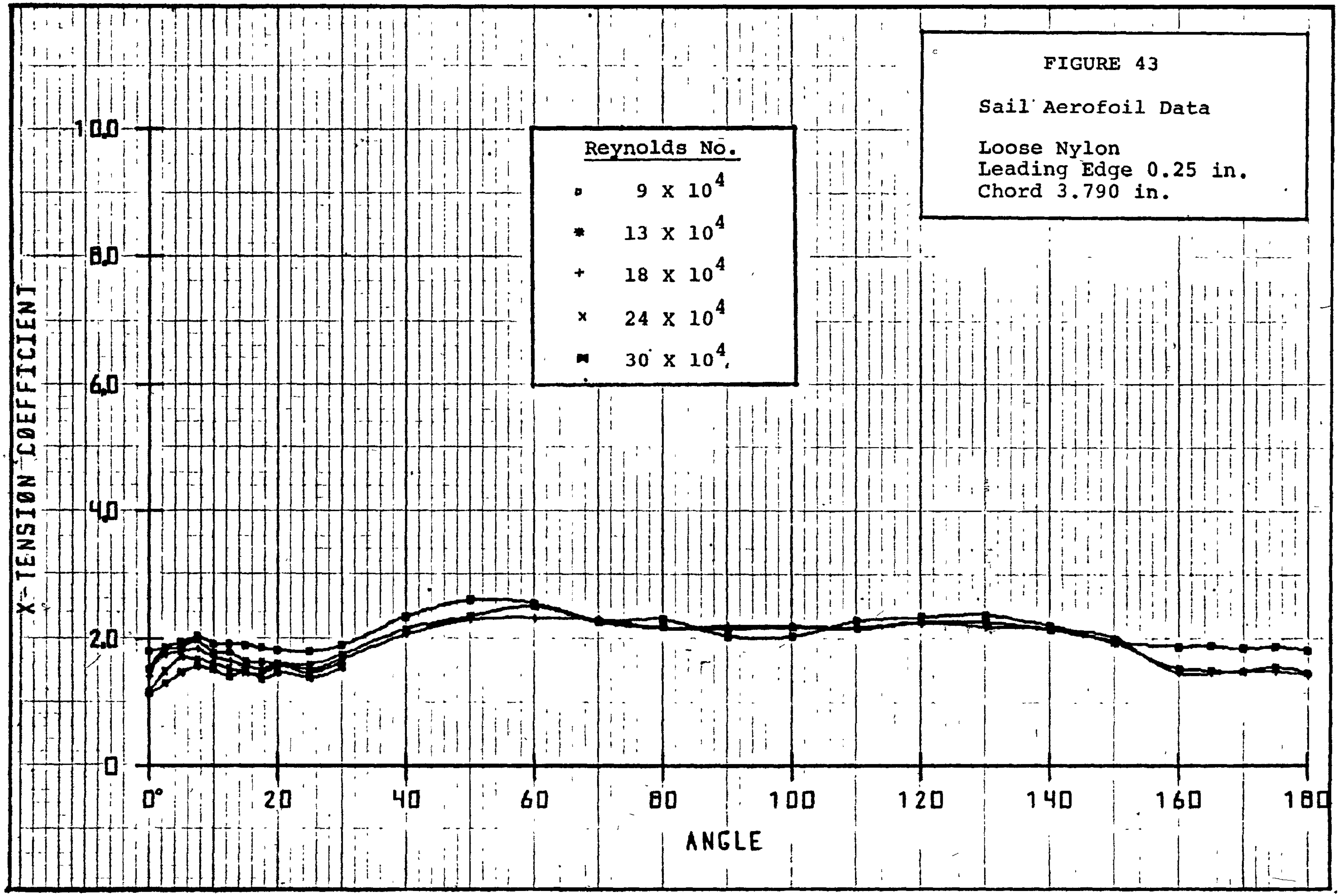
FIGURE 43
Sail Aerofoil Data
Loose Nylon
Leading Edge 0.25 in.
Chord 3.790 in.
Reynolds No.
9 X 10^4
13 X 10^4
18 X 10^4
24 X 10^4
30 X 10^4
X-TENSION COEFFICIENT
10.0
8.0
6.0
4.0
2.0
0
0°
20
40
60
80
100
120
140
160
180
ANGLE

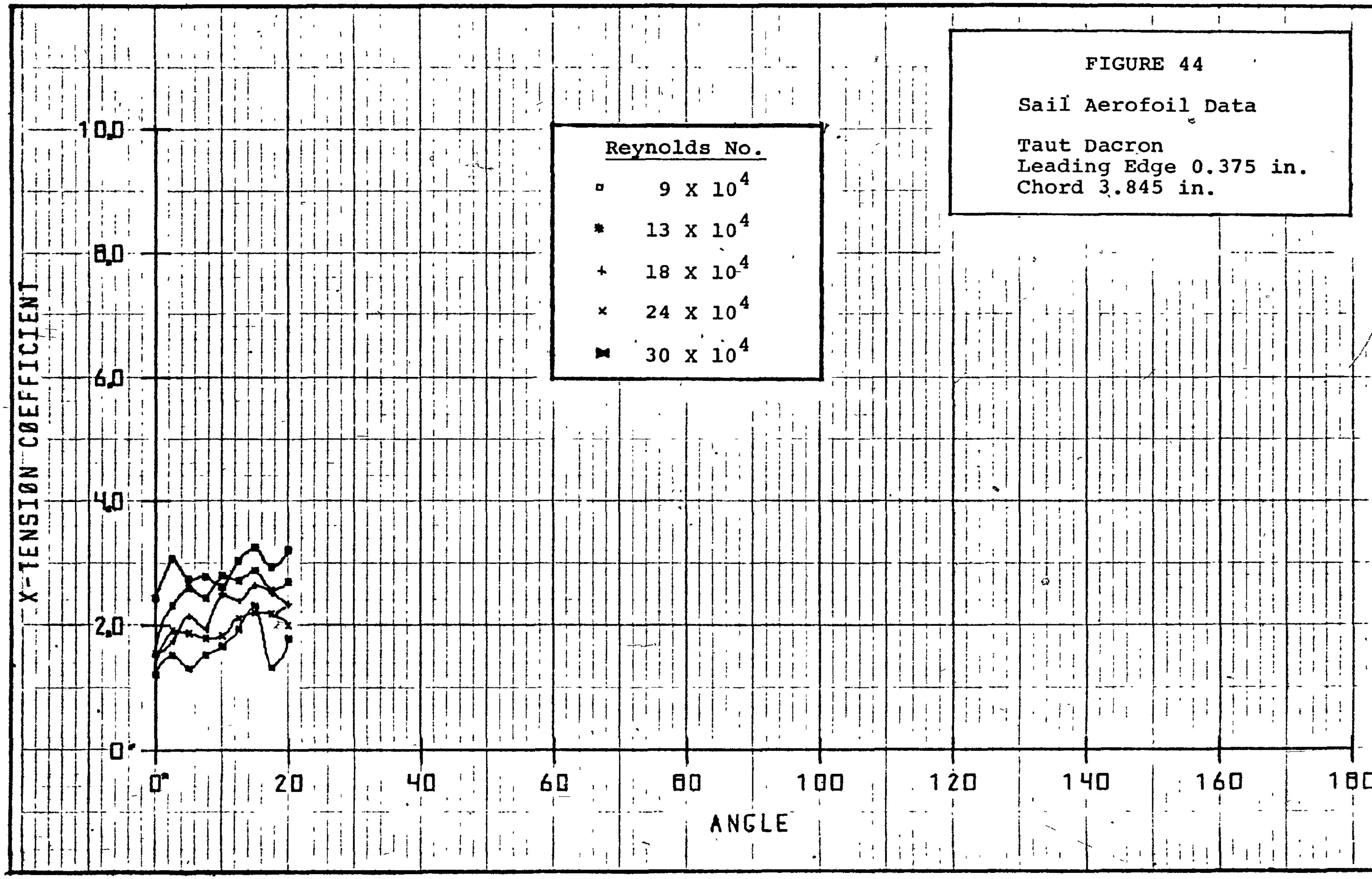
FIGURE 44
Sail Aerofoil Data
Taut Dacron
Leading Edge 0.375 in.
Chord 3.845 in.
Reynolds No.
9 X 10^4
13 X 10^4
18 X 10^4
24 X 10^4
30 X 10^4
X-TENSION COEFFICIENT
10.0
8.0
6.0
4.0
2.0
0
0°
20
40
60
80
100
120
140
160
180
ANGLE

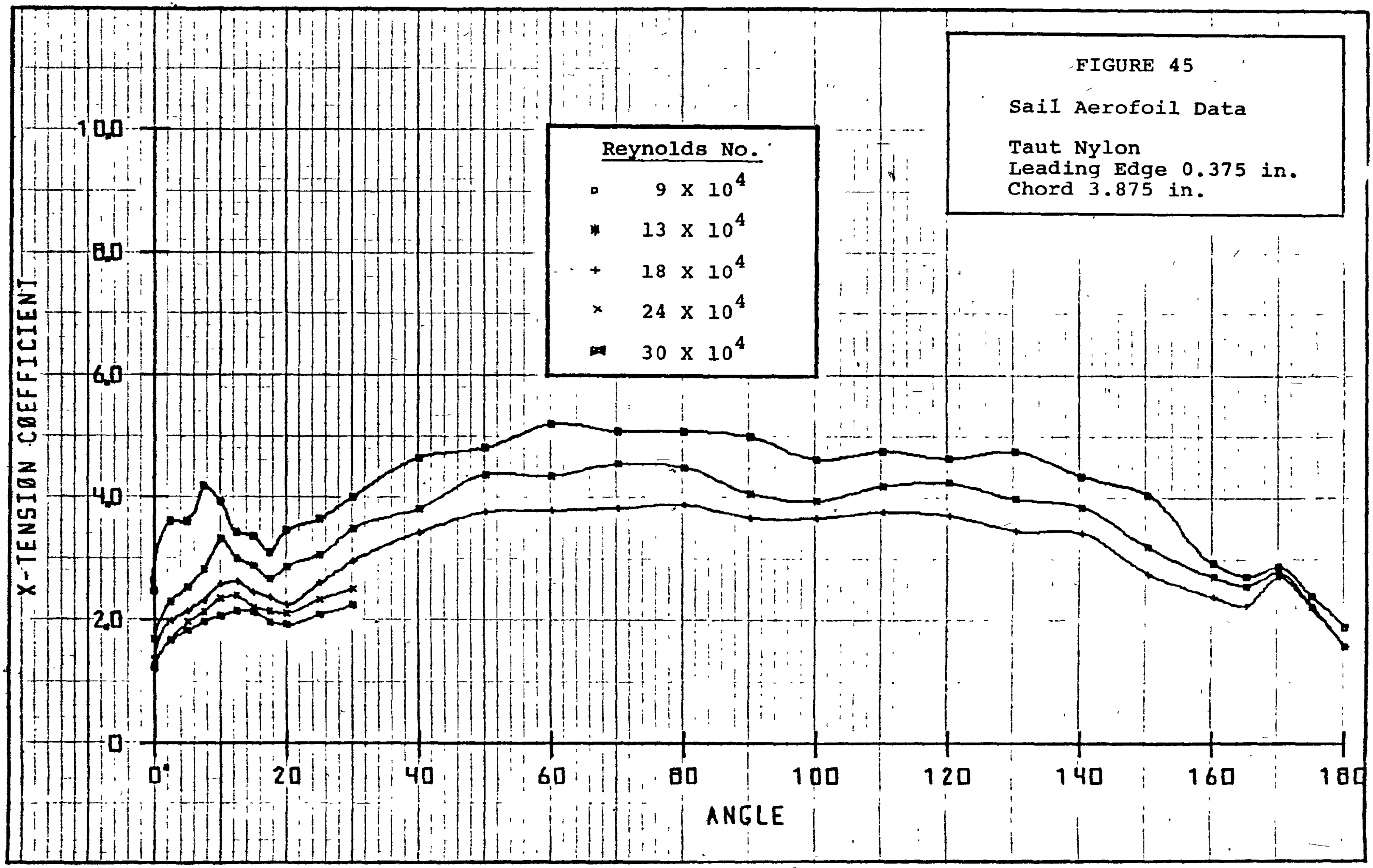
FIGURE 45
Sail Aerofoil Data
Taut Nylon
Leading Edge 0.375 in.
Chord 3.875 in.
Reynolds No.
9 X 10^4
13 X 10^4
18 X 10^4
24 X 10^4
30 X 10^4
X-TENSION COEFFICIENT
10.0
8.0
6.0
4.0
2.0
0
0°
20
40
60
80
100
120
140
160
180
ANGLE

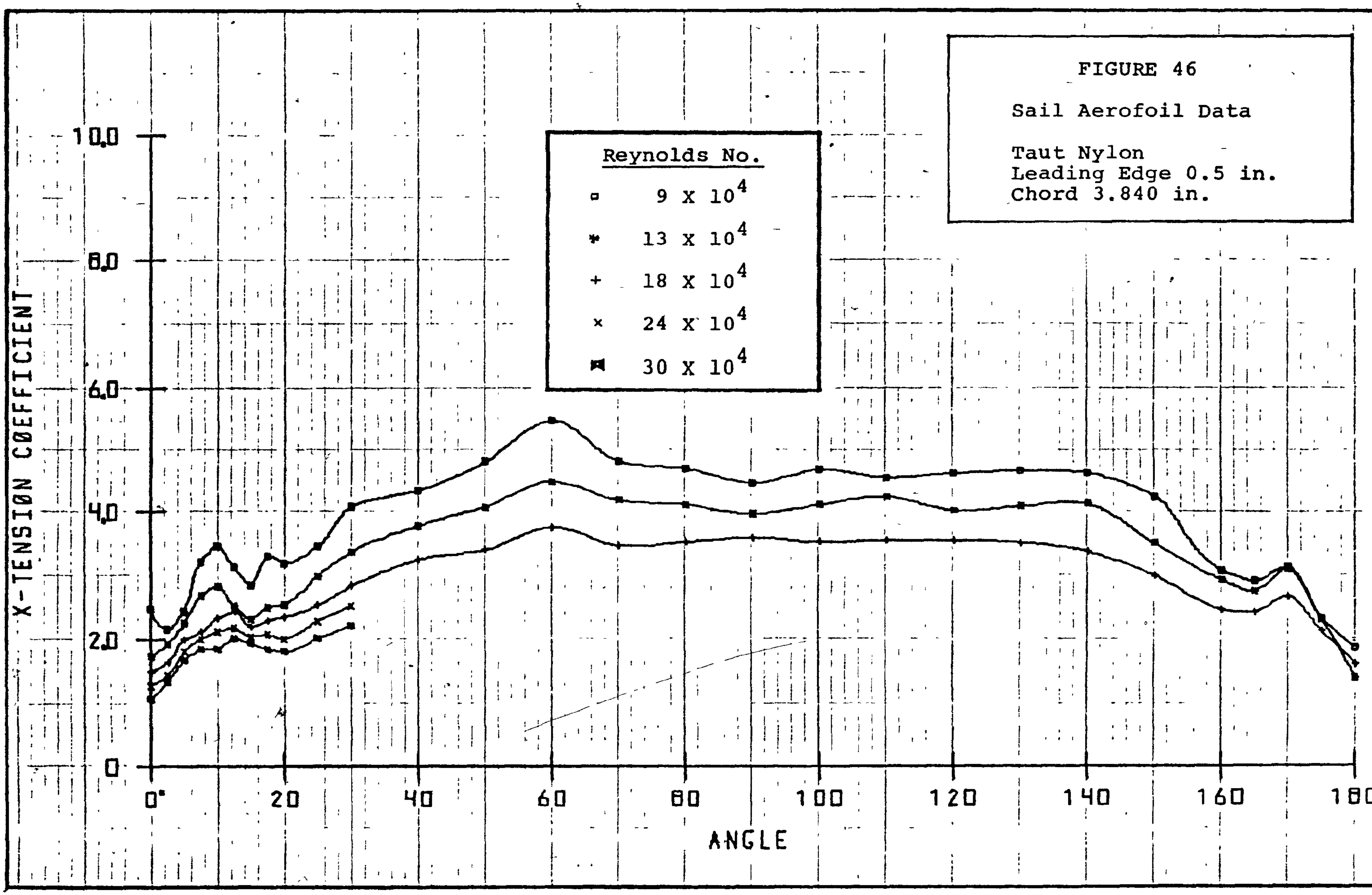

FIGURE 46
Sail Aerofoil Data
Taut Nylon
Leading Edge 0.5 in.
Chord 3.840 in.
Reynolds No.
9 X 10^4
13 X 10^4
18 X 10^4
24 X 10^4
30 X 10^4
X-TENSION COEFFICIENT
10.0
8.0
6.0
4.0
2.0
0
0°
20
40
60
80
100
120
140
160
180
ANGLE

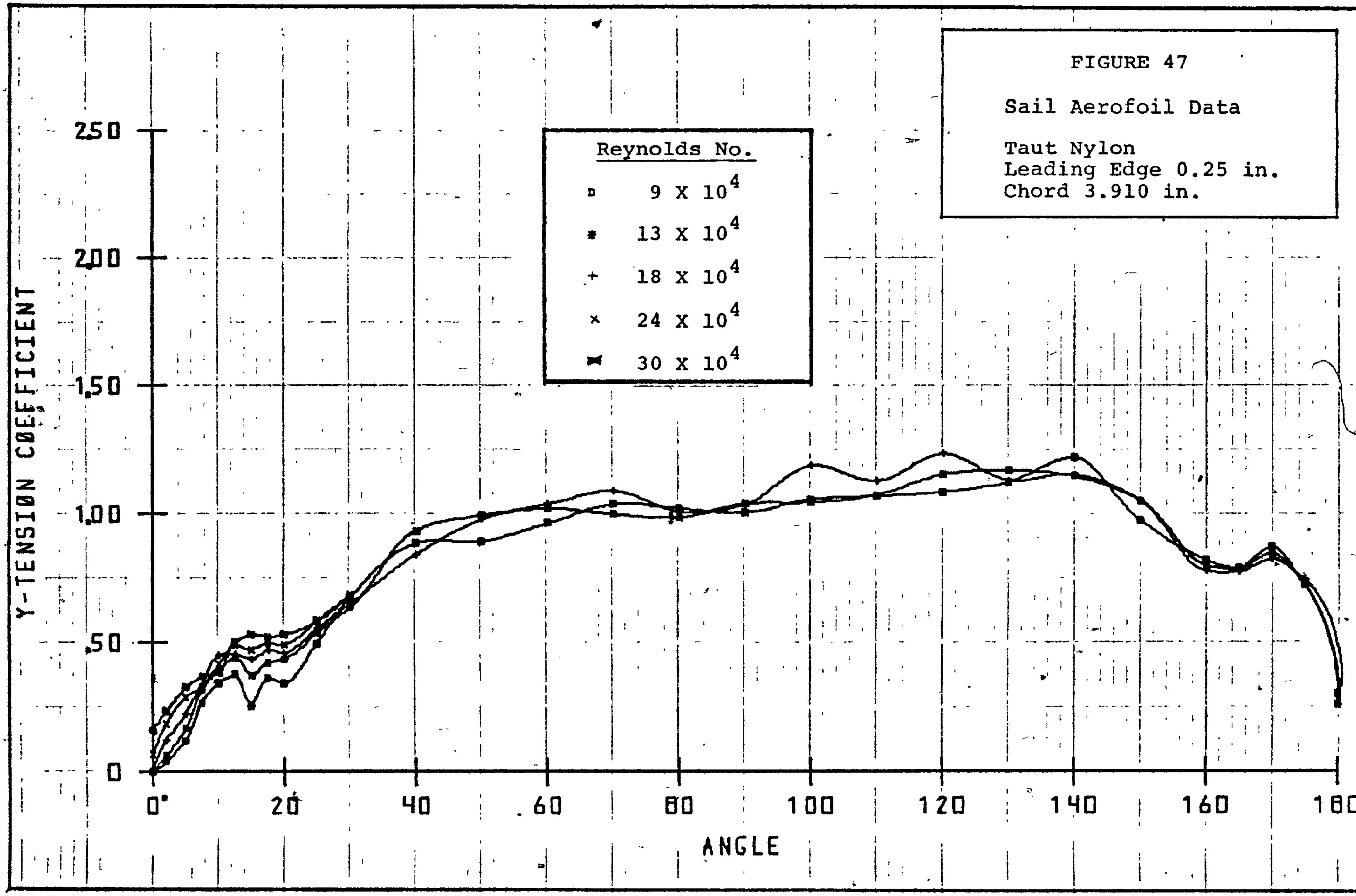

FIGURE 47
Sail Aerofoil Data
Taut Nylon
Leading Edge 0.25 in.
Chord 3.910 in.
Reynolds No.
9 X 10^4
13 X 10^4
18 X 10^4
24 X 10^4
30 X 10^4
Y-TENSIØN CØEFFICIENT
2.50
2.00
1.50
1.00
.50
0
0°
20
40
60
80
100
120
140
160
180
ANGLE

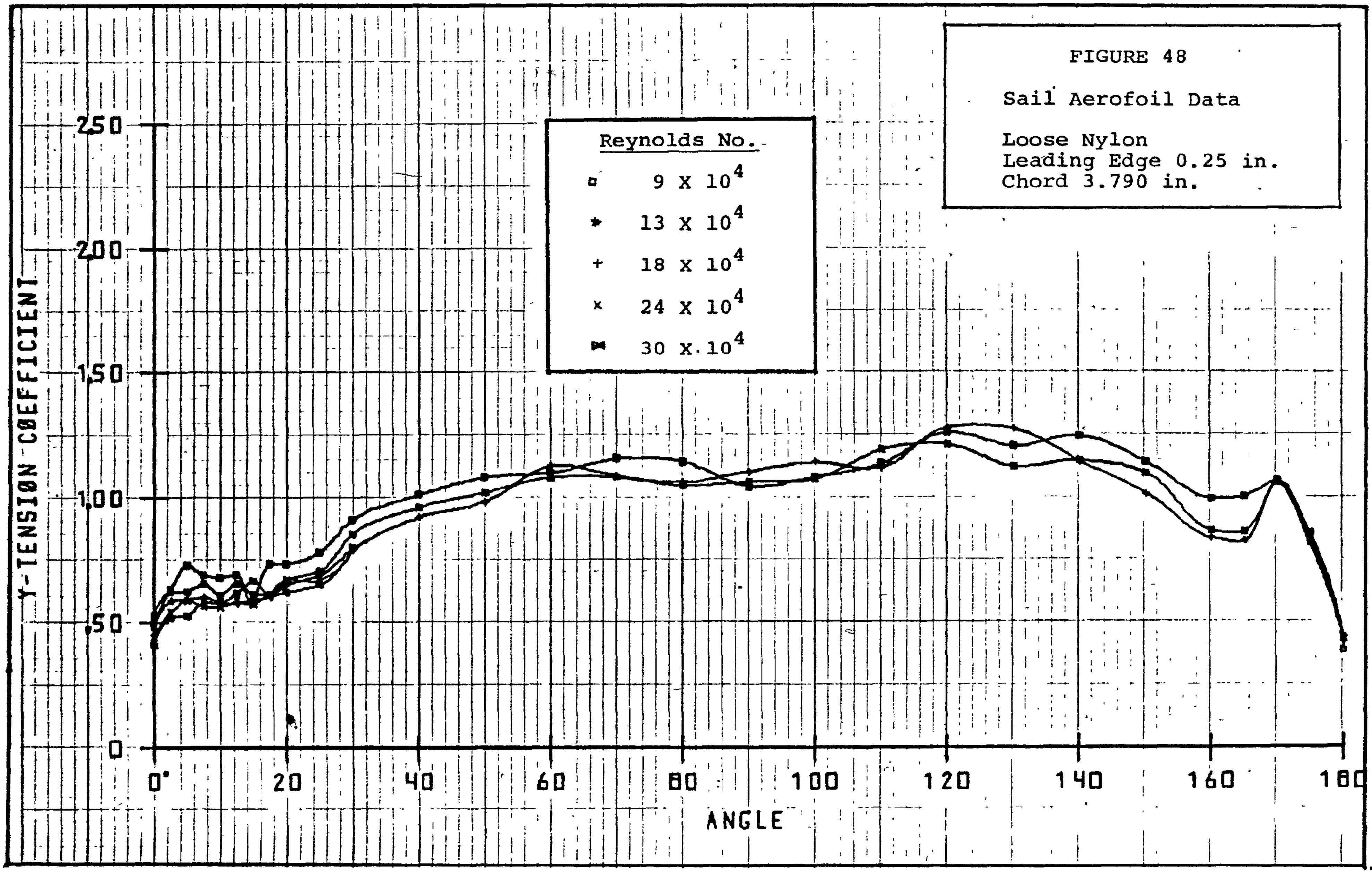

FIGURE 48
Sail Aerofoil Data
Loose Nylon
Leading Edge 0.25 in.
Chord 3.790 in.
Reynolds No.
9 X 10^4
13 X 10^4
18 X 10^4
24 X 10^4
30 X 10^4
Y-TENSION COEFFICIENT
2.50
2.00
1.50
1.00
.50
0
0°
20
40
60
80
100
120
140
160
180
ANGLE

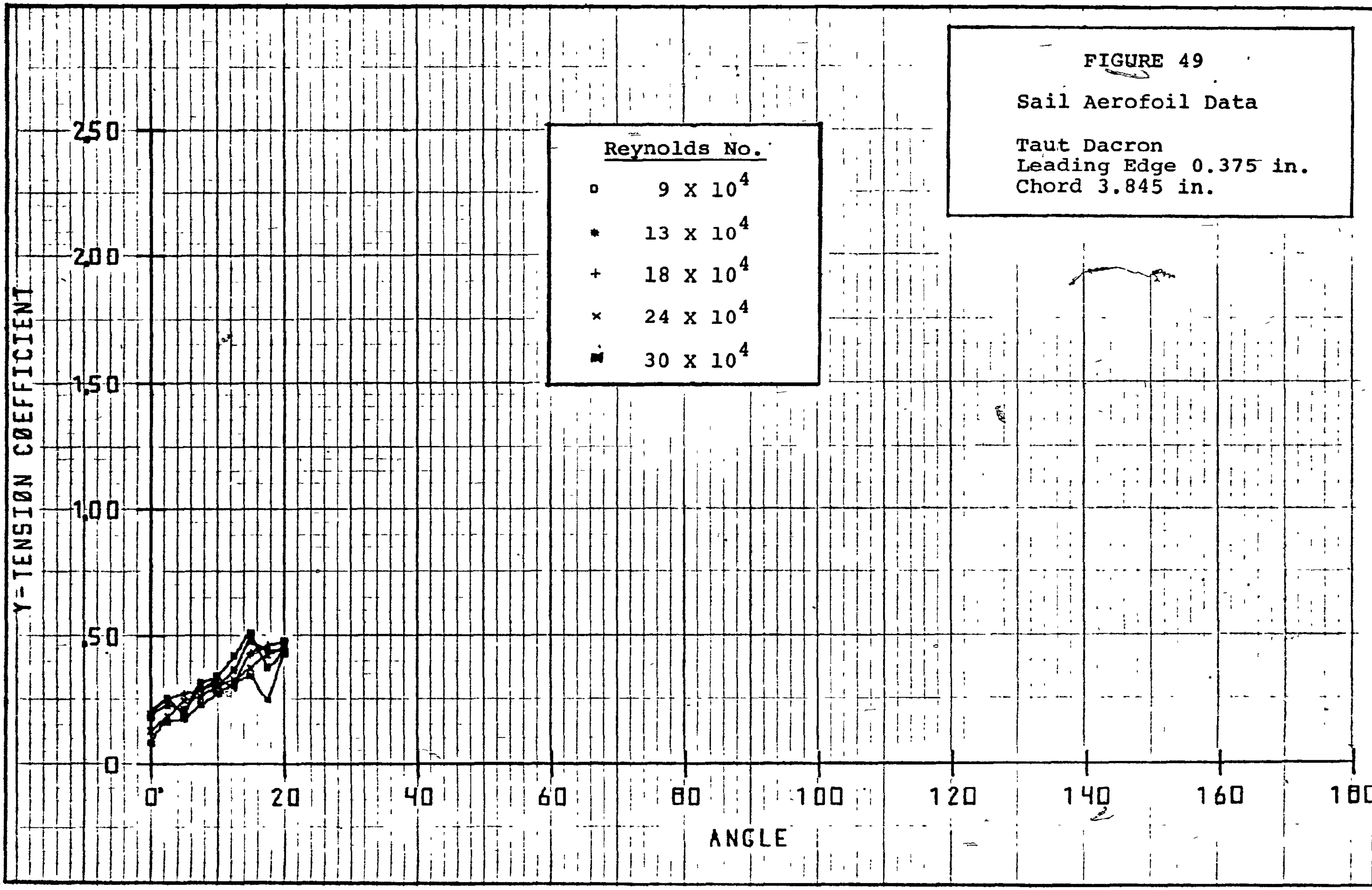
FIGURE 49
Sail Aerofoil Data
Taut Dacron
Leading Edge 0.375 in.
Chord 3.845 in.
Reynolds No.
9 X 10^4
13 X 10^4
18 X 10^4
24 X 10^4
30 X 10^4
Y-TENSIØN CØEFFICIENT
2.50
2.00
1.50
1.00
.50
0
0°
20
40
60
80
100
120
140
160
180
ANGLE

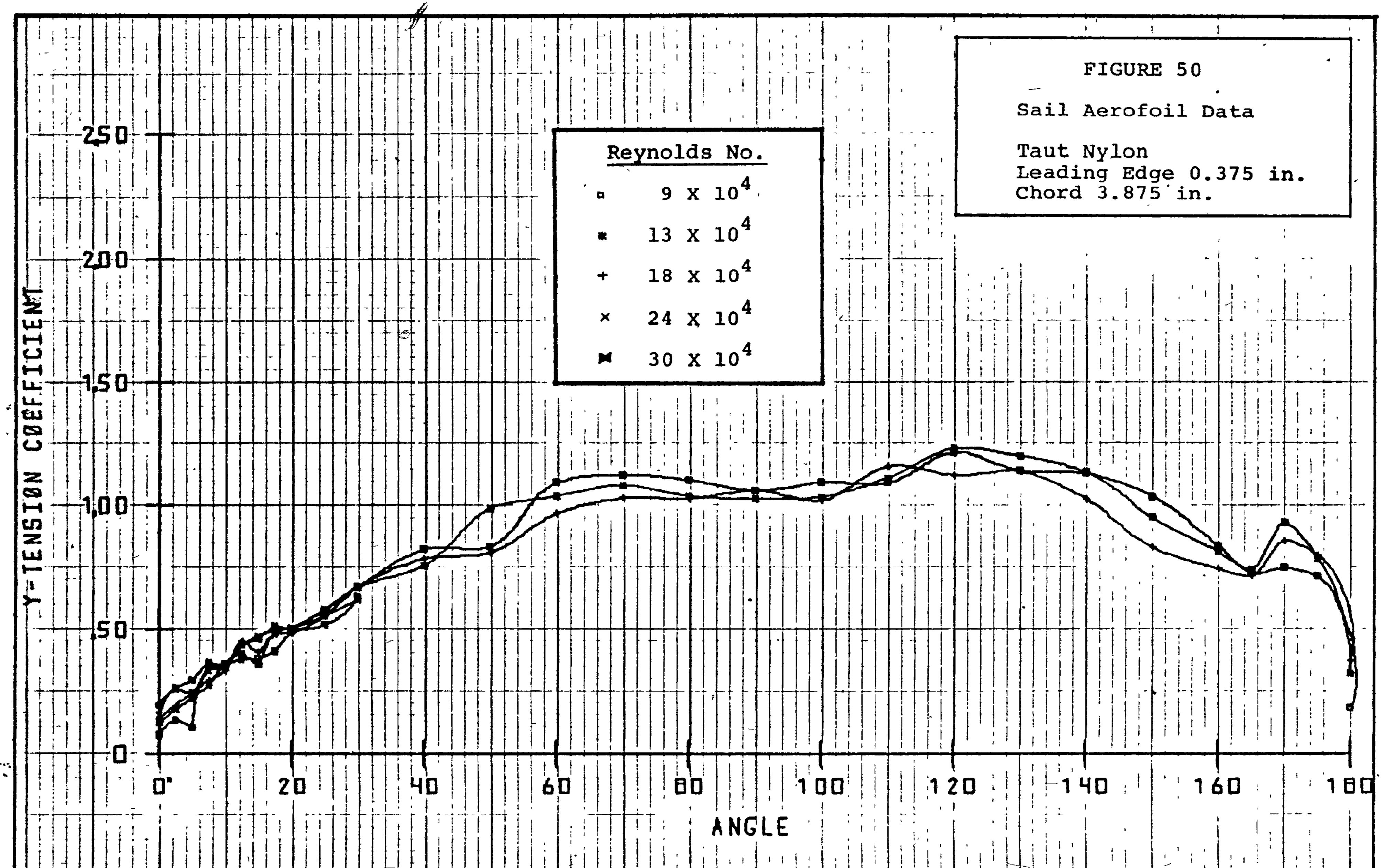
FIGURE 50
Sail Aerofoil Data
Taut Nylon
Leading Edge 0.375 in.
Chord 3.875 in.
Reynolds No.
9 X 10^4
13 X 10^4
18 X 10^4
24 X 10^4
30 X 10^4
Y-TENSION COEFFICIENT
2.50
2.00
1.50
1.00
.50
0
0°
20
40
60
80
100
120
140
160
180
ANGLE

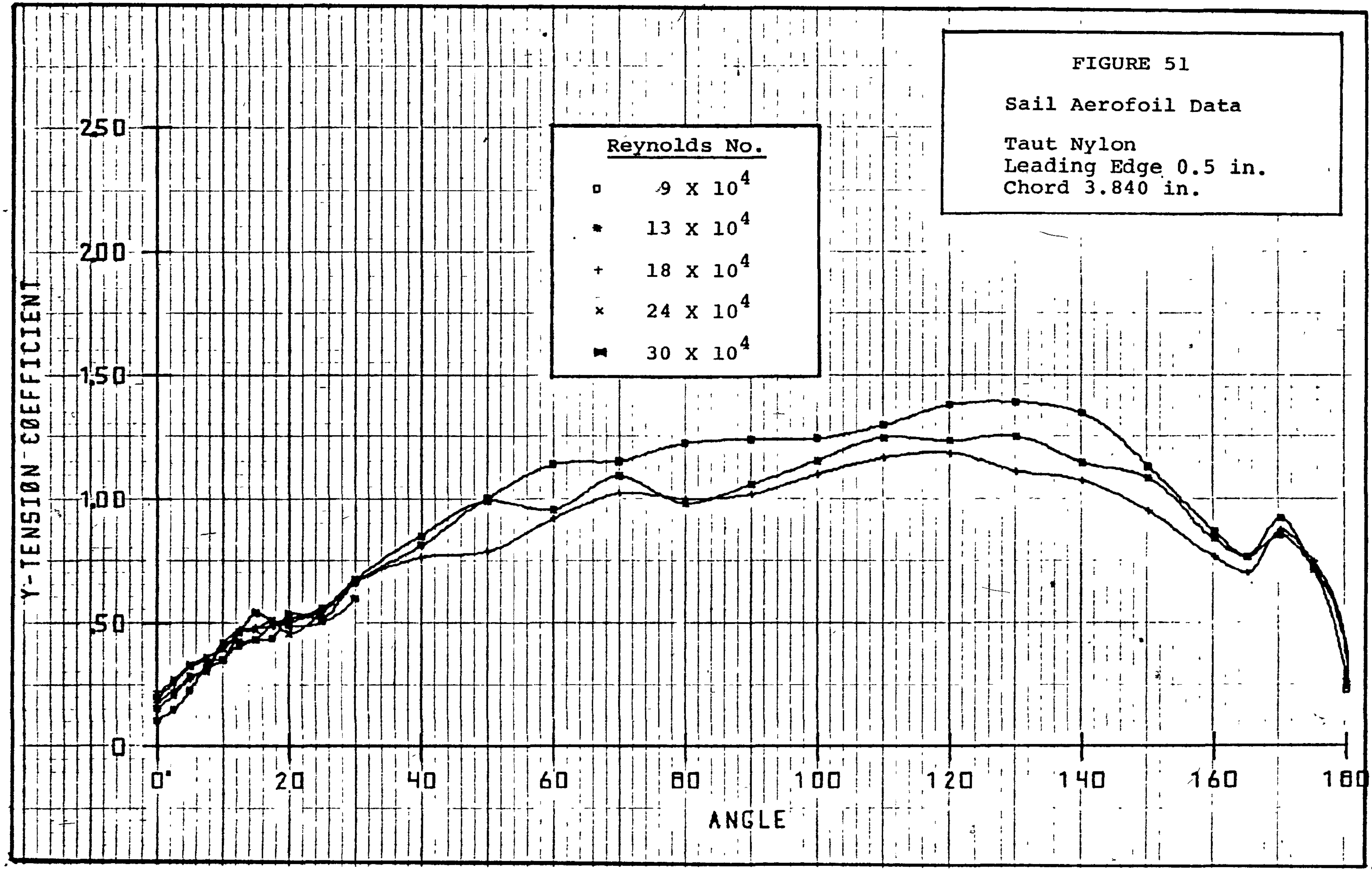
FIGURE 51
Sail Aerofoil Data
Taut Nylon
Leading Edge 0.5 in.
Chord 3.840 in.
Reynolds No.
9 X 10^4
13 X 10^4
18 X 10^4
24 X 10^4
30 X 10^4
Y-TENSION COEFFICIENT
2.50
2.00
1.50
1.00
.50
0
0°
20
40
60
80
100
120
140
160
180
ANGLE

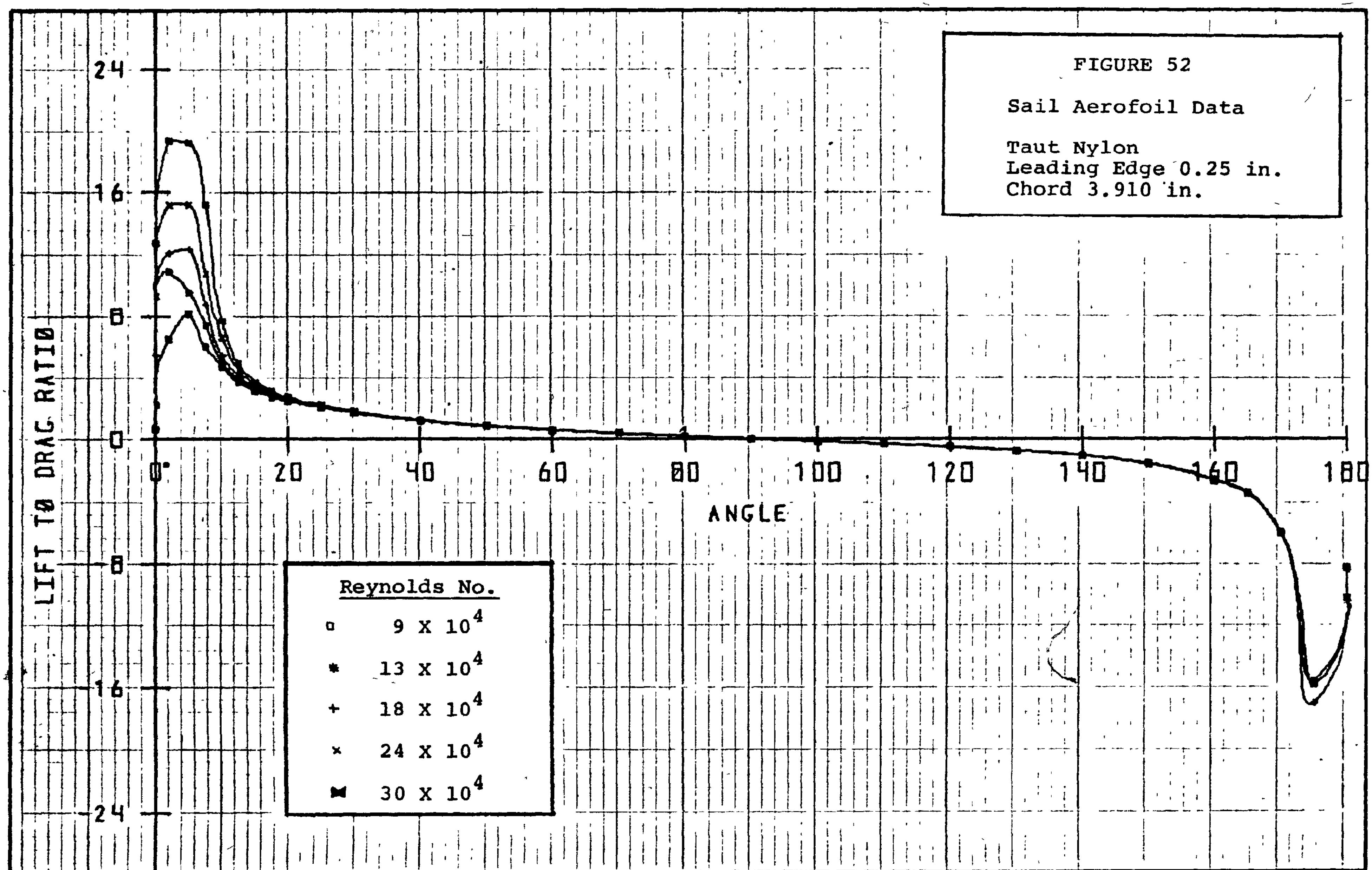

FIGURE 52
Sail Aerofoil Data
Taut Nylon
Leading Edge 0.25 in.
Chord 3.910 in.
LIFT TØ DRAG RATIØ
ANGLE
24
16
8
0
8
16
24
0°
20
40
60
80
100
120
140
160
180
Reynolds No.
9 X 10^4
13 X 10^4
18 X 10^4
24 X 10^4
30 X 10^4

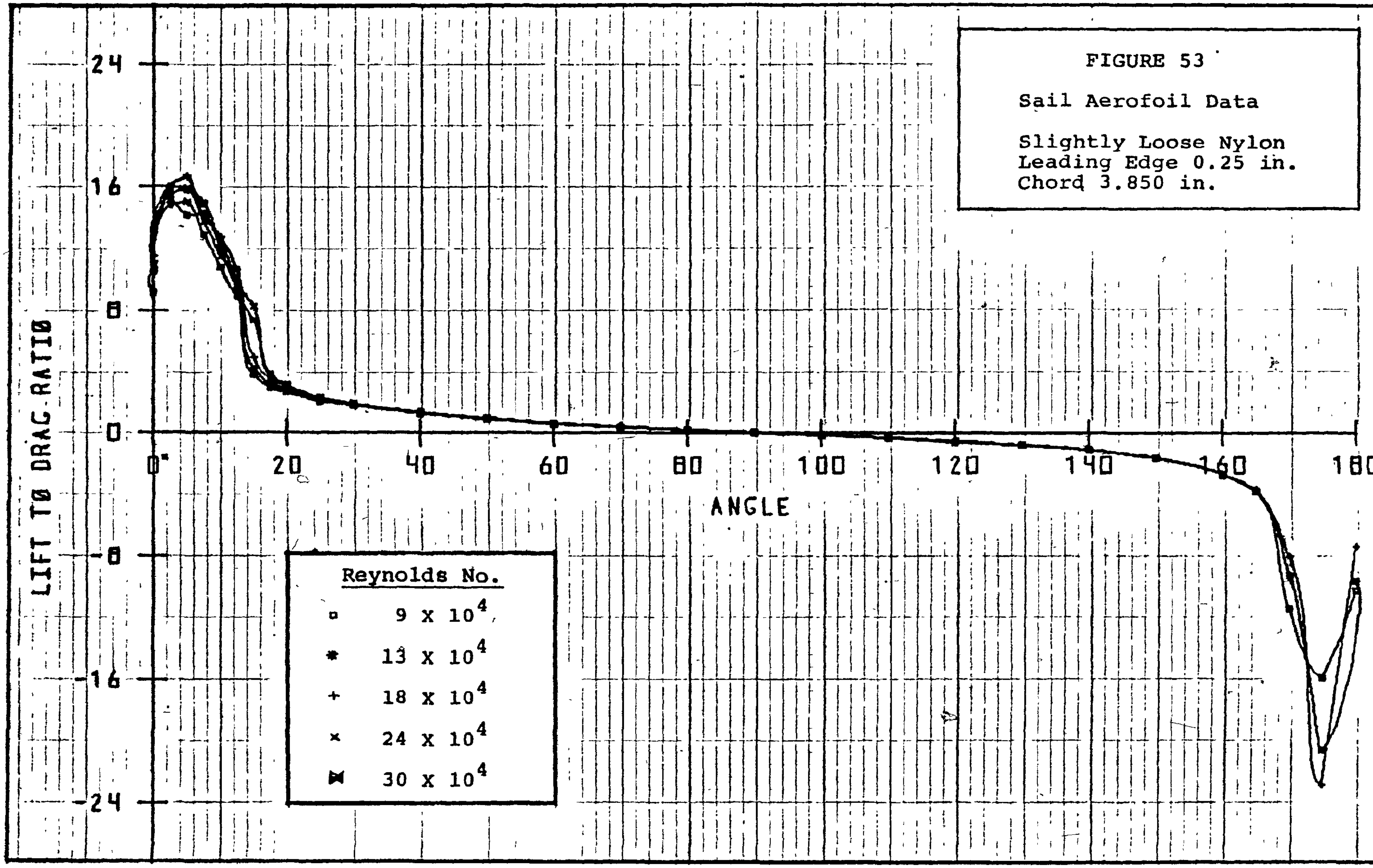
FIGURE 53
Sail Aerofoil Data
Slightly Loose Nylon
Leading Edge 0.25 in.
Chord 3.850 in.
LIFT TØ DRAG RATIØ
24
16
8
0
-8
-16
-24
0°
20
40
60
80
100
120
140
160
180
ANGLE
Reynolds No.
9 x 10^4
13 x 10^4
18 x 10^4
24 x 10^4
30 x 10^4

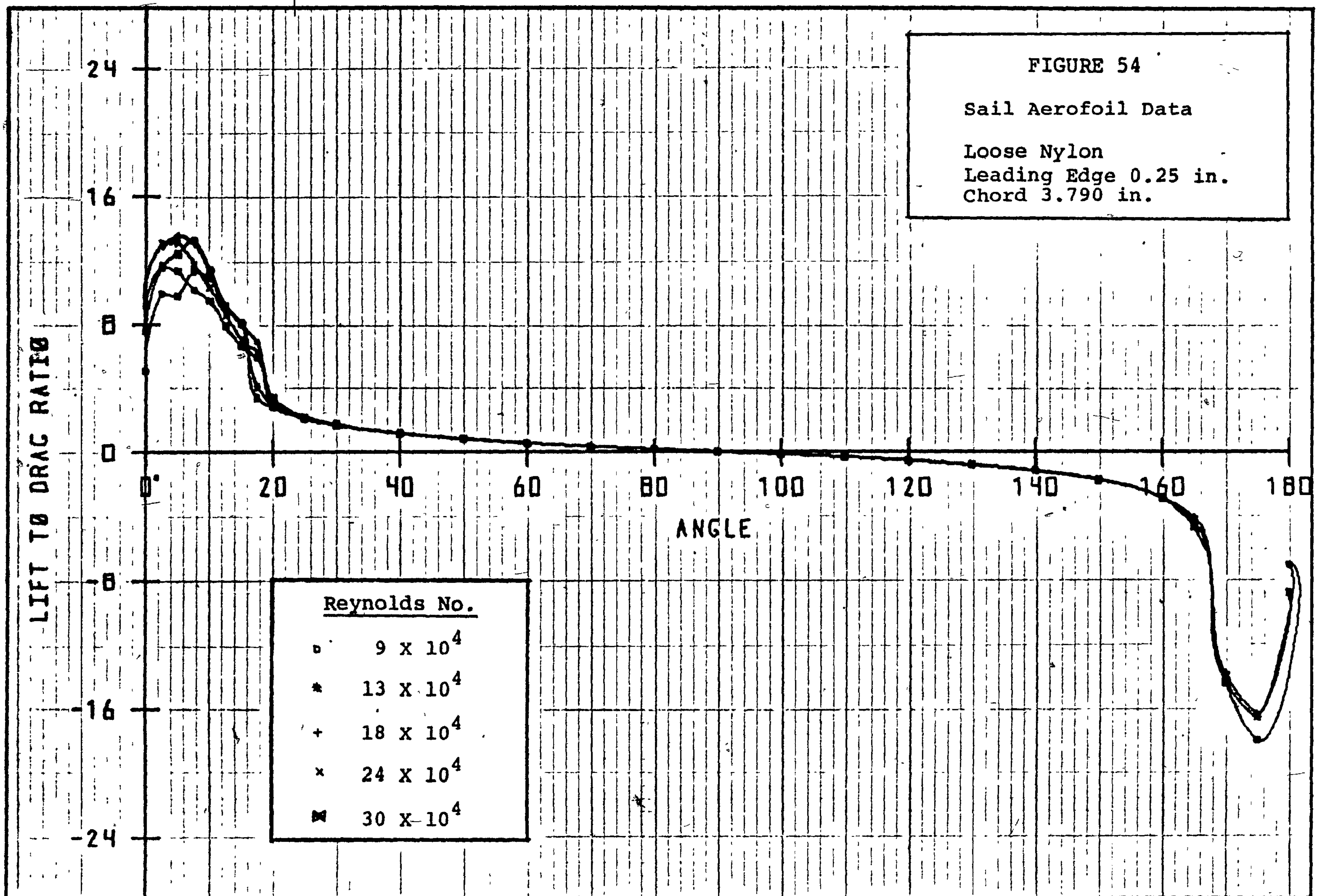
FIGURE 54
Sail Aerofoil Data
Loose Nylon
Leading Edge 0.25 in.
Chord 3.790 in.
Reynolds No.
9 X 10^4
13 X 10^4
18 X 10^4
24 X 10^4
30 X 10^4
LIFT TØ DRAG RATIØ
ANGLE
24
16
8
0
-8
-16
-24
0°
20
40
60
80
100
120
140
160
180

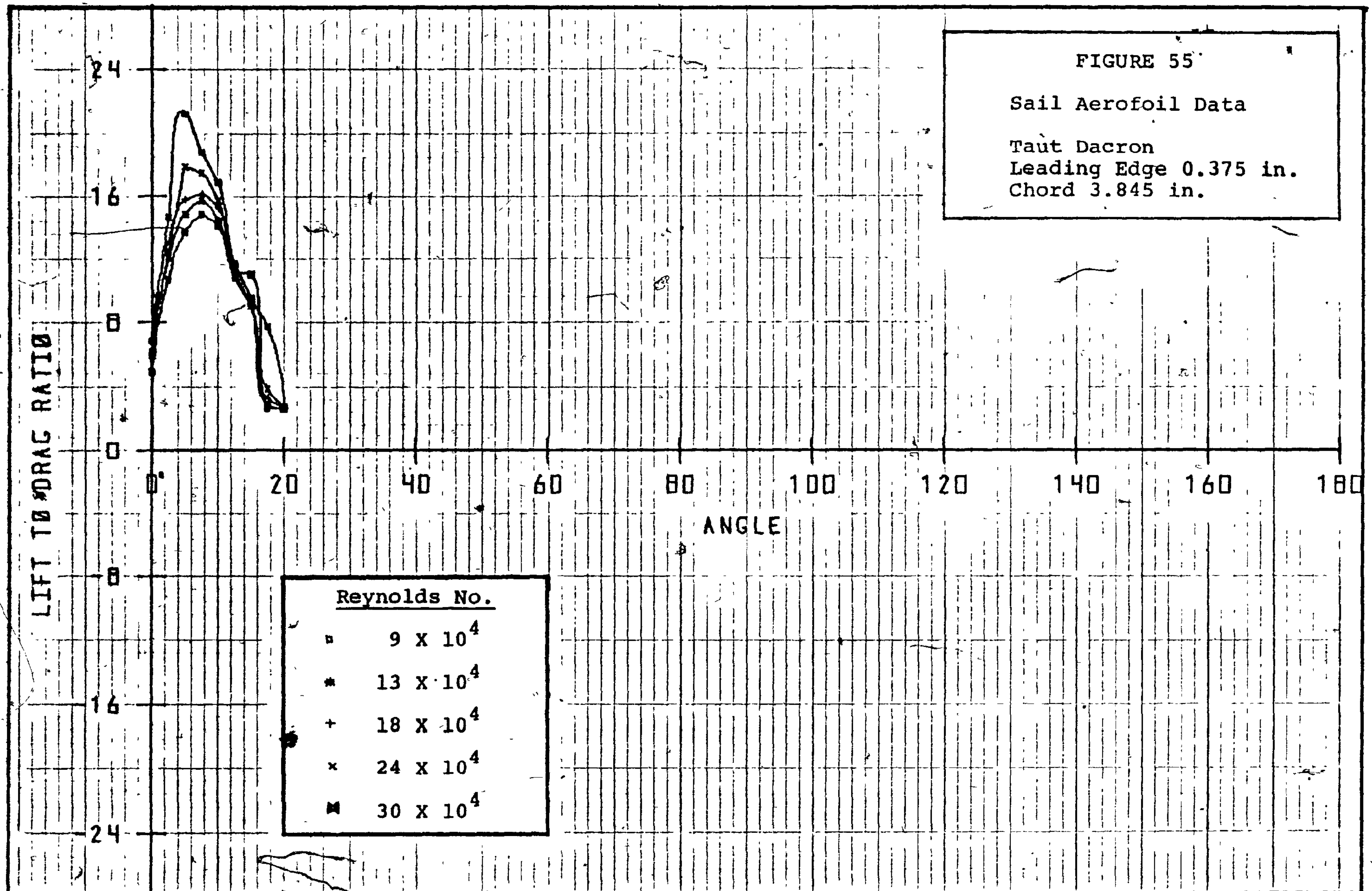
FIGURE 55
Sail Aerofoil Data
Taut Dacron
Leading Edge 0.375 in.
Chord 3.845 in.
LIFT TØ DRAG RATIØ
24
16
8
0
-8
-16
-24
0°
20
40
60
80
100
120
140
160
180
ANGLE
Reynolds No.
9 X 10⁴
13 X 10⁴
18 X 10⁴
24 X 10⁴
30 X 10⁴

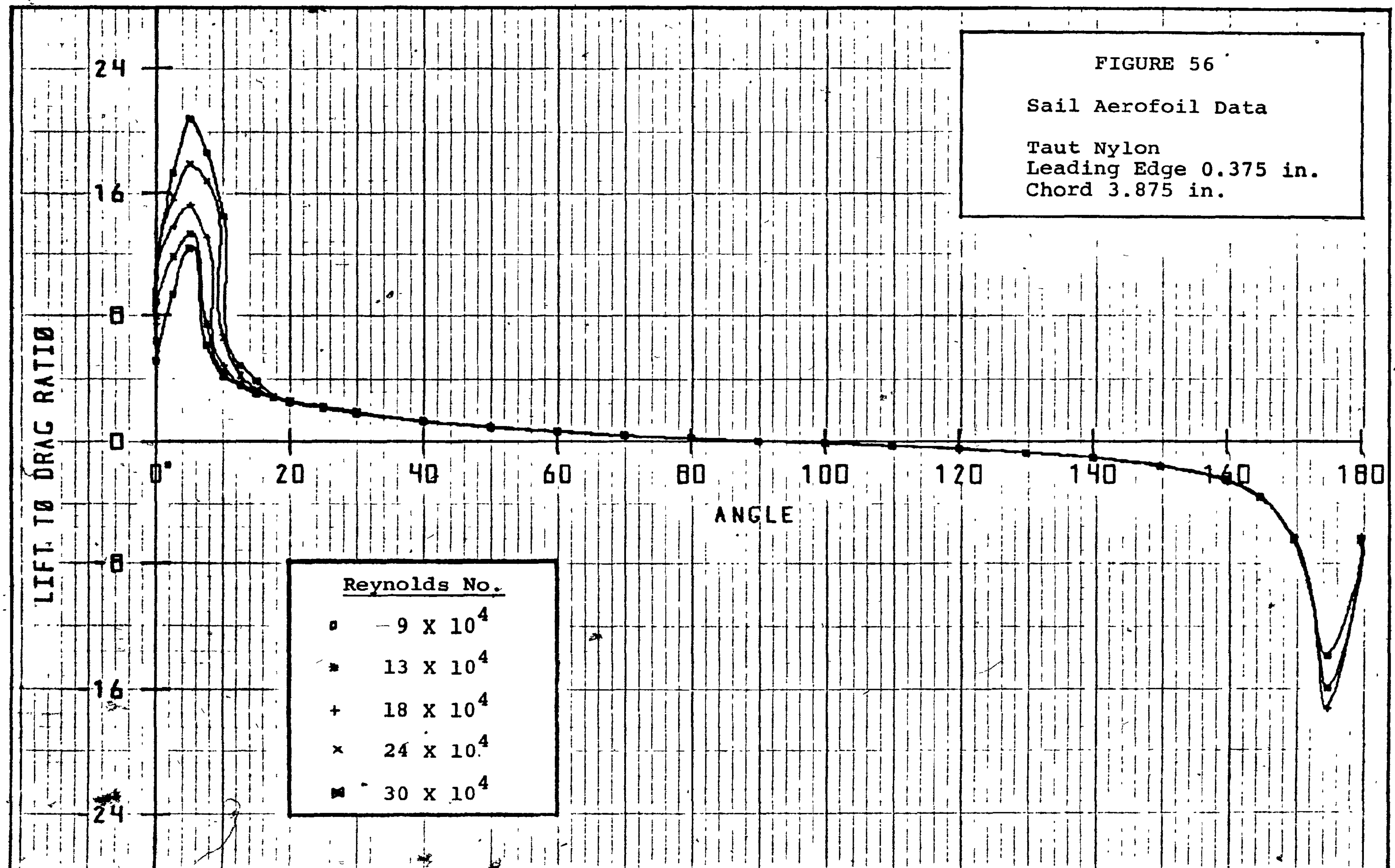
FIGURE 56
Sail Aerofoil Data
Taut Nylon
Leading Edge 0.375 in.
Chord 3.875 in.
LIFT TØ DRAG RATIØ
ANGLE
24
16
8
0
8
16
24
0°
20
40
60
80
100
120
140
160
180
Reynolds No.
9 X 10^4
13 X 10^4
18 X 10^4
24 X 10^4
30 X 10^4

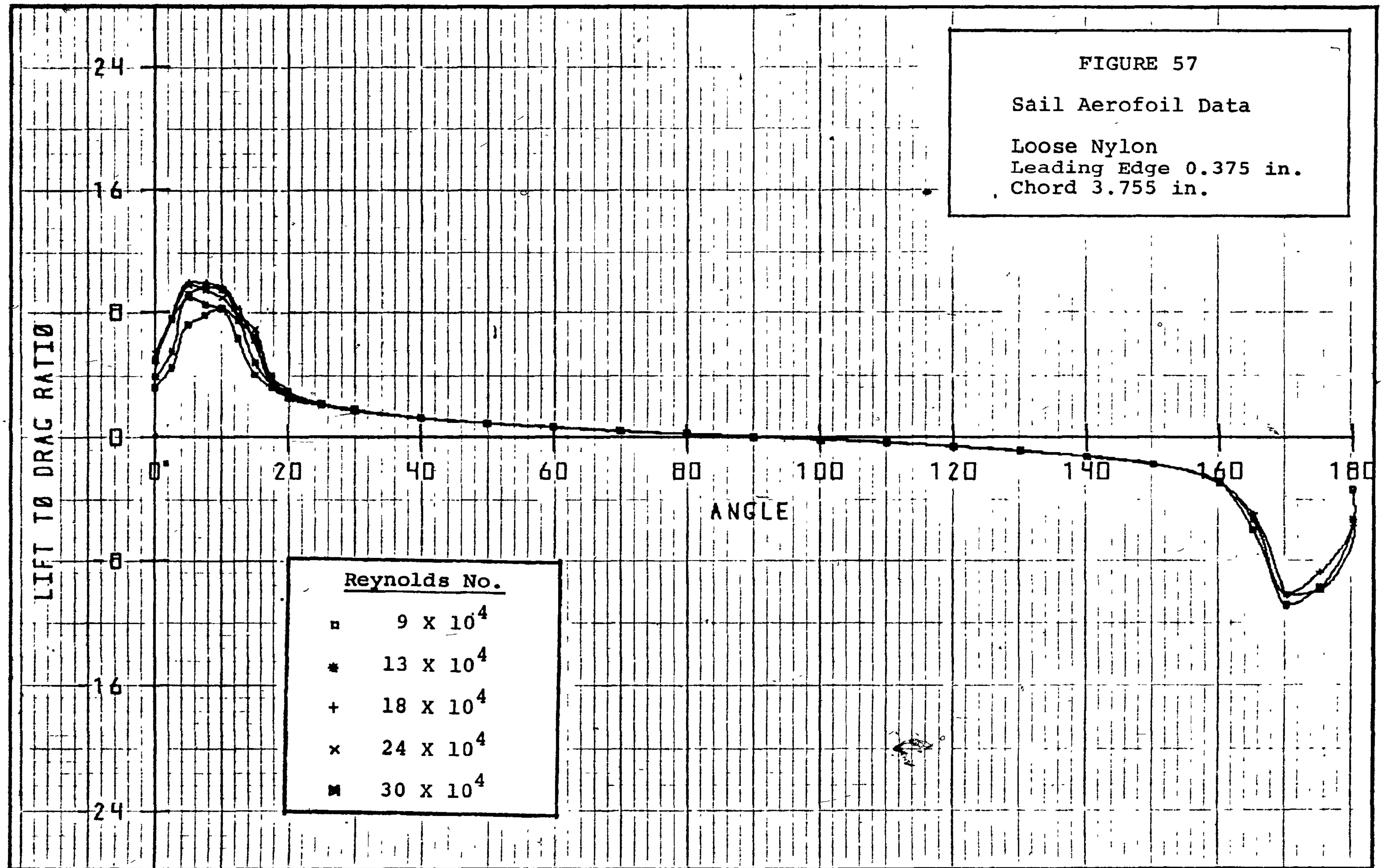
FIGURE 57
Sail Aerofoil Data
Loose Nylon
Leading Edge 0.375 in.
Chord 3.755 in.
Reynolds No.
9 X 10^4
13 X 10^4
18 X 10^4
24 X 10^4
30 X 10^4
LIFT TØ DRAG RATIØ
ANGLE
24
16
8
0
-8
-16
-24
0°
20
40
60
80
100
120
140
160
180

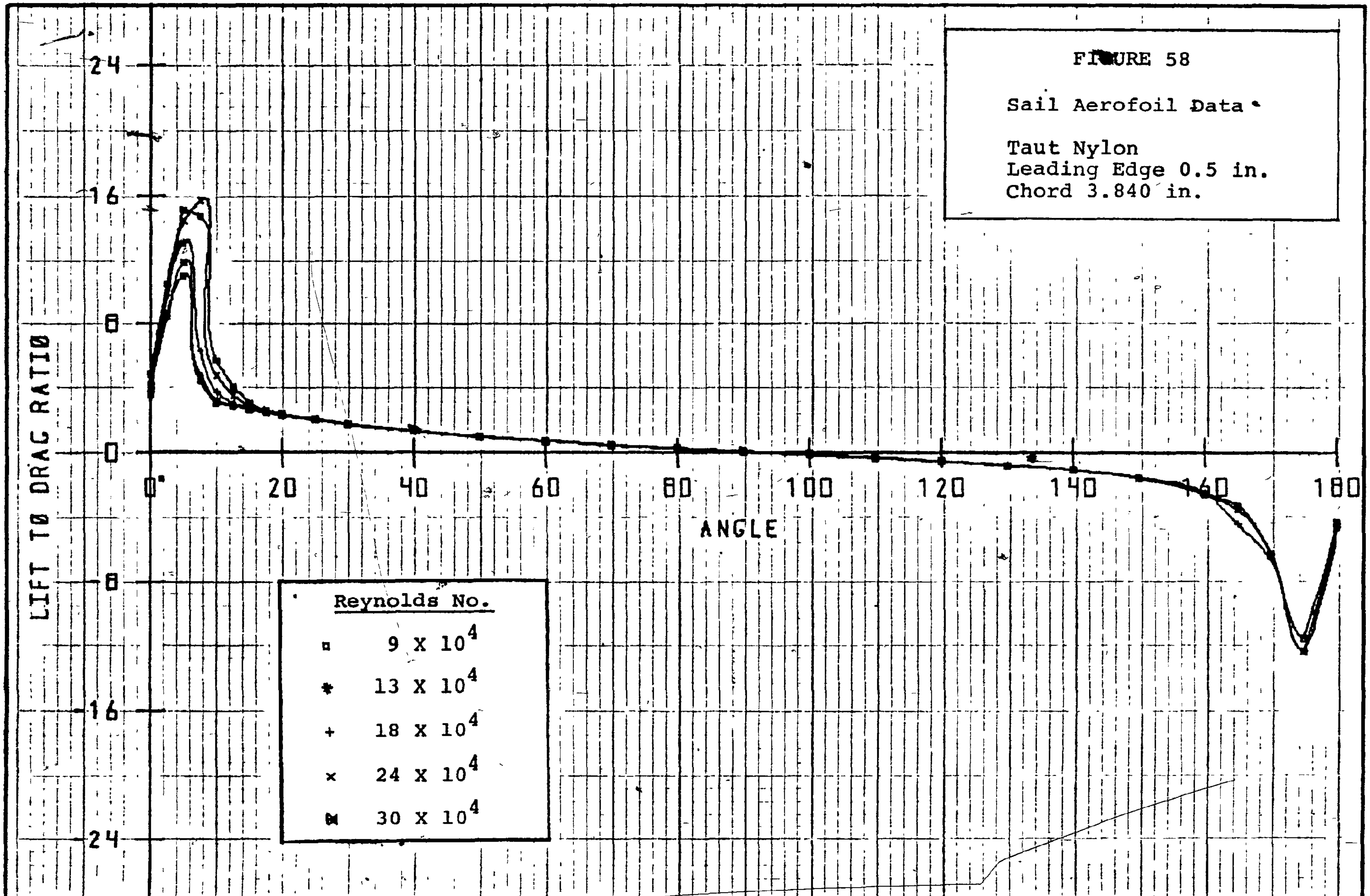
FIGURE 58
Sail Aerofoil Data
Taut Nylon
Leading Edge 0.5 in.
Chord 3.840 in.
LIFT TO DRAG RATIO
ANGLE
24
16
8
0
8
16
24
0°
20
40
60
80
100
120
140
160
180
Reynolds No.
9 X 10⁴
13 X 10⁴
18 X 10⁴
24 X 10⁴
30 X 10⁴

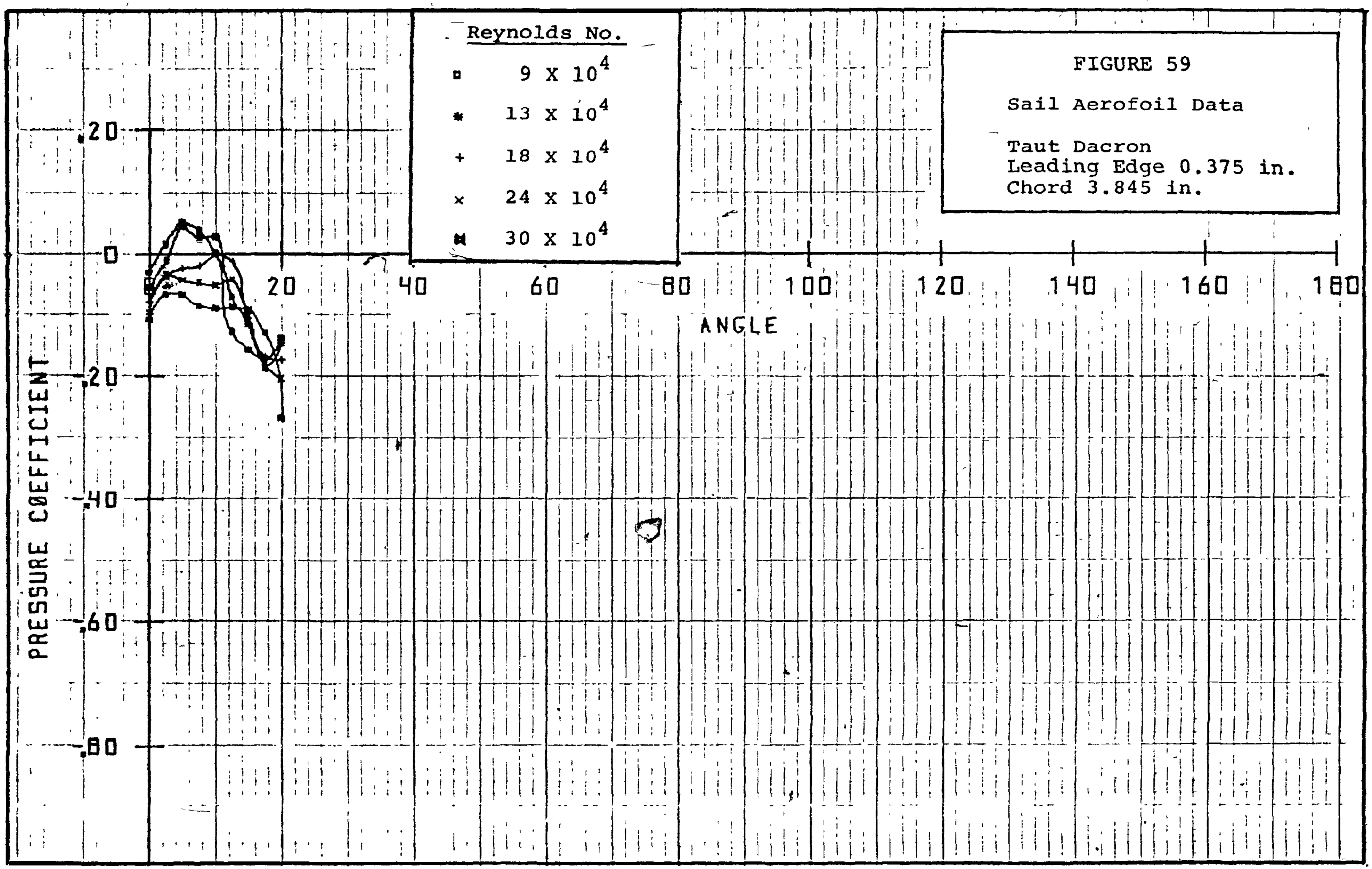

FIGURE 59

Sail Aerofoil Data

Taut Dacron
Leading Edge 0.375 in.
Chord 3.845 in.

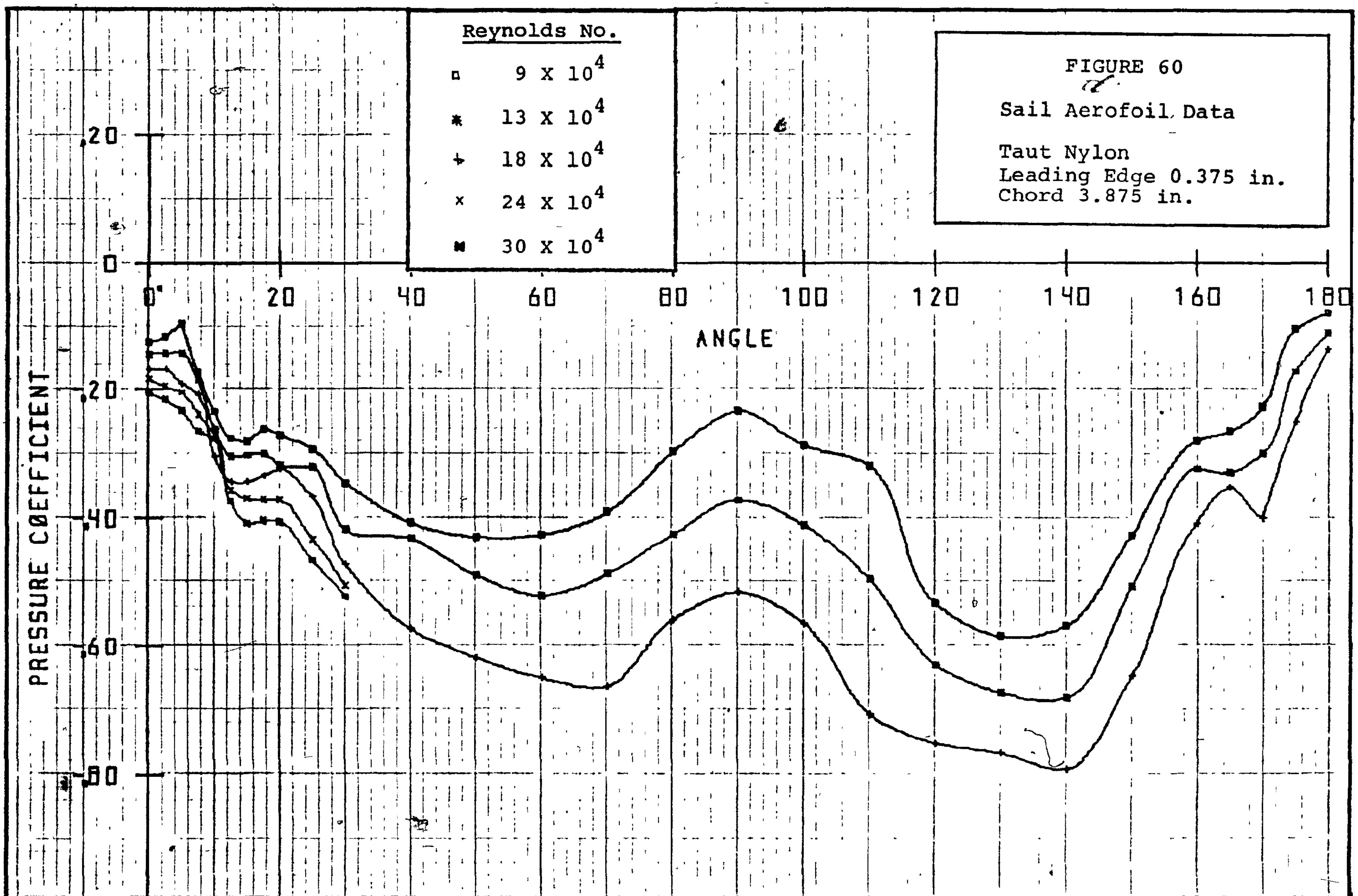

Reynolds No.
9 X 10^4
13 X 10^4
18 X 10^4
24 X 10^4
30 X 10^4
FIGURE 60
Sail Aerofoil Data
Taut Nylon
Leading Edge 0.375 in.
Chord 3.875 in.
.20
0
-.20
-.40
-.60
-.80
0°
20
40
60
80
100
120
140
160
180
ANGLE
PRESSURE CØEFFICIENT

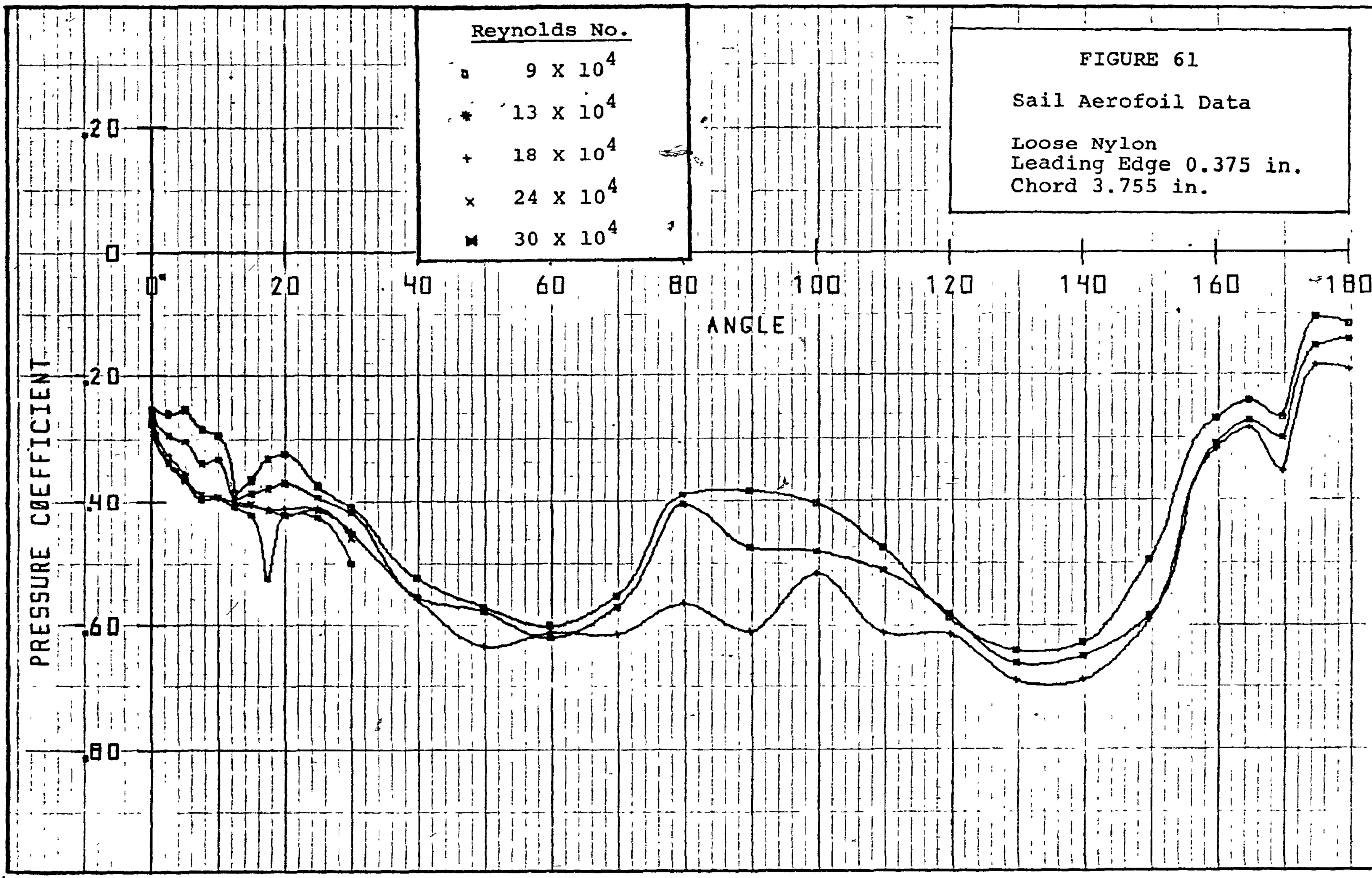
Reynolds No.
9 X 10^4
13 X 10^4
18 X 10^4
24 X 10^4
30 X 10^4
FIGURE 61
Sail Aerofoil Data
Loose Nylon
Leading Edge 0.375 in.
Chord 3.755 in.
.20
0
-.20
.40
.60
.80
0°
20
40
60
80
100
120
140
160
180
ANGLE
PRESSURE COEFFICIENT

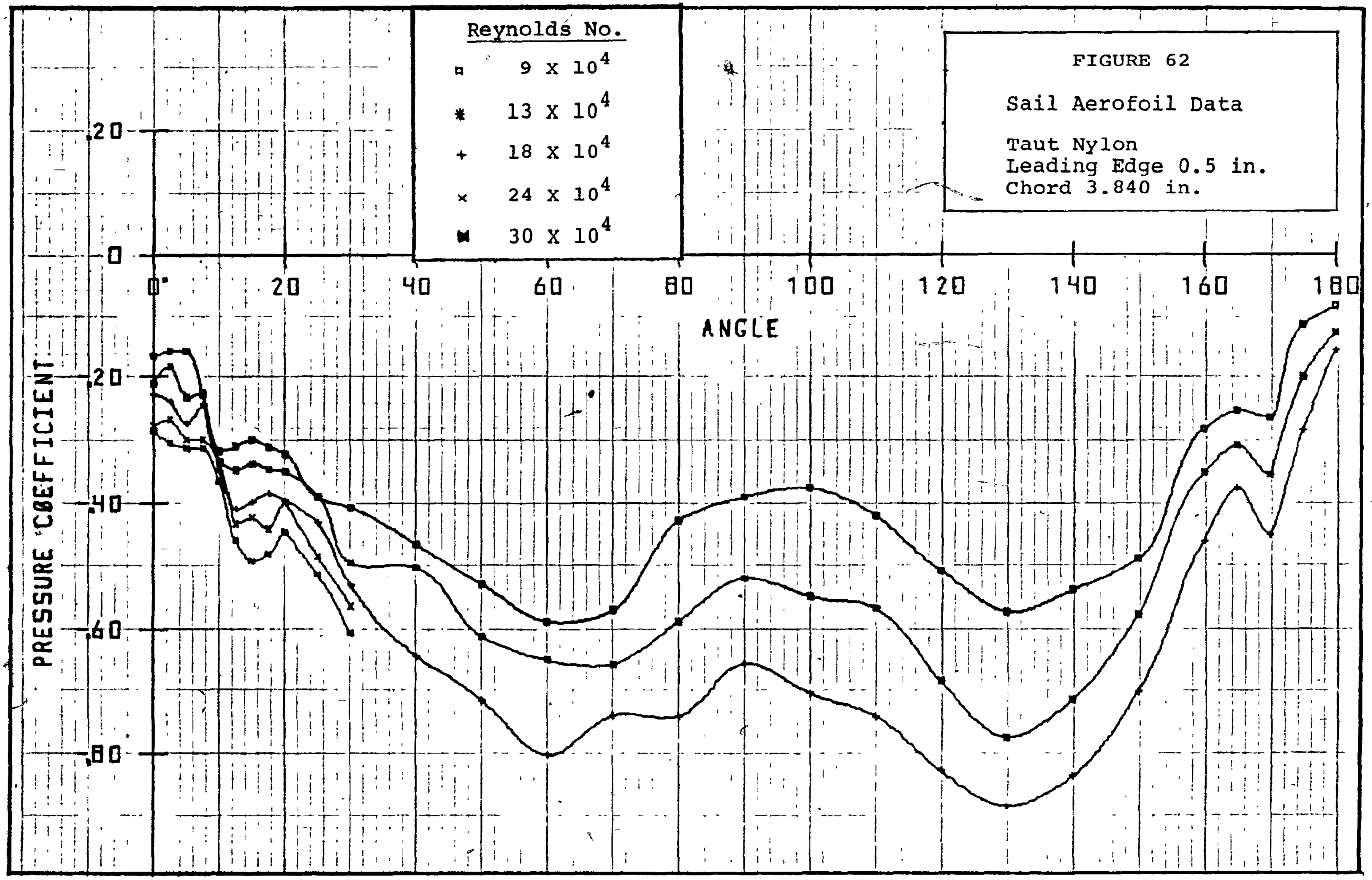

FIGURE 62
Sail Aerofoil Data
Taut Nylon
Leading Edge 0.5 in.
Chord 3.840 in.
Reynolds No.
9 X 10^4
13 X 10^4
18 X 10^4
24 X 10^4
30 X 10^4
PRESSURE COEFFICIENT
ANGLE
.20
0
-.20
-.40
-.60
-.80
0°
20
40
60
80
100
120
140
160
180

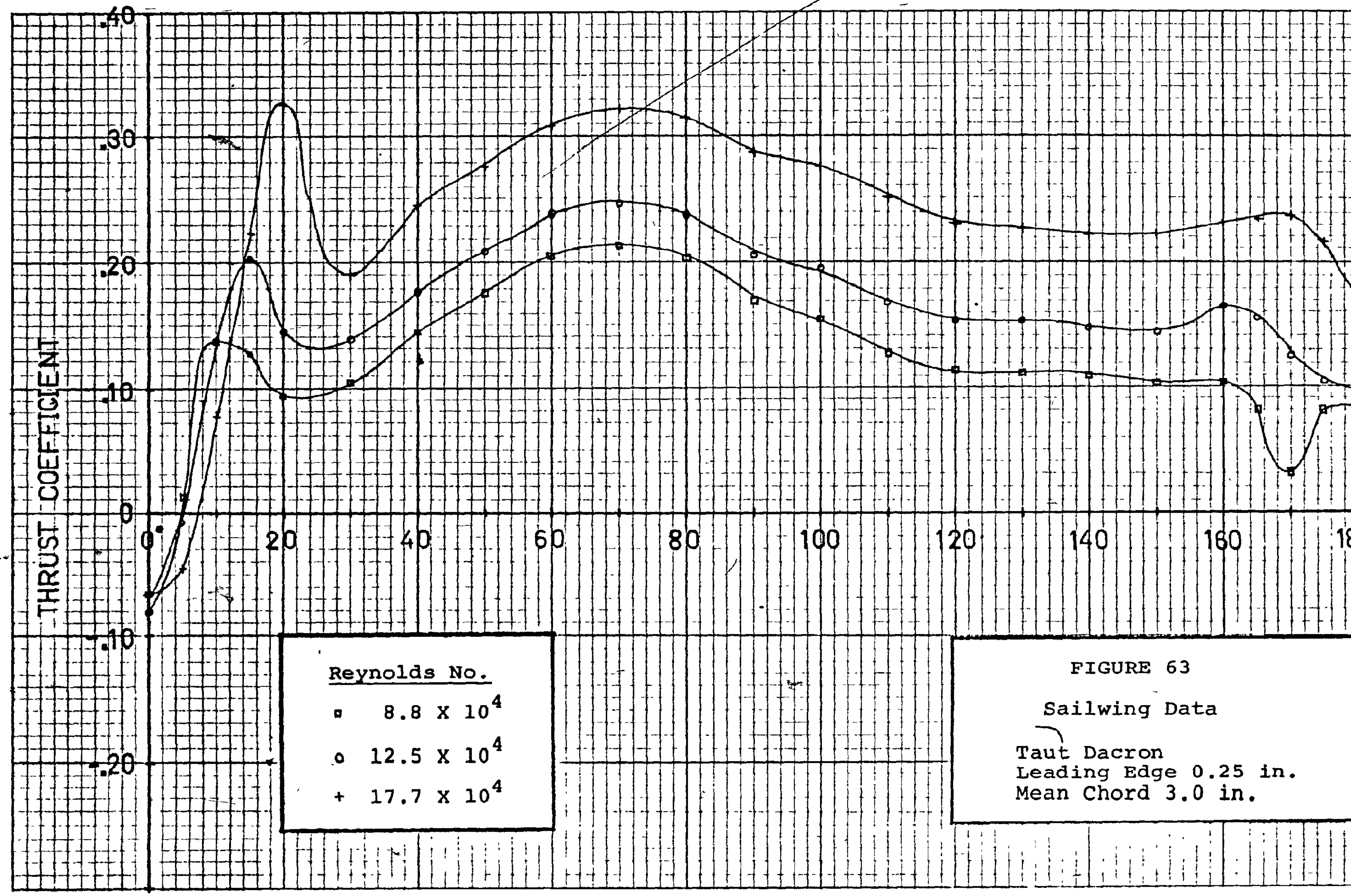

FIGURE 63

Sailwing Data

Taut Dacron
Leading Edge 0.25 in.
Mean Chord 3.0 in.

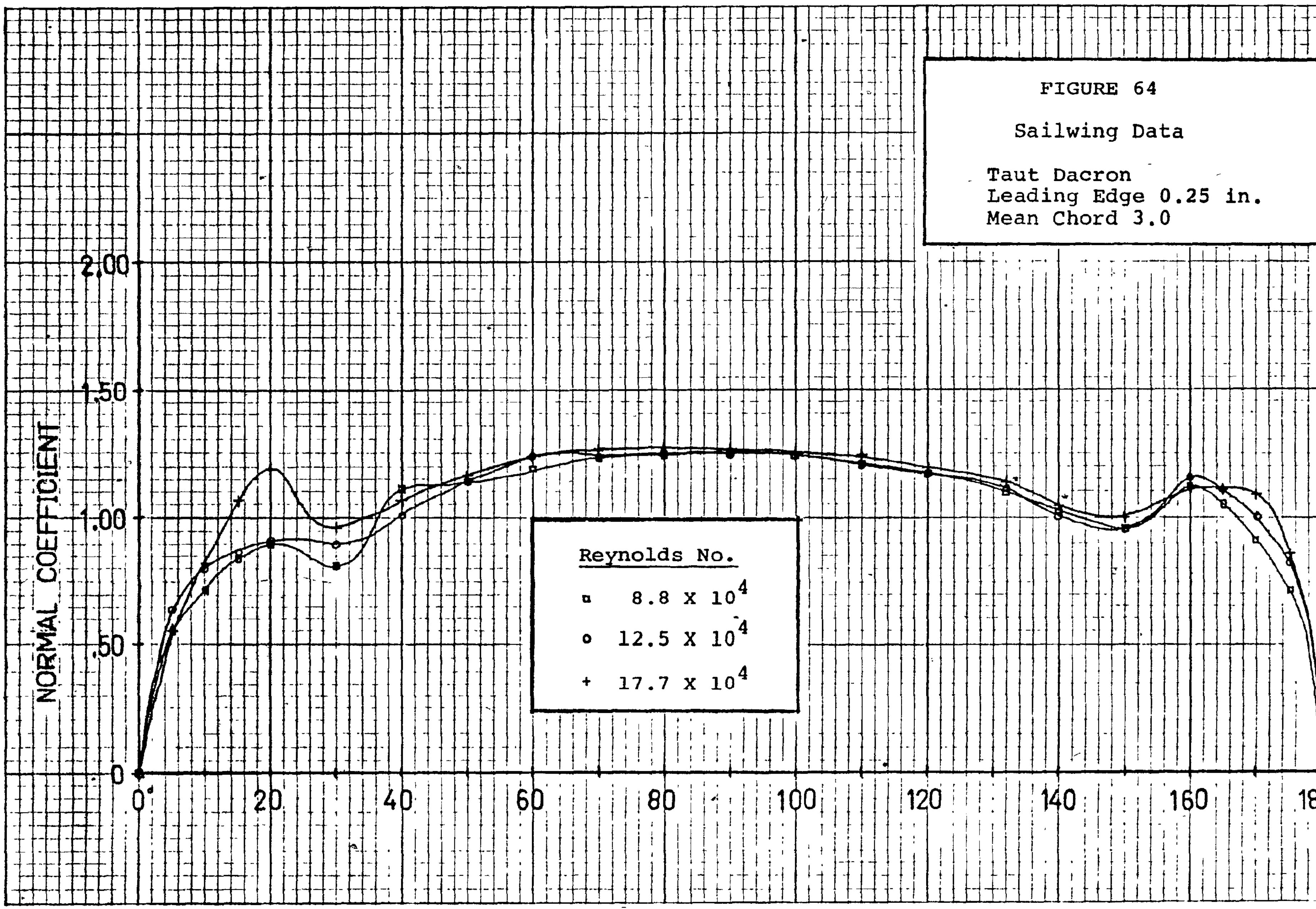
FIGURE 64
Sailwing Data
Taut Dacron
Leading Edge 0.25 in.
Mean Chord 3.0
Reynolds No.
8.8 X 10^4
12.5 X 10^4
17.7 X 10^4
NORMAL COEFFICIENT
2.00
1.50
1.00
.50
0
0°
20
40
60
80
100
120
140
160
180°

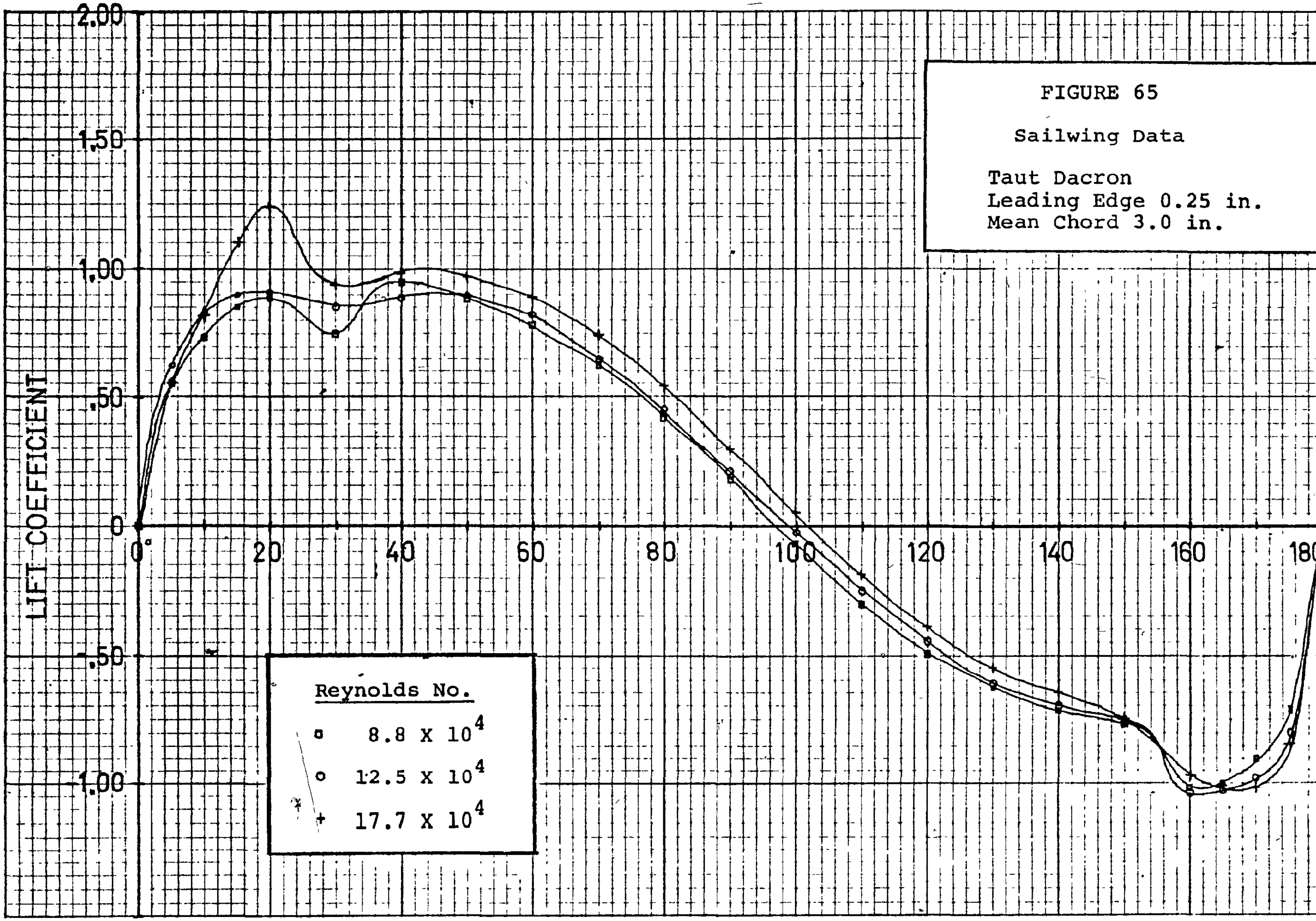
FIGURE 65
Sailwing Data
Taut Dacron
Leading Edge 0.25 in.
Mean Chord 3.0 in.
LIFT COEFFICIENT
2.00
1.50
1.00
.50
0
-.50
-1.00
0°
20
40
60
80
100
120
140
160
180°
Reynolds No.
8.8 X 10^4
12.5 X 10^4
17.7 X 10^4

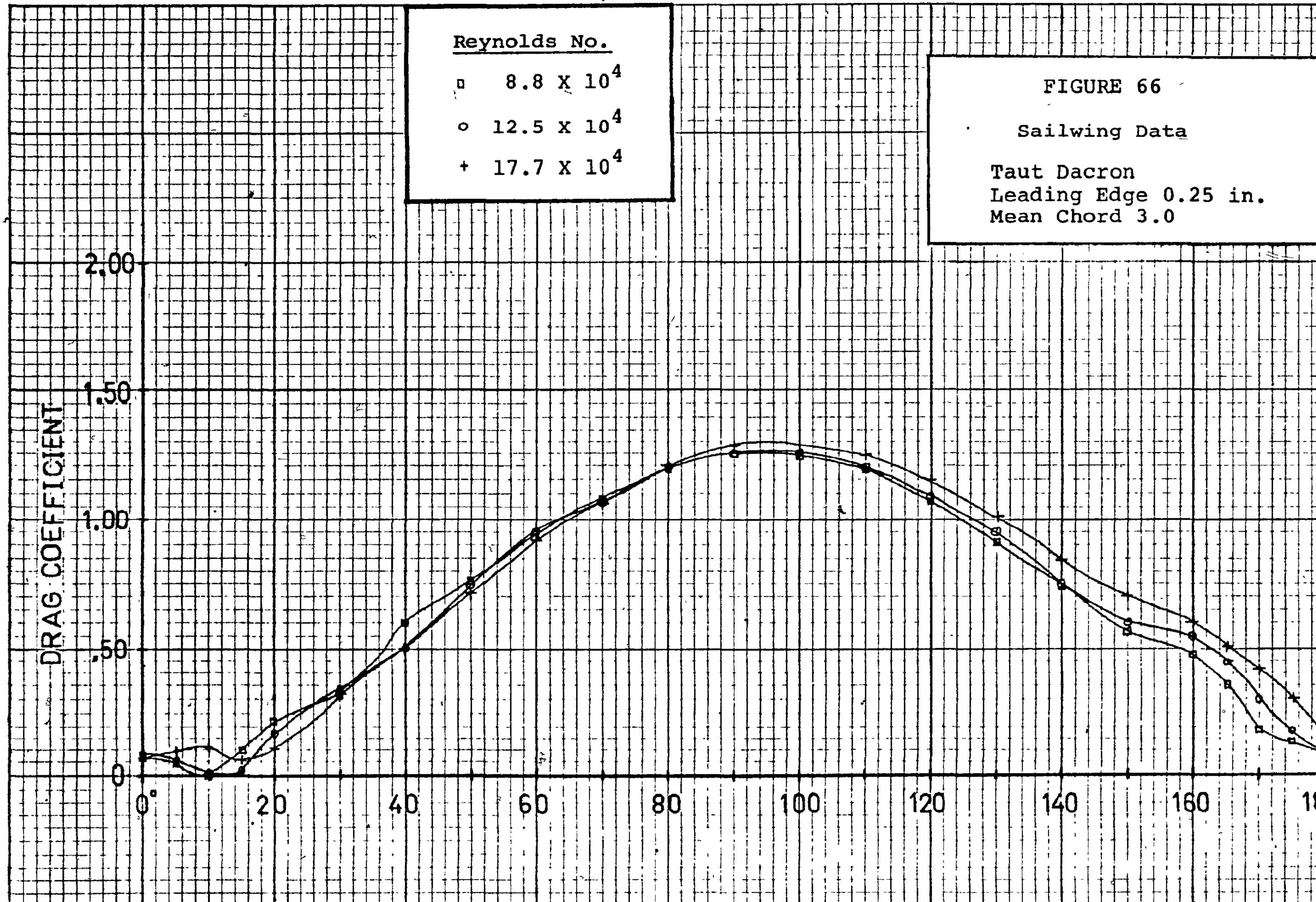

Reynolds No.
8.8 X 10^4
12.5 X 10^4
17.7 X 10^4
FIGURE 66
Sailwing Data
Taut Dacron
Leading Edge 0.25 in.
Mean Chord 3.0
DRAG COEFFICIENT
2.00
1.50
1.00
.50
0
0°
20
40
60
80
100
120
140
160
180°

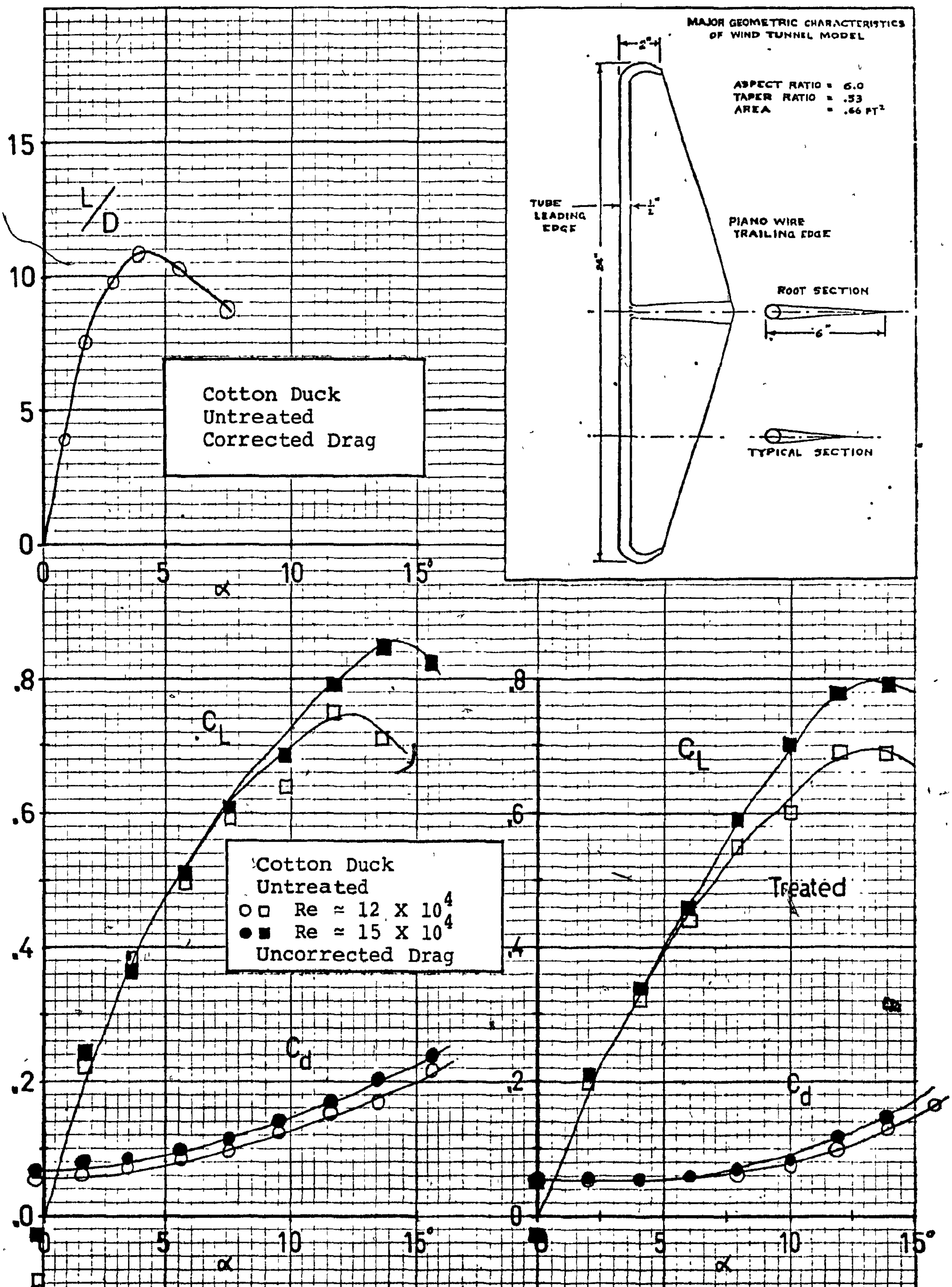

FIGURE 67 : The Princeton sailwing (Sweeney 1961)

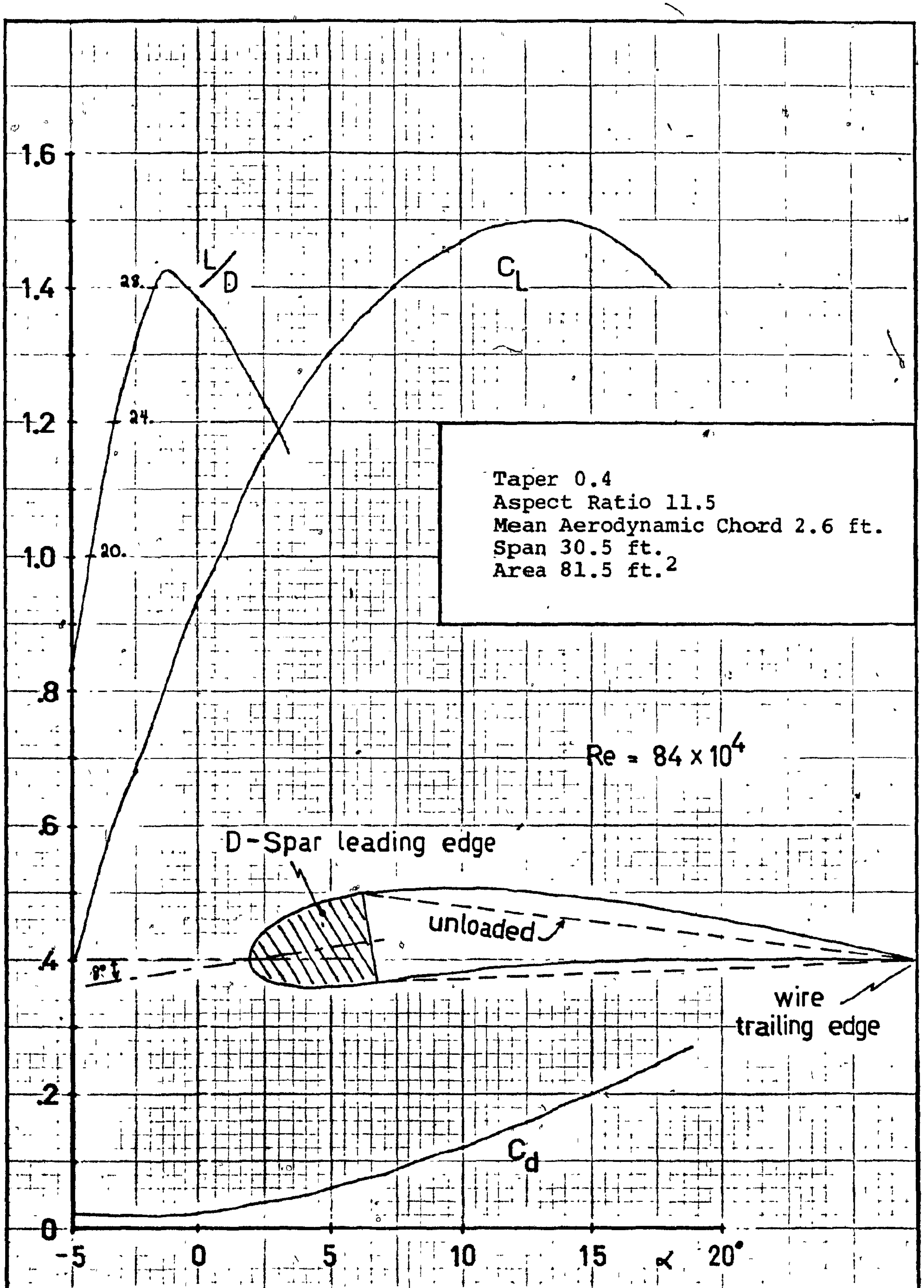

FIGURE 68 : The NASA sailwing (Fink 1967).

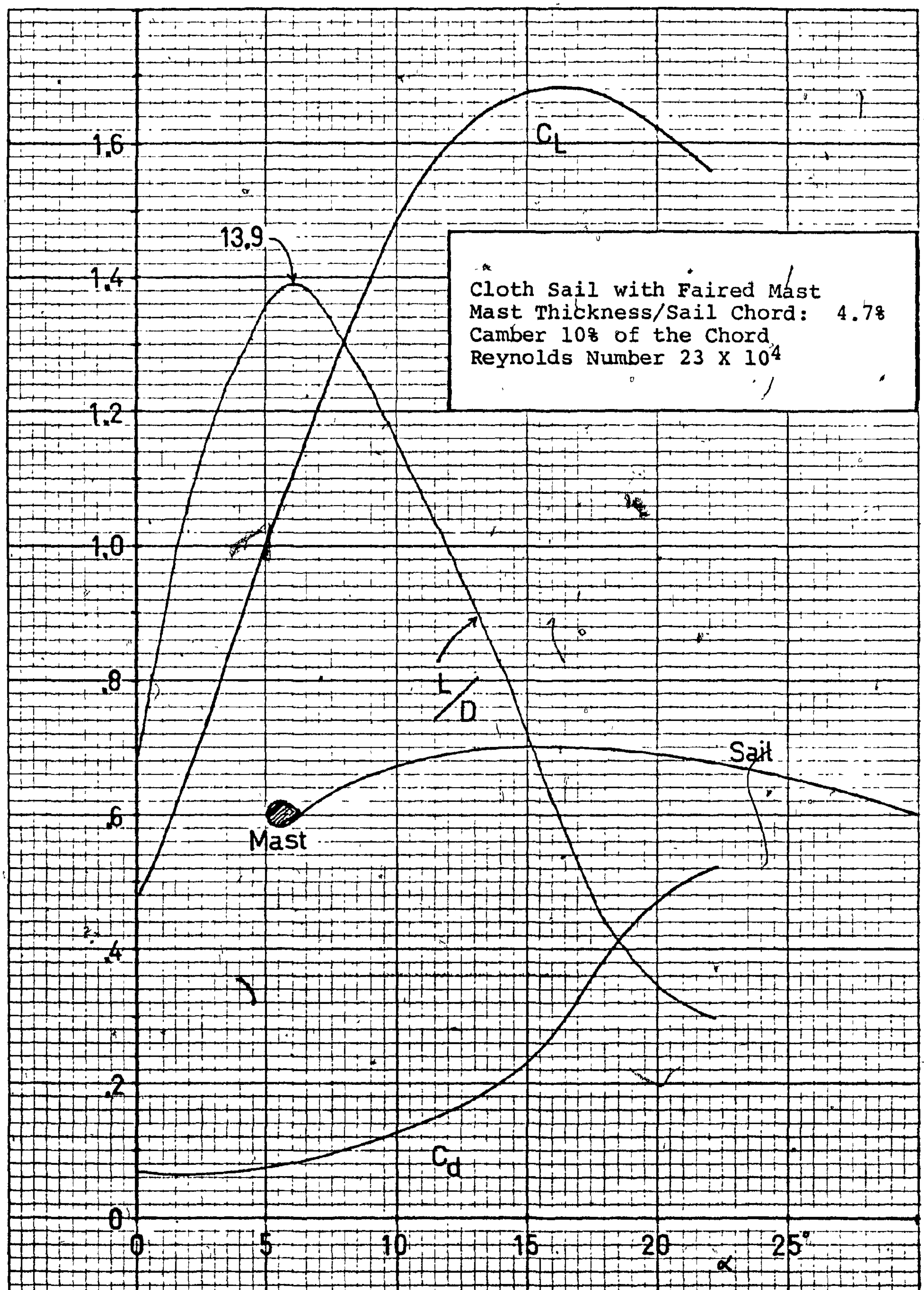

FIGURE 69 : Characteristics of a 2-D sail (Chapleo 1968)

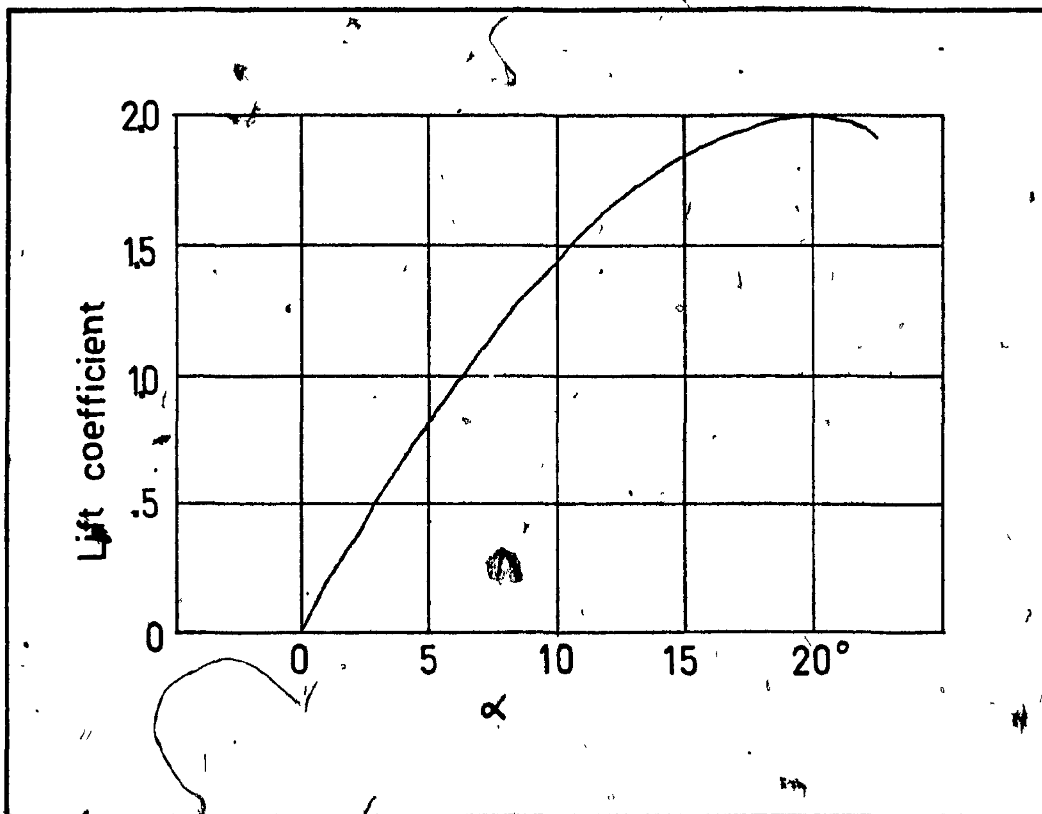

Aspect Ratio 7.25:1
Taper Ratio 3:1
Area 158 ft.^{2}
Span 34 ft.
Estimated Leading Edge/Chord 12%
Estimated Re = 90×10^4 to 180×10^4

FIGURE 70 : Coefficient of lift of a sailwing used in a "hang-glider" (Stong 1974).

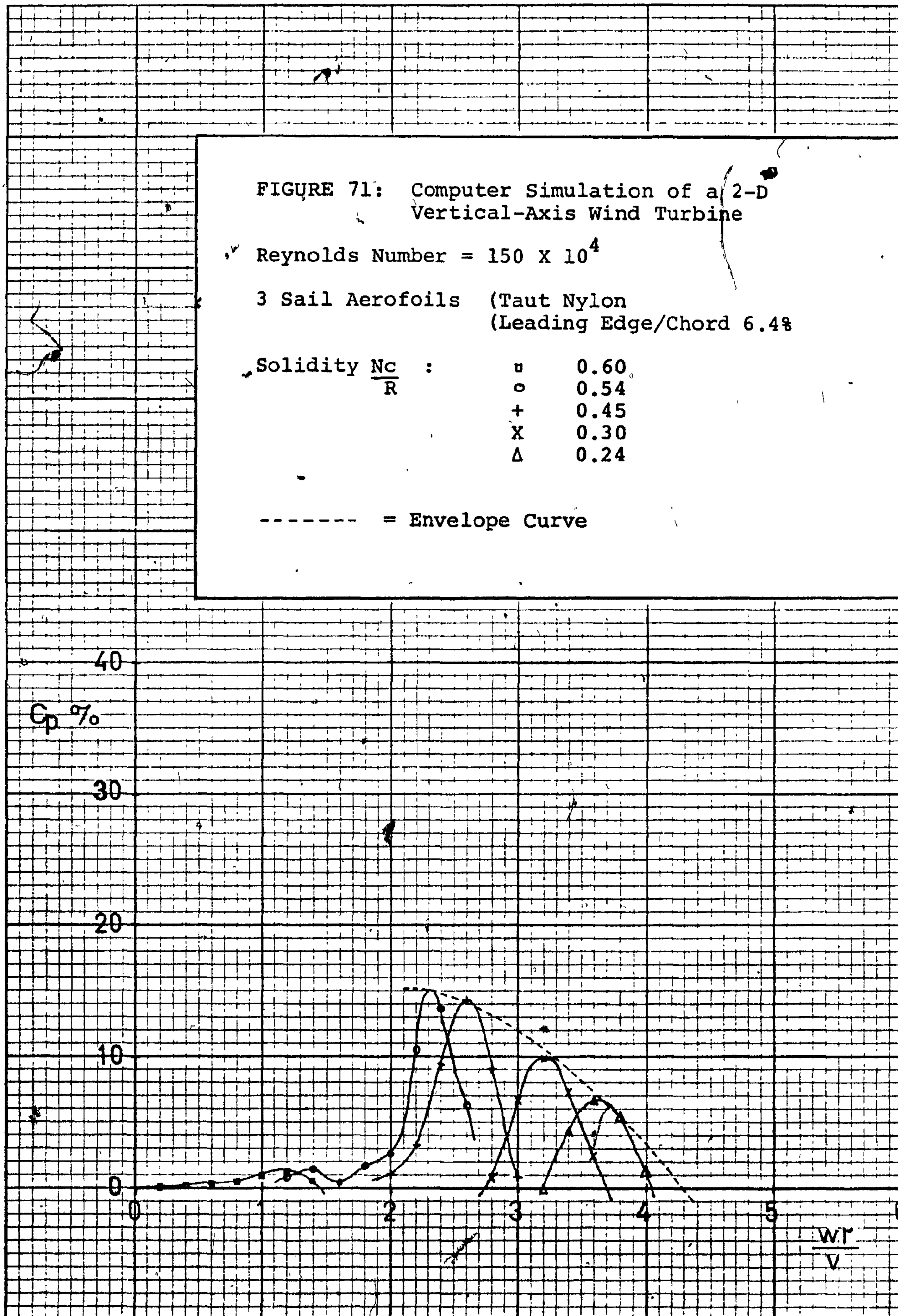

FIGURE 71: Computer Simulation of a 2-D Vertical-Axis Wind Turbine

Reynolds Number = 150×10^4

3 Sail Aerofoils (Taut Nylon (Leading Edge/Chord 6.4%

Solidity $\frac{Nc}{R}$:

▫	0.60
o	0.54
+	0.45
X	0.30
Δ	0.24

------- = Envelope Curve

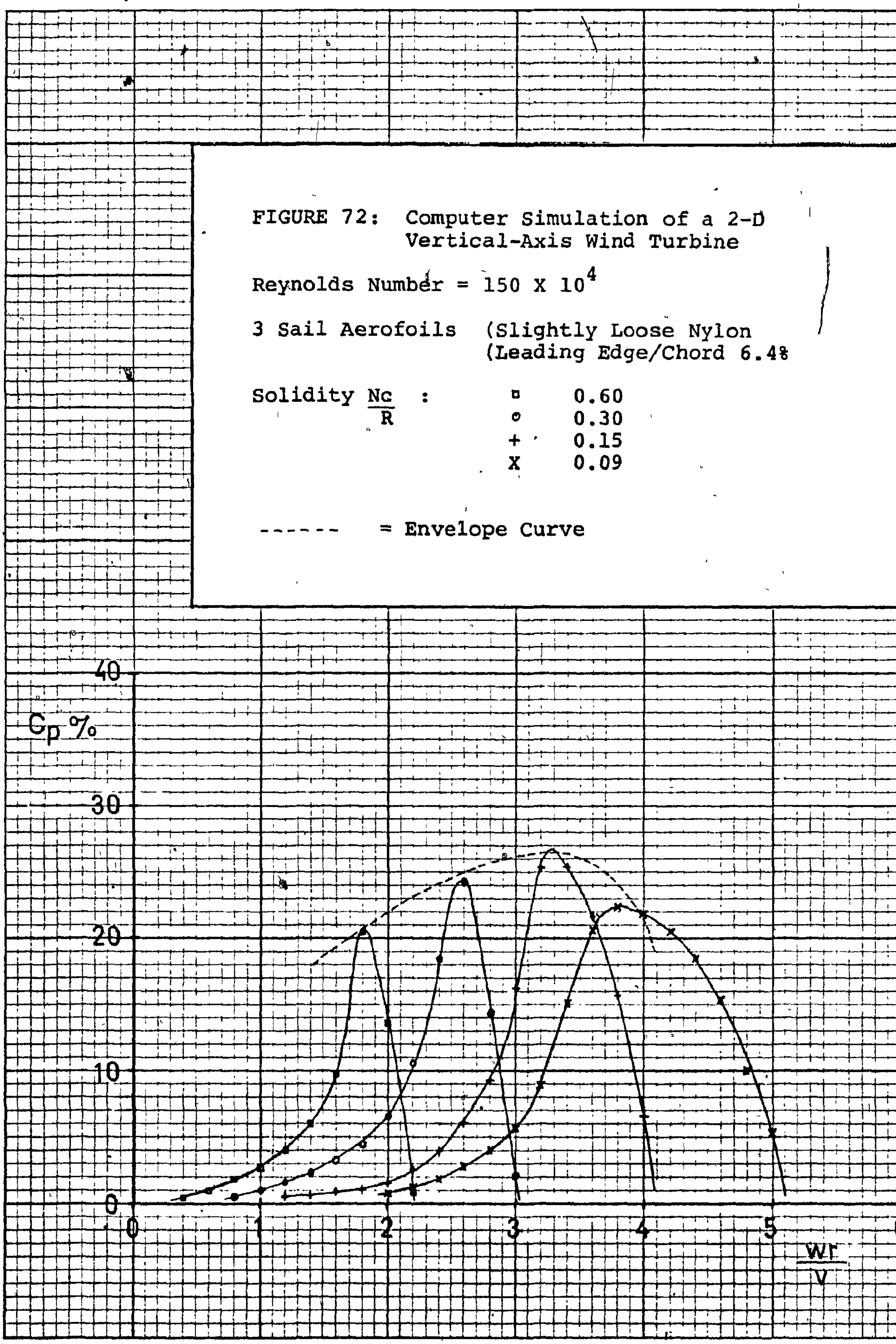

FIGURE 72: Computer Simulation of a 2-D Vertical-Axis Wind Turbine

Reynolds Number = 150 X 10^4

3 Sail Aerofoils (Slightly Loose Nylon (Leading Edge/Chord 6.4%

Solidity $\frac{Nc}{R}$:

□	0.60
o	0.30
+	0.15
X	0.09

------ = Envelope Curve

FIGURE 73: Computer Simulation of a 2-D Vertical-Axis Wind Turbine

Reynolds Number = 150 X 10^4

3 Sail Aerofoils (Loose Nylon (Leading Edge/Chord 6.4%

Solidity $\frac{Nc}{R}$:

□	0.60
o	0.30
+	0.15
X	0.09

------ = Envelope Curve

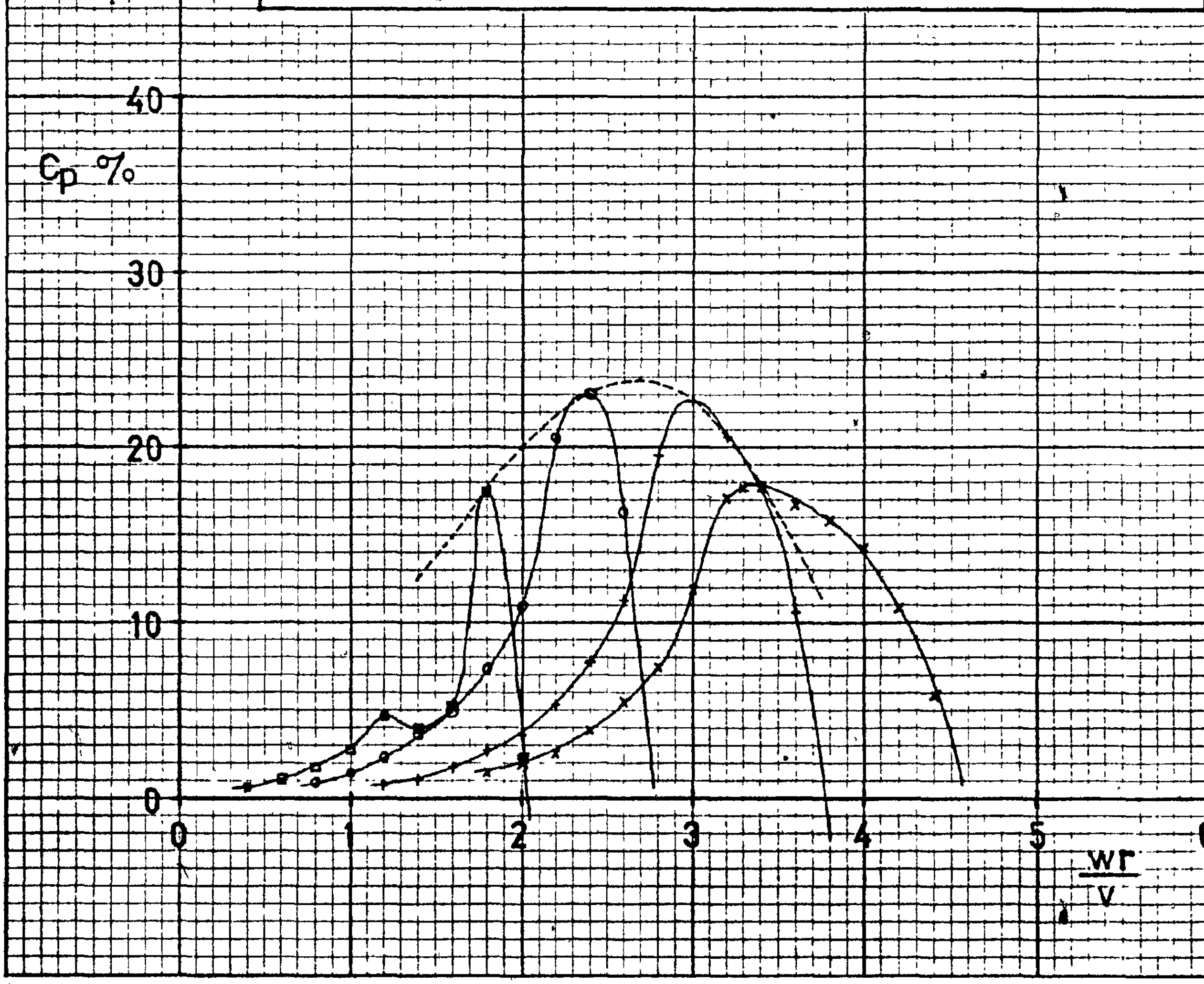

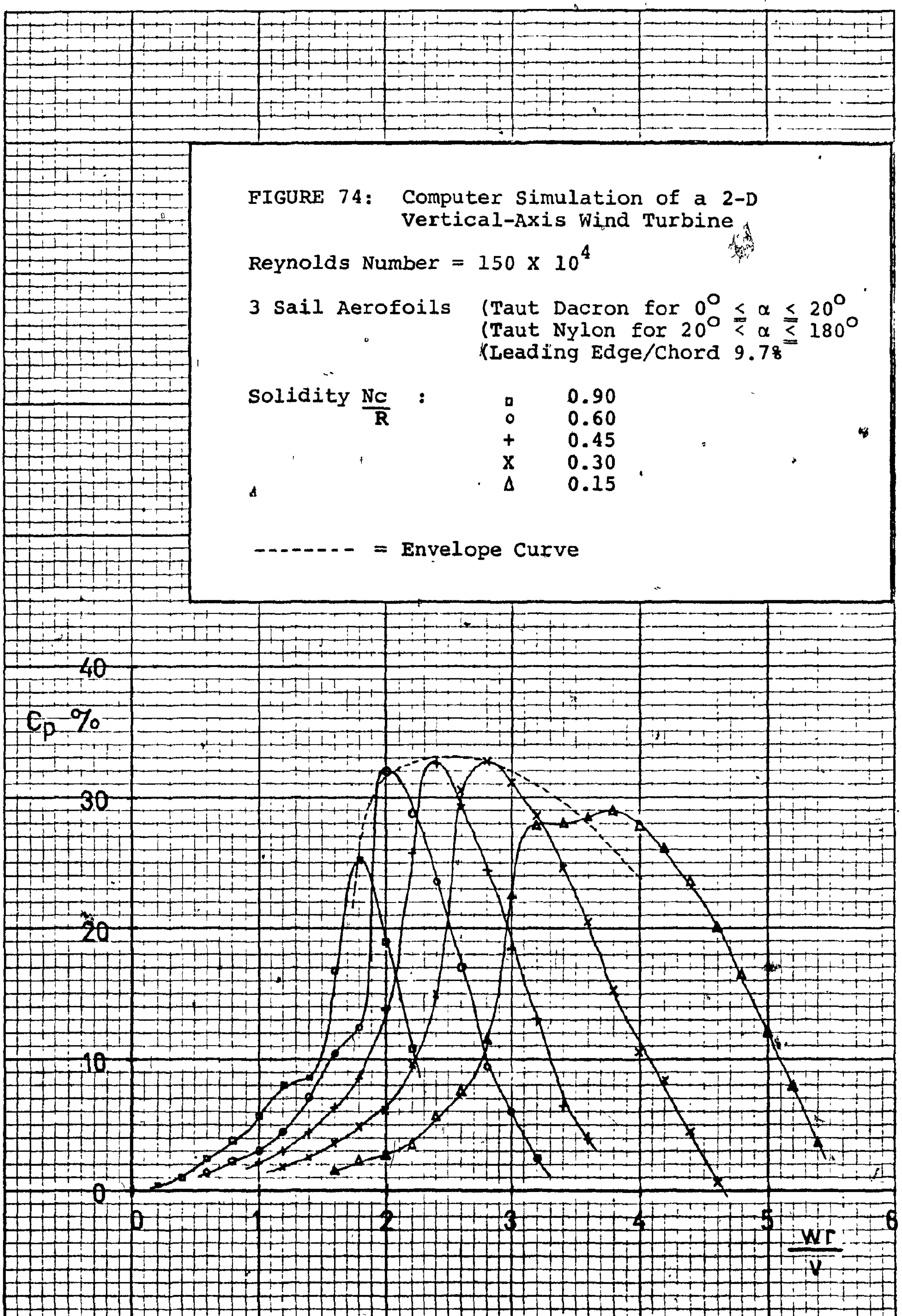

FIGURE 74: Computer Simulation of a 2-D Vertical-Axis Wind Turbine

Reynolds Number = 150 X 10^4

3 Sail Aerofoils (Taut Dacron for $0^o \leq \alpha \leq 20^o$
(Taut Nylon for $20^o \leq \alpha \leq 180^o$
(Leading Edge/Chord 9.7%

Solidity $\frac{Nc}{R}$:

□	0.90
o	0.60
+	0.45
X	0.30
Δ	0.15

-------- = Envelope Curve

FIGURE 75: Computer Simulation of a 2-D Vertical-Axis Wind Turbine

Reynolds Number = 150×10^4

3 Sail Aerofoils (Taut Nylon
(Leading Edge/Chord 9.7%

Solidity $\frac{Nc}{R}$:

□	0.60
o	0.30
+	0.15

------- = Envelope Curve

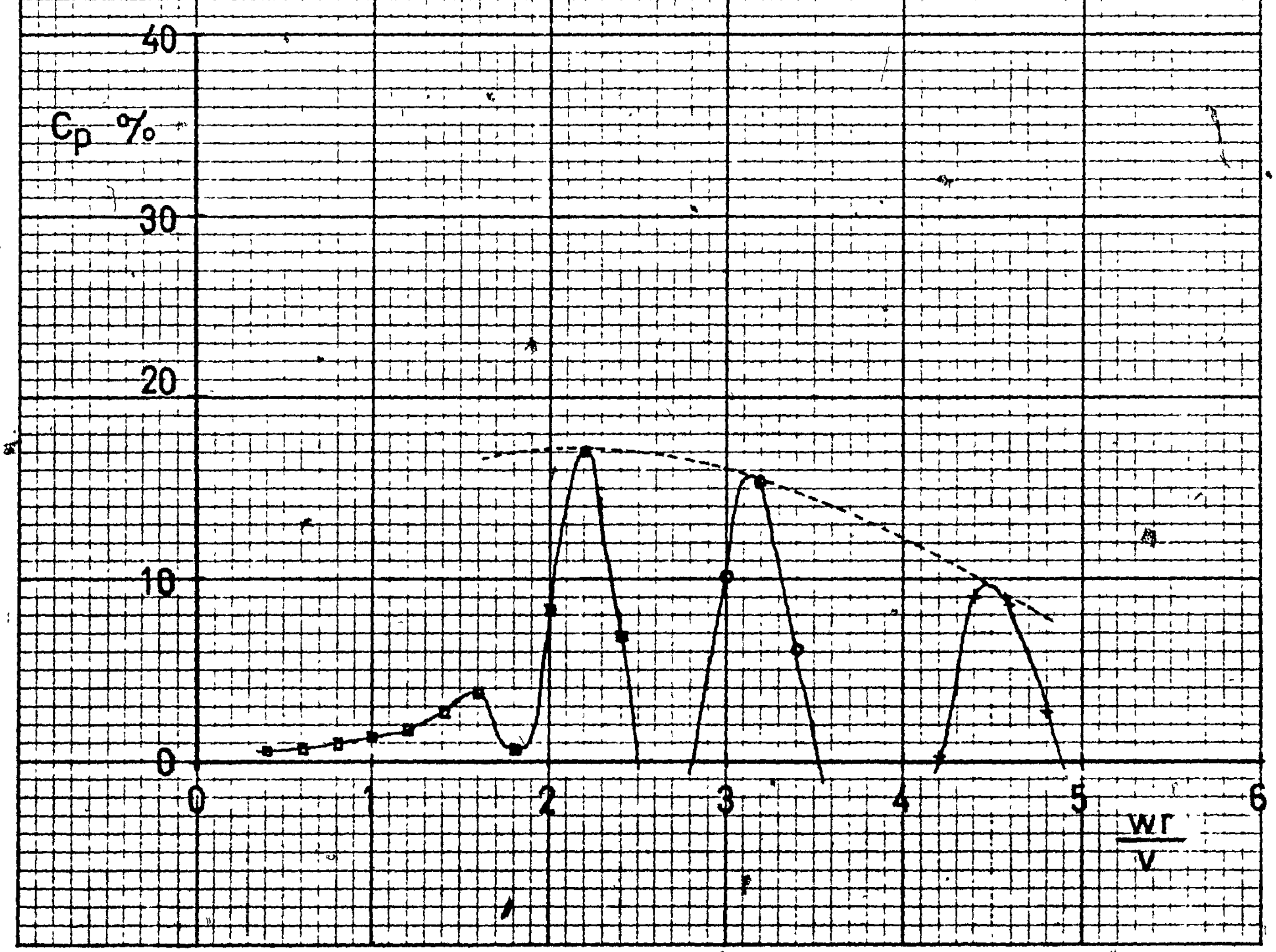

FIGURE 76: Computer Simulation of a 2-D Vertical-Axis Wind Turbine

Reynolds Number = 150 X 10^4

3 Sail Aerofoils (Loose Nylon
(Leading Edge/Chord 9.7%

Solidity $\frac{Nc}{R}$:

▫	0.60
o	0.45
+	0.30
X	0.15

------- = Envelope Curve

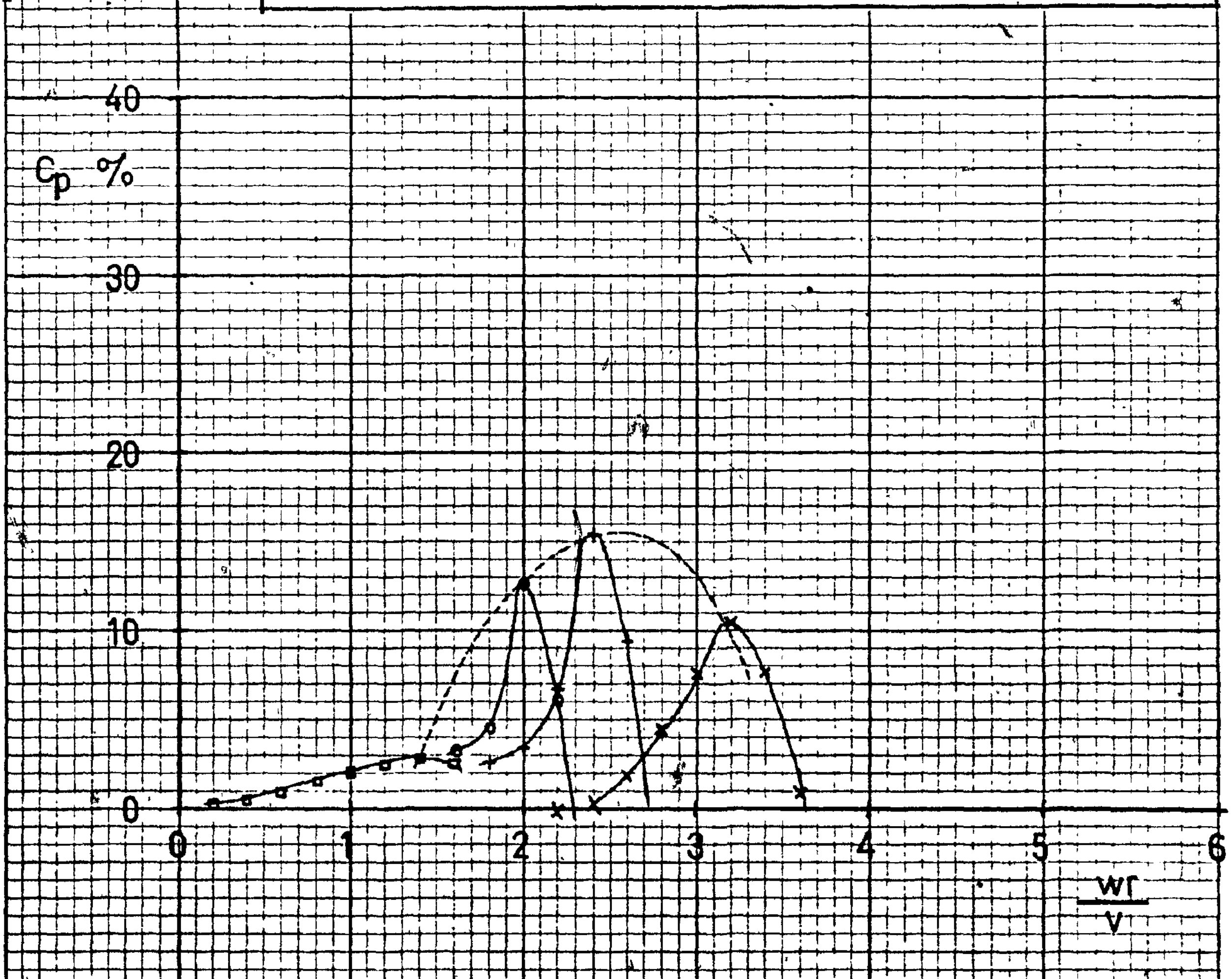

FIGURE 77: Computer Simulation of a 2-D Vertical-Axis Wind Turbine

Reynolds Number = 150 X 10^4

3 Sail Aerofoils (Taut Nylon
(Leading Edge/Chord 13%

Solidity $\frac{Nc}{R}$:

□	0.60
o	0.45
+	0.30

------- = Envelope Curve

FIGURE 78: Computer Simulation of a 2-D Vertical-Axis Wind Turbine

Reynolds Number
- □ 50×10^4
- o 150×10^4
- + 200×10^4
- X 250×10^4

3 Sail Aerofoils (Slightly Loose Nylon (Leading Edge/Chord 6.4%

Solidity $\frac{Nc}{R} = 0.15$

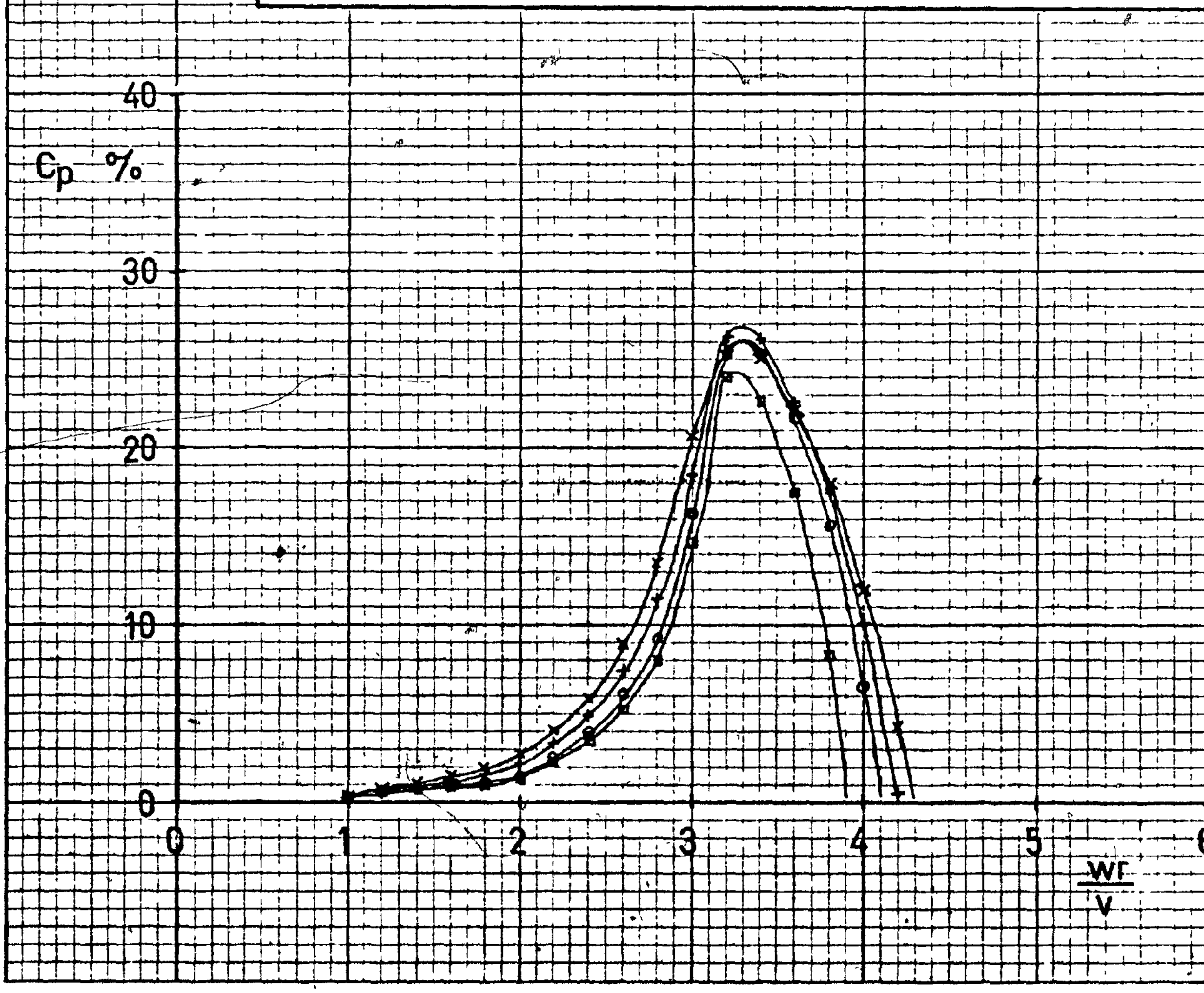

APPENDIX A

Program Listing

Program Notation

WIND TURBINE WED. 15 SEP. 1976

```
0001      JOB, START=10205
0002      JOB, REMOVE, JRTURB
0003      JOB, COMPILE, JRTURB, NOLIST
0004      C  UTILITY CARDS
0005            EXTERNAL F1V, F2V
0006            COMMON/BT/REYNCT( 10 ), ALFCT( 30 ), CTV( 30, 10 ), NCT, NCTR
0007            COMMON/BN/REYNCN( 10 ), ALFCN( 30 ), CNV( 30, 10 ), NCN, NCNR
0008            COMMON/BCR/CRR
0009            COMMON/WD/PI, WRV, REYNWD, VDV
0010            DIMENSION Y( 25 ), VDVYX( 25 ), EFFIC( 25 ), CD( 25 )
0011            DIMENSION VPVW( 25 ), VDVX( 25 ), WRVX( 25 ), CQ( 25 ), CP( 25 ), VDVW( 25 )
0012            LOGICAL ISSW     ⟶ ISSW (5) is an interrupt switch to stop the program (see line 72)
0013            PI=3 141592
0014            HR2A=0 25
0015            READ (5, 38 ) REYNWD
0016      38    FORMAT ( F10 2)
0017            READ( 5, 37 ) WRVA, WRVB, NWRV       } Parameters defining the turbine
0018      37    FORMAT( 2F5 1, I5 )
0019            READ( 5, 46 ) N, CRR
0020      46    FORMAT( I5, F5 2 )
0021      C     READING CT AND CN
0022            READ( 5, 31 )NCT, NCTR
0023            NCTR2 = NCTR - 2
0024            READ( 5, 42 )( REYNCT( J ), J=1, NCTR )
0025            READ( 5, 43 )( ALFCT( I ), ( CTV( I, J ), J=1, NCTR ), I=1, 11 )
0026            READ( 5, 44 )( ALFCT( I ), ( CTV( I, J ), J=1, NCTR2 ), I=12, NCT )
0027            READ( 5, 31 )NCN, NCNR
0028            NCNR2 = NCNR - 2
0029            READ( 5, 42 )( REYNCN( J ), J=1, NCNR )         } Reading thrust
0030            READ( 5, 43 )( ALFCN( I ), ( CNV( I, J ), J=1, NCNR ), I=1, 11 )    and normal force
0031            READ( 5, 44 )( ALFCN( I ), ( CNV( I, J ), J=1, NCNR2 ), I=12, NCN )    coefficients
0032      31    FORMAT( 2I5 )
0033      42    FORMAT( 10X, 5F10 3 )
0034      43    FORMAT( 6F10 3 )
0035      44    FORMAT( 4F10 3 )
0036      C  PERFORMANCE OF THE WINDMILL -  SPILLAGE EFFECT + AMBIENT WIND V
0037            EXPN=0 254
0038            CDPL=1. 11467
0039            NX=10                 } Constants for turbine theory
0040            NY=0                    and blade element analysis
0041            NMAX=15
0042            EPS=0 02
0043            NWRV1=NWRV+1
0044            WRVX( 1 )=WRVA        ⟵ Starting value of tip speed ratio
0045            WRITE ( 6, 123 )
0046      123   FORMAT( 1H1, 50H   TIP SPEED     CQ        CP        EFF       VD/V ,
0047          1 15H      CD     IT  //)
0048              DO 20 IW=1, NWRV1
0049              IWFIX=IW
0050              IF( NWRV. NE. 0 )WRVX( IW )=WRVA+FLOAT( IW-1 )*( WRVB-WRVA )/FLOAT( NWRV )
                  ↑ Incrementing the tip speed ratio.
```

WIND TURBINE WED. 15 SEP. 1976

```
      WRV=WRVX( IW )
      VDVX( 1 ) = 0.          } The assumed disc velocity ratio
      VDVX( 2 ) = 1.          }    is given two extreme values : 0.0 and 1.0.
      VDVYX( 1 ) = 1.
      VDV = VDVX( 2 )                                   } { Turbine drag coefficient integrated
      CALL SIMPS( 0. ,PI, 0 ,1 ,NX, NY, F1V, C )        } { with an assumed disc velocity
          CD( IW )=FLOAT( N )/PI*2 *HR2A*C              } { ratio  VDVX = 1.0
          BA=CD( IW )/CDPL
          IF( BA. GE  1. 0 )VDVY=0                      } { Turbine theory used to calculate
          IF( BA  LT  1  0 )VDVY=( 1 -BA )**EXPN        } {  VDVY
      VDVYX( 2 ) = VDVY -VDVX( 2 )
          DO 22 IV=3, NMAX           <—— iteration loop limited to NMAX
          IVFIX=IV                                        | Next assumption VDVX
          CALL  TERPL1( VDVYX, VDVX, IV-1, 0. 0, VDV )  <—| is estimated by
          VDVX( IV )=VDV                                  | interpolation.
          CALL  SIMPS( 0. , PI, 0  ,1  ,NX, NY, F1V, C ) <-|
          CD( IW )=FLOAT( N )/PI*2. *HR2A*C               |_ Turbine drag integrated
          BA=CD( IW )/CDPL                                 | using the last assumed VDVX.
          IF( BA. GE  1. 0 )VDVY=0
          IF( BA. LT  1  0 )VDVY=( 1 -BA )**EXPN
          VDVYX( IV )=VDVY-VDVX( IV )                 Switch #5 to interrupt the program.
          IF( IV. NE. NMAX. AND. . NOT  ISSW( 5 )) GO TO 23
          WRITE( 6, 24 )WRV, VDVX( IV ), VDVYX( IV ), CD( IW ), IVFIX
 24       FORMAT( 1H  , 8X, 5HWR/V   , 9X, 5HVDVX   , 9X, 5HVDVYX  , 9X, 2HCD, 7X, 1HN/
     1    4F14. 6, I3 )
          GO  TO  27                                      | Iterations stop when calculated
 23       IF( ABS( VDVYX( IV ) )-EPS )25, 25, 22  <——     | and assumed disc velocities are
 22       CONTINUE                                        | close enough.
 25     VDV=VDV+0. 5*VDVYX( IVFIX )
        VDVW( IW )=VDV
        CALL  SIMPS( 0. , PI, 0  , 1. , NX, NY, F2V, C )  <——   Integration of the torque
        CQ( IW )=FLOAT( N )/PI*HR2A*C
        CP( IW )=CQ( IW )*WRV*2.  * 100
        EFFIC( IW )=CP( IW )*( 27. /16  )
      WRITE( 6, 124 )WRVX( IW ), CQ( IW ), CP( IW ), EFFIC( IW ), VDVW( IW ), CD( IW ), IVFIX
 124  FORMAT( 1H  , F10. 2, F10. 4, 2F10 3, 2F10 4, I3 )      ↑_ Printing the results
 20     CONTINUE  <——> Tip speed ratio incremented
 27   CONTINUE                  and procedure repeated
C  PRINTING THE CONSTANTS
      WRITE( 6, 116 )REYNWD, HR2A, N, NX, NY, EPS
 116  FORMAT( 1HO/21HWINDMILL REYNOLDS NO.  , F8 1/5HHR/2A , F10. 3/
     1  13HNO.  OF BLADES  , I7/23HNO  OF ANGLE INCREMENTS , I7/
     2  24HNO.  OF HEIGHT INCREMENTS  , I7/9HPRECISION  , F10. 3/
     3  12HCHORD/RADIUS /17HBLADE TILT, DELTA /12HRADIUS RATIO /
     4  37HNO.  OF POINTS FOR ANGLE INTERPOLATION /14X,
     5  23HFOR SPEED INTERPOLATION /14HZERO-LIFT DRAG /11HDATA SOURCE  )
      WRITE( 6, 117 )CDPL, EXPN
 117  FORMAT( 1H  , 15HCD OF THE PLATE  , F10. 3/11HTHEORY USED  /
     1    16HEXPONENT FOR B/A  , F10. 2 )
      STOP
```

```
      END
C     SHAPE OF WINDMILL
      FUNCTION RR( YR )
      RR=1. 0
      RETURN
      END
```

The radius ratio r/R is defined as a function of height. Here it is constant

```
      FUNCTION DEL( YR )
      DEL=0 0
      RETURN
      END
```

The blade tilt angle may also vary with the height Here it is constant

```
      FUNCTION CR( YR )
      COMMON/BCR/CRR
      CR = CRR
      RETURN
      END
```

The chord to radius ratio may vary with the height Here it is constant

```
C     FINDING CT
      FUNCTION CT( ALF, REYNBL )
      COMMON/BT/REYNCT( 10 ), ALFCT( 30 ), CTV( 30, 10 ), NCT, NCTR
      MM=4
      NN=3
      NTR = NCTR
      REYN=REYNBL
      IF( ALF. GT ALFCT( 10 ) ) NTR = NCTR - 2
      IF( REYNBL LT REYNCT( 1 ) )REYN  =REYNCT( 1 )
      IF( REYNBL. GT REYNCT( NTR ) ) REYN = REYNCT( NTR ) + 0. 01
      CALL TERPL2( ALFCT, REYNCT, CTV, NCT, NTR, MM, NN, ALF, REYN, CT )
      RETURN
      END
```

(This subroutine interpolates the thrust coefficient at any Re and α from the data stored.)

```
C     FINDING CN
      FUNCTION CN( ALF, REYNBL )
      COMMON/BN/REYNCN( 10 ), ALFCN( 30 ), CNV( 30, 10 ), NCN, NCNR
      MM=4
      NN=3
      NNR = NCNR
      REYN=REYNBL
      IF( ALF GT. ALFCN( 10 ) ) NNR = NCNR - 2
      IF( REYNBL. LT. REYNCN( 1 ) )REYN  =REYNCN( 1 )
      IF( REYNBL. GT. REYNCN( NNR ) ) REYN = REYNCN( NNR ) + 0. 01
      CALL TERPL2( ALFCN, REYNCN, CNV, NCN, NNR, MM, NN, ALF, REYN, CN )
      RETURN
      END
```

(This subroutine interpolates the normal coeffecient at any Re and α from the data stored).

```
C     DRAG COEFFICIENT BASED ON AMBIENT WIND V
      FUNCTION F1V( TE, YR )
      COMMON/WD/PI, WRV, REYNWD, VDV
      X=RR( YR )*WRV+VDV*COS( TE )
      Y=VDV*SIN( TE )*COS( DEL( YR ) )
      ALF=ABS( ATAN2( Y, X )/PI*180. )
      VAVS=X*X+Y*Y
      REYNBL=SQRT( VAVS )*0. 5*CR( YR )*REYNWD
      F1V=VAVS*CR( YR )*( CN( ALF, REYNBL )*SIN( TE )-CT( ALF, REYNBL )*COS( TE )
```

This function calculates the integrand of the numerical integration of the drag coefficient

```
     1   /COS( DEL( YR )))
      RETURN
      END
C  TORQUE COEFFICIENT BASED ON AMBIENT WIND V
      FUNCTION F2V( TE, YR )
      COMMON/WD/PI, WRV, REYNWD, VDV
      X=RR( YR )*WRV+VDV*COS( TE )
      Y=VDV*SIN( TE )*COS( DEL( YR ))
      ALF=ABS( ATAN2( Y, X )/PI*180  )
      VAVS=X*X+Y*Y
      REYNBL=SQRT( VAVS )*0 5*CR( YR )*REYNWD
      F2V=VAVS*CR( YR )*RR( YR )*CT( ALF, REYNBL )/COS( DEL( YR ))
      RETURN
      END
```

This function calculates the integrand of the numerical integration of the torque coefficient.

```
C     INTERPOLATION FOR ONE DIMENSION WITHOUT SEEKING THE REGION
      SUBROUTINE TERPL1 ( X, Z, M, A, C )
      DIMENSION X( 25 ), Z( 25 )
      C=0.
        DO 50 I=1, M
        P=1
          DO 51 J=1, M
          IF( J. EQ. I )GO TO 51
          P=P*( A-X( J ))/( X( I )-X( J ))
51        CONTINUE
50      C=C+P*Z( I )
      RETURN
      END
```

All the available points are used to estimate the value of the function Z = f(x) at a new value X = A.

```
C   INTERPOLATION IN 2 DIMENSIONS AND SEARCH FOR THE REGION
      SUBROUTINE TERPL2( X, Y, Z, M, N, MM, NN, A, B, C )
      DIMENSION  X( 30 ), Y( 10 ), Z( 30, 10 )
      DIMENSION  F( 5 ), G( 5 ), W( 5, 5 )
        DO 10 I=1, M
        IF( A. GT  X( I )) GO TO 10
        KK=I-2
        GO TO 11
10      CONTINUE
11    KK = KK-( MM/4 )
      IF( KK. LE. -1 ) KK=0
      IF( KK+MM. GT. M ) KK=M-MM
        DO 12 I=1, N
        IF( B  GT. Y( I )) GO TO 12
        LL=I-2
        GO TO 13
12      CONTINUE
13    LL=LL-( NN/4 )
      IF( LL. LE. -1 ) LL=0
      IF( LL+NN. GT. N ) LL=N-NN
        DO 14 I=1, MM
      DO 14 J=1, NN
        KKI=KK+I
```

The desired value C = f(A,B) is interpolated from an array of data points Z = f(X,Y) by using several points surrounding the region of interest.

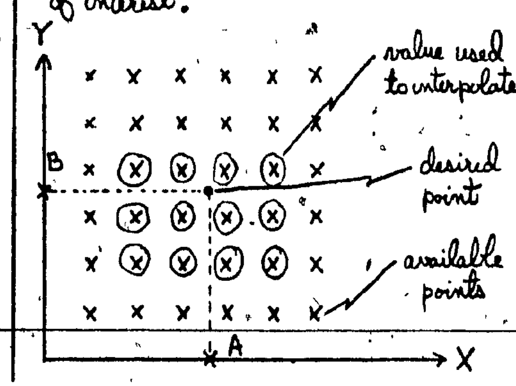

```
            LLJ=LL+J
            W( I, J )=Z( KKI, LLJ )
            F( I )=X( KKI )
      14    G( J )=Y( LLJ )
```

This section of the subroutine locates the region of interest.

```
         C=0
            DO 20 I=1, MM
            H=0.
              DO 21 J=1, NN
              P=1.
                DO 22 K=1, NN
                IF( K. EQ. J ) GO TO 22
                P=P*( B-G( K ))/( G( J )-G( K ))
      22        CONTINUE
      21      H=H+P*W( I, J )
            P=1.
              DO 23 L=1, MM
              IF ( L. EQ. I ) GO TO 23
              P=P*( A-F( L ))/( F( I )-F( L ))
      23      CONTINUE
      20    C=C+P*H
         RETURN
         END
```

This section of the subroutine actually performs the interpolation.

```
      C  NUMERICAL INTEGRATION = SIMPSON S' RULE
         SUBROUTINE SIMPS ( A, B, C, D, NX, NY, F, S )
         MX = 2*NX+1
         MY=2*NY+1
         IF( NX. NE. 0 )DX=( B-A )/FLOAT( NX )/2.
         IF( NY. NE. 0 )DY=( D-C )/FLOAT( NY )/2.
         IF( NX. EQ 0 )DX=3.
         IF( NY. EQ 0 )DY=3.
         Y=C
         S=0.
            DO 40 IY=1, MY
            X=A
            SUM=0.
              DO 41 IX=1, MX
              MULT = 4-2*MOD( IX, 2 )
              IF( IX. EQ. 1. OR. IX. EQ. MX )MULT=1
              SUM=SUM+FLOAT( MULT )*F( X, Y )
      41      X=X+DX
            SUM = SUM*DX/3
            MULT=4-2*MOD( IY, 2 )
            IF( IY. EQ 1. OR. IY EQ. MY )MULT=1
            S=S+FLOAT( MULT )*SUM
      40    Y=Y+DY
         S=S*DY/3
         RETURN
         END
      JOB, RELEASE, JRTURB
      JOB, END
```

(Numerical integration in two dimensions)

NOTATION IN THE PROGRAM

Name in the Program	Meant Notation	Description
ALF	α	Local angle of attack of a blade (degrees).
ALFCN(I)	α_{C_N}	Angles of attack in the data array of normal coefficients (degrees).
ALFCT(I)	α_{C_T}	Angles of attack in the data array of thrust coefficients (degrees).
BA	B/A	Ratio of the drag of the wind turbine to the drag of a "solid" turbine as used in the theory allowing high solidity.
BCR	Block c/R	Common block containing the value of c/R when it is constant along the height of the turbine.
BN	Block N	Common block containing information pertaining to the data array of normal coefficients.
BT	Block T	Common block containing information pertaining to the data array of thrust coefficients.
C		Temporary variable: crude result of a numerical integration.
CD(IW)	C_D	Drag coefficient of the wind turbine.
CDPL	$C_{D_{plate}}$	Drag of a "solid" turbine as used in the theory allowing high solidity.
CN(ALF,REYNBL)	$C_N(\alpha, Re_{blade})$	Function finding the normal coefficient from the data array.
CNV(I,J)	C_N values	Data array of normal coefficients.
CP(IW)	C_P	Power coefficient.
CQ(IW)	C_Q	Torque coefficient.
CR(YR)	c/R $(\frac{Y}{H/2})$	Chord to radius ratio as a function of height.
CRR	c/R	Chord to radius ratio when it is constant along the height of the turbine.
CT(ALF,REYNBL)	$C_T(\alpha, Re_{blade})$	Function finding the thrust coefficient from the data array.
CTV(I,J)	C_T values	Data array of thrust coefficients.
DEL(YR)	δ $(\frac{Y}{H/2})$	Tilt angle of the blades from the vertical as a function of height (radians).
EFFIC(IW)	η	Turbine efficiency (Betz) $(= \frac{27}{16} C_P)$
EPS	ε (epsilon)	Precision margin allowed when finding the disc velocity ratio.
EXPN	Exponent_x	Exponent in the theory allowing high solidity.
F1V(TE,YR)	$f_1(\theta, Y/R)$	Integrand in the numerical integration of the turbine drag.
F2V(TE,YR)	$f_2(\theta, Y/R)$	Integrand in the numerical integration of the turbine torque.
HR2A	$\frac{HR}{2A}$	Dimensionless shape factor of the turbine.
ISSW(5)	Switch	Logical variable whose truth depends on the position of the external switch no. 5 on the computer console (special feature of the computer used).
IV		Incremental index for the iterations required to find the disc velocity ratio.
IVFIX	IV_{fixed}	Current value of IV. May be used outside the iteration loop.
IW		Incremental index for tip speed ratio.
IWFIX	IW_{fixed}	Current value of IW. May be used outside the loop.

Name in the Program	Meant Notation	Description
MM		Number of points to be used in the angle interpolation of the data array.
N	N	Number of blades on the turbine.
NCN	No. of C_N	Number of angles in the data array of normal coefficients.
NCNR	No. of Re_{C_N}	Number of Reynolds numbers in the data array of normal coefficients.
NCNR2	= NCNR-2	
NCT	No. of C_T	Number of angles in the data array of thrust coefficients.
NCTR	No. of Re_{C_T}	Number of Reynolds numbers in the data array of thrust coefficients.
NCTR2	= NCTR-2	
NMAX	N_{max}	Desired maximum number of iterations allowed to find the disc velocity ratio.
NN		Number of points to be used for the Reynolds number interpolation in the data array.
NNR		Temporary variable for NCTR or NCTR2.
NTR		Temporary variable for NCNR or NCNR2.
NWRV	No. of $\frac{WR}{V}$	Number of tip speed ratios at which performance are evaluated.
NWRV1	NWRV + 1	
NX	n_x	Half the number of intervals for numerical integration in the θ direction.
NY	n_y	Half the number of intervals for numerical integration in height.
PI	π	3.141592
REYN	Re	Temporary variable for the Reynolds number of the blade ($/10^4$).
REYNBL	Re_{blade}	Blade Reynolds number ($/10^4$).
REYNCN(J)	Re_{C_N}	Reynolds numbers ($/10^4$) in the data array of normal coefficients.
REYNCT(J)	Re_{C_T}	Reynolds numbers ($/10^4$) in the data array of thrust coefficients.
REYNWD	$Re_{wind\ turbine}$	Turbine Reynolds number based on the diameter.
RR(YR)	$r/R(\frac{y}{H/2})$	Radius ratio as a function of height.
SIMPS(A,B,C,D,NX,NY,F,S)		Numerical integration $S = \int_{CA}^{DB}\int f(x,y)\,dx\,dy$ using 2NX and 2NY intervals in x and y (Simpson's rule).
TE	θ	Angle in the horizontal plane, with respect to the position of a turbine blade facing the wind (radians).
TERPL1 (X,Z,M,A,C)		Interpolation in an array Z = f(x) of the value C = f(A) using M points.
TERPL2(X,Y,Z,M,N,MM,NN,A,B,C)		Interpolation in an MxN array Z = f(x,y) of the value C = f(A,B) using MM by NN points.
VAVS	$(\frac{V\alpha}{V})^2$	Ratio of the horizontal local windspeed relative to a blade to the ambient wind velocity.
VDV	$\frac{V_D}{V}$	Disc velocity ratio.
VDVW(IW)	$\frac{V_D}{V}$	Disc velocity ratio.
VDVX(IV)	$(\frac{V_D}{V})_x$	Assumed disc velocity ratio.
VDVY(IV)	$(\frac{V_D}{V})_y$	Calculated disc velocity ratio using the turbine theory.
VDVYX(IV)	$(\frac{V_D}{V})_y - (\frac{V_D}{V})_x$	Difference between calculated and assumed disc velocity ratios.
WD	Block WD	Common block containing information on the wind turbine.

Name in the Program	Meant Notation	Description
WRV	$\frac{wR}{V}$	Tip speed ratio.
WRVA	$(\frac{wR}{V})_a$	Lowest tip speed ratio at which performances are evaluated.
WRVB	$(\frac{wR}{V})_b$	Largest tip speed ratio at which performances are evaluated.
WRVX(IW)	$\frac{wR}{V}$	Tip speed ratio.
X (as used in F1V and F2V)		Tangential component of the local windspeed $V\alpha$ relative to a turbine blade.
Y (as used in F1V and F2V)		Radial component (in a horizontal plane) of the local windspeed $V\alpha$ relative to a turbine blade.
Y(I)		Not used in this version of the program.

APPENDIX B

Sample of Data Cards

Explanation Note for the Data Cards

Sample Output of the Program

Explanation Note for the Output

```
WIND  TURBINE                          WED,  15  SEP,  1

     JOB,START=10205
     JOB,JRTURB
      150.
   0.0   6.0   30
     3 0.05
    28     5
                     9.0       13.0      18.0      24.0      30.0
         0.0      -0.088    -0.076    -0.069    -0.070    -0.066
         2.5      -0.033    -0.026    -0.022    -0.020    -0.023
         5.0       0.024     0.034     0.037     0.031     0.025
         7.5       0.094     0.098     0.091     0.083     0.073
        10.0       0.147     0.149     0.152     0.133     0.121
        12.5       0.191     0.197     0.206     0.184     0.168
        15.0       0.008     0.038     0.096     0.227     0.200
        17.5      -0.026     0.003     0.028     0.057     0.079
        20.0      -0.020    -0.011     0.005     0.035     0.055
        25.0      -0.037    -0.002     0.009     0.010     0.022
        30.0       0.004     0.019     0.021     0.026     0.035
        40.0       0.028     0.042     0.049
        50.0       0.024     0.041     0.047
        60.0      -0.030     0.013     0.016
        70.0      -0.009    -0.007     0.004
        80.0      -0.021    -0.007    -0.003
        90.0       0.008     0.014     0.021
       100.0       0.040     0.051     0.053
       110.0       0.078     0.075     0.078
       120.0      -0.075     0.044     0.081
       130.0       0.017     0.047     0.068
       140.0       0.039     0.048     0.045
       150.0       0.016     0.030     0.031
       160.0      -0.004     0.002     0.002
       165.0      -0.006    -0.004     0.002
       170.0      -0.136    -0.101    -0.073
       175.0      -0.030    -0.050    -0.059
       180.0       0.072     0.071     0.081
    28     5
                     9.0       13.0      18.0      24.0      30.0
         0.0       0.812     0.836     0.789     0.748     0.696
         2.5       1.472     1.223     1.168     1.083     0.996
         5.0       1.438     1.408     1.368     1.299     1.227
         7.5       1.547     1.529     1.493     1.432     1.378
        10.0       1.600     1.592     1.578     1.514     1.473
        12.5       1.693     1.678     1.658     1.599     1.561
        15.0       1.405     1.518     1.589     1.603     1.588
        17.5       1.297     1.361     1.432     1.507     1.527
        20.0       1.364     1.356     1.378     1.448     1.493
        25.0       1.575     1.577     1.569     1.563     1.573
        30.0       1.826     1.851     1.832     1.833     1.797
        40.0       2.040     2.057     2.067
        50.0       2.120     2.099     2.089
```

WIND TURBINE WED, 15 SEP, 1

0051	60.0	1.874	1.749	1.734
0052	70.0	1.883	1.888	1.846
0053	80.0	1.974	1.976	1.941
0054	90.0	2.009	1.971	1.958
0055	100.0	1.983	1.979	1.973
0056	110.0	1.932	1.945	1.940
0057	120.0	2.141	2.024	1.879
0058	130.0	2.189	2.183	2.188
0059	140.0	2.156	2.154	2.162
0060	150.0	1.854	1.874	1.870
0061	160.0	1.425	1.434	1.420
0062	165.0	1.499	1.456	1.436
0063	170.0	1.548	1.521	1.483
0064	175.0	1.243	1.301	1.351
0065	180.0	0.736	0.681	0.599
0066	JOB, END			

Explanation Note for the Data Cards

Line Number	Variables Read	Explanation
0003	REYNWD	Turbine Reynolds Number ($/10^4$)
0004	WRVA, WRVB NWRV	Tip Speed Ratio Range Number of Runs Within this Range
0005	N CRR	Number of Blades Chord to Radius Ratio
0006	NCT NCTR	Number of Angles of Attack for C_T Number of Reynolds Numbers for C_T
0007	REYNCT	5 Reynolds Numbers for C_T
0008-0018	ALFCT, CTV	Angle + 5 Values of C_T ($0^\circ \leq \alpha \leq 30^\circ$)
0019-0035	ALFCT, CTV	Angle + 3 Values of C_T ($40^\circ \leq \alpha \leq 180^\circ$)
0036	NCN NCNR	Number of Angles of Attack for C_N Number of Reynolds Numbers for C_N
0037	REYNCN	5 Reynolds Numbers for C_N
0038-0048	ALFCN, CNV	Angle + 5 Values of C_N ($0^\circ \leq \alpha \leq 30^\circ$)
0049-0065	ALFCN, CNV	Angle + 3 Values of C_N ($40^\circ \leq \alpha \leq 180^\circ$)

SAMPLE OUTPUT OF THE PROGRAM

TIP SPEED	CQ	CP	EFF	VD/V	CD	IT
0. 00	0. 0001	0. 000	0. 000	0. 9790	0 0885	3
0 20	0 0003	0 011	0 018	0. 9784	0 0910	3
0. 40	0. 0006	0. 052	0. 088	0 9763	0. 0994	3
0. 60	0. 0005	0. 064	0. 108	0. 9727	0 1143	3
0 80	0. 0007	0 107	0. 181	0. 9674	0 1355	3
1 00	0. 0017	0 343	0. 579	0 9608	0. 1618	3
1 20	0 0025	0 599	1. 010	0 9526	0 1941	3
1. 40	0. 0025	0 708	1 194	0 9436	0. 2277	3
1. 60	0 0028	0 903	1. 524	0 9339	0 2642	3
1 80	0. 0029	1. 044	1. 762	0. 9234	0. 3013	3
2. 00	0. 0038	1 501	2. 533	0. 9122	0. 3400	3
2. 20	0 0058	2 531	4 270	0 8994	0 3852	3
2. 40	0 0083	3. 976	6. 710	0 8838	0 4394	3
2 60	0. 0117	6. 062	10 229	0. 8643	0. 5048	3
2. 80	0. 0166	9. 290	15 677	0. 8277	0 5876	4
3. 00	0. 0270	16 229	27. 386	0 7803	0 7002	4
3. 20	0. 0396	25 354	42. 785	0 7169	0 8142	4
3 40	0. 0373	25. 360	42. 795	0 6655	0 8888	5
3 60	0. 0302	21 737	36. 681	0 6069	0. 9573	5
3. 80	0. 0206	15. 669	26. 441	0 5298	1 0199	4
4. 00	0. 0082	6. 527	11. 014	0. 4436	1. 0667	5
4. 20	−0 0065	−5. 441	−9 182	0 3487	1 0961	7
4 40	−0. 0214	−18 874	−31. 849	0. 2592	1. 1091	8
4. 60	−0. 0337	−31 016	−52. 339	0. 1923	1. 1129	11

WR/V	VDVX	VDVYX	CD	N
4. 799988	0. 119019	0. 273983	1. 086472	12

WINDMILL REYNOLDS NO 150. 0
HR/2A 0. 250
NO. OF BLADES 3
NO. OF ANGLE INCREMENTS 10
NO OF HEIGHT INCREMENTS 0
PRECISION 0. 020
CHORD/RADIUS 0.05
BLADE TILT, DELTA 0°
RADIUS RATIO 1.0
NO. OF POINTS FOR ANGLE INTERPOLATION 4
FOR SPEED INTERPOLATION 3
ZERO-LIFT DRAG
DATA SOURCE *Slightly loose nylon d = 0.25 in.*
CD OF THE PLATE 1 115
THEORY USED *Extension for high solidity*
EXPONENT FOR B/A 0. 25

115705 09-15-76 JOB. END
357 . SECONDS
115707 09-15-76 JOB. HALT

Explanation Note for the Output

TIP SPEED	Tip Speed Ratio
CQ	Torque Coefficient
CP	Power Coefficient
EFF	Turbine Efficiency
VD/V	Disc Velocity Ratio
CD	Turbine Drag Coefficient
IT	Number of Iterations